

**Preparation and characterisation of diamond based  
stationary phases for high performance  
liquid chromatography**

---

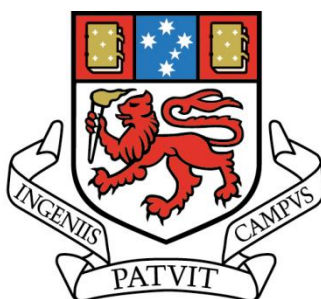
by

**Anton Peristy**

Specialist in Chemistry

Submitted in fulfilment of the requirements for the degree of

**Doctor of Philosophy**



**UNIVERSITY  
OF TASMANIA**

School of Physical Sciences,  
University of Tasmania

**July 2015**

## **Declaration**

### **Declaration of Originality**

This thesis contains no material which has been accepted for a degree or diploma by the University or any other institution, except by way of background information and duly acknowledged in the thesis, and to the best of my knowledge and belief no material previously published or written by another person except where due acknowledgement is made in the text of the thesis, nor does the thesis contain any material that infringes copyright.

**/Anton Peristyy**

### **Authority of Access**

This thesis may be made available for loan and limited copying and communication in accordance with the Copyright Act 1968.

**/Anton Peristyy**

### **Statement regarding published work contained in thesis (where applicable)**

The publishers of the papers comprising Chapters 1, 3 and 4 hold the copyright for that content, and access to the material should be sought from the respective journals. The remaining non published content of the thesis may be made available for loan and limited copying and communication in accordance with the Copyright Act 1968.

**/Anton Peristyy**

University of Tasmania

Hobart,

Date: \_\_\_\_\_

## Statement of co-authorship

The following people and institutions contributed to the publication of work undertaken as part of this thesis:

Paper 1: Candidate<sup>1</sup> (60%), P. N. Nesterenko<sup>2</sup> (25%), B. Paull<sup>3</sup> (10%), O. N. Fedyanina<sup>4</sup> (5%)

Paper 2: Candidate<sup>1</sup> (70%), P. N. Nesterenko<sup>2</sup> (20%), B. Paull<sup>3</sup> (10%)

Details of the Authors role:

Paper 1: Author 1 contributed to the design of the overall concept, executed the literature overview and wrote the draft manuscript. Author 2 contributed to the concept, publication refinement and submission. Author 3 assisted in proof reading, corrections and publication refinement. Author 4 contributed to the literature overview.

Paper 2: Author 1 contributed to the design of the overall concept, executed all laboratory work and wrote the draft manuscript. Author 2 contributed to the concept, publication refinement and submission. Author 3 assisted in proof reading, corrections and publication refinement.

We the undersigned agree with the above stated “proportion of work undertaken” for each of the above published (or submitted) peer-reviewed manuscripts contributing to this thesis:

*Signed:* \_\_\_\_\_

*Date:* \_\_\_\_\_

*Prof. Pavel Nesterenko*

*Primary Supervisor*

*School of Physical Sciences*

*University of Tasmania*

*Prof. John Dickey*

*Head of School*

*School of Physical Sciences*

*University of Tasmania*

## Statement of co-authorship

The following people and institutions contributed to the publication of work undertaken as part of this thesis:

School of Physical Sciences, University of Tasmania = **Anton Peristy** (Candidate)

School of Physical Sciences, University of Tasmania = **Pavel Nesterenko** (Author 1)

School of Physical Sciences, University of Tasmania = **Brett Paull** (Author 2)

School of Chemistry, Moscow State University = **Olga Fedyanina** (Author 3)

### Author details and their roles:

#### Paper 1.

Peristy, A.A., Fedyanina, O.N., Paull, B., Nesterenko, P.N. **Diamond based adsorbents and their application in chromatography**, *Journal of chromatography A*, 1357 (2014) 68-86.

This paper comprises Chapter 1. Candidate was the primary author and conducted the majority of literature search, literature analysis and wrote the manuscript. Pavel Nesterenko, Brett Paull and Olga Fedyanina contributed to the idea, its formalisation and development.

#### Paper 2.

Peristy, A.A., Paull, B., Nesterenko, P.N. **Chromatographic performance of synthetic polycrystalline diamond as a stationary phase in normal phase high performance liquid chromatography**, *Journal of chromatography A*, 1391 (2015) 49-59.

This paper comprises Chapter 4 and partially Chapter 3. Candidate was the primary author and conducted all the experiments, analysed data and wrote the manuscript. Pavel Nesterenko and Brett Paull contributed to the idea, its formalisation and development.

We the undersigned agree with the above stated “proportion of work undertaken” for each of the above published (or submitted) peer-reviewed manuscripts contributing to this thesis:

Signed:           Candidate  
                          Pavel Nesterenko  
                          Brett Paull  
                          Olga Fedyanina

Date: 17/04/15

## List of publications and presentations

1. Peristy A.A., Fedyanina O.N., Paull B., Nesterenko P.N. **Diamond based adsorbents and their application in chromatography**, *Journal of chromatography A*, 1357 (2014) 68-86. (Chapter 1).
2. Peristy A.A., Paull B., Nesterenko P.N. **Diamond based adsorbents and their application in chromatography**, *Journal of chromatography A*, 1391 (2015) 49-59. (Chapter 3 and 4).
3. Peristy A.A., Paull B., Nesterenko P.N. **Chromatographic properties of synthetic high pressure high temperature diamond in hydrophilic interaction liquid chromatography**. *Manuscript in preparation*. (Chapter 5).
4. Peristy A.A., Paull B., Nesterenko P.N. **Ion-exchange properties of microdispersed sintered detonation nanodiamond**. *Manuscript in preparation*. (Chapter 6).
5. Peristy A.A., Nesterenko P.N., Paull B. **Adsorption of inorganic ions by sintered detonation nanodiamond**. *40<sup>th</sup> International Symposium on High Performance Liquid Phase Separations and Related Techniques, HPLC-2013*. Hobart, Australia, 18-21 November 2013. P. 277. (Chapter 6).
6. Nesterenko P.N., Fedyanina O.N., Peristy A.A., Paull, B. **Diamond based stationary phases in chromatography: emphasise on separation selectivity, hydrolytic and thermal stability**. *40<sup>th</sup> International Symposium on High Performance Liquid Phase Separations and Related Techniques, HPLC-2013*. Hobart, Australia, 18-21 November 2013. P. 273. (Chapter 3).
7. Peristy A.A., Nesterenko P.N., Paull B. **Synthetic Diamond Microparticles as a Stationary Phase for Elevated Temperature and Ultra-high Pressure Liquid Chromatography**. *41<sup>st</sup> International Symposium on High Performance Liquid Phase Separations and Related Techniques, HPLC-2014*. New Orleans, USA, 11-15 May 2014. L-062. (Chapters 4 and 6).

8. Nesterenko P.N., Fedyanina O.N., Paull B., Peristy A.A., Mitev D., Duffy E. **Prospectives of using diamond based adsorbents in chromatography.** *Abstract of IX Conference on Analytical Chemistry of Siberia and Far East*, 8-13 October 2012, Krasnoyarsk, Russia. P.165.
9. Paull B., Nesterenko P.N., Connolly D., Nesterenko E., Alwael H., Collins D., Peristy A.A., Duffy E., He X. **Application of metallic and carbonaceous nano-particle modified phases in micro-extraction and liquid chromatography.** *38<sup>th</sup> International Symposium on High Performance Liquid Phase Separations and Related Techniques, HPLC-2012*. 16-21 June 2012, Anaheim, USA. L-03-20.
10. Paull B., Nesterenko P.N., Mitev D., Peristy A.A., Duffy E. **Diamond Based Phases for Chromatography, from Micro to Nano: Production, Characterisation and Application.** *Pittsburgh Conference on Analytical Chemistry and Applied Spectroscopy, Pittcon 2013*. 17-21 March 2013, Philadelphia, PA, USA. 930-1.

## Acknowledgement

This research was supported under Australian Research Council's Discovery Projects funding scheme (Discovery Grants DP110102046 and DP150102608). The tuition fee was kindly provided by the Tasmanian government through the Department of Economic Development, Tourism and the Arts.

I owe my sincere gratitude to the following people for their involvement in this project:

- My supervisors, Prof. Pavel Nesterenko and Prof. Brett Paull for their deep knowledge, suggestions and invaluable help throughout entire course of PhD. Without their encouragement and guidance this work would have not been possible
- People who have been involved in this project at different stages for fruitful discussions and feedback – Ms Emer Duffy, Dr Dimitar Mitev, Prof. Zhenggui Wei and Dr Tom Kazarian
- Australian Centre for Research on Separation Science (ACROSS) – for providing facilities and pleasant working environment
- The author gratefully acknowledges use of the services and instruments of Central Science Laboratory of University of Tasmania. Special thanks to Dr Karsten Goemann and Dr Sandrin Feig for their assistance in acquisition and interpretation of SEM images and EDS spectra, and to Dr Thomas Rodemann for the help with FTIR spectra measurements
- Dr John Ford for the valuable discussions regarding the purification of diamond and column packing
- Prof. Andrew Shalliker for the suggestions about the conducting of the van Deemter experiments
- Friends who have helped me in many ways during past few years – Mr Daniel Gstoettenmayr, Ms Esme Candish, Dr Sara Sandron, Dr Dario Arrua, Mr Alfonso Rojas Cardona, Mr Alain Wuethrich, Dr Laura Tedone, Ms Mari Egeness, Mr Matthew Jacobs, Mr Milos Dvorak, Mr Yabin Wen, Mr Yan Li, Dr Tom Lawson, Dr Sinead Currivan and others. Special thanks to Emer, Matt, Sinead and Esme for their help in the Thesis refinement
- Mr Peter Dove, Mr John Davis, Mr Chris Young, Mr Murray Frith and Ms Jennifer Nield for their assistance
- My wife, daughter, parents, brother and other family members for support during all these years

## List of Abbreviations

ACN – acetonitrile	ICP-MS – inductive coupled plasma mass spectroscopy
ANP – aqueous normal phase chromatography	ID – internal diameter
ATA – aurintricarboxylic acid	IPA – isopropyl alcohol
BET – Brunauer–Emmett–Teller	IR – infrared
BTBA - benzyltributylammonium chloride	KHP – potassium hydrogen phthalate
BTMA – benzyltrimethylammonium chloride	LbL – layer by layer
BuLi – butyl lithium	MeOH – methanol
CVD – chemical vapour deposition	MPCVD – microwave plasma assisted chemical vapour deposition
CZE – capillary zone electrophoresis	MSDN – microdispersed sintered detonation nanodiamond
DFT – density functional theory	ND – nanodiamond
DHBA – dihydroxybenzoic acid	NP-HPLC – normal phase HPLC
DIW – deionised water	ODS – octadecyl silica
DMSO – dimethylsulfoxide	PAH – polycyclic aromatic hydrocarbon
DND – detonation nanodiamond	PAAm – polyallyl amine
DSC – differential scanning calorimetry	PAR – 4-(2-pyridylazo)-resorcinol
EDS – energy dispersive X-ray spectroscopy	PEG – polyethylene glycol
EELS – electron energy loss spectroscopy	PGC – porous graphitic carbon
FTIR – Fourier transform infrared spectroscopy	PS-DVB – polystyrene-divinylbenzene
GC – gas chromatography	PTFE - polytetrafluoroethylene
HBSA – hydroxybenzenesulphonic acid	RP-HPLC – reversed phase chromatography
HETP – height equivalent to theoretical plate	SDND – single digit nanodiamond
HILIC – hydrophilic interaction liquid chromatography	SEM – scanning electron microscopy
HPHT diamond – high pressure high temperature diamond	SPE – solid-phase extraction
HPLC – high performance liquid chromatography	SWCNT – single wall carbon nanotube
IC – ion chromatography	TFA – trifluoroacetic acid
	TGA – Thermogravimetric analysis
	TMAOH – tetramethylammonium hydroxide
	TNT – trinitrotoluene



UHP – ultra high purity

UHPLC – ultra high performance liquid chromatography

US – ultrasound

UV – ultraviolet

XPS – X-ray photoelectron spectroscopy

### List of letter designations

$A$  – adsorption,  $\mu\text{mol}\cdot\text{g}^{-1}$

$A_{max}$  – adsorption capacity,  $\mu\text{mol}\cdot\text{g}^{-1}$

$D_p$  – pore size, nm

$d_p$  – particle size,  $\mu\text{m}$

$d$  – diameter, m

$F$  – flow rate,  $\text{mL}\cdot\text{min}^{-1}$

$g = 10 \text{ m}\cdot\text{s}^{-2}$  – gravitational acceleration

$H$  – height, m

$h$  – reduced plate height

$\Delta H^\circ$  – enthalpy,  $\text{kJ}\cdot\text{mol}^{-1}$

$K_D$  – distribution coefficient,  $\text{mL}\cdot\text{g}^{-1}$

$K_L$  – Langmuir adsorption constant,  $\text{mL}\cdot\mu\text{mol}^{-1}$

$K_F$  – Freundlich adsorption constant

$k$  – retention factor

$L$  – column length, mm

$\log P$  – octanol/water partitioning coefficient

$m$  – mass, g

$N$  – theoretical plate count,  $\text{plates}\cdot\text{m}^{-1}$

$p_p$  – particle perimeter,  $\mu\text{m}$

$\Delta P$  – pressure drop in the column, psi

$Q_x$  – fraction of particles with size  $> x$

$q_x$  – fraction of particles with size  $\approx x$

$R$  – gas constant =  $8.31 \text{ J}\cdot\text{mol}^{-1}\cdot\text{K}^{-1}$

$r$  – radius, m

$S$  – surface area,  $\text{m}^2\cdot\text{g}^{-1}$

$S_p$  – particle area,  $\mu\text{m}^2$

$\Delta S^\circ$  – entropy,  $\text{kJ}\cdot\text{mol}^{-1}\cdot\text{K}^{-1}$

$T$  – temperature,  $^\circ\text{C}$

$t$  – time, min

$t_R$  – retention time, min

$U$  – velocity,  $\text{m}\cdot\text{s}^{-1}$

$u$  – linear velocity,  $\text{mm}\cdot\text{s}^{-1}$

$V$  – volume, L

$W$  – weight, g

$X$  – molar fraction

$\alpha$  – selectivity

$\alpha_T$  – thermal expansion,  $\text{K}^{-1}$

$\beta$  – phase ratio

$\Phi$  – column resistance factor

$\zeta$  – zeta potential, mV

$\eta$  – viscosity,  $\text{Pa}\cdot\text{s}$

$\Theta$  – wettability,  $^\circ$

$\rho$  – density,  $\text{kg}\cdot\text{m}^{-3}$

$\varphi$  – volume fraction

## Abstract

The idea of using diamond and diamond containing materials in separation sciences has attracted a strong interest in the past decade. The combination of a unique range of properties, such as chemical inertness, mechanical, thermal and hydrolytic stability, excellent thermal conductivity with minimal thermal expansion and intriguing adsorption properties makes diamond a promising material for use in various modes of chromatography. This Thesis is dedicated to the preparation and investigation of diamond based stationary phases for ultra high-performance liquid chromatography. The Thesis consists of 6 chapters: introduction and literature review, experimental Chapter, and four research Chapters.

The information about the recent research on the preparation of diamond based stationary phases, their properties and chromatographic performance is summarised in Chapter 1. Special attention is devoted to the dominant retention mechanisms evident for particular diamond related materials, and their subsequent applicability to various modes of liquid chromatography, including liquid chromatography carried out under the conditions of high temperature and pressure. Advantages and drawbacks of diamond-based stationary phases described in literature are analysed. According to the literature review, it is decided to investigate chromatographic performance of non-modified non-porous high pressure high temperature (HPHT) diamond with 1.6  $\mu\text{m}$  particles and a surface area 5.1  $\text{m}^2\cdot\text{g}^{-1}$ .

Chapter 2 contains the general information on materials and instrumentation used in this work, as well as the description of methods and calculations.

A purification procedure for HPHT diamond is developed and its surface properties are characterised using various physical chemical methods in Chapter 3. It is shown that this material possesses a hydrophilic surface which displays various oxygen-containing groups, including carboxyl, carbonyl, hydroxyl, and others. Next, optimisation of particle shape and size distribution is performed by means of oxidative digestion and sedimentation. After that, the column packing procedure is developed. It is shown that better column packings can be achieved by using a water-based slurry with an addition of 10 mM NaOH, while use of organic solvents does not provide stable packed beds. Finally, it is established that packing pressure has to be kept as high as possible, and column after-packing conditioning with  $\text{HNO}_3$  helps to improve peak shape.

The resultant columns exhibit a maximum efficiency of 128,200 theoretical plates per meter in normal phase (NP) liquid chromatography, as shown in Chapter 4. The retention behaviour of several classes of compounds, including alkyl benzenes, polyaromatic

hydrocarbons, alkylphenylketones, phenols, and aromatic acids and bases are studied using *n*-hexane – IPA mixtures as a mobile phase. The results are compared with those observed for microdispersed sintered detonation nanodiamond (MSDN) and porous graphitic carbon. HPHT diamond revealed distinctive separation selectivity, which is orthogonal to that observed for porous graphitic carbon (Hypercarb); while selectivities of HPHT diamond and MSDN are similar. Owing to the non-porous nature of the particles, columns packed with HPHT diamond exhibit excellent mass transfer, and separations of 4, 6 and 9 model compounds are presented.

Furthermore, HPHT diamond is tested as a stationary phase in aqueous normal phase (HILIC/ANP) chromatography using acetonitrile/water and methanol/water mobile phases in Chapter 5. The retention of several classes of compounds is investigated, including nucleobases, quaternary ammonium salts, carboxylic acids, phenols and their derivatives. The column performance is studied within a large pH range (2.2-12.7) using several buffering mixtures (trifluoroacetic, ammonium formate, ammonia and several hydroxides). The main retention mechanisms for HPHT diamond include cation exchange and hydrogen bonding. Both buffer and organic modifier (acetonitrile/methanol) have a crucial influence on the HPHT diamond column selectivity. A complete selectivity reversal is observed for different groups of solutes as a result of changes in mobile phase composition.

During the research on chromatographic properties of HPHT diamond, an assumption is made that the adsorption of cations and anions on the surface of diamond has a strong effect on its chromatographic performance. For example, it is shown that column conditioning with HNO<sub>3</sub>, H<sub>2</sub>SO<sub>4</sub> or H<sub>3</sub>PO<sub>4</sub> leads to different column selectivities in NP-HPLC, and the use of NaOH and KOH solutions of equal concentration in ANP-HPLC results in different retention of nucleobases and phenolic compounds. Therefore, the adsorption of cations and anions on the diamond surface is studied in Chapter 6. MSDN is used for the investigation of the adsorption of inorganic cations and anions due to the higher surface area of MSDN as compared to HPHT diamond.

The selectivity series  $\text{Fe}^{3+} > \text{Al}^{3+} > \text{Cu}^{2+} > \text{Mn}^{2+} > \text{Zn}^{2+} > \text{Cd}^{2+} > \text{Co}^{2+} > \text{Ni}^{2+}$  is found for MSDN, and the adsorption capacity for these metals is between 2 and 5  $\mu\text{mol}\cdot\text{g}^{-1}$ . Counter ions can contribute to the adsorption mechanism for transition metals, and the buffer influence on the adsorption of metals is revealed. Accordingly, the adsorption of inorganic anions ( $\text{CH}_3\text{COO}^-$ ,  $\text{Cl}^-$ ,  $\text{B}_4\text{O}_7^{2-}$ ,  $\text{ClO}_4^-$ ,  $\text{I}^-$ ,  $\text{SO}_4^{2-}$ ,  $\text{C}_2\text{O}_4^{2-}$ ,  $\text{PO}_4^{3-}$ ) on MSDN is investigated. The adsorption capacity for inorganic anions is at levels of 50-150  $\mu\text{mol}\cdot\text{g}^{-1}$ , depending on the anion. For the first time, an anion exchange capacity is detected for detonation nanodiamond,

exceeding its cation-exchange capacity. Electrostatic interactions, formation of complexes with hydroxyls and interactions with metal impurities contribute to the anion adsorption mechanism, so anion adsorption selectivity over MSDN is different from common anion exchangers. It is shown that the adsorption on MSDN obeys Langmuir law. The pH affects the adsorption of  $\text{SO}_4^{2-}$ ,  $\text{PO}_4^{3-}$  and  $\text{B}_4\text{O}_7^{2-}$  differently due to different adsorption mechanisms.

## Table of Content

<i>Chapter 1. Literature review: Diamond based adsorbents and their application in chromatography</i>	1
1.1. Introduction	1
1.2. Properties of various forms of diamond and preparation of adsorbents	2
1.2.1. General properties of diamond	2
1.2.2. HPHT diamond	8
1.2.3. Detonation nanodiamond	9
1.2.3.1. Single digit nanodiamond	13
1.2.3.2. Microdispersed sintered detonation nanodiamond	13
1.2.4. CVD and related techniques	14
1.2.5. Composite adsorbents	14
1.3. Modification of diamond surface chemistry	17
1.4. Application of diamond materials in adsorption and chromatography	21
1.4.1. Gas adsorption chromatography	21
1.4.2. Liquid chromatography	28
1.4.2.1. Normal phase and hydrophilic interaction liquid chromatography (HILIC)	28
1.4.2.2. Reversed-phase and related mixed-mode HPLC	32
1.4.2.3. Ion-exchange chromatography	35
1.4.2.4. Electro modulated liquid chromatography	38
1.4.3. Microfluidic separations	38
1.4.4. Low pressure column liquid chromatography	39
1.4.5. High temperature liquid chromatography	41
1.5. Conclusions	43
1.6. Reference List	44
<i>Chapter 2. General experimental</i>	54
2.1. Instrumentation	54
2.2. Reagents	55
2.3. Methods	56
2.3.1. Preparation of HPHT diamond microparticles	56
2.3.2. Aqueous titration	57
2.3.3. Titration in water-organic mixtures	58
2.3.4. Column packing	58
2.4. Calculations	59

2.4.1. Sedimentation analysis of particle size distribution	59
2.4.2. Determination of void volume and phase ratio of HPHT diamond column	62
2.4.3. Van't Hoff plots	63
2.5. Reference List	63
<i>Chapter 3. Preparation and characterisation of synthetic diamond stationary phase for liquid chromatography and optimisation of column packing procedure</i>	65
3.1. Introduction	65
3.2. Experimental	67
3.2.1. Calcination of HPHT diamond	67
3.2.2. Determination of adsorption capacity of diamond	67
3.3. Results and discussion	67
3.3.1. Purification and characterisation of diamond packing material	67
3.3.1.1. Purification of HPHT diamond particles	67
3.3.1.2. Surface characterisation of purified HPHT diamond	70
3.3.1.3. Quantification of functional groups by means of acid base titration	72
3.3.2. Fabrication of HPHT diamond particles with improved shape and particle size distribution	74
3.3.2.1. Improvement of particle shape by means of thermal oxidation	76
3.3.2.2. Slurry solvent selection for particle sedimentation and column packing	81
3.3.2.3. Sedimentation	85
3.3.3. Development of column packing procedure for HPHT diamond	88
3.3.3.1. Influence of packing conditions on the performance of the column	88
3.3.3.2. Influence of post-packing conditioning on the performance of the column	90
3.3.3.3. Comparison of HPHT diamond column performance with other carbonaceous phases in HPLC	94
3.3.3.4. Comparison of HPHT diamond column hydrodynamic characteristics with other carbonaceous phases in HPLC	98
3.3.3.5. Packing repeatability	100
3.4. Conclusions	102
3.5. Reference List	103
<i>Chapter 4. Chromatographic performance of synthetic polycrystalline diamond as a stationary phase in normal phase high performance liquid chromatography</i>	106
4.1. Introduction	106
4.2. Experimental	106

4.2.1. Instrumentation	106
4.2.2. Column conditioning in NP-HPLC	107
4.3. Results and discussion	107
4.3.1. Characterisation of the prepared HPHT diamond fraction	107
4.3.2. Retention mechanism and separation selectivity	108
4.3.3. Influence of column conditioning on the retention in NP-HPLC	115
4.3.4. Comparison with other carbonaceous adsorbents	117
4.3.4.1. Comparison with MSDN	117
4.3.4.2. The effect of alkyl chain length on retention of alkylbenzenes and alkyl phenyl ketones	120
4.3.5. Chromatographic performance	123
4.3.5.1. HPHT diamond column loading capacity	123
4.3.5.2. Separations with HPHT diamond column	123
4.4. Conclusions	128
4.5. Reference List	128
<i>Chapter 5. Chromatographic behaviour of synthetic high pressure high temperature diamond in hydrophilic interaction liquid chromatography</i>	131
5.1. Introduction	131
5.2. Experimental	132
5.3. Results and discussion	132
5.3.1. Characterisation of the prepared HPHT diamond column	132
5.3.2. Behaviour of HPHT diamond in acetonitrile based mobile phases	134
5.3.2.1. Influence of pH and type of buffer	138
5.3.2.2. Operation under alkaline conditions	141
5.3.2.3. Selectivity of retention in water – ACN mixtures	143
5.3.3. Performance of HPHT diamond in methanol based mobile phases	144
5.3.4. Selectivity of HPHT in ACN and MeOH based mobile phases	147
5.3.5. Thermodynamics of retention on HPHT diamond in ANP chromatography	152
5.4. Conclusions	154
5.5. Reference List	154
<i>Chapter 6. Ion-exchange properties of microdispersed sintered detonation nanodiamond</i>	157
6.1. Introduction and literature review	157
6.2. Experimental	160
6.2.1. Experiments with transition metals	160

6.2.2. Experiments with anions	161
6.2.3. Adsorption isotherms	161
6.3. Results and discussion	162
6.3.1. Characterisation of MSDN	162
6.3.1.1. Scanning electron microscopy	162
6.3.1.2. Surface characterisation	162
6.3.2. Investigation of adsorption of metals	164
6.3.2.1. pH dependence	164
6.3.2.2. Kinetics of adsorption	167
6.3.2.3. Buffer dependence	168
6.3.2.4. Isotherms of adsorption	168
6.3.3. Investigation of anion adsorption	174
6.4. Conclusions	178
6.5. Reference List	180
<i>Chapter 7. General conclusions and future work</i>	184
7.1. Conclusions	184
7.2. Future work	188
7.3. Reference List	189
<i>Chapter 8. Supplementary information</i>	190



# Chapter 1. Literature review: Diamond based adsorbents and their application in chromatography.

## 1.1. Introduction

Current trends in chromatography are based upon a growing need for an increase in column performance, in terms of both resolution and efficiency, whilst simultaneously reducing analysis times. One route to improved chromatographic performance is to operate at the higher regions of both temperature and pressure. However, this route demands additional requirements for the stationary phases, namely greater mechanical strength, better thermal stability and enhanced chemical resistance to the solvents. Traditional stationary phases, including silica or alumina, do not satisfy these emerging requirements, and as such cannot be used under these severe conditions. Silica and alumina based sorbents cannot be used at higher temperatures due to limited hydrolytic stability, particularly outside of a rather narrow operational pH range (~pH 2–8). In addition, often it is very difficult to eliminate all residual polar hydroxyl groups from these materials during or following the attachment of non-polar ligands to the surface of the substrate. Such bonded phases are often themselves brittle and unstable, especially once again at conditions of high pressure and temperature. For these reasons, the search for new materials with improved chromatographic performance under a wider variety of conditions is an important task, which requires on-going attention [1].

Diamond, in various forms, has recently become easily accessible, and at relatively low costs, following a series of developments in the technologies available for diamond production [2-6]. Such developments, which have taken place sporadically over the last 40–50 years, include advances in high pressure, high temperature synthesis (HPHT), chemical vapour deposition (CVD), and detonation synthesis (DND). Diamond combines mechanical, thermal and chemical and hydrolytic stability with excellent thermal conductivity and negligible thermal expansion, absence of shrinking or swelling in the presence of inorganic or organic solvents. The surface of diamond can be relatively easily modified in order to produce either hydrophilic or hydrophobic properties. Together, all of these advantages make diamond a very promising material for use as a potential stationary phase for various types of chromatography, particularly those operational under so-called ‘harsh’ separation conditions, such as high temperature and ultra-high pressure modes of liquid chromatography [1,7].

With the development of new diamond manufacturing technologies, as well as those for related carbon-based materials, interest in their application within chromatography has

obviously grown, and this is reflected in the steadily growing number of publications in this area [8,9]. The growth in publications is certainly likely to continue, as commercial manufacturing of diamond composed HPLC columns has now become a reality [10,11].

This review is therefore focused upon recent progress in the chromatographic application of diamond-based materials. The review begins by covering the main physical and chemical properties of various diamond containing materials. Considerable emphasis will be placed upon the properties of diamond, which are important for chromatographic purposes, including particle size distribution and shape, porous structure, types and concentration of functional groups at the surface and stability/reactivity of particles. Properties of diamond may vary significantly with the type of production and nature of purification methods, so surface modification has become common practice to attune the diamond surface for subsequent applications. Therefore, the most common ways of diamond surface modification and functionalisation, as relevant to preparation of diamond based stationary phases, including composite materials, will also be covered within. Finally, the application of diamond-based adsorbents in different modes of chromatography will be critically reviewed, and the future opportunities and directions considered.

## **1.2. Properties of various forms of diamond and preparation of adsorbents**

### **1.2.1. General properties of diamond**

Diamond is a transparent crystalline substance, colourless or pale yellow (diamonds of other colours are also known), consisting of pure  $sp^3$ -carbon in a face-centred cubic lattice. Diamond possesses an outstanding hardness of 10 on the Mohs scale, a density of  $3.5 \text{ g}\cdot\text{cm}^{-3}$ , excellent thermal conductivity of  $800\text{--}2300 \text{ W}\cdot\text{m}^{-1}\text{K}^{-1}$ , negligible thermal expansion with a linear thermal expansion coefficient of  $8 \times 10^{-7} \text{ K}^{-1}$ , and Young's modulus of 1050 GPa [1]. Undoped diamond is an excellent insulator with electrical resistivity in the order of  $10^{20} \text{ }\Omega\cdot\text{cm}$  at  $20 \text{ }^\circ\text{C}$ . However, doping with boron can result in a substantial decrease in electrical resistivity between 5 and 100  $\text{m}\Omega\cdot\text{cm}$ . Typical boron dopant concentrations in diamond are between 500 and 10 000 ppm or  $10^{19}\text{--}10^{21} \text{ atoms}\cdot\text{cm}^{-3}$  [2,12]. Facet dependence of certain properties, including electrical properties is also reported for diamond nanocrystals [13]. Diamond is a chemically inert material, stable until  $1000 \text{ }^\circ\text{C}$  under vacuum and until  $400 \text{ }^\circ\text{C}$  in the air [14].

Natural diamond has obviously been a valuable resource for man for three millennia. Attempts to produce synthetic diamond were first undertaken towards the end of nineteenth century, although the first reproducible methods only emerged in the 1950s. Unsurprisingly,

since that time the number of publications in this area has increased dramatically [2]. Unfortunately, natural diamond is a low abundant precious mineral of very high value. Thus, the use of natural diamond in chromatography is obviously rather impractical. However, the demonstration of natural diamond particles as a chromatographic sorbent has indeed been reported [15].

Currently, between 8 and 10 methods for the synthesis of diamond have been developed, of which a number have practical value for the preparation of diamond and diamond composite based chromatographic stationary phases. These include (a) high pressure high temperature (HPHT) diamond synthesis, (b) detonation synthesis producing single digit detonation nanodiamond (SDND), and subsequent aggregates, including microdispersed sintered detonation nanodiamond (MSDN), and (c) diamond obtained by chemical vapour deposition (CVD) or by microwave plasma assisted CVD (MPCVD). Table 1.1 summarises the main methods of synthesis of diamond used for the preparation of chromatographic adsorbents and their properties, whilst Fig. 1.1 shows SEM images of a number of basic forms of diamond, prepared using the above synthetic technologies, suitable for the preparation of chromatographic stationary phases.

In practical terms, only HPHT technology is currently used for the preparation of diamond particles of diameters greater than a few microns, which is appropriate for direct use as column packing, whilst CVD based processes are more suited to the preparation of nanofilms and nanodiamond coatings. HPHT synthetic diamond, which can be produced at the centimetre scale, has the closest characteristics to natural diamond, related to the fact that HPHT synthesis induces direct phase transitions from graphite to diamond, similar to the natural process. Mechanisms for other, less popular methods of diamond manufacturing such as laser assisted [34], electrochemical [35] or hydrothermal synthesis from silicon carbide [36] may vary, but normally involve the assembling of diamond crystallites from carbon atoms, ions or multi-atom fragments from the gas or liquid phase. Technically, such processes are possible at much lower temperatures and pressures, and tend to lead to smaller particle formation (3–200 nm).

Table 1.1. Types and characteristics of diamond containing materials used in chromatography.

Substrate	Comments	$d_p, \mu\text{m}$	$S, \text{m}^2\cdot\text{g}^{-1}$	$D_p, \text{nm}$	Separation mode	Refs.
Natural diamond	Properties vary on origin, impurities content may be very high and inconsistent	10	$\sim 1.71/d_p$	nonporous	RP-HPLC	[15]
HPHT diamond crystalline particles	Contaminated by metal catalysts (Co, Ni and others), lattice defects and morphology depend on synthesis, surface free of functionalities	1-6	$\sim 1.71/d_p$	nonporous	NP- and RP-HPLC, mixer for post column reactions	[16-18]
Polymer embedded HPHT diamond particles	Polymer layer provides different adsorption properties, and makes adsorbent less mechanically and thermally stable	1-2	$\sim 1.71/d_p$	nonporous	RP HPLC	[16]
Polycrystalline aggregates formed by 5-30 nm NDs	Both DND and HPHT nanoparticles can form stable aggregates, high backpressure in columns	< 0.15	160-220	no data	GC	[19]
Solid support (CaF <sub>2</sub> , SiO <sub>2</sub> , Al <sub>2</sub> O <sub>3</sub> , PTFE, etc) mixed with NDs or coated	1 – 20 w/w % of DNDs in adsorbents, bare, hydrogenated and chlorinated DNDs are studied	200-630	-	-	GC	[20-22]
MSDN	Sintered DND nanoparticles with developed porous structure; surface contains residual $sp^2$ carbon, various functional groups and elemental impurities	2-5	153-216	1.2-7.5	IC, NP- and RP HPLC, HILIC, high-temperature chromatography	[23-26]
Macroporous polysaccharide particles, pores filled with DND hydrosols	Adsorbents contains 8.2-12.0 mg·mL <sup>-1</sup> of specially treated DND aggregates of 3-250 nm size	60-200	no data	no data	Low-pressure affinity chromatography	[27,28]
Core-shell composites with DND/polymer layers	Spherical glassy carbon or amorphous carbon microparticles LbL coated with PEI and DNDs; amino groups from PEI layer may be additionally modified with alkyl- and hydroxyl- groups	3.3-4.0 <sup>a</sup>	15-45 <sup>a</sup> ,	28-70 <sup>a</sup> ,	RP-HPLC, HILIC, mixed mode chromatography	[29,30]
	Diamond microparticles LbL coated with PEI and 10-50 nm particles of HPHT diamonds	1.7	19.4-30.3	20.4	NP- and RP-HPLC	[31]
Microspherical particles of aggregated NDs coated with diamond layer	Spray dried formation of DND/PEG or HPHT/PEG particles followed by oxidation, MPCVD diamond coating, oxidation and hydrogen plasma treatment	3.5-9.0	295-333	8.1-10.2	RP-HPLC	[32]
MPCVD diamond	Smooth surface independent on the film thickness used for coating of diamond aggregates; crushed grains of boron doped diamond	8-12	1.0	-	electromodulated chromatography, preparation of adsorbents	[32,33]

<sup>a</sup> Shell thickness 0.2–0.25  $\mu\text{m}$ .

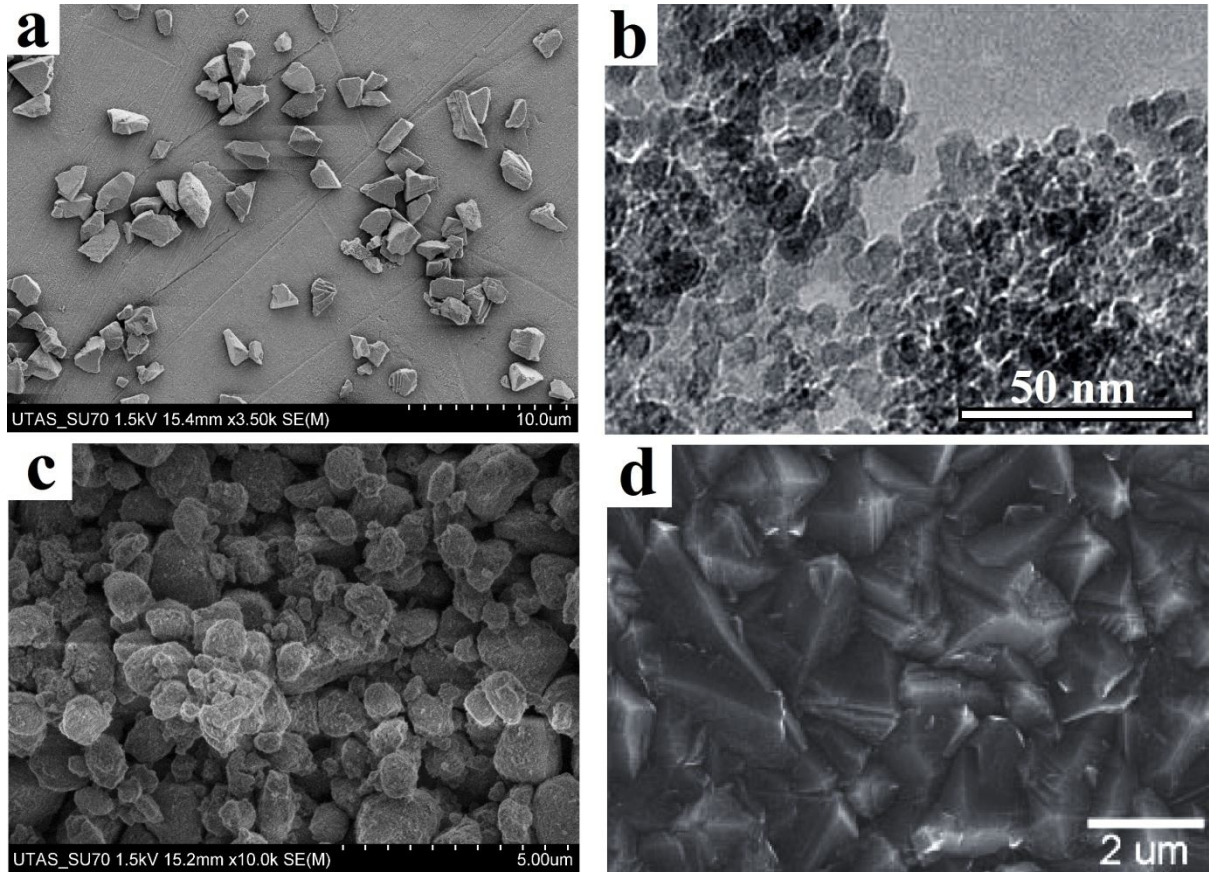


Fig. 1.1. SEM/TEM images of various forms of synthetic diamond, including (a) HPHT diamond, (b) SDND, (c) MSDN and (d) CVD diamond.

The properties of diamond, especially of nanodiamond, depend on size, shape, crystal structure and surface chemistry of particles [37,38]. Cubic, 3C is the most abundant and stable crystalline form of diamond, which usually occurs in nature and is produced by HPHT synthesis. Hexagonal, 2H diamond, also known as lonsdaleite, was discovered in 1967 in meteorite residues, and lately found in DND and CVD diamond. More rare diamond polytypes were also recorded in CVD diamond. Obviously, electronic properties, surface tension, and, more significantly, adsorption properties of diamond are related to planar atom density at the surface of diamond and number of dangling (missing bonds with neighbour atoms or broken atom bonds) bonds for carbon atoms [39]. For the characteristic planes in a *face-centered cubic* (fcc) lattice of diamond crystal structure the planar density decreases in the following order  $4/a^2$  (111)  $>$   $2\sqrt{2}/a^2$  (110)  $>$   $2/a^2$  (100), where  $a$  is the lattice constant. Each surface carbon atom has one dangling bond in the hexagonal (111) and square (110) array of atoms and two dangling bonds in case of square arrays of atoms (100). The difference in the surface properties could be significant for the different planes. For example, theoretical calculations show a possibility of the formation of different charge-transfer complexes between graphene and diamond (111) surfaces and no charge transfer is detected between graphene and diamond (100) surfaces [40].

The polarity of the diamond surface is important for understanding its application as a stationary phase for HPLC, which can be estimated by measuring contact angles ( $\theta$ , degrees) formed for a drop of water on a polished surface. The surface is considered hydrophobic if  $\theta > 90^\circ$ . Data on the wettability of the surface with water for various carbon materials is presented in Table 1.2. Normally, diamond is less hydrophobic ( $\theta = 36\text{--}72^\circ$ ) than graphite and glassy carbon, however oxidation and hydrogenation can change the polarity of the surface. Accordingly, CVD diamond film oxidised in air has a contact angle of  $\theta_{\text{O}} = 32^\circ$ , but hydrogenation of the surface increases this value significantly, to  $\theta_{\text{H}} = 93^\circ$  [41]. Obviously, the polarity of DND and MSND, having many polar functional groups at their surfaces following oxidative purification, is much higher than for CVD or HPHT diamonds. Importantly, the hydrophobicity of diamond materials depends on their nanostructure and on the  $sp^3/sp^2$  ratio of carbon at their surfaces. For comparison, the most popular HPLC adsorbent, octadecylsilica (ODS), exhibits contact angles of  $106\text{--}113^\circ$  [42]. Usually, polar adsorbents are better suited to normal-phase mechanism and HILIC separation modes, and non-polar or hydrophobic adsorbents are more applicable in reversed-phase mode of HPLC.

Table 1.2. Wettability of carbon materials with water as contact angles ( $\theta$ , degrees) [33,42].

Type of material	$\theta_{NO}$	$\theta_H$	$\theta_O$
Single crystal natural diamond, plane (111)	36 - 72	$93 \pm 4$	$32 \pm 2$
Smooth polished surface of polycrystalline diamond	$40 \pm 2$	$93 \pm 2$	$32 \pm 2$
Nanocrystalline diamond films	$40 \pm 3$	$70 \pm 2$	$3 \pm 2$
Nanoporous diamond		$124 \pm 3$	
Graphite	78-86		
Glassy carbon	76		
Octadecyl silica	106-113		

Note: NO – naturally oxidised or as prepared, H – hydrogenated, O – oxidised.

### 1.2.2. HPHT diamond

Among all the methods for diamond production, high pressure high temperature synthesis (HPHT) is by far the most common. Properties of ND produced by HPHT are dependent upon precise conditions of the synthetic process [6]. Commonly HPHT techniques are unable to produce very fine particles, typically producing diamond and diamond aggregates of 200 nm and upwards. Control over the particle size distribution using HPHT technology is also a significant challenge.

Particles produced from HPHT processes generally have greater homogeneity and a uniform surface chemistry, as compared to other techniques. Additionally, lattice defects are less common. However, it has been reported that the nature of the carbon precursor can influence the structure of the resultant diamond material. For example, using amorphous carbon and C<sub>60</sub> can provide uniform and homogeneous ND particles, whilst using graphitic carbon can lead to a mixed texture ND [43].

The actual mechanism of diamond phase formation is also different for different precursor substrates. Diamond forms due to a diffusion process and two-step martensitic process from graphite, whereas it forms only by the diffusion process without graphitisation or formation of intermediate phases from non-graphitic carbon [43]. Physical conditions of synthesis also have a significant effect on the structure of resultant particles. Increasing pressure makes the formation of the diamond phase thermodynamically favourable, whilst increasing temperature provides faster kinetics between graphite and diamond phases [2]. In practice, it is necessary to find an appropriate balance between thermodynamic and kinetic processes to achieve slow particle growth, providing high particle crystallinity and low levels of lattice defects. The size and shape in HPHT synthesis is much less controllable, particularly compared to other methods of ND synthesis.

The above processes result in diamond materials with relatively hydrophobic and passivated surfaces, which potentially makes them suitable as stationary phase substrates for RP-HPLC or GC separations (see Table 1.1). On the other hand, passive surfaces make functionalisation and modification of particles produced by HPHT more complicated, particularly compared to other method of production, such as detonation synthesis. The surface of HPHT diamond is terminated with hydrogen or carbon, although nitrogen impurities in HPHT diamond are quite common [44]. It has been estimated that approximately 50 ppm of surface carbon atoms are connected to ionisable functional groups. These surface functionalities can have positive or negative charges (but these values are considerably lower than the equivalents for DND), with a zeta-potential ( $\zeta$ ) of zero at pH 6.6 reported by



Hongthani and Fermin [45]. At pH above 8, ND particles produced using HPHT have been reported as exhibiting a  $\zeta = -40$  mV, while under acid conditions,  $\zeta = +40$  mV was observed [45]. At high pH  $\zeta$  can be modified by chemical oxidation of the surface, as approximately 0.1% of the carbon atoms at the ND surface are associated with redox active  $sp^2$  surface states.

Usually industrial HPHT diamond powders contain admixtures of dispersing or flowing agent at the surface such as silicates, fatty acids or surfactants, so cleaning of the surface is recommended by heating and alkali washing.

### 1.2.3. Detonation nanodiamond

Detonation nanodiamond (DND) is produced in a dynamic synthetic environment, based upon a controlled explosive blast, using high-grade explosives such as TNT, hexogen or mixtures thereof, under oxygen-deficient conditions [5,46,47]. The resultant reaction soot contains amorphous graphite and up to 2–10% of DND, which has to be isolated using gas phase or wet oxidation of the graphite. The DND must also be purified from various elemental impurities by washing with mineral acids [48,49].

Despite the yield of 2–10%, detonation synthesis of nanodiamond can generate relatively large amounts of material, which cannot be achieved by other synthetic methods with proportionally higher yields (such as CVD). DND is produced by detonation of explosive precursors within an enclosed blast chamber, and the amount of precursor can be tens of kilograms [48]. Thus, manufacturing of up to 10 tons of DND per year is possible using a single chamber. A further potential advantage of DND arises from the non-equilibrium conditions of synthesis, which results in a heterogeneous particle surface and a polyfunctional surface. This provides greater opportunity for particle modification, widening the potential application scope of the material, including preparation of chromatographic adsorbent.

Nanodiamond particles produced during detonation synthesis consist of a diamond core coated with a carbon shell containing various amorphous or  $sp^2$  carbon inclusions and metal impurities. Oxidation of non-diamond carbon phase and removal of the impurities results in smooth surface of nanoparticles containing monolayer of graphene-like sheets and various functional groups at the surface.

Table 1.3 includes the elemental composition of DND according to Mitev and Kulakova [4,49-51], with compositional data for minor impurities shown graphically within Fig. 1.2. The characterisation of DND has revealed a very specific set of common impurities. Apart

from amorphous  $sp^2$ -carbon content, non-carbon impurities are typically present within DND particles at significant concentrations. These include chemically bonded and adsorbed oxygen, nitrogen and hydrogen, as well as metal oxides, carbides and sulfates [49]. Such impurities can be situated mainly on the surface of DND particles and some of them (N, Si, P) may be locked within the crystal structure. In the latter instance, their removal can represent a significant challenge.

Numerous studies have been conducted regarding the surface properties of DND and how they can be influenced by post-production purification procedures. These data have been summarised in recent publications [4,52,53]. Wet oxidation with concentrated mineral acids ( $\text{HClO}_4$ ,  $\text{HNO}_3$ ,  $\text{H}_2\text{SO}_4$ ,  $\text{HF}$ , etc.), various oxidising agents ( $\text{CrO}_3$ ,  $\text{H}_2\text{O}_2$ , etc.) is the most common approach applied for surface treatment, which, as mentioned above, effectively removes non-diamond carbon and metal impurities. Different functional groups can be also formed during such purification, including carbonyls, carboxyls, hydroxyls, lactones, anhydrides, and others connected with both  $sp^3$  and residual  $sp^2$  carbon as shown in Fig. 1.3. This process provides a more hydrophilic surface with a more negative  $\zeta$ -potential (see Fig. 1.3). Similar results have been achieved by purification of DND through heating under an air/ $\text{O}_2$ / $\text{O}_3$  atmosphere, though metal oxides and non-volatile impurities cannot be removed in this process. Heating of DND in an inert atmosphere (Ar or vacuum) results in DND sintering and desorption of functional groups, leading to a more homogeneous surface. This route may be more beneficial for potential GC applications. Heating under a  $\text{H}_2$  atmosphere, as well as the reduction of DND in liquid phase using  $\text{LiAlH}_4$  can be also applied. This type of purification provides a hydrophobic hydrogen terminated surface, which can provide a potential substrate for application in RP-HPLC.

As should be noted, despite a wide range of purification methods, it is evident that any purification procedure results in unique surface properties for DND [54,55]. However, when referring to chromatographic applications of DND, it is crucially important to have reproducible technology for production of diamond materials with consistent surface properties. Currently, the development of a standard approach to the normalisation of DND from different origins is necessary before the full advantage of DND based stationary phases can be further realised. The typical procedure includes oxidation of DND in air at 420–450 °C followed by hydrogenation in atmosphere of  $\text{H}_2$  at 800 °C and, sometimes, photochemical or gas-phase chlorination [56,57].

Table 1.3. Chemical composition of DND [4,49-51].

Element content of DND particles wt%	Chemical forms	Comments
C, 85-92%	$C_{\text{diam}}$ – 98.0-98.8% $C_{\text{nondiam}}$ – 0.8-1.1%	$sp^2$ -Carbon is difficult to remove completely
O (5-10%), H (0.1-1%), N (2-3%)	Adsorbed gases, chemisorbed water, functional groups	Up to 20-25 various functional groups, difficulties in preparation of chemically homogeneous surface
Metals (0.2-5.5)	Metal oxides, carbides sulphates, silicates, etc.)	Level of metal impurities can be reduced by using strong inorganic acids and complexing reagents

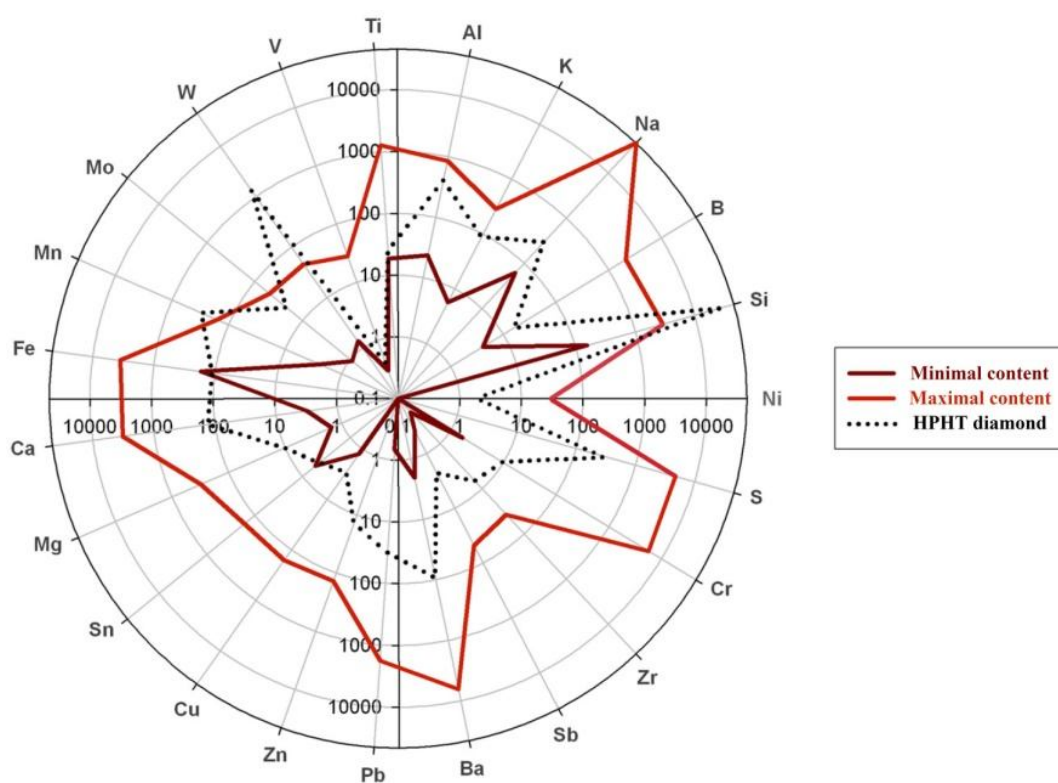


Fig. 1.2. Profiles of maximum and minimum content of 23 elemental impurities in DND and comparison with profile of impurities in a sample of HPHT diamond [51].

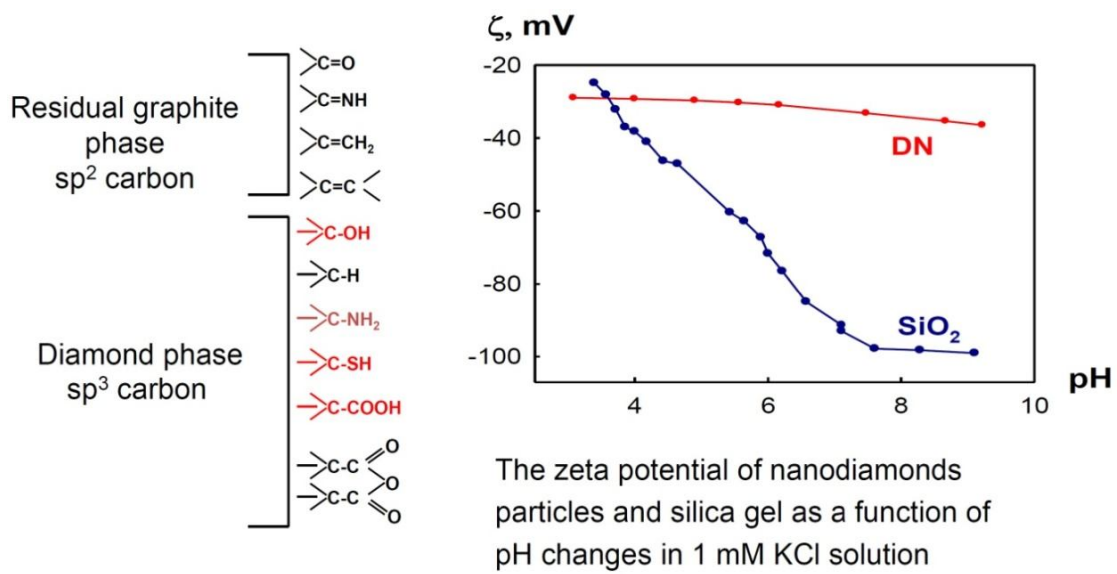


Fig. 1.3. Functional groups on the surface of DND and its  $\zeta$ -potential dependence on pH (as compared to SiO<sub>2</sub>) [26].

The presence of various polar functional groups at the surface of DND is responsible for the adsorption of ions and accumulation of impurities from solvents. Also, polar groups provide hygroscopic properties to dried powders of DND [58].

#### **1.2.3.1. Single digit nanodiamond**

Many publications refer to the application of single digit nanodiamond (SDND), such that this sub-classification of DND is worthy of specific consideration herein. As the name suggests, SDND is material with a very narrow particle size distribution, typically between 3 and 6 nm, with average particle size of 5 nm [59]. Stable suspensions of SDND are both difficult to achieve (given a strong tendency to spontaneous aggregation) and stabilise.

Similar to all other nanomaterials, the size of SDND has a great influence on the chemical and physical properties of material. Such properties, including reactivity, suspension stability, surface composition and  $\zeta$ -potential, may vary significantly with particle size [38]. Hence, disaggregation of DND into stable SDND suspensions represents an important step on the route to their utilisation for production of efficient stationary phases, particularly where diamond nanoparticle monolayer type structures are of interest.

Disaggregation of DND aggregates can involve both mechanical (ball milling) and chemical treatments to achieve more or less stable suspensions of SDND, often requiring the ultrasonication in concentrated NaCl solutions [60]. It should be noted that the preparation of SDND suspensions is always connected with extra contamination of the surface by metals, for example, zirconium from milling balls or metals impurities from NaCl [51].

#### **1.2.3.2. Microdispersed sintered detonation nanodiamond**

Similar to obtaining stable SDND suspensions, creating stable forms of larger DND agglomerates is equally challenging. Since the use of adsorbents with particles of diameter less than 1  $\mu\text{m}$  in chromatography limited by high backpressure, the production of stable DND agglomerates with appropriate mechanical properties and size (e.g. 1–10  $\mu\text{m}$ ) is required. To achieve this, sintering of DND at high temperatures (1500  $^{\circ}\text{C}$ ) and pressures (8 GPa) is considered the easiest and most effective solution [14]. Sintering of DND leads to the formation of mechanically stable particles up to 50  $\mu\text{m}$  in size and a well-developed porous structure. Micron size sintered nanodiamond particles (MSND) preserve a high surface area (130–200  $\text{m}^2/\text{g}$ ), bimodal distribution of pores on size with maxima at 1.5 nm and 3.0 nm and heterogeneous surface functionality as shown in Fig. 1.3. MSND is particularly beneficial for application in different modes of liquid chromatography [23,24,26,61,62].

#### 1.2.4. CVD and related techniques

The chemical vapour deposition (CVD) method of growing diamond from the gas phase using hydrocarbons as a source of carbon has been known since the late 1980s [63]. CVD or the more common microwave plasma assisted CVD (MPCVD) diamond growth process does not require high pressure, so it can be easily used in research laboratories.

With CVD, incorporation of non-carbon impurities into the diamond lattice and on the surface is unlikely and much less common than in the case of detonation synthesis [2,6]. Therefore the preparation of very pure diamond is possible. The CVD preparation of diamond precisely doped with other elements (boron, nitrogen, phosphorus, etc.) is also possible in order to modify the physico-chemical properties of diamond. For example, electrical conductivity of boron doped diamond is substantially higher than of pure diamond [12]. Importantly, CVD methods provide the production of diamond particles and films of controlled dimensions. Therefore, CVD process should be useful for the preparation of composite adsorbents [32] and for construction of microfluidic separation units [64].

Overall, the surface of CVD-formed diamond is relatively hydrophobic as it is normally terminated with hydrogen. The terminal hydrogen atoms are quite reactive, so the surface of this material can be additionally modified, e.g. with 1-octadecene, to increase its hydrophobic properties for potential use in RP-HPLC [32]. Also, there are some possibilities for production of diamond with different polytype crystal structures as described in Section 1.2.1.

#### 1.2.5. Composite adsorbents

Clearly, using the above technologies, diamond materials with a broad range of physico-chemical properties can be produced [65]. This diversity is further amplified when such materials are used to produce composite phases.

One of the major disadvantages of using diamond based materials in chromatography is the difficulty associated with the preparation of microspherical particles with sufficiently developed porous structures. Existing sintering technology applied to nanodiamond can be used for the preparation of porous micro-particles of irregular or oval shape, as shown in Fig. 1.1 (c). However, recently significant progress in the development of diamond composite stationary phases was reported by Linford *et al.* [29-31,66], who designed a new type of pellicular phase, consisting of a central core (diamond, glassy carbon or carbonised microporous PS-DVB microspheres), covered with multilayers of ND particles and poly(allylamine) (PAA) “glue” (see Fig. 1.4, top left). The layer-by-layer structure in these composite particles is cross-linked with 1,2,5,6-diepoxyoctane [31] or 1,2,7,8-

diepoxyoctane [29,30], and residual amino groups from PAA can be additionally modified with octylisocyanate [66], 1,2-epoxyoctadecane [29-31], octadecylisocyanate or 3,3,4,4,5,5,6,6,7,7,8,8,9,9,10,10-heptadecafluorodecyl isocyanate [66] to adjust the hydrophobicity of the resulting adsorbent. The geometrical structure of the prepared adsorbents includes a central core of diameter 2.8–4.0  $\mu\text{m}$ , and up to 25–30 bilayers formed by PAA of Mw 17,000 or 65,000, and NDs of size 4–400 nm. The average composite particle diameter  $d_{p,total}$  can be described by the following equation:

$$d_{p,total} = d_{p,core} + 0.0398 \cdot n \quad (\text{Equation 1.1})$$

where  $d_{p,core}$  is the diameter of the central core in microns and  $n$  is the number of bilayers [29]. The surface areas of these composites are between 15 and 45  $\text{m}^2 \cdot \text{g}^{-1}$ , with pore diameters of 30–70 nm, depending on the size of NDs forming the shell. The prepared phases are stable over the pH range 1–13, and can operate at temperatures up to 100  $^{\circ}\text{C}$ .

Obviously, in the case of the above composite materials, having both anion-exchange and hydrophobic functional groups, the stationary phase should be considered as a mixed-mode substrate. Three variants of this type of phase are now commercially available from Diamond Analytics (USA), under the trade names, FlareC18 Mixed-Mode, Flare C18+ and Flare HILIC. The latest Flare C18+ phase is similar to that described above, namely Flare C18 Mixed Mode phase, but with all amino groups quaternised to provide a permanent positive charge to the surface across the whole pH range.

The preparation and characterisation of a new composite micro-spherical porous particle (Fig. 1.4, right), produced solely from diamond materials, was recently described by Kondo *et al.* [32]. The authors applied spray-drying technology for the preparation of microspherical ND aggregates, using a suspension of 20, 30 or 50 nm nanoparticles of HPHT diamond in 1% aqueous polyethylene glycol (PEG). The PEG was subsequently removed by air oxidation at 300  $^{\circ}\text{C}$  for 1 h, and the prepared ND-agglomerated spherical particles were coated by an additional layer of diamond using microwave plasma assisted CVD (MPCVD), in order to improve mechanical properties. The composite particles were oxidised in air at 425  $^{\circ}\text{C}$  for 5 h to remove  $sp^2$ -carbon impurities, followed by treatment with hydrogen plasma to produce a reactive hydrogenated surface. Finally, octadecyl groups were grafted to the surface by reaction of the hydrogenated surface with 1-octadecene in an argon atmosphere.

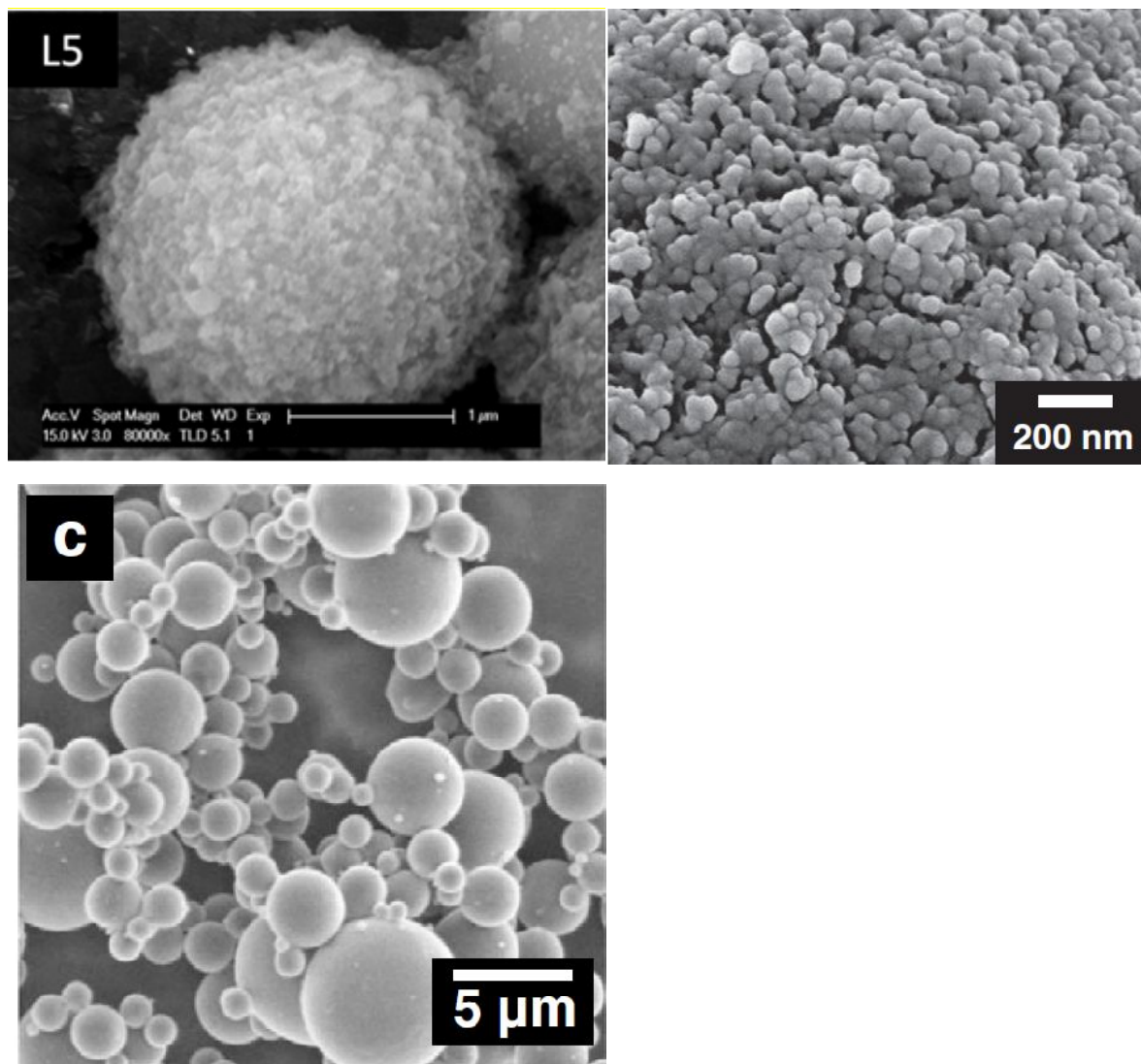


Fig. 1.4. SEM images of pellicular particles comprising glassy carbon central core and 5 bilayers of PAA and NDs of particle size 10–400 nm (top left), and of surface structure of microspherical porous particles fabricated from ND particles using spray drying and MPCVD coating for 10 min (top right and bottom left). [30,32].



The porous structure of the above composites depends on size of NDs used. The use of three fractions of ND particles, with sizes of  $24\pm 6$ ,  $35\pm 9$  and  $52\pm 12$  nm resulted in products having  $D_p$  of 4.6, 5.9 and 9.3 nm, respectively, and specific surface areas of 201, 152 and  $85\text{ m}^2\cdot\text{g}^{-1}$ . Clearly, such material only consists of HPHT and CVD diamond, and thus exhibits great potential for application under harsh separation conditions. Obviously, there is also potential for immobilisation of other functional groups on the surface of hydrogenated intermediate, to produce stationary phases for different HPLC modes. The only drawback of the reported process is a relatively broad particle size distribution, as shown in Fig. 1.4, (bottom left), so careful size fractionation of particles in the future is required before column packing.

### **1.3. Modification of diamond surface chemistry**

Diamond materials produced by different methods have different physical and chemical properties. Producers of diamond materials often use special additives (silicates, fatty acids, amines, etc.) in order to modify product properties for particular applications (prevent caking, improve suspendability, adjust mechanical properties). However, for the use in chromatography diamond based phases often require homogeneous surfaces. Hence, physical and chemical surface modification is an important and necessary step in preparation of diamond adsorbents. There are three main objectives from surface modification:

- The removal of undesirable additives from the surface
- The homogenisation of the diamond surface (to-date a standard approach is not available)
- The introduction of new selectivity to the diamond surface towards specific chromatographic applications.

Aside from the above, surface functionalisation of such diamond based materials provides an opportunity to control the stability of diamond suspensions in various solvents, improves interfacial adhesion of ND within composite matrices, and influences the electronic properties of ND crystallites [67]. Modification techniques applied to diamond particles can involve physical and chemical modification (or both), the latter of which may involve either covalent or non-covalent surface functionalisation (see Fig. 1.5). Physical modification does not typically aim to change the surface properties of diamond phases, but normally is used to modify the mechanical and structural properties of the material, such as particle aggregation, particle size distribution, sintering of nanodiamond, etc.

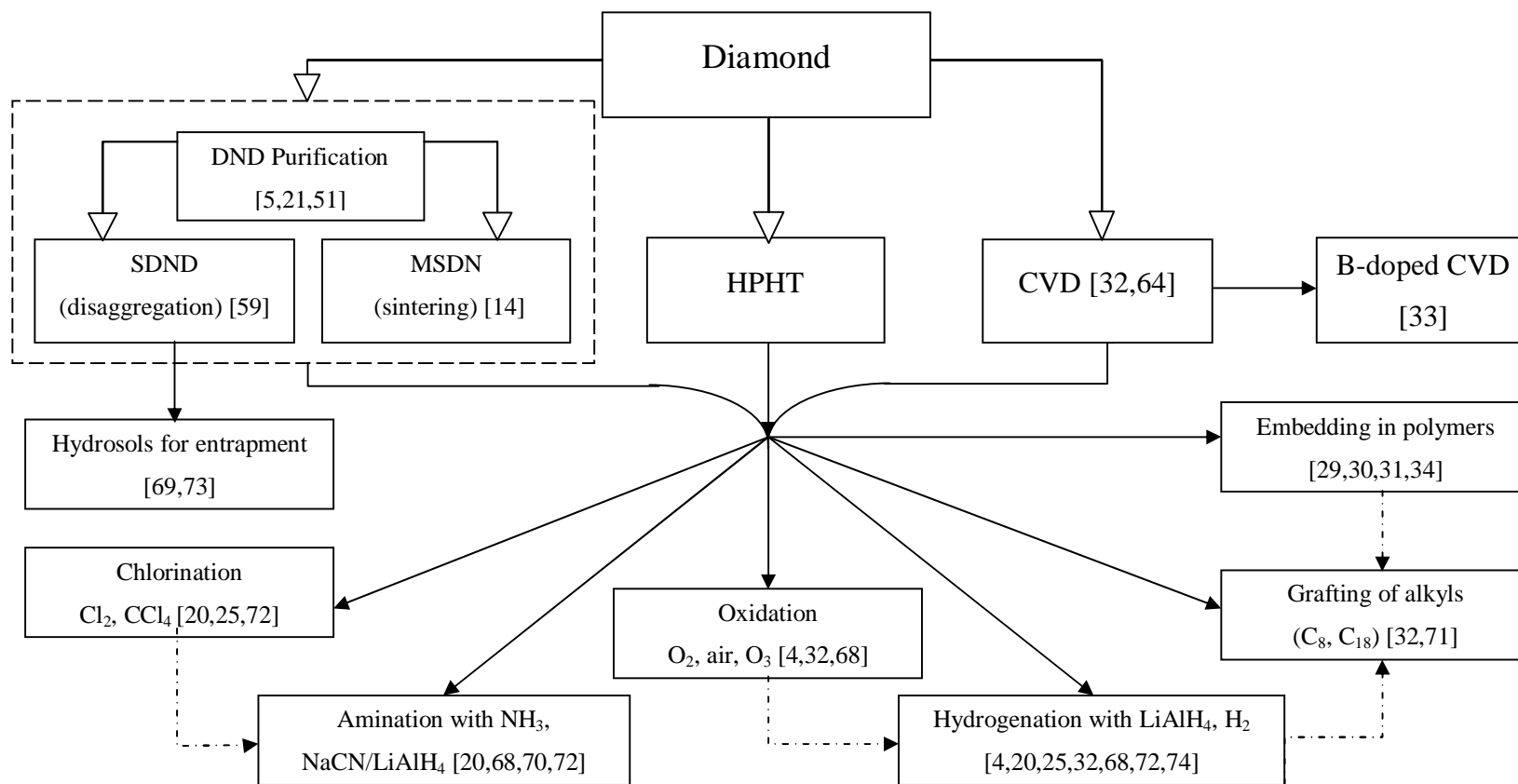


Fig. 1.5. Modification of diamond materials for use in chromatography and solid-phase extraction.

As mentioned previously, obtaining stable disaggregated ND suspensions is an important step prior to further modification, and narrow particle size distribution is required to improve column packing.

A simple and effective method for the disaggregation of DND agglomerates and reducing particle size is ultrasonication [75]. This not only allows a reduction in average particle size of DND aggregates, but also can change the surface chemistry and  $\zeta$ . This shift in  $\zeta$  is related to the appearance of new hydroxyl groups at the surfaces during ultrasonication of DND. The size distribution of ND agglomerates can be controlled by adjusting the ultrasound intensity. It has been demonstrated that ultrasonically treated particles can conserve suspension stability and particle size distribution for a period of up to 150 days [76].

In the case of increasing diamond agglomerate sizes, sintering within the thermodynamic boundaries of diamond stability can be done [14]. As mentioned previously, sintering can improve the morphology of agglomerates and lead to materials with high porosity and homogeneous surfaces.

In terms of chemical modification of diamond surfaces, the simplest route is liquid phase acid treatment [55,77]. Oxidative treatment with  $\text{HNO}_3$  or  $\text{HClO}_4$  can be used both for removal of on-diamond carbon and metal impurities and for creating additional oxygen containing functional groups (carbonyls, carboxyls, hydroxyls, etc.) [74]. Simultaneously the presence of non-diamond carbon and impurities of metal oxides can be reduced [51]. Oxidised diamond can be used in cation-exchange chromatography [26].

Heating of diamond in various controlled atmospheres, or within the presence of a plasma, is another efficient way for chemical modification of the diamond surface [78,79]. Oxidation of diamond in the air starts at 430–650 °C, depending on the type of diamond, and increases the concentration of carboxyl groups at the surface of diamond and its cation-exchange capacity. Alternatively, heating of diamond at 800–900 °C in the presence of  $\text{H}_2$  can be used for hydrophobisation and surface homogenation [71]. Chlorination at 400–600 °C has been shown to be effective in the introduction of C-Cl bonds onto diamond surfaces [56]. Somewhat similar results can also be achieved via plasma treatment. Both  $\text{H}_2$  and Ar plasmas have been applied to remove functionalities from ND surfaces and increase particle hydrophobicity [32], whilst treatment with  $\text{O}_2$  plasma resulted in more hydrophilic particles with higher content of carbonyl and carboxyl groups [80].

The non-covalent functionalisation of diamond surfaces can be achieved through adsorption of specific molecules. Adsorption modification has been frequently used to stabilise ND suspensions [81,82], or as a step for the preparation of ND composites [30,32].

For example, simple addition of surfactants, such as sodium oleate [83] or  $\text{AlCl}_3$  [81], can increase the absolute value of the ND surface  $\zeta$  and electrostatically stabilise ND suspensions in non-polar solvents and water, respectively [83].

The surface modification of diamond particles with inorganic material layers is a less common approach, but has been demonstrated with materials such as  $\text{SiO}_2$  or  $\text{SnO}_2$  [84]. In this case the diamond particle simply acts as a stable, inert and heat dissipating core, while the attached shell, with its different adsorption properties, could be used for the construction of the stationary phase for UHPLC as reported recently by Waters [10].

Covalent modification of the surface of diamond is a very significant topic, as this approach can bring a selectivity desired for specific chromatographic applications. Since diamond surfaces are normally covered by weakly acidic carboxylic groups, using various amines has become the most common way of attaching different moieties to the diamond surface. For example, long-chain aliphatic amines have been used for preparation of amide coatings with a reduced surface charge and enhanced hydrophobicity [31]. The use of poly(allylamine) coated NDs is reported for solid-phase extraction (SPE) and as intermediate for the preparation of various composite adsorbents functionalised with octadecyl-, octyl- and heptafluorodecyl- groups [30,66,85,86]. Another useful approach includes conversion of carboxyl groups at diamond surface into primary hydroxyls by reaction with  $\text{LiAlH}_4$  and subsequent treatment either with alkyl isocyanates, chloroanhydrides or other reactive substances to introduce a desired functional group [87].

Another useful approach to the covalent functionalisation of diamond surfaces involves radical reactions using benzoyl peroxide to attach carboxylic or alkyl groups [88]. This method is less common than using nitrogen containing substances; however, it can potentially lead to the formation of more stable bonds between diamond and the attached functional group, as compared to amide or diazo bonds.

The use of radical initiator di-*tert*-amyl peroxide for mono- and multi-layer coating of hydrogen terminated diamond particles of 70  $\mu\text{m}$  size is reported by Linford *et al.* [89]. The prepared adsorbent is used for SPE of pesticide cyanazine. Lately this research group used similar surface chemistry for diamond surface initiation and encapsulation of particles into poly(styrene-divinylbenzene) layer [90,91]. The prepared adsorbent and its sulfonated analogue are tested for SPE of 1-naphtylamine.

Overall, in practice, multistep modification is usually required for the preparation of diamond based adsorbents with desirable surface characteristics. Theoretically, presence of

reactive carboxyl-, hydroxyl and hydrogen groups allows attachment of all types of functional groups normally used in chromatographic stationary phases.

#### **1.4. Application of diamond materials in adsorption and chromatography**

Diamond adsorbents were first applied as column packings for GC and HPLC separations in 1965–1973 [15,19]. These early studies into applications within adsorption GC and RP-HPLC attracted only limited interest of the mainstream chromatographers, as diamond packed columns had serious practical limitations including high backpressure, poor separation efficiencies [19], limited loading capacities [15] and poorly characterised retention mechanism. A renewed interest emerged 30 years later, possibly following the development of new technologies for the preparation of nanodiamond adsorbents [1,92], improvements in chromatographic equipment and a better understanding of the properties and chemistry of ND in particular [5]. Importantly, ultra-high performance liquid chromatography (UHPLC) and high-temperature liquid chromatography (HTLC) also appeared at this time, and initiated an intensive search for new separation media having improved mechanical, chemical and thermal stability. To some degree, porous graphitic carbon (PGC) satisfied these requirements, and numerous applications of this type adsorbent in HPLC emerged [8,9]. An intriguing property of carbonaceous adsorbents including active carbon, graphitised carbon black, glassy carbon, etc. is their unique separation selectivity [9]. The complex surface chemistry of diamond, and DND in particular, provides unique selectivity, so multiple separation mechanisms can be realised with diamond based stationary phases, as detailed within Table 1.4.

##### **1.4.1. Gas adsorption chromatography**

Excellent thermal stability and intriguing selectivity of carbonaceous adsorbents produced an interest to diamond as a promising stationary phase for use in gas chromatography (GC). Indeed, the first use of “diamantiferous material” in GC relates back to 1965, when Allied Chemical Corporation applied for a patent on the preparation of, “synthetic diamond containing material, consisting of individual diamond particles with mean size less than 0.1  $\mu\text{m}$ , surface area 40–400 square meters per gram and having at least 10% of the surface area containing hydroxyl, carbonyl and carboxyl groups” [19]. The column used in this early work was 244  $\times$  0.64 cm I.D. and packed with 5–30 nm DND particles ( $S = 200 \text{ m}^2 \cdot \text{g}^{-1}$ ).

Table 1.4. Chromatographic applications of diamonds and diamond containing phases.

Stationary phase	Structure	Column size, L x ID	Eluent	Separated compounds	Ref.
<b>GC</b>					
DND aggregates	< 0.1 $\mu\text{m}$ , 40-400 $\text{m}^2\cdot\text{g}^{-1}$	244 cm x 6.4 mm	Helium	$\text{CF}_4$ , $\text{C}_2\text{F}_4$ , $\text{C}_2\text{H}_2\text{F}_2$ , $\text{CH}_2\text{F}_2$ ,	[19]
DND aggregates (10%) deposited on surface of $\text{CaF}_2$ carrier (90%)	<b>DND:</b> 10 nm, 200-260 $\text{m}^2\cdot\text{g}^{-1}$ , <b>Carrier:</b> 0.2-0.6 mm, < 1 $\text{m}^2\cdot\text{g}^{-1}$	549 cm x 3.2 mm	Helium, argon, 350-500°C	HF, HCl, $\text{ClF}_3$ , $\text{F}_2$	[22,93]
Various DND aggregates (10%) deposited on surface of Chromaton-N-AW DMCS carrier (90%)	<b>DND:</b> 10-12 nm, 246-300 $\text{m}^2\cdot\text{g}^{-1}$ , <b>Carrier:</b> 0.40-0.63 mm, < 1 $\text{m}^2\cdot\text{g}^{-1}$	250 x 3.0 mm	Nitrogen, 120-200°C	Alkanes, benzene, nitromethane, acetonitrile, acetone, methanol, ethanol, diethyl ether	[20,21,68,72,94]
<b>RP HPLC</b>					
Natural diamond particles	10 $\mu\text{m}$ , nonporous	250 x 3.0 mm	50% methanol – 50% water	benzene, anthracene	[15]
HPHT diamond particles	2 $\mu\text{m}$ , nonporous	290 mm x 75 $\mu\text{m}$	70% acetonitrile – 30% 10 mM $\text{NH}_4\text{Ac}$ , pH 3.5	Methyl-, ethyl-, propyl- and butyl-parabens	[16]
	1 $\mu\text{m}$ , nonporous	215 mm x 75 $\mu\text{m}$			
HPHT diamond particles with chemically grafted octyl groups	2 $\mu\text{m}$ , nonporous	200 mm x 75 $\mu\text{m}$	70% acetonitrile – 30% water	Methyl-, ethyl-, propyl- and butyl 4-hydroxybenzoates	[16]
Polybutadiene coated HPHT diamond particles	2 $\mu\text{m}$ , nonporous	188 mm x 75 $\mu\text{m}$	30% acetonitrile – 70% water	Methyl-, ethyl-, propyl- and butyl 4-hydroxybenzoates	[16]
	1 $\mu\text{m}$ , nonporous	160 mm x 75 $\mu\text{m}$			
MSND	3-6 $\mu\text{m}$ , 153-216 $\text{m}^2\cdot\text{g}^{-1}$ , 1.2-7.5 nm pores	100 x 4.6 mm, 150 x 4.0 mm, 100 x 4.0 mm	Methanol – water, acetonitrile - water	Phenols, benzoic acids, benzene derivatives, nucleic bases, nucleosides, alkylanilines	[7,23,24,95-97]
CVD diamond coated HPHT aggregated particles	3-5 $\mu\text{m}$ , 109 $\text{m}^2\cdot\text{g}^{-1}$ , 4.6-9.3 nm	150 x 2.0 mm	Acetonitrile - water	Alkylbenzenes, uracil, methyl benzoate, toluene, naphthalene	[32]
Core-shell composite with up to 25 nanodiamond/PAA bilayers treated with 1.2-epoxyoctadecane	2.8-4.0 $\mu\text{m}$ , 15–45 $\text{m}^2\cdot\text{g}^{-1}$ , 30-70 nm pores	50 x 4.6 mm; 50 x 2.1 mm	Acetonitrile - water	Alkylbenzenes, phenols, pesticides, essential oils, pharmaceuticals	[29-31]

Table 1.4 (continued). Chromatographic applications of diamonds and diamond containing phases.

<b>NP HPLC</b>					
MSND	3-6 $\mu\text{m}$ , 153-216 $\text{m}^2\cdot\text{g}^{-1}$ , 1.2-7.5 nm pores	150 x 4.0 mm	Isooctane, pentane, hexane-IPA	Alkylbenzenes, dialkylphthalates, derivatives of benzene	[7,25,61,96,98,99]
	4 $\mu\text{m}$ , 216 $\text{m}^2\cdot\text{g}^{-1}$ , 1.2-7.5 nm pores	100 x 4.6 mm	Heptane, pentane	Positional isomers of xylenes	[95-97]
Core-shell composite with 28 nanodiamond/PAA bilayers	1.7 $\mu\text{m}$ , 30 $\text{m}^2\cdot\text{g}^{-1}$ , 20.4 nm pores	30 x 4.6 mm	70% hexane –30% ethylacetate (each containing 0.2% triethylamine)	Benzophenone, nitrobenzene	[31]
<b>HILIC</b>					
MSND	4 $\mu\text{m}$ , 216 $\text{m}^2\cdot\text{g}^{-1}$ , 1.2-7.5 nm pores	100 x 4.6 mm	80% methanol – 20% water	Methyl- and ethylanilines	[95,97]
	3-6 $\mu\text{m}$ , 153-216 $\text{m}^2\cdot\text{g}^{-1}$ , 1.2-7.5 nm pores	150 x 4.0 mm, 100 x 4.0 mm	Methanol – water, acetonitrile - water	Phenols, benzoic acids, nucleic bases, nucleosides	[23,24,62]
<b>IC</b>					
MSND	3-6 $\mu\text{m}$ , 153-216 $\text{m}^2\cdot\text{g}^{-1}$ , 1.2-7.5 nm pores	150 x 4.0 mm	$\text{HNO}_3$ with 0.1-0.5 M $\text{KNO}_3$ $\text{HNO}_3$	Alkaline-earth and transition metals Alkali metals	[26] [100]
<b>Electromodulated chromatography</b>					
HPHT, covered with a layer of boron doped CVD diamond	8-12 $\mu\text{m}$ , 1 $\text{m}^2\cdot\text{g}^{-1}$ ,	78 x 3.0 mm	0.1M $\text{LiClO}_4$ , -1.2 to +1.2V	aromatic sulphonates	[33]
<b>Low pressure ion-exchange chromatography</b>					
Hydrosol of particles entrapped in polysaccharide matrix	<b>DND:</b> 4-250 nm; <b>Carrier:</b> Sepharose 2B	60 x 16 mm	Gradient 20 mM Tris-HCl, pH 7.0 - 100 mM TrisHCl, pH 8.8 with 50 mM EDTA and 10 mM dithiothreitol	luciferase, apoobelin	[27]

It was used for the GC separation of  $\text{CF}_4$ ,  $\text{C}_2\text{F}_4$ ,  $\text{C}_2\text{H}_2\text{F}_2$  and  $\text{CH}_2\text{F}_2$  using  $30 \text{ mL}\cdot\text{min}^{-1}$  of He as the carrier gas and a column temperature  $40 \text{ }^\circ\text{C}$ . This diamond material was shown to maintain its efficiency during heating up to  $350 \text{ }^\circ\text{C}$ . However, application of diamond, treated in a  $\text{H}_2$  atmosphere at  $800 \text{ }^\circ\text{C}$  was also demonstrated in this work [19].

Two years later, researchers from Allied Chemical Corporation patented the use of mixed-bed columns in GC, where the stationary phase comprised  $0.2\text{--}0.6 \text{ mm}$  particles of inert support ( $\text{CaF}_2$ , diatomaceous earth, firebrick, silica, alumina, PTFE, etc.) containing at least 1 wt% of above described ND type material [93]. The use of larger particles loaded with ND aggregates of diameter less than  $0.15 \text{ }\mu\text{m}$ , was in response to high backpressures seen for columns packed with ND aggregates only. A stationary phase comprising 80%  $\text{CaF}_2$  and 20% ND, with a surface area of  $160\text{--}200 \text{ m}^2\cdot\text{g}^{-1}$  was successfully applied for the separation of gases ( $\text{F}_2$ ,  $\text{Cl}_2$ , HF, carbon and nitrogen oxides, etc.), fluorinated alkanes and alkenes, hydrocarbons ( $\text{CF}_4$ ,  $\text{C}_2\text{F}_4$ ,  $\text{C}_2\text{H}_2\text{F}_2$ ,  $\text{CH}_2\text{F}_2$ ,  $\text{CHClF}_2$ ,  $\text{C}_3\text{F}_8$ ), various organic compounds (alkanes, alkenes, cycloalkenes, etc.), and inorganic compounds, such as  $\text{WF}_6$ ,  $\text{SF}_6$  and  $\text{ClF}_3$ . It should be noted that the contribution of  $\text{CaF}_2$  to the surface area was approximately  $0.15 \text{ m}^2\cdot\text{g}^{-1}$ , so the retention of the above species was almost entirely due to interaction with the incorporated ND aggregates.

Soon after, the excellent thermal stability and chemical resistance of diamond was once again confirmed by Hirshmann and Mariani [22], who separated  $\text{F}_2$ , HCl,  $\text{ClF}_3$  and HF using a  $548 \times 0.32 \text{ cm}$  I.D. nickel column packed with a mixed bed stationary phase containing 90%  $\text{CaF}_2$  particles ( $d_p = 0.2\text{--}0.6 \text{ mm}$ ) and 10% DND aggregates ( $d_p = 10 \text{ nm}$ ,  $S = 200\text{--}260 \text{ m}^2\cdot\text{g}^{-1}$ ). An example of the early separation achieved is shown in Fig. 1.6. No indications of reactions between these corrosive species and the stationary phase were reported.

GC was also used to investigate specific adsorption properties and retention mechanisms on diamond surfaces, providing data which can still be used in other areas of chromatographic separations [72]. This information includes specific and dispersive interactions between various molecules and the stationary phase, adsorption energy and selectivity. An intensive GC characterisation of the thermodynamic parameters of adsorption and retention mechanisms was accomplished by Belyakova *et al.* [20,21,68,72,94,101], which was obtained using a mixed bed type adsorbent containing various types of DND, that are listed within Table 1.5. PTFE columns, of dimensions  $25 \text{ cm}$  long and  $3 \text{ mm}$  I.D., and packed with diatomite matrix, Chromaton-N-AW-DMCS ( $d_p = 0.40\text{--}0.63 \text{ mm}$ ,  $S = 1 \text{ m}^2\cdot\text{g}^{-1}$ ), with various immobilised DND aggregates, were used with a nitrogen carrier gas.



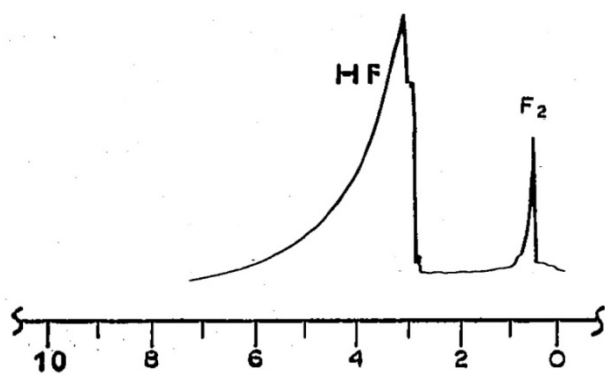


Fig. 1.6. GC separation of  $F_2$  and HF at room temperature on a 548x0.32 cm I.D. column, packed with stationary phase comprising 10% DND and 90%  $CaF_2$ , carrier gas –helium, 80  $mL \cdot min^{-1}$  [22].

The authors calculated and compared the differential enthalpy of adsorption ( $-\Delta H$ ) and the standard differential molar entropy of adsorption ( $\Delta S$ ) for the adsorbent listed, using a set of probes (four n-alkanes, benzene, acetonitrile, acetone, nitromethane, methanol, ethanol, diethyl ether and ethyl acetate). The corresponding data are shown in Table 1.6. According to authors, the adsorption properties of the initial DND-DP samples were similar to the properties of activated carbon [102,103], while modified samples behaved similarly to graphitised carbon black [104]. The impact of the methylene group upon adsorption enthalpy was estimated as  $20 \text{ kJ}\cdot\text{mol}^{-1}$ . This value is close to the value obtained for activated carbon, which may indicate the presence of amorphous carbon on the surface of the DND. Subsequent modifications of DND-DP led to the removal of the main portion of amorphous carbon from the surface and changed the adsorption properties. Surprisingly, all modifications caused a decrease of retention times for the majority of the compounds, as compared to the original DND-DP. Partly, this decrease in retention times can be attributed to a decrease in specific surface area for modified DNDs.

Despite the fact that trends within the above data are rather inconsistent, some conclusions on the properties of the modified DND surface can be made through comparison of the thermodynamic parameters for differently modified DNDs. Modification with  $\text{H}_2$  or  $\text{CCl}_4$  resulted in a more hydrophobic surface and higher enthalpy values for the adsorption of hydrocarbons and other nonpolar molecules. Modification with  $\text{Cl}_2$  provided surface passivation, with subsequent reduced adsorption enthalpies for all the classes of compounds. Ozone is a much stronger oxidising agent than the  $\text{K}_2\text{Cr}_2\text{O}_7/\text{H}_2\text{SO}_4$  mixture, so ozone treatment of DND resulted in hydrophilic charged surface having higher affinity to polar molecules such as alcohols, ketones and nitriles.

In a separate study, Vereshchagin *et al.* suggested the preparation of an adsorbent for GC by heating DND agglomerates in argon at  $1000 \text{ }^\circ\text{C}$  [105]. A chromatographic column of  $1000 \times 3 \text{ mm}$  I.D. was packed with  $100\text{--}160 \text{ }\mu\text{m}$  diameter particles with surface area of  $40\text{--}400 \text{ m}^2\cdot\text{g}^{-1}$ , and applied to the GC separation of common gases using helium as the carrier gas. The column was shown to be operational at temperatures up to  $500 \text{ }^\circ\text{C}$  without notable changes in adsorption properties. However, some caution should be applied, as the transformation of diamond into amorphous graphite is possible under heating of diamond in an inert atmosphere at such high temperatures [57,106].

Table 1.5. Properties of DND samples used for GC characterisation (see Table 1.6).  $K_D$  and  $K_A$  are electron-donor and electron acceptor characteristics, respectively [72,94].

Adsorbent	Preparation	$S, \text{m}^2\cdot\text{g}^{-1}$	$D_p, \text{nm}$	$K_D, \text{kJ}\cdot\text{mol}^{-1}$	$K_A, \text{kJ}\cdot\text{mol}^{-1}$
DND-DP	DND purified with overheated $\text{HNO}_3$	300	12		
DND-DP- $\text{H}_2$	$\text{H}_2$ , 850 °C, 1h	286	12	0.60-0.65	0.5-0.73
DND-DP- $\text{CCl}_4$	$\text{CCl}_4$ , 500 °C, 1h, Ar	246	-	0.20-0.28	0.25-0.4
DND-DP- $\text{Cl}_2$ - $\text{NH}_3$	$\text{Cl}_2$ , 600 °C, 1h; $\text{NH}_3$ , 400 °C, 1h	289	10	0.30-0.85	0.80-1.26
DND-DP-Cr	boiling $\text{K}_2\text{Cr}_2\text{O}_7/\text{H}_2\text{SO}_4$	258	-	0.40	1.4
DND-DP- $\text{Cl}_2$	$\text{Cl}_2$ , 450 °C, 1h	258	-	0.2-0.5	0.4-0.9
DND-E	oxidized with $\text{O}_3$	218	-	-	-

Table 1.6. Adsorption enthalpy ( $\Delta H, \text{kJ}\cdot\text{mol}^{-1}$ ) and entropy ( $\Delta S, \text{J}\cdot\text{mol}^{-1}\cdot\text{K}^{-1}$ ) for model compounds [20,21,68,72,94,101]. For description of types of DND see Table 1.4.

Analyte	DND-DP		DND-DP- $\text{H}_2$		DND-DP- $\text{CCl}_4$		DND-DP- $\text{Cl}_2$ - $\text{NH}_3$		DND-DP-Chr		DND-DP- $\text{Cl}_2$		DND-E	
	$\Delta H$	$\Delta S$	$\Delta H$	$\Delta S$	$\Delta H$	$\Delta S$	$\Delta H$	$\Delta S$	$\Delta H$	$\Delta S$	$\Delta H$	$\Delta S$	$\Delta H$	$\Delta S$
n- $\text{C}_6\text{H}_{14}$	-25	-26	-49	-71	-49	-81	-36	-40	-29	-59	0	0	-35	-79
n- $\text{C}_7\text{H}_{16}$	-46	-63	-60	-83	-56	-91	-	-	-31	-55	0	0	-43	-87
n- $\text{C}_8\text{H}_{18}$	-63	-90	-68	-89	-61	-94	-	-	-33	-54	0	0	-55	-106
n- $\text{C}_9\text{H}_{20}$	-90	-139	-78	-103	-70	-107	-	-	-36	-57	-	-	-60	-109
$\text{C}_6\text{H}_6$	-38	-45	-58	-82	-45	-66	-	-	-35	-62	-	-	-42	-79
$\text{CH}_3\text{CN}$	-43	-75	-35	-36	-35	-39	-41	-50	-17	-19	-24	-50	-33	-61
$(\text{CH}_3)_2\text{CO}$	-38	-32	-46	-61	-28	-24	-	-	-28	-36	-	-	-57	-94
$\text{CH}_3\text{OH}$	-26	-15	-25	-25	-21	-	-22	14	-42	-79	-1.6	-10	-95	-190
$\text{C}_2\text{H}_5\text{OH}$	-30	-20	-36	-35	-	-	-	-	-61	-119	-2	-6	-53	-91
$\text{CH}_3\text{NO}_2$	-62	-86	-38	-36	-37	-48	-27	42	-	-	-9	-27	-	-
$(\text{C}_2\text{H}_5)_2\text{O}$	-31	-30	-	-	-39	-56	-	-	-	-	-	-	-	-

### 1.4.2. Liquid chromatography

The majority of diamond based adsorbents are hydrolytically stable and fully compatible with various types of organic solvents. The surface of bare diamond is usually oxidised and hydrophilic due to presence hydroxyl-, carboxyl- and other polar groups, but it can be easily converted to hydrophobic or to more specific types of functional groups. So, depending on the surface properties these adsorbents can be used in various LC modes. In many cases, the occurrence of a single retention mechanism is impossible, so mixed-mode interactions should be expected, particularly for stationary phases comprising DND, MSND and composite phases.

A special attention should be paid to the packing of HPLC columns with diamond based adsorbents. A special care should be taken for standard slurry packing procedures due to friability and strong abrasive and cutting capabilities of diamond particles. This may result in blockage or cuts of column frits. The use of gravity or gradient of pressure as well as of more concentrated slurry can eliminate these problems [17,100].

#### 1.4.2.1. Normal phase and hydrophilic interaction liquid chromatography (HILIC)

As indicated in Table 1.2 both natural and synthetic diamonds can be considered as rather hydrophilic materials. As both normal-phase (NP) and HILIC modes of LC are based on the use of polar adsorbents and non-polar mobile phases, many types of diamond (prepared without additional chemical modification) can potentially be applied in these areas.

In 2002, Patel *et al.* [97] were the first to publish a report on the use of MSND in NP-HPLC of organic compounds. The study used a  $100 \times 4.6$  mm ID chromatographic column packed with  $3.8 \pm 0.1$   $\mu\text{m}$  MSND particles, with a surface area of  $216 \text{ m}^2 \cdot \text{g}^{-1}$ , using heptane as the mobile phase for the separation of *ortho*- and *para*-xylenes. Despite very low column efficiency (only  $1300 \text{ N} \cdot \text{m}^{-1}$ ) and incomplete resolution of solute peaks due to tailing, interesting separation selectivity ( $\alpha = k_{\text{ortho}}/k_{\text{para}} = 2.63/2.29 = 1.15$ ) was observed for these positional isomers. No such selectivity could be seen with a bare silica column for these analytes in heptane.

Emelina *et al.* [98] used NP-HPLC for comparison of the adsorption properties of two MSND phases: the first purified with  $\text{CrO}_3/\text{H}_2\text{SO}_4$  mixture and the second gas-phase purified with ozone. Two columns (75–80 mm long, 2.0 mm ID) were dry packed with 3–4  $\mu\text{m}$  sintered DND particles. The authors did not find any substantial difference in separation selectivity between the two adsorbents, but slightly stronger retention selected analytes was found for ozone treated MSND, which is in good agreement with data showing a higher

concentration of polar groups for this phase (see discussion in Section 1.4.1). The retention order for the following solutes was obtained, toluene < bromobenzene < *o*-dichlorobenzene < benzophenone < anisole. However, no actual separations were reported due to very low column efficiencies, of the order 630–790 N·m<sup>-1</sup>. Later, the same group used NP-HPLC for characterisation of the adsorption properties of hydrogenated MSND, although once more no separations were demonstrated [25]. Using benzylamine as a probe, the authors identified the presence of hydroxyl groups of varied acidity at the surface of hydrogenated MSND.

The first successful NP-HPLC separation was reported by Nesterenko *et al.* [7,26,61] in 2007, who used a 150 × 4.0 mm ID column, packed with carefully fractionated 3–6 μm MSND particles, and a bimodal pore size distribution, with a surface area of 153 m<sup>2</sup>·g<sup>-1</sup>. Separations of 8 alkylbenzenes and 10 dialkylphthalates were achieved using *n*-hexane/IPA (95:5, v/v) or pure pentane as mobile phases (see Fig. 1.7). Nesterenko and co-authors compared the selectivity of their diamond phase with that of PGC and conventional NP adsorbents, such as silica and alumina [26]. Obviously, hydrogen bonding plays a very important role in retention of polar molecules under NP-HPLC conditions, however results indicated the presence of a graphitic layer on the surface of the sintered ND, resulting in selectivity close to that of the planar PGC. As expected, selectivity of silica and alumina were very different to that of the MSND substrate (see Fig. 1.8).

The high concentration of very polar groups on the surface of MSND could result in an adsorbed water layer and, hence, be applicable in “aqueous normal-phase chromatography”, more commonly known as hydrophilic interaction liquid chromatography (HILIC). Fedyanina and Nesterenko [23,24] studied the retention mechanism of substituted phenols and benzoic acids on an MSND column using both methanol-water and acetonitrile-water mobile phases. In both cases the retention of solutes decreased with increases of organic solvent, up to 75–80%. Beyond this, any further increase of organic solvent caused an increase in the retention time for all solutes, as shown in Fig. 1.9, left. Interestingly, it was noted that the retention order of ionogenic solutes did not depend on the concentration of organic solvent in the mobile phase. Linear correlations for  $\log k - \text{p}K_a$  and  $\log k - C_{\text{methanol}}$  were obtained for both phenols and benzoic acids. The corresponding plot of  $\log k - \text{p}K_a$  for phenols is in Fig. 1.9, right. These observations indicate that the main retention mechanism in this system is in fact hydrogen bonding, though some hydrophobic interactions were also present. However, both selectivity and efficiency did depend on the nature of the organic solvent. In the case of water–methanol, the column efficiency was on average 1.3 times higher than in the case of a water–acetonitrile based mobile phase.

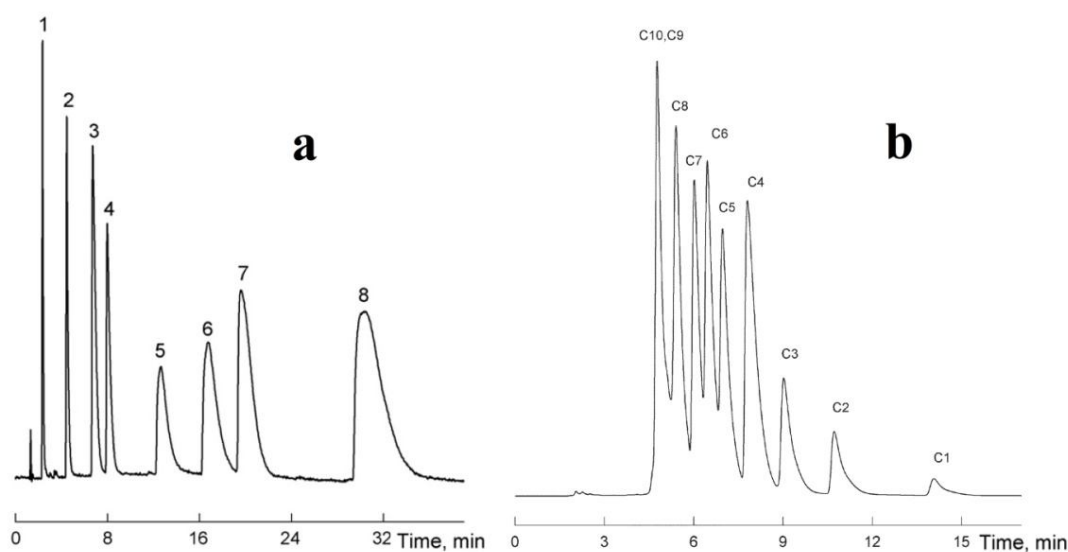


Fig. 1.7. Separation of 8 alkylbenzenes (a) and 10 dialkyl phthalates (b) on MSDN. Conditions: *n*-pentane, 1.0 mL·min<sup>-1</sup>, detection UV 254 nm (a); *n*-hexane/IPA (95:5,v/v), 0.6 mL·min<sup>-1</sup>, 30 °C, detection UV 254 nm (b). Analytes, (a): (1) 1,3,5-triisopropylbenzene, (2) 1,3-diisopropylbenzene, (3) tert-butylbenzene, (4) isopropylbenzene, (5) benzene, (6) toluene, (7) *n*-amylbenzene, (8) *n*-nonylbenzene. Analytes, (b): in order from di-*n*-decyl- (C10) to di-*n*-methyl-phthalate (C1) [61].

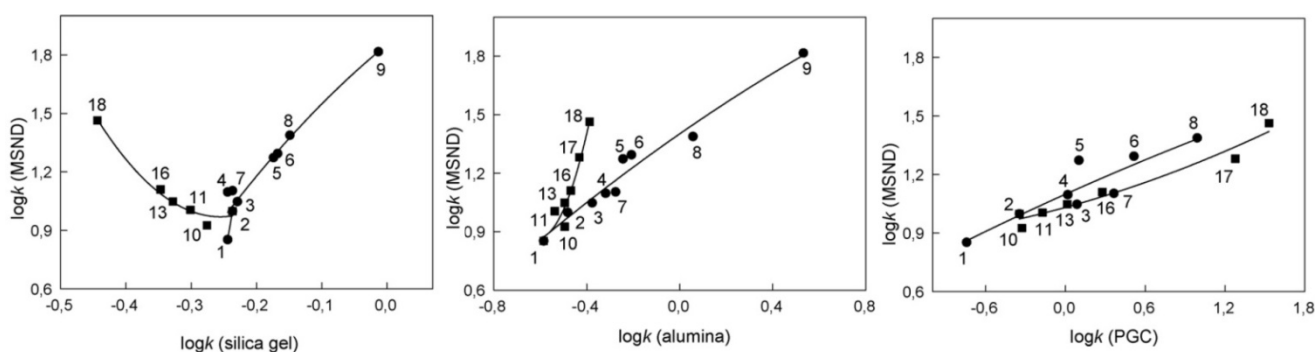


Fig. 1.8. Comparison of selectivity of MSND with silica gel, alumina and PGC [26]. The left side of the plot presents data obtained for polymethylbenzenes (data points 10, 11, 13, 16 and 18) and right side presents data for monoalkylbenzenes with differing chain length of *n*-alkyl groups.

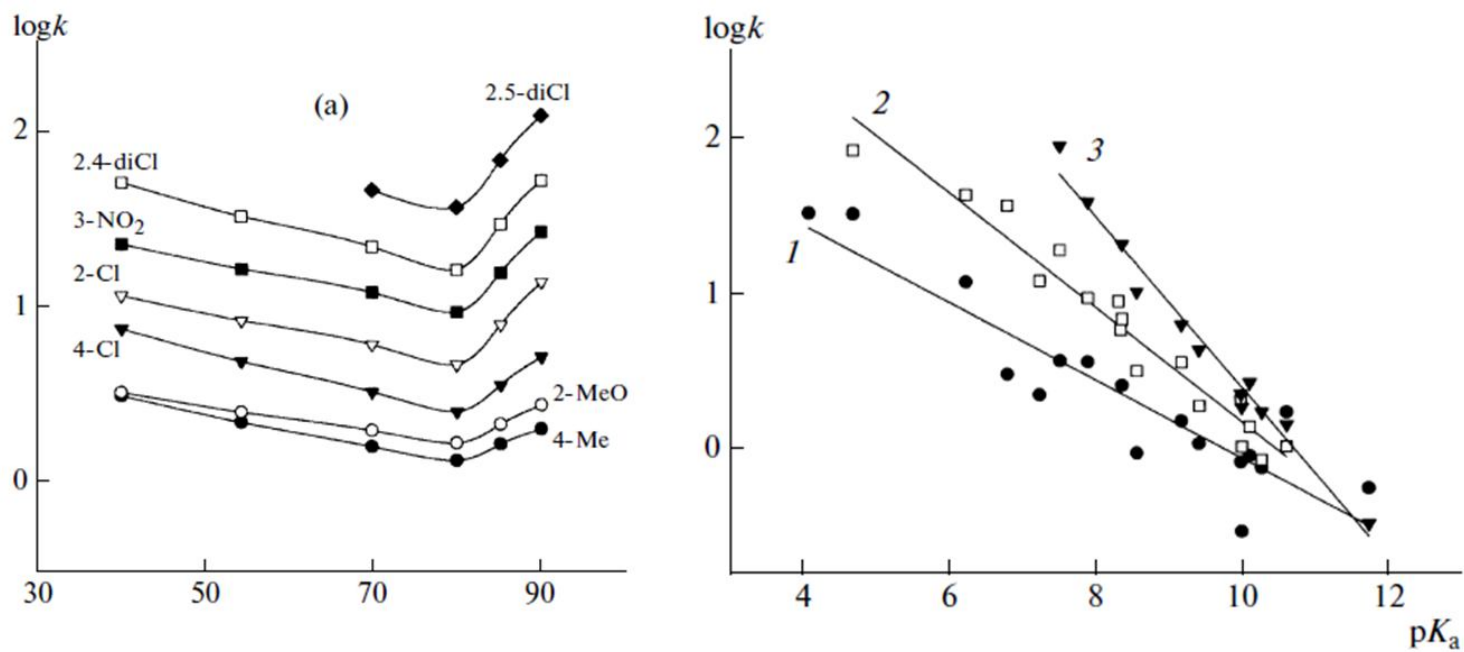


Fig. 1.9. Indication of typical HILIC retention behaviour for derivatives of phenol on MSND column with an increase of methanol content (left) and correlations between  $\log k$  and  $pK_a$  obtained for phenols (right) on porous graphite (1) and MSND (2,3) columns in mobile phases containing 90% methanol (1, 3) and acetonitrile (2). [23].

This comparative study also showed how DND exhibits a high separation selectivity for structural isomers, such as 2,4- and 2,5-dichlorophenols, which can be separated on MSND, but cannot be separated on the Hypercarb PGC phase. Some indications of the impact of hydrophobic and  $\pi$ - $\pi$  interactions on the retention of phenols and benzoic acids were also observed [23,24].

#### **1.4.2.2. Reversed-phase and related mixed-mode HPLC**

For reversed-phase liquid chromatography (RP-HPLC) it is important to have a hydrophobic surface as the stationary phase. Potentially, diamond materials produced using HPHT synthesis or CVD could therefore be applied without surface modification, as their surfaces are typically free of functionalities and relatively hydrophobic, as presented in Table 1.2. The first study of adsorption and chromatographic properties of HPHT synthetic diamonds in HPLC was reported in 2000 by Ford *et al.* [107]. It was found that the retention on the surface of HPHT diamond appears to involve both typical RP interactions and an element of hydrogen bonding, that depended on the origin of substrate [17,107]. Natural diamond also possesses similar properties [15], but due to its obvious drawbacks, including cost, presence of various impurities and availability, it is impractical. However, an attempt to use natural diamond in HPLC was reported in 1973 (see details in Table 1.3).

As stated previously, the outstanding mechanical properties of diamond make it a candidate material for chromatography at ultra-high pressures. Liu *et al.* packed 1 and 2 micron particles of non-porous synthetic diamond into 75  $\mu\text{m}$  capillaries of length 215 and 290 mm, respectively, and used them for the reverse-phase separation of polar phenols and parabens at pressures up to 180 MPa [16]. Within these studies, the authors also used modified diamond phases, using butadiene coatings in an unsuccessful attempt to improve separation selectivity for the bare diamond phase. The efficiency achieved in this work, which ranged from 10,000 to 126,000 N/m for bare diamond phase, and 16,000–112,000 N/m for the diamond-poly(butadiene)phase. The same researchers also tried to prepare diamond with a more hydrophobic surface by heating diamond microparticles in a  $\text{H}_2$  atmosphere at 900  $^\circ\text{C}$  with subsequent radical grafting of octyl groups. The surface of the prepared adsorbent was extremely hydrophobic and strong retention for test compounds was achieved. However, no improvements in separation selectivity or efficiencies were obtained.

The surface of MSND is very hydrophilic, so the retention of hydrophobic neutral molecules is much weaker than upon other types of diamond. So far, no separation of neutral organic molecules has been reported for MSND. Clearly, the retention and separation of polar



solutes like phenols or benzoic acid on this type of material is due to other types of interactions, as discussed in the previous section.

Considerable progress in the application of diamond based phases in RP-HPLC became evident after the appearance of new pellicular phases in 2010 [29-31]. As discussed in Section 1.2.5, these phases consist of a diamond or carbon core, covered with multilayers of ND particles and a polyamine bonding agent (see Fig. 1.4). These particles can be cross-linked with 1,2,5,6-diepoxyoctane to create a mixed-mode stationary phase containing amino, hydroxyl, and cyclooctyl groups. Particles that were 2–3  $\mu\text{m}$  in size with a much improved surface area were produced using this method and packed into 4.6 mm  $\times$  30 mm columns. Chromatographic applications of these phases, in both HILIC and RP-HPLC modes for separations of polar compounds, alkylbenzenes, phenols, pharmaceuticals and pesticides have been shown [29-31]. The results have demonstrated that despite the complicated structure of this form of stationary phase, stability and efficiency are impressive and separations reproducible. For example, a mixture of four alkylbenzenes can be separated within 9 min (Fig. 1.10), showing ca. 36,300 N/m for the peak of mesitylene, respectively. Efficiency of the majority of these composite adsorbents was significantly higher than values mentioned previously for many alternative diamond based phases, reaching HETP = 18  $\mu\text{m}$  for diazinon in RP-HPLC, using a 50/50 v/v water/methanol mobile phase.

Wiest *et al.* extended the above work, using similar composite phases obtained by layer-by-layer deposition of ND and PAAm, but instead using 3 micron spherical glassy carbon as the core support, in-place of micron-sized diamond [30]. The ND-PAAm composite was also cross-linked with 1,2,7,8-diepoxyoctane and packed within 50  $\times$  4.6 mm ID columns, for application in RP and mixed-mode HPLC. Not only did the cross-linked phase show admirable efficiencies for a diamond-based phase, ca. 71,000 N/m on a conventional HPLC system, but it also exhibited good stability under extreme pH conditions: pH 11.3–13. Efficiencies of HETP = 9-10  $\mu\text{m}$  could be achieved using these columns with UHPLC chromatographs, applying “sandwich” injections. Separations of pharmaceuticals at high (11.3) and low (2.7) pH were performed, and phenols and phenolic derivatives were separated under acidic conditions. While no stability studies were performed under acidic conditions, there appeared to be no degradation of the phases under these conditions.

Recently, the same research group evolved the structure of this type of composite phase once more, with the development of carbonised PS-DVB particles, of diameter 2  $\mu\text{m}$  as the central core in place of the above glassy carbon, or non-porous diamond particles.

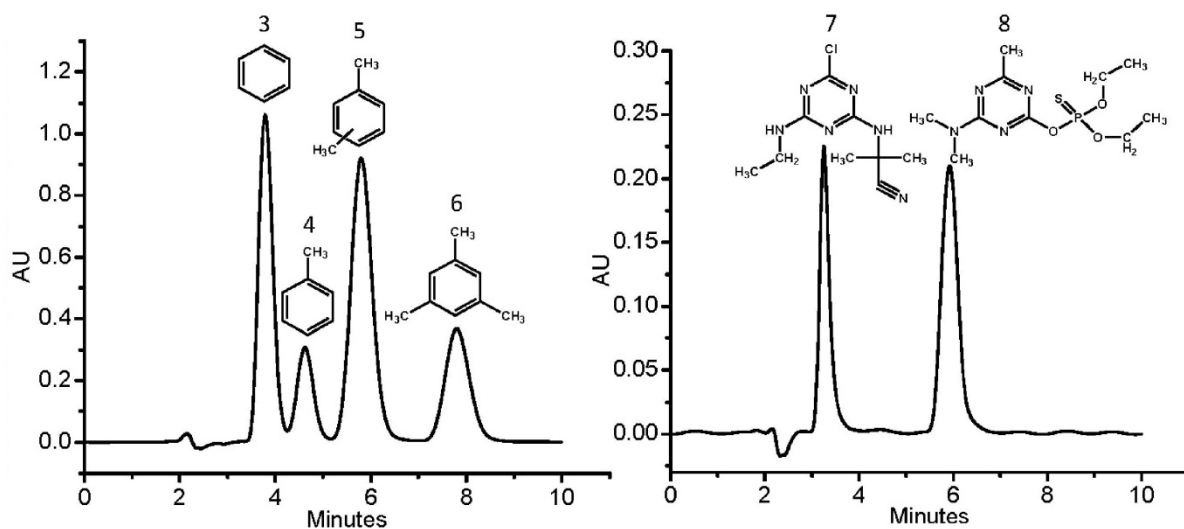


Fig. 1.10. Reversed-phase (mixed-mode) separations on  $30 \times 4.6$  mm ID column packed with diamond/polyamine/ND composite. Mixed mode conditions, eluent –  $0.2 \text{ mL} \cdot \text{min}^{-1}$  of acetonitrile–water (50:50) + 0.1% triethylamine [31].

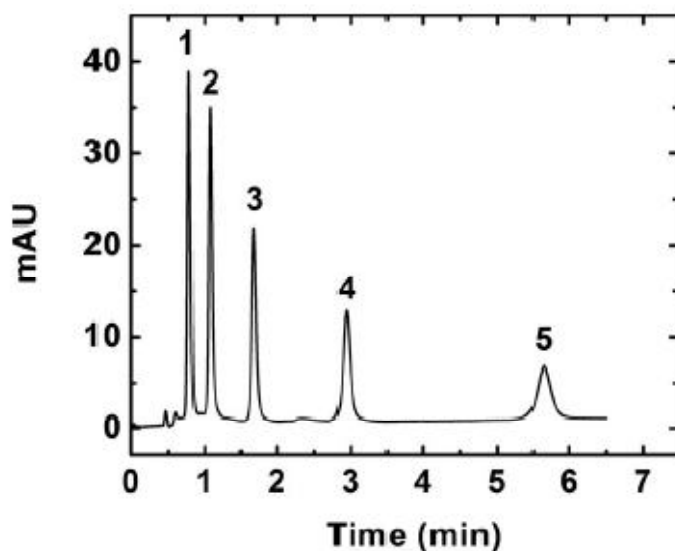


Fig. 1.11. UHPLC separation of alkylbenzenes (1. ethyl-, 2. butyl-, 3. hexyl-, 4. octyl-, and 5. decylbenzene) using a  $2.1 \times 50$  mm ID column packed with the particles  $3.3 \mu\text{m}$ . The mobile phase was 40:60  $\text{H}_2\text{O}/\text{ACN}$  at  $35 \text{ }^\circ\text{C}$  with a flow rate of  $0.15 \text{ mL} \cdot \text{min}^{-1}$ . The efficiency of the decylbenzene peak was 89,000  $\text{N}/\text{m}$  with a tailing factor of 1.08 [29].

The new adsorbent offers extremely high separation efficiencies of up to 112,000 N/m, a typical example of which is shown in Fig. 1.11. However, this type of stationary phase includes a significant concentration of protonated amino groups, due to presence of poly(allylamine) within the shell structure, so the resulting retention mechanism must be considered as mixed reversed-phase/anion-exchange, with limited suitability for the separation of aromatic organic acids [29].

A unique type of technology based on microwave plasma-assisted CVD (MPCVD) deposition of diamond layers upon microspherical aggregates of ND has recently been developed by Kondo *et al.* [32]. A detailed description of the synthesis of the composite is given in Section 1.2.5. This method for the preparation of pure diamond composite offers new possibilities for the control of the porous structure of particles, and for modification of the surface chemistry. The RP-HPLC separation of a model mixture of n-alkylbenzoates (see separation conditions in Table 1.3) was obtained, although column efficiency was poor, in the range 700–1700 N.

#### **1.4.2.3. Ion-exchange chromatography**

HPHT and CVD produced diamonds have no charged groups at the surface and do not exhibit any significant ion-exchange selectivity without oxidative treatment. Hence, retention of neither anions nor of cations has not been reported using HPHT diamond based phases. However, DND possesses pronounced cation exchange properties, due to the functionalisation of its surface with carboxyl and hydroxyl groups, following the oxidative treatment applied during isolation and purification of DND from detonation soot. According to the results of potentiometric titrations [108,109], Boehm titrations [110] and FT-IR spectroscopic data [4], the surface of this form of synthetic diamond contains three types of cation-exchange groups, including strong acidic carboxylic, weak acidic carboxylic and phenolic. The type and surface concentration of such ionogenic groups depends on the type of oxidative purification procedure applied. Chukhaeva and Cheburina evaluated cation-exchange capacity of DND purified with strong oxidising acids as being equal to 0.7 mmol·g<sup>-1</sup> [111]. Chiganova [110] reported the total concentration of protogenic groups as 0.66 and 0.91 meq·g<sup>-1</sup> for DND samples with surface areas of 270 m<sup>2</sup>·g<sup>-1</sup>, which had been purified by wet (nitric acid) or gas phase oxidation in the air, respectively. The corresponding values for total surface concentrations of acidic functional groups were 1.47 and 2.02 groups per nm<sup>2</sup>, while the concentrations of strongly acidic carboxylic groups in these samples were 0.47 and 1.33 groups·nm<sup>-2</sup>. These values are comparable with the maximum concentration of

silanols known for silica, namely  $4.6 \text{ groups}\cdot\text{nm}^{-2}$  [42]. The ratio of strong and weakly acidic functional groups evaluated by the Boehm method is significantly higher for the gas phase oxidised sample ( $0.60 \text{ mmol}\cdot\text{g}^{-1}$  against  $0.18 \text{ mmol}\cdot\text{g}^{-1} = 3.33$ ), as compared with wet oxidised sample ( $0.21 \text{ mmol}\cdot\text{g}^{-1}$  against  $0.39 \text{ mmol}\cdot\text{g}^{-1} = 0.54$ ). Obviously, the latter sample has a less charged surface ( $\zeta = -30.1 \text{ mV}$ ) than gas phase sample ( $\zeta = -36.6 \text{ mV}$ ) [110]. pKa values of carboxylic groups at the surface of diamond are usually around 4–6 [108,109].

As expected, most of the publications in this area are devoted to the investigation of cation-exchange properties of DND, while only a few papers have reported data on adsorption of inorganic anions [112]. Cation exchange selectivity of the following order,  $\text{Ca}^{2+} > \text{Ba}^{2+} > \text{Li}^{+} > \text{Na}^{+} > \text{K}^{+}$  has been reported for both oxidised synthetic diamond [113] and DND [110]. This selectivity is in agreement with the ion-exchange selectivity of nonaromatic carboxylic type cation exchangers towards alkali metal ( $\text{Li}^{+} > \text{Na}^{+} > \text{Cs}^{+} > \text{K}^{+}$ ) and alkaline-earth metal ions ( $\text{Ca}^{2+} > \text{Sr}^{2+} > \text{Ba}^{2+}$ ), as recorded in basic media [114]. This typical retention order for alkali and alkaline-earth metals were obtained in acidic eluent on a column packed with MSND, and is shown in Fig. 1.12b. Obviously, MSND exhibits strong ion-exchange selectivity, as the baseline separation of alkali metal cations was possible (Fig. 1.12a). However, all chromatographic peaks tailed due to the microporous structure of MSND and slow diffusion of metal cations within these pores.

The complexing properties of the same type of MSND were evaluated by Nesterenko *et al.* [26]. A chromatographic column of dimensions  $100 \times 4 \text{ mm I.D.}$  was used for the separation of  $\text{Cd}^{2+}$ ,  $\text{Ca}^{2+}$ ,  $\text{Zn}^{2+}$ ,  $\text{Co}^{2+}$ ,  $\text{Mn}^{2+}$ ,  $\text{Mg}^{2+}$ ,  $\text{Sr}^{2+}$ ,  $\text{Ba}^{2+}$ ,  $\text{Ni}^{2+}$ ,  $\text{Pb}^{2+}$ ,  $\text{Cu}^{2+}$ , using  $1.5\text{--}5.0 \text{ mM HNO}_3\text{--}0.1 \text{ M KNO}_3$  as the eluent. Alkaline-earth, transition and heavy metal cations were retained under these conditions in an order correlating to the stability of the complexes formed with carboxylic groups at the surface of MSND [115]. Under optimised conditions, a mixture of  $\text{Cd}^{2+}$ ,  $\text{Co}^{2+}$ ,  $\text{Mn}^{2+}$ ,  $\text{Mg}^{2+}$  could be separated within 20 min. The retention order for these metals on DND was similar to that obtained on commercially available carboxylic type cation exchangers. The effect of the column temperature and ionic strength on the retention of cations was evaluated, and the results confirmed the dominance of surface complexation within the retention mechanism.

For DND, there are some indications on the significant effect of counter-ions on the adsorption of cations [100], whilst no effect of counter ions was recorded for adsorption of cations on natural diamond [116].

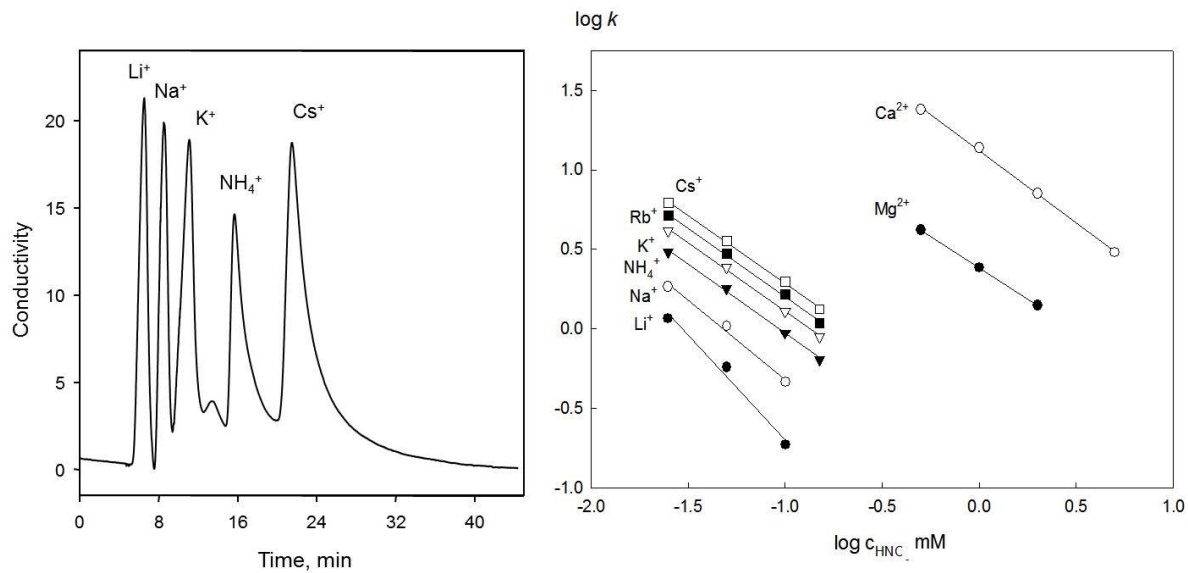


Fig. 1.12. Separation of alkali metal cations on MSDN column  $150 \times 4.0$  mm I.D. ( $d_p = 3\text{--}6$   $\mu\text{m}$ ). Eluent:  $0.05$  mM  $\text{HNO}_3$ ,  $0.35$   $\text{mL}\cdot\text{min}^{-1}$ ,  $23$   $^\circ\text{C}$ . Conductivity detector. Unpublished results.

#### 1.4.2.4. Electro modulated liquid chromatography

The elevated electrical conductivity of boron doped diamond powder facilitates its use as a stationary phase in electromodulated chromatography [33]. This type of chromatography exploits the possibility of retention and selectivity control through changing the electric potential applied to the surface of the conducting stationary phase. The electric resistivity measured for 8–12  $\mu\text{m}$  HPHT diamond particles powder was greater than  $40 \text{ M}\Omega\cdot\text{cm}$ , however after the coating of these particles with a boron doped CVD diamond layer, this resistivity dropped to  $2.4 \Omega\cdot\text{cm}$  [33]. Therefore, boron doped diamond powder was packed in specially constructed columns, dimensions of  $78 \times 3.0 \text{ mm}$  I.D., and applied to the electrochemically modulated separation of a mixture containing benzenesulfonate, 4-toluenesulfonate, 1,3-benzenedisulfonate and 1,5-naphthalenedisulfonate, with  $0.1 \text{ M LiClO}_4$  as the mobile phase, delivered at a flow rate of  $0.4 \text{ mL}\cdot\text{min}^{-1}$  [33]. A rise in applied electric potential from  $-1.2 \text{ V}$  to  $+1.2 \text{ V}$  increased the retention times for all solutes, in the order of 0.5–10 min. A linear correlation between voltage and retention factors was demonstrated for all solutes and separation of three aromatic acids within 3 min was achieved. Due to its inert nature and the wide potential window of conductive diamond, there is a possibility to use this adsorbent at higher positive and negative potentials without undesirable effects, such as surface oxidation, microstructural changes or solvent electrolysis, which are more likely with other carbon-based materials commonly applied to this niche variant of liquid chromatography. However, the very low specific surface area of nonporous borondoped diamond powder ( $\sim 1 \text{ m}^2\cdot\text{g}^{-1}$ ) greatly limits column loading capacity and influences interaction strength between solutes and such stationary phases.

#### 1.4.3. Microfluidic separations

The capabilities of CVD based methods for the growth of diamond films and coatings make it an ideal tool for preparation of microfluidic chips. As discussed earlier in Section 1.2.1, diamond can be converted from an insulator into an electric conductor by doping with B or N, thus making it a suitable material for chemically resistant electrodes. Also the excellent thermal conductivity of diamond allows very efficient dissipation of Joule heating during electrophoresis in the narrow channels of microfluidic chips [70,117], which is a problem in CZE at high voltage. CVD can therefore provide formation of both conducting and non-conducting, smooth and homogeneous diamond films on various surfaces, with great flexibility for the preparation of diamond microfluidic chips of varying geometries [101].

Such devices present inert surfaces and perfect mechanical stability, and can be used under extreme separation conditions.

Application of a diamond based microfluidic chips for the fast chromatography of proteins was reported by Bjorkman *et al.* [64]. The authors used CVD deposited diamond films of 10–20  $\mu\text{m}$  on top of a silica carrier with subsequent lithography and sacrificial silica etching with HF, for the fabrication of a purely diamond microfluidic device. The resulting platforms had separation channels of 4.0 cm length, with rectangular,  $40 \times 100$  or  $70 \times 100$   $\mu\text{m}$ , cross sections (see Fig. 1.13). The hydrophobicity of the prepared diamond films was estimated using contact angle measurements with water, and was reported as  $47^\circ$  and  $65^\circ$  for the original and a hydrogenated surface of diamond, respectively. Obviously, the surface of the diamond surface is rather hydrophilic, and serves to eliminate hydrophobic interactions between proteins and the channel walls of the microfluidic chip. In this case, the channels were filled with continuous polymer beds derivatised with ammonium groups and the chromatographic separation of myoglobin, conalbumin, ovalbumin and trypsin inhibitor was achieved in 30 s with a 20 mM phosphate buffer (pH 7.8), and a linear gradient of sodium chloride concentration delivered at a flow rate of  $0.1 \mu\text{L}\cdot\text{min}^{-1}$  and pressure of 9 bar. The resolution of chromatographic peaks was comparable with that obtained with continuous beds synthesised in fused-silica capillaries and quartz microfluidic chips [118]. Although diamond only plays the role of a support here, whilst the separation takes place upon the polymer bed, this work does represent a new approach to creating microfluidic chips with improved mechanical and chemical stability, and also shows increased possibilities for on-chip electrochemical, spectrophotometric and fluorescent detection.

#### **1.4.4. Low pressure column liquid chromatography**

A further type of diamond containing adsorbent is described by Bondar' *et al.* [60,73,119], who used a 5% DND hydrosol, entrapped within 60–200  $\mu\text{m}$  particles of the macroporous polysaccharide adsorbent, Serpharose 2B. This sorbent was packed in  $80 \times 16$  mm I.D. columns and used for the low pressure ion-exchange chromatography of proteins, using a 20 mM Tris-HCl buffer (pH 7.0) as the eluent, delivered at  $1 \text{ mL}\cdot\text{min}^{-1}$ . The authors isolated 40% of luciferase from a crude extract of proteins in a single step separation in 140 min [27]. Chemical inertness, low cytotoxicity, biocompatibility and the unique selectivity of DND towards cytochrome C, luciferase, lysozyme and others, as discovered by this research group, make this new adsorbent potentially very significant for the separation and purification of biomolecules [69].

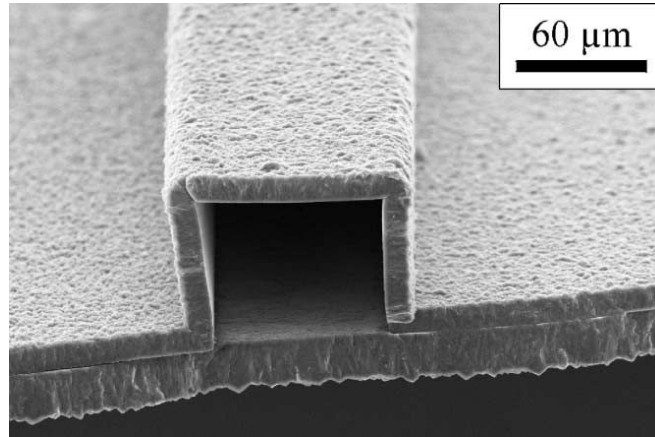


Fig. 1.13. SEM image of capillary microchip constructed from diamond using CVD [64].



However, the application of the polysaccharide phase is limited by a narrow pH window of hydrolytic stability (pH 4–9), and a relatively soft matrix. Additionally, the exact role of DND in this experiment is yet to be established, although the authors believe that the DND played a key role in the chromatographic performance of the composite material.

Sevostyanova *et al.* [28] described an application of a similar adsorbent for the separation of proteins. Laboratory made highly permeable diacetate cellulose microspherical particles, of diameter 100–300  $\mu\text{m}$ , were used in place of Sepharose 2B, which contained differing amounts of DND. A column of internal diameter 4.8 mm, with a 3.9 cm bed of the prepared adsorbents, produced selective and efficient separations of insulin and ribonuclease in 0.1 M acetate (pH 2.5) and 0.1 M phosphate buffers (pH 6.5), respectively, at flow rates of  $0.1 \text{ mL}\cdot\text{min}^{-1}$ . Adsorbents with higher concentrations of DND demonstrated more favourable thermodynamics of adsorption for targeted proteins, while phases with lower content of DND had faster kinetics of adsorption due to an optimum porous structure for the diffusion of proteins inside of the particles.

#### **1.4.5. High temperature liquid chromatography**

The combination of very high thermal conductivity ( $900\text{--}2300 \text{ W}\cdot\text{m}^{-1}\text{K}^{-1}$ ), and extremely low linear thermal expansion coefficients, in the order of  $5 \times 10^{-8} \text{ K}^{-1}$  [1], mechanical stability and high thermal stability up to  $400 \text{ }^\circ\text{C}$ , make diamond a perfect stationary phase for HPLC at high temperatures. Diamond sorbents can be used under harsh separation conditions, where conventional phases like silica, alumina, and organic polymers are not stable. In liquid chromatography, an increase in column temperature decreases viscosity of the mobile phase and provides for faster diffusion and kinetics of sorption–desorption processes, which in turn allows the use of higher flow rates, and the development of faster separations with increased column efficiency. Recently, Nesterenko *et al.* demonstrated a 14-fold increase in the number of plates for a column packed with MSDN following an increase of column temperature from  $35$  to  $180 \text{ }^\circ\text{C}$  (see Fig. 1.14a) [99]. Additionally, an improvement in resolution of chromatographic peaks for a three-component model mixture on the MSDN phase was noted for the separation at elevated column temperature (see Fig. 1.14b), although the increase of column temperature decreased the retention of the solutes.

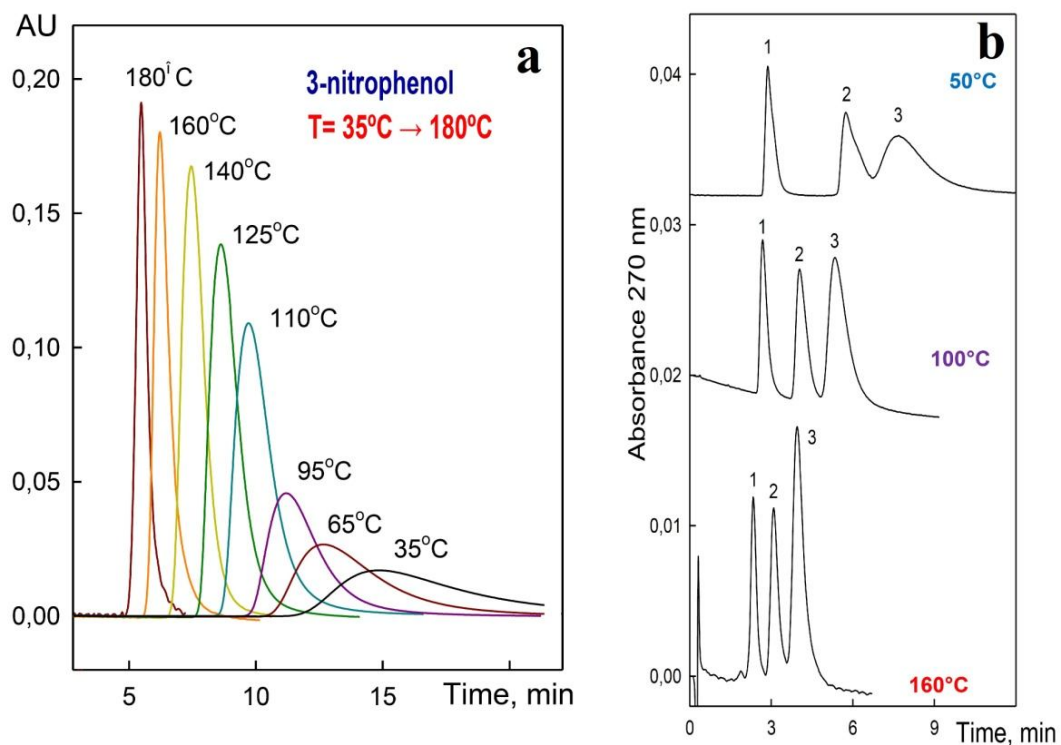


Fig. 1.14. The effect of column temperature on separation efficiency (a) and resolution of chromatographic peaks (b).  $150 \times 4.0$  mm I.D. column packed with 3–6  $\mu\text{m}$  MSDN. Eluent: 90:10 (v/v) methanol – 5 mM MES buffer pH 6.0,  $0.3 \text{ mL} \cdot \text{min}^{-1}$ . Peaks: 3-nitrophenol (a); (1) toluene, (2) aniline, (3) 4-chlorophenol (b). Unpublished results.

## 1.5. Conclusions and aims

Diamond is a unique material with extraordinary physical and chemical properties, which potentially may be beneficial for its use in chromatography. However, for many years the application of diamond based materials in chromatography was limited by the absence of porous materials having developed surface area, optimum pore size and of good understanding of surface chemistry and adsorption properties for different types of diamond. The remarkable progress in all these areas has been achieved in the last decade.

Three main types of diamond materials, including 1-2 micron particles of HPHT diamond, 3–4 micron particles of HPHT diamond and MSND, are found to be the most suitable for various chromatographic applications. The application of new technologies for the preparation of diamond based composites opens new possibilities in construction of special stationary phases such as fully porous microspherical diamond particles with chemically grafted molecules or pellicular type particles with multiple nanodiamond/polyamine bilayered structure of porous shell. The maximum separation efficiency reached the level of 10,800–112,000 theoretical plates per meter for both microparticulated HPHT diamond and composite adsorbent. The clear future for diamond based stationary phases is associated with UHPLC at elevated column temperatures. The possibility of using MSND packed column in HPLC at 200 °C has been demonstrated.

Significant progress has been made towards understanding retention mechanisms and the separation selectivity of diamond adsorbents in various chromatographic modes. However, a systematic study of pure diamond particles in different modes of liquid chromatography has not been reported. Therefore, the overall aim of this Thesis is the development of stationary phases based upon unmodified synthetic polycrystalline high pressure high temperature (HPHT) diamond and investigation of their chromatographic properties. The specific aims are:

- the preparation and characterisation of HPHT diamond stationary phases and development of a column packing procedure for this sorbent
- investigation of the performance of HPHT diamond columns in NP-HPLC with a focus on the retention mechanism, separation selectivity, and comparison with other carbon based stationary phases
- investigation of the performance of HPHT diamond columns in HILIC conditions. Special attention will be dedicated to the influence of mobile phase composition on the

retention mechanism and selectivity, as well as to the performance of the HPHT diamond column under the conditions of elevated temperature and high pH.

- Investigation of the ion-exchange properties of microdispersed sintered detonation nanodiamond (MSDN). Adsorption of both anions and cations on MSDN will be studied, and the influence of cations and anions on the adsorption of each other will be explored.

### 1.6. Reference List

1. P.N. Nesterenko, P.R. Haddad, Diamond-related materials as potential new media in separation science, *Anal.Bioanal.Chem.*, 396 (2010) 205-211.
2. S. Ferro, Synthesis of diamond, *J.Mater.Chem.*, 12 (2002) 2843-2855.
3. A. Krueger, Diamond nanoparticles: Jewels for chemistry and physics, *Adv.Mater.*, 20 (2008) 2445-2449.
4. I.I. Kulakova, V.V. Korolkov, R.Yu. Yakovlev, G.V. Lisichkin, The Structure of Chemically Modified Detonation-Synthesized Nanodiamond Particles, *Nanotechnologies in Russia*, 5 (2010) 474-485.
5. V.N. Mochalin, O. Shenderova, D. Ho, Y. Gogotsi, The properties and applications of nanodiamonds, *Nat.Nanotechnol.*, 7 (2012) 11-23.
6. O.A. Williams, Nanocrystalline diamond, *Diam.Relat.Mater.*, 20 (2011) 621-640.
7. A. Matheson, P.N. Nesterenko, Diamonds are a Chromatographer's Best Friend?, *Lc Gc Europe*, 23 (2010) 120-123.
8. L. Pereira, Porous graphitic carbon as a stationary phase in HPLC: Theory and applications, *J.Liq.Chromatogr.R.T.*, 31 (2008) 1687-1731.
9. C. West, C. Elfakir, M. Lafosse, Porous graphitic carbon: A versatile stationary phase for liquid chromatography, *J.Chromatogr.A*, 1217 (2010) 3201-3216.
10. B. Muriithi, K. Wyndham, P. Iraneta, I. Bouvier, T. Walter, 21 Apr. 2014, San Francisco, CA, USA, 2014, p.p. RR9.18.
11. Flare columns information sheet, <http://diamond-analytics.com>, Accessed on 17 Mar. 2014. <http://diamond-analytics.com/uploads/Datasheet-Diamond%20Analytics.pdf>
12. A. Kraft, Doped diamond: A compact review on a new, versatile electrode material, *Int.J.Electrochem.Sc.*, 2 (2007) 355-385.
13. A.S. Barnard, E. Osawa, The impact of structural polydispersivity on the surface electrostatic potential of nanodiamond, *Nanoscale*, 6 (2014) 1188-1194.

14. G.N. Yushin, S. Osswald, V.I. Padalko, G.P. Bogatyreva, Y. Gogotsi, Effect of sintering on structure of nanodiamond, *Diam.Relat.Mater.*, 14 (2005) 1721-1729.
15. M.J. Telepchak, The Mechanism of Reverse Phase Liquid-Solid Chromatography, *Chromatographia*, 6 (1973) 234-236.
16. Y. Liu, Investigation of novel microseparation techniques, Masters Thesis, Brigham Young University, 2007.
17. A.K. Badu-Tawiah, Adsorption isotherms of diamond-packed columns in reverse phase liquid chromatography, Masters Thesis, Indiana University of Pennsylvania, 2010.
18. Information sheet for Metrosep BP 1 Guard/2.0, <http://metrohm.com>, Accessed on 28.02.2014  
[http://metrohm.com/com/Produkte2/Accessories/index.html?identifier=61015100&language=en&name=61015100\(2014](http://metrohm.com/com/Produkte2/Accessories/index.html?identifier=61015100&language=en&name=61015100(2014)
19. Allied Chemical Corporation, Great Britain Patent Application, No GB19660039411 19660902 (1969).
20. L.D. Belyakova, O.G. Larionov, S.A. Parkaeva, B.V. Spitsyn, Investigation of surface chemistry of ultradispersed diamond by means of gas chromatography, *Sorption Chromatogr.Processes*, 8 (2008) 66-74.
21. L.D. Belyakova, A.N. Kudinova, A.O. Larionova, O.G. Larionov, B.V. Spitsyn, The surface properties of nanodiamonds as examined by gas chromatography, *Russ.J.Phys.Chem.A*, 82 (2008) 420-423.
22. R.P. Hirschmann, T.L. Mariani, Synthetic Diamond - A Solid Absorbent for Corrosive Gases, *J.Chromatogr.*, 34 (1968) 78-80.
23. O.N. Fedyanina, P.N. Nesterenko, Regularities of Chromatographic Retention of Phenols on Microdispersed Sintered Detonation Nanodiamond in Aqueous-Organic Solvents, *Russ.J.Phys.Chem.A*, 84 (2010) 476-480.
24. O.N. Fedyanina, P.N. Nesterenko, Regularities of retention of benzoic acids on microdispersed detonation nanodiamonds in water-methanol mobile phases, *Russ.J.Phys.Chem.A*, 85 (2011) 1773-1777.
25. V.V. Korolkov, M.V. Kochetova, O.G.Larionov, S.V.Emelina, Investigation of adsorption properties of porous disperse diamond by means of HPLC, *Sorption Chromatogr.Processes*, 8 (2008) 507-512.

26. P.N. Nesterenko, O.N. Fedyanina, Y.V. Volgin, P.Jones, Ion chromatographic investigation of the ion-exchange properties of microdisperse sintered nanodiamonds, *J.Chromatogr.A*, 1155 (2007) 2-7.
27. K.V. Purtov, A.P. Puzyr, V.S. Bondar, Nanodiamond sorbents: New carriers for column chromatography of proteins, *Dokl.Biochem.Biophys.*, 419 (2008) 72-74.
28. A.A. Sevostyanova, A.N. Melenevsky, A.A. Demin, E.N. Pavlova, E.S. Nikiforova, Nanodiamonds in cellulose matrix for protein chromatographic purification, *Sorption Chromatogr.Processes*, 11 (2011) 742-753.
29. C.H. Hung, L.A. Wiest, B. Singh, A. Diwan, M.J.C. Valentim, J.M. Christensen, R.C. Davis, A.J. Miles, D.S. Jensen, M.A. Vail, A.E. Dadson, M.R. Linford, Improved efficiency of reversed-phase carbon/nanodiamond/polymer core-shell particles for HPLC using carbonized poly(divinylbenzene) microspheres as the core materials, *J.Sep.Sci.*, 36 (2013) 3821-3829.
30. L.A. Wiest, D.S. Jensen, C.H. Hung, R.E. Olsen, R.C. Davis, M.A. Vail, A.E. Dadson, P.N. Nesterenko, M.R. Linford, Pellicular Particles with Spherical Carbon Cores and Porous Nanodiamond/Polymer Shells for Reversed-Phase HPLC, *Anal.Chem.*, 83 (2011) 5488-5501.
31. G. Saini, D.S. Jensen, L.A. Wiest, M.A. Vail, A. Dadson, M.L. Lee, V. Shutthanandan, M.R. Linford, Core-Shell Diamond as a Support for Solid-Phase Extraction and High-Performance Liquid Chromatography, *Anal.Chem.*, 82 (2010) 4448-4456.
32. T. Kondo, M. Kobayashi, T. Saito, Y. Kadota, T. Kameshima, T. Aikawa, T. Kawai, M. Yuasa, Micrometer-sized mesoporous diamond spherical particles, *Diam.Relat.Mater.*, 43 (2014) 72-79.
33. G.W. Muna, V.M. Swope, G.M. Swain, M.D. Porter, Electrochemically modulated liquid chromatography using a boron-doped diamond particle stationary phase, *J.Chromatogr.A*, 1210 (2008) 154-159.
34. M.V. Baidakova, Y.A. Kukushkina, A.A. Sitnikova, M.A. Yagovkina, D.A. Kirilenko, V.V. Sokolov, M.S. Shestakov, A.Y. Vul', B. Zousman, O. Levinson, Structure of nanodiamonds prepared by laser synthesis, *Phys.Solid State*, 55 (2013) 1747-1753.
35. V.P. Novikov, V.P. Dymont, Synthesis of diamondlike films by an electrochemical method at atmospheric pressure and low temperature, *Appl.Phys.Lett.*, 70 (1997) 200-202.

36. Y.G. Gogotsi, K.G. Nickel, P. Kofstad, Hydrothermal synthesis of diamond from diamond-seeded beta-SiC powder, *J.Mater.Chem.*, 5 (1995) 2313-2314.
37. A.S. Barnard, M. Sternberg, Crystallinity and surface electrostatics of diamond nanocrystals, *J.Mater.Chem.*, 17 (2007) 4811-4819.
38. O.A. Williams, J. Hees, C. Dieker, W. Jager, L. Kirste, C.E. Nebel, Size-Dependent Reactivity of Diamond Nanoparticles, *Acs Nano*, 4 (2010) 4824-4830.
39. B.B. Pate, *Diamond: Electronic Properties and Applications*, Kluwer Academic Publishers, 1995
40. W. Hu, Z.Y. Li, J.L. Yang, Diamond as an inert substrate of graphene, *J.Chem.Phys.*, 138 (2013)
41. L.Y. Ostrovskaya, V.G. Ral'chenko, I.I. Vlasov, A.A. Khomich, A.P. Bol'shakov, Hydrophobic diamond films, *Prot.Met.Phys.Chem.Surf.*, 49 (2013) 325-331.
42. G.V. Lisichkin, Yu.A. Fadeev, A.A. Serdan, P.N. Nesterenko, P.G. Mingalev, D.B. Furman, *Chemistry of grafted surface compounds (Khimiya privitykhpoverkhnostnykh soedinenii)*, Fizmatlit, 2003.
43. H. Sumiya, H. Yusa, T. Inoue, H. Ofuji, T. Irifune, Conditions and mechanism of formation of nano-polycrystalline diamonds on direct transformation from graphite and non-graphitic carbon at high pressure and temperature, *High Pressure Res.*, 26 (2006) 63-69.
44. M. Chaigneau, G. Picardi, H.A. Girard, J.C. Arnault, R. Ossikovski, Laser heating versus phonon confinement effect in the Raman spectra of diamond nanoparticles, *J.Nanopart.Res.*, 14 (2012) 955-955.
45. W. Hongthani, D.J. Fermin, Layer-by-Layer assembly and redox properties of undoped HPHT diamond particles, *Diam.Relat.Mater.*, 19 (2010) 680-684.
46. V.Y. Dolmatov, Detonation synthesis ultradispersed diamonds: Properties and applications, *Usp.Khim.*, 70 (2001) 687-708.
47. B.I. Kharisov, O.V. Kharissova, L. Chavez-Guerrero, *Synthesis Techniques, Properties, and Applications of Nanodiamonds*, *Synth.React.Inorg., Metal-Organic, Nano-Metal Chem.*, 40 (2010) 84-101.
48. V.Ju. Dolmatov, *Detonation nanodiamonds*, NPO Professional (in Russian), 2011.
49. D.F. Mitev, A.T. Townsend, B. Paull, P.N. Nesterenko, Direct sector field ICP-MS determination of metal impurities in detonation nanodiamond, *Carbon*, 60 (2013) 326-334.

50. I.I. Kulakova, *Innovative Superhard Materials and Sustainable Coatings for Advanced Manufacturing*, Springer Netherlands, 2005 (Chapter 29).
51. D.F. Mitev, A.T. Townsend, B. Paull, P.N. Nesterenko, Screening of elemental impurities in commercial detonation nanodiamond using sector field inductively coupled plasma-mass spectrometry, *J.Mater.Sci.*, 49 (2014) 3573-3591.
52. V.Y. Dolmatov, Detonation nanodiamonds: Synthesis, structure, properties and applications, *Usp.Khim.*, 76 (2007) 375-397.
53. D.F. Mitev, A.T. Townsend, B. Paull, P.N. Nesterenko, Microwave-assisted purification of detonation nanodiamond, *Diam.Relat.Mater.*, 48 (2014) 37-46.
54. A.P. Koshcheev, P.V. Gorokhov, M.D. Gromov, A.A. Perov, U. Ott, The chemistry of the surface of modified detonation nanodiamonds of different types, *Russ.J.Phys.Chem.A*, 82 (2008) 1708-1714.
55. A.P. Koshcheev, Thermodesorption mass spectrometry in the light of solution of the problem of certification and unification of the surface properties of detonation nanodiamonds, *Russ.J.Gen.Chem.*, 79 (2009) 2033-2044.
56. G.V. Lisichkin, V.V. Korol'kov, B.N. Tarasevich, I.I. Kulakova, A.V. Karpukhin, Photochemical chlorination of nanodiamond and interaction of its modified surface with C-nucleophiles, *Russ.Chem.B+*, 55 (2006) 2212-2219.
57. S. Osswald, G. Yushin, V. Mochalin, S.O. Kucheyev, Y. Gogotsi, Control of sp<sup>2</sup>/sp<sup>3</sup> carbon ratio and surface chemistry of nanodiamond powders by selective oxidation in air, *J.Am.Chem.Soc.*, 128 (2006) 11635-11642.
58. M.V. Korobov, N.V. Avramenko, A.G. Bogachev, N.N. Rozhkova, E. Osawa, Nanophase of water in nano-diamond gel, *J.Phys.Chem.C.*, 111 (2007) 7330-7334.
59. E. Osawa, Monodisperse single nanodiamond particulates, *Pure Appl.Chem.*, 80 (2008) 1365-1379.
60. V.S. Bondar', A.P. Puzyr', Nanodiamonds for biological investigations, *Phys.Solid State*, 46 (2004) 716-719.
61. P.N. Nesterenko, O.N. Fedyanina, Y.V. Volgin, Microdispersed sintered nanodiamonds as a new stationary phase for high-performance liquid chromatography, *Analyst*, 132 (2007) 403-405.
62. P.N. Nesterenko, O.N. Fedyanina, E. Candish, Proceedings of V Staverovskie Chteniya, 15 Oct. 2009, Krasnoyarsk, Russia, 2009, p.265.
63. B.V. Spitsyn, L.L. Bouilov, B.V. Derjaguin, Vapor Growth of Diamond on Diamond and Other Surfaces, *J.Crystal Growth*, 52 (1981) 219-226.



64. H. Bjorkman, C. Ericson, S. Hjerten, K. Hjort, Diamond microchips for fast chromatography of proteins, *Sensors Actuators B-Chem.*, 79 (2001) 71-77.
65. A.V. Nojkina, N.A. Kolchemanov, P.Y. Dedkov, Sintering of nanodiamond in thermodynamic stability area of diamonds, *Euro PM 2002: Diamond Tool.Proc.*, *Eur.Conf.Hard Mater.Diamond Tool.*, 4 (2002) 151-155.
66. G. Saini, M.A. Vail, A. Dadson, M.R. Linford, Highly stable core shell diamond for solid phase extraction and high performance liquid chromatography, *Abstr.Pap.Am.Chem.S.*, 237 (2009) 343-343.
67. V.R. Dhanak, Y.V. Butenko, A.C. Brieva, P.R. Coxon, L. Alves, L. Siller, Chemical Functionalization of Nanodiamond by Amino Groups: An X-Ray Photoelectron Spectroscopy Study, *J.Nanosci.Nanotechnol.*, 12 (2012) 3084-3090.
68. L.D. Belyakova, S.A. Borovikova, O.G. Larionov, A.A. Revina, L.N. Kolomietz, Physicochemical properties of surfaces of various nanomaterials according to gas-chromatography data, *Prot.Met.Phys.Chem.Surf.*, 47 (2011) 691-697.
69. V.S. Bondar', I.O. Pozdnyakova, A.P. Puzyr', Applications of nanodiamonds for separation and purification of proteins, *Phys.Solid State*, 46 (2004) 758-760.
70. S.C. Hens, G. Cunningham, T. Tyler, S. Moseenkov, V. Kuznetsov, O. Shenderova, Nanodiamond bioconjugate probes and their collection by electrophoresis, *Diam.Relat.Mater.*, 17 (2008) 1858-1866.
71. V.V. Korolkov, I.I. Kulakova, B.N. Tarasevich, G.V. Lisichkin, Dual reaction capacity of hydrogenated nanodiamond, *Diam.Relat.Mater.*, 16 (2007) 2129-2132.
72. S.A. Parkaeva, L.D. Belyakova, O.G. Larionov, Adsorption properties of modified detonation nanodiamond powders based on gas-chromatography data, *Sorption Chromatogr.Processes*, 10 (2010) 283-292.
73. A.P. Puzyr', V.S. Bondar', Patent Application, No 2003119416/15 (2005).
74. J. Xu, E. Bowden, USA Patent Application, No 11/068628 (2005).
75. T. Uchida, A. Hamano, N. Kawashima, S. Takeuchi, Disaggregation and surface modification of nano-sizes diamond by ultrasound exposure - relationships among acoustic intensity, disaggregation, and surface modification, *Trans.Institute Electronics, Information and Communication Engineers A*, J89-A (2006) 93-100100.
76. T. Uchida, A. Hamano, N. Kawashima, S. Takeuchi, Disaggregation and surface modification of nano-size diamond by ultrasound exposure: Relationships among acoustic intensity, disaggregation, and surface modification, *Electron.Commun.Japan Part Iii-Fundament.Electron.Sci.*, 90 (2007) 10-18.

77. D. Mitev, R. Dimitrova, M. Spassova, C. Minchev, S. Stavrev, Surface peculiarities of detonation nanodiamonds in dependence of fabrication and purification methods, *Diam.Relat.Mater.*, 16 (2007) 776-780.
78. I.I. Kulakova, I.T. Gubarevich, V. Dolmatov, A. Rudenko, Chemical properties of detonation-synthesized ultradispersed diamond, *J.Superhard.Mater.*, 22 (2000) 42-4848.
79. V.N. Mochalin, S. Osswald, C. Portet, G.N. Yushin, C. Hobson, M. Havel, Y.G. Gogotsi, *Proceedings of Mater. Res. Soc. Symp.*, 2008, Warrendale, PA USA, 2008, p.1089.
80. C. Popov, W. Kulisch, S. Bliznakov, G. Ceccone, D. Gilliland, L. Sirghi, F. Rossi, Surface modification of nanocrystalline diamond/amorphous carbon composite films, *Diam.Relat.Mater.*, 17 (2008) 1229-1234.
81. G.A. Chiganova, V.A. Bondar, A.S. Chiganov, Electrophoretic Behavior of Hydrosols of Ultradisperse Diamond and Modification of Its Surface, *Colloid J.Russ.Acad.Sci.*, 55 (1993) 774-775.
82. G.A. Chiganova, Aggregation of particles in ultradispersed diamond hydrosols, *Colloid J.*, 62 (2000) 238-243.
83. X. Xu, Zh. Yu, Y. Zhu, B. Wang, Effect of sodium oleate adsorption on the colloidal stability and zeta potential of detonation synthesized diamond particles in aqueous solutions, *Diam.Relat.Mater.*, 14 (2005) 206-212212.
84. U. Maitra, A. Gomathi, C.N.R. Rao, Covalent and noncovalent functionalisation and solubilisation of nanodiamond, *J.Exp.Nanosci.*, 3 (2008) 271-278.
85. L.A. Wiest, G. Saini, S.S. Tartakoff, S.L. Castle, M.A. Vail, A. Dadson, M.R. Linford, Direct attachment of epoxides and isocyanates to hydroxyl-terminated microdiamond surfaces for use in chemical separations, *Abstr.Pap.Am.Chem.S.*, 237 (2009) 337-337.
86. G. Saini, L. Yang, M.L. Lee, A. Dadson, M.A. Vail, M.R. Linford, Amino-modified diamond as a durable stationary phase for solid-phase extraction, *Anal.Chem.*, 80 (2008) 6253-6259.
87. M.R. Linford, D.S. Jensen, L.A. Wiest, Patent Application, No US 12/557,503 (2012).
88. S. Ida, T. Tsubota, S. Tanii, M. Nagata, Y. Matsumoto, Chemical modification of the diamond surface using benzoyl peroxide and dicarboxylic acids, *Langmuir*, 19 (2003) 9693-9698.

89. L. Yang, M.A. Vail, A. Dadson, M.L. Lee, M.C. Asplund, M.R. Linford, Functionalization of Deuterium- and Hydrogen-Terminated Diamond Particles with Mono- and Multilayers using Di-tert-Amyl Peroxide and Their Use in Solid Phase Extraction, *Chem.Mater.*, 21 (2009) 4359-4365.
90. M.R. Linford, L. Yang, L.A. Wiest, Patent Application, No US 12/463,414 (2012).
91. L. Yang, M.A. Vail, A. Dadson, M.R. Linford, Direct polymer attachment on hydrogen/deuterium-terminated diamond particles with solid phase extraction on the resulting sorbents, *Abstr.Pap.Am.Chem.S.*, 237 (2009) 323-323.
92. E.P. Nesterenko, P.N. Nesterenko, D. Connolly, X.Y. He, P. Floris, E. Duffy, B. Paull, Nano-particle modified stationary phases for high-performance liquid chromatography, *Analyst*, 138 (2013) 4229-4254.
93. T.L. Mariani, R.P. Hirschmann, D.A. Cupolo, C.J. Peterman, Patent Application, No GB19670010258 19670303 (1967).
94. L.D. Belyakova, A.K. Buryak, O.G. Larionov, Chromatography: Method of Investigation of Surface Chemistry and Interface Processes, *Prot.Met.Phys.Chem.Surf.*, 49 (2013) 605-626.
95. S.V. Mikhailovsky, K.J. Rutt, B.A. Patel, V.I. Padalko, V.V. Turov, V.M. Bogatyrev, V.M. Gun'ko, *Innovative Superhard Materials and Sustainable Coatings for Advanced Manufacturing*, Springer Netherlands, 2005 (Chapter 11).
96. P.N. Nesterenko, O.N. Fedyanina, Properties of microdispersed sintered nanodiamonds as a stationary phase for normal-phase high performance liquid chromatography, *J.Chromatogr.A*, 1217 (2010) 498-505.
97. B.A. Patel, K.J. Rutt, V.I. Padalko, S.V. Mikhailovsky, Use of industrial diamonds in HPLC, *J.Superhard.Mater.*, 6 (2002) 51-55.
98. S.A. Emelina, O.G. Larionov, B.V. Spitsyn, Proceedings of X International Conference: "Theoretical problems of chemistry of the surface, adsorption and chromatography", 24 Apr. 2006, Moscow, Klyasma, 2006, p.125.
99. P.N. Nesterenko, O.N. Fedyanina, A.A. Peristy, B. Paull, Proceedings of HPLC-2013, 18 Nov. 2013, Hobart, Australia, 2013,
100. A.A. Peristy, P.N. Nesterenko, B. Paull, Proceedings of HPLC-2013, 18 Nov. 2013, Hobart, Australia, 2013,
101. B.V. Spitsyn, S.A. Denisov, N.A. Skorik, A.G. Chopurova, S.A. Parkaeva, L.D. Belyakova, O.G. Larionov, The physical-chemical study of detonation nanodiamond application in adsorption and chromatography, *Diam.Relat.Mater.*, 19 (2010) 123-127.

102. I.A. Bardina, N.V. Kovaleva, Y.S. Nikitin, Chromatographic retention and the thermodynamic characteristics of adsorption on an active carbon for a number of organic compounds in the Henry region, *Russ.J.Phys.Chem.*, 78 (2004) 970-974.
103. L.D. Belyakova, A.M. Voloshchuk, L.M. Vorobeva, A.O. Larionova, O.G. Larionov, Effect of Carbon Adsorbents of Porous Structure on Chromatographic Retaining of Different Adsorbates, *Zh.Fiz.Khim.*, 69 (1995) 501-505.
104. A.V. Kiselev, Ya.I. Yashin, Gas-adsorption chromatography, New York : Plenum Press, 1969.
105. A. Vereshchagin, E. Petrov, G. Sakovich, V. Komarov, A. Klimov, N. Kozyrev, Russia Patent Application, No 2051092 (1995).
106. Y. Gogotsi, T. Kraft, K.G. Nickel, M.E. Zvanut, Hydrothermal behavior of diamond, *Diam.Relat.Mater.*, 7 (1998) 1459-1465.
107. A. Nuamthanom, P.M. Donaldson, J. Stokes, J.C. Ford, Proceedings of Duquesne University 2000 Summer Research Symposium, 26 June 2008, Pittsburgh, PA, 2008,
108. N.A. Skorik, A.L. Krivozubov, A.P. Karzhenevskii, B.V. Spitsyn, Physicochemical study of the nanodiamond surface, *Prot.Met.Phys.Chem.Surf.*, 47 (2011) 54-58.
109. A.N. Zhukov, F.R. Gareeva, A.E. Aleksenskii, A.Y. Vul, Surface charge of detonation nanodiamond particles in aqueous solutions of simple 1: 1 Electrolytes, *Colloid J.*, 72 (2010) 640-646.
110. G.A. Chiganova, Investigation of surface properties of ultradispersed diamond, *Colloid J.*, 56 (1994) 266-268.
111. S.I. Chukhaeva, L.A. Cheburina, Sorption activity of nanodiamonds on cesium, *J.Superhard.Mater.*, 2 (2000) 43-48.
112. H. Sakurai, N. Ebihara, E. Osawa, M. Takahashi, M. Fujinami, K. Oguma, Adsorption characteristics of a nanodiamond for oxoacid anions and their application to the selective preconcentration of tungstate in water samples, *Anal.Sci.*, 22 (2006) 357-362.
113. S.K. Gordeev, O.G. Taushkanova, E.P. Smirnov, L.M. Martynova, Reaction of Solutions of Alkali Hydroxides and Alkali Earth Metals with Diamond Preparations, *Zh.Obshch.Khim.*, 53 (1983) 2426-2428.
114. Y.A. Kokotov, Ionites and ion exchange, Leningrad: Chemistry, 1980.
115. P.N. Nesterenko, P. Jones, B. Paull, High Performance Chelation Ion Chromatography, RSC, 2011.
116. V.I. Kuchuk, E.V. Golikova, Y.M. Chernoberezhskii, Potentiometric Titration of A Natural Diamond Micropowder, *Colloid J.USSR*, 46 (1984) 982-987.

117. A.T. Karczemska, D. Witkowski, V. Ralchenko, A. Bolshakov, D. Sovyk, J.M. Lysko, M. Fijalkowski, J. Bodzenta, J. Hassard, Diamond electrophoretic microchips- Joule heating effects, *Mater.Sci.Eng., B*, 176 (2011) 326-330.
118. P. Khanna, A. Villagra, S. Kim, E. Seto, M. Jaroszeski, A. Kumar, S. Bhansali, Use of nanocrystalline diamond for microfluidic lab-on-a-chip, *Diam.Relat.Mater.*, 15 (2006) 2073-2077.
119. K.V. Purtov, V.S. Bondar', A.P. Puzyr', Russia Patent Application, No RF2352387 (2009).

## Chapter 2. General experimental

### 2.1. Instrumentation

Thermogravimetric analysis (TGA) and differential scanning calorimetry (DSC) were carried out on a Labsys EVO instrument (Setaram, Box Hill, VIC, Australia); Calisto Processing software was used for data acquisition and management. All runs were performed using UHP nitrogen or air, with Al<sub>2</sub>O<sub>3</sub> crucibles and a scanning rate of 10 °C per minute.

Titration experiments were done with a Metrohm 809 Titrando autotitrator with Tiamo 1.2 software (Mitcham, VIC, Australia). Fytik software (GitHub, San-Francisco, CA, USA) was used for Gaussian peak-fitting.

A Nanoseries zetasizer Model Zen3600 (Malvern Instruments, Malvern, Worcestershire, UK) was used for  $\zeta$ -potential measurements. The Smoluchowski approximation for large particle sizes (1-2  $\mu$ m) and high ionic strengths (100 mM) was used according to [1]. pH of suspensions was adjusted with either NaOH or HNO<sub>3</sub>.

Specific surface areas were calculated based upon BET adsorption/desorption method using a TriStar II 3020 (Micrometrics Gemini, Georgia, USA) instrument. Before measurements the samples were heated at 100 °C in vacuum overnight.

Imaging of HPHT diamond particles was carried out using Hitachi SU-70 (Hitachi Ltd., Chiyoda, Tokyo, TKY, Japan) field emission scanning electron microscope and 1.5 keV electron beam. All samples were platinum-sputtered prior to analysis. An Oxford AZtec 2.3 EDS/EBSD system was used for the investigation of diamond surface composition and the presence of impurities by EDS\*.

FTIR spectra of HPHT diamond were obtained using Bruker MPA infrared spectrometer (Billerica, MA, USA). Prior to measuring FTIR spectra, HPHT diamond powder was dried overnight at 100 °C in a vacuum oven (0.4 atm). Potassium bromide tablets containing 5% w/w dried diamond powder were used for collecting spectra. Raman spectra were measured with Bruker FRA 106 Raman spectrometer coupled with a Raman Scope (microscope) (Billerica, MA, USA)\*.

Accela 1250 UHPLC (Thermo Fisher Scientific, Waltham, MA, USA) was used for evaluation of HPHT diamond and PGC columns. Photometric detection at 254 nm was used

---

\* The author gratefully acknowledges use of the services and instruments of Central Science Laboratory of University of Tasmania. Special thanks to Dr Karsten Goemann and Dr Sandrin Feig for their assistance in acquisition and interpretation of SEM images and EDS spectra, and to Dr Thomas Rodemann for the help with FTIR spectra measurements

unless otherwise stated. ChromQuest<sup>TM</sup> software (Thermo Fisher Scientific, Waltham, MA, USA) was used for operating the UHPLC system and processing the chromatographic data. Retention factors for the analytes were calculated based on the peak maximum, and void volume was determined as described in the Section 2.4.2. Column efficiency and peak asymmetry were calculated according to IUPAC recommendations [2] using peak width at 10% height. For the peaks with high asymmetry factors ( $A_s > 1.2$ ), Exponentially Modified Gaussian (EMG) model was applied for the calculation of peak parameters [3].

## 2.2. Reagents

Industrial non-porous high pressure high temperature (HPHT) diamond (Grade 2, fraction of 1-2  $\mu\text{m}$  particle size) was purchased from Hunan Real Tech Superabrasive & Tool Co. Ltd. (Changsha city, Hunan, China). Empty stainless steel columns (100  $\times$  4.6 mm ID and 50  $\times$  4.6 mm ID) were purchased from Phenomenex (Lane Cove West, NSW, Australia). A Hypercarb<sup>TM</sup> column (100  $\times$  4.6 mm ID) packed with 5  $\mu\text{m}$  porous graphitic carbon (PGC) particles (Shandon HPLC, Runcorn, Cheshire, UK) and a 150  $\times$  4.0 mm ID column packed with 3-6  $\mu\text{m}$  particles of microdispersed sintered detonation nanodiamond (MSDN, see description in [4]) were used for comparative studies.

Deionised water (DIW) was obtained from a Milli-Q (USA) system and was used for the sedimentation and purification of diamond, as well as for mobile phases and solute standards. 2-propanol (IPA), *n*-hexane (both from Chem-Supply, Gillman, SA, Australia), dimethyl sulfoxide (DMSO), acetonitrile (ACN), methanol (MeOH) (all from Sigma-Aldrich, Castle Hill, NSW, Australia),  $\text{CH}_3\text{COONH}_4$  (Univar, Ingleburn, NSW, Australia), formamide (Ajax Chemicals, Thermo Fisher, Scoresby, VIC, Australia), were used for the preparation of mobile phases, titration experiments and column packing. Solutions of NaOH and  $\text{HNO}_3$  (both from Chem-Supply, Gillman, SA, Australia) were used for fractionation by sedimentation, and purification of HPHT diamond. KOH (Sigma-Aldrich, Castle Hill, NSW, Australia),  $\text{NH}_4\text{OH}$  (Chem-Supply, Gillman, SA, Australia), tetramethylammonium hydroxide (TMAOH) (Sigma-Aldrich, Castle Hill, NSW, Australia), NaCl (Ajax Chemicals, Thermo Fisher, Scoresby, VIC, Australia), formic acid (Univar, Downers Grove, IL, USA), acetic acid (BDH chemicals, Murarrie, QLD, Australia), trifluoroacetic acid (TFA) (Sigma-Aldrich, Castle Hill, NSW, Australia) and HCl (Merck KGaA, Darmstadt, Germany) were used for the preparation of buffers and titration experiments. Potassium hydrogen phthalate (KHP) (Sigma-Aldrich, Castle Hill, NSW, Australia) was used for standardisation of buffers and titration standards. Pure solute standards for the chromatographic characterisation of

HPHT diamond were supplied by Sigma-Aldrich (Castle Hill, NSW, Australia). All solvents were HPLC grade; all chemicals used in buffer preparation were at least >99% grade, and all solute standards were at least >98% grade. All solvents were degassed prior to use and stored in airtight containers. All aqueous solutions were handled in plastic containers, and solutions containing organic phase were stored in glass bottles and vials.

KOH (Sigma-Aldrich, Castle Hill, NSW, Australia), methanesulphonic acid (Thermo Fisher, Scoresby, VIC, Australia), NaNO<sub>3</sub> (VWR International, Murarrie, QLD, Australia), Na<sub>3</sub>PO<sub>4</sub> (VWR International, Murarrie, QLD, Australia), Na<sub>2</sub>SO<sub>4</sub> (Sigma-Aldrich, Castle Hill, NSW, Australia) and Na<sub>2</sub>CO<sub>3</sub> (Ajax Chemicals, Thermo Fisher, Scoresby, VIC, Australia) were used for the preparation of buffers, and for the investigation of the influence of column conditioning upon the retention.

The following substances were used for the preparation of adsorbate solutions of cations and anions, buffer solutions and as reagents for UV-determination: MnSO<sub>4</sub>, NaClO<sub>4</sub>, Hexamine (99%, all from AJAX Chemicals, Thermo Fisher, Scoresby, VIC, Australia), Zn(NO<sub>3</sub>)<sub>2</sub>, CoSO<sub>4</sub>, CuCl<sub>2</sub>, CuSO<sub>4</sub>, Na<sub>2</sub>SO<sub>4</sub>, Cu(NO<sub>3</sub>)<sub>2</sub>, Na<sub>2</sub>C<sub>2</sub>O<sub>4</sub>, NaCl, Na<sub>2</sub>B<sub>4</sub>O<sub>7</sub>, o-Cresolphthalein (99%, all from Sigma-Aldrich, Castle Hill, NSW, Australia), Cd(NO<sub>3</sub>)<sub>2</sub>, NiSO<sub>4</sub>, Al(NO<sub>3</sub>)<sub>3</sub>, Na<sub>3</sub>PO<sub>4</sub>, NaI, CH<sub>3</sub>COOH (99%, all from VWR International, Murarrie, QLD, Australia), Fe(NO<sub>3</sub>)<sub>3</sub>, HNO<sub>3</sub>, H<sub>2</sub>SO<sub>4</sub> (99%, all from Chem-Supply, Gillman, SA, Australia), 4-(2-pyridylazo)resorcinol (98%, Kodak, Rochester, NY, USA), Chromeazurol-S (85%, Riedel-de-Haën, Sigma-Aldrich, Seelze, Germany), CH<sub>3</sub>COONa, KH<sub>2</sub>PO<sub>4</sub>, H<sub>3</sub>PO<sub>4</sub> (99%, all from Univar, Ingleburn, NSW, Australia), NaOH (99% Scharlau, Sentmenat, Barcelona, Spain).

## **2.3. Methods**

### **2.3.1. Preparation of HPHT diamond microparticles**

As it was previously reported, this batch of diamond powder showed the presence of the following major impurities: Si, W, Ta, Al, and Mn [5,6]. According to Dolmatov, treatment with concentrated HNO<sub>3</sub> is the most effective method for removal of metal impurities and non-diamond carbon from diamond materials [7]. Accordingly, it was decided to use this method in order to eliminate W, Ta, Al and Mn from HPHT diamond. Additionally, purification with boiling 40% NaOH (2.5 mL per 1.0 g of diamond) was applied for 30 min in order to dissolve silica (or silicate) impurities, which have amphoteric character and are soluble in hot concentrated NaOH. Since Si is a major impurity (see Section 3.3.1.1), the treatment with NaOH was done first and the excess of 5 M HNO<sub>3</sub> was applied



afterwards, followed by intensive flushing with DIW between and after treatments. The HPHT diamond was removed from the solutions by means of centrifugation with subsequent decanting. The washoffs after the treatment with 40% NaOH were used for the determination of silica presence, as described in the Section 3.3.1.1.

After the HPHT diamond had been purified, it was subjected to multiple sedimentations in the presence of 10 mM aqueous NaOH. This solution was chosen based on test sedimentation experiments described in Sections 3.3.2.2. Sedimentations were carried out in tall measuring cylinders (500 cm<sup>3</sup> or 1000 cm<sup>3</sup>, height of solvent (*H*) 21 cm was used, see Fig. 2.1). Slurry with a concentration of 10 mg·mL<sup>-1</sup> was used. Fractionation was done in two steps. First, long time intervals were applied (18 or 24 hours), after which the supernatant along with the fine fractions of diamond (<1 μm particle size) were discarded. This step was performed at least 30 times, until the supernatant was clear and did not precipitate agglomerates of fine diamond dust upon acidification. During the second step, shorter time intervals were used (6 or 12 hours). Particles of diamond which were large enough (>1.4 μm) to sediment during this time were discarded, and the supernatant was re-dispersed and subjected to another 6 or 12 hour sedimentation. This was repeated until no sediment was formed within 6 or 12 hours (at least 30 times). Finally, after the last sedimentation cycle, the diamond was washed with the excess of DIW and dried in air. The yield of fractionated diamond was typically within 10-20% (w/w).

### **2.3.2. Aqueous titration**

An aqueous solution of ~5 mM KOH and of 1 M NaCl (for the maintaining of the ionic strength) was used for titration. Prior to each run, KOH was standardised by titration with KHP. The HPHT diamond was previously subjected to the sedimentation in the presence of 10 mM NaOH (see Section 2.3.1), so it was assumed that all surface COOH groups would be dissociated. 1.000 g of HPHT diamond was placed in an 80 mL beaker followed by an addition of 30.0 mL of 2.271 mM HCl (again, 1 M NaCl was added to HCl solution for maintaining ionic strength). This ensured that all surface groups were reprotonated (pH of suspension was around 3.0). During titration, the excess of HCl was titrated first. The second titration peak was a broad one and can be attributed to carboxyl groups which have different pK<sub>a</sub> values depending on their environments. By subtracting the total amount of KOH used for the titration from the amount of HCl added prior to the titration, the amount of the residual NaOH can be obtained, which was present in the HPHT diamond after the

sedimentation. Overall, the value for the amount of carboxylic groups per gram of HPHT diamond was calculated from each experiment.

### **2.3.3. Titration in water-organic mixtures**

Volumetric titration in water-organic mixtures was performed using in 80% CAN – 20% DIW and 80% MeOH – 20% DIW. TMAOH, standardised with KHP was used as titration agent. Again, 1.000 g of HPHT diamond was taken and an excess of HCl (23.6  $\mu\text{mol}$ ) was added in order to protonate all surface groups. Similar to above, two values were obtained for the excess of HCl added prior to titration and the amount of COOH groups per gram of the HPHT diamond. Last value was compared with the results obtained in aqueous conditions to understand how the dissociation processes on the diamond surface are affected by the presence of an organic phase.

### **2.3.4. Column packing**

The system for column packing consisted of a Haskel DSF-122 air driven liquid pump (Haskel International Inc., Burbank, CA, USA), a 30 mL stainless steel slurry reservoir, 150  $\times$  4.6 mm ID column connection and 100  $\times$  4.6 mm ID or 50  $\times$  4.6 mm ID empty columns with 0.5  $\mu\text{m}$  pore size frits. For comparison purposes, another 50  $\times$  4.6 mm ID column was packed into a Thermo Fisher column body (Thermo Fisher Scientific, Waltham, MA, USA), in order to assess the influence of column design on the chromatographic performance of HPHT diamond\*. A slurry containing 0.2  $\text{g}\cdot\text{mL}^{-1}$  of HPHT diamond powder was prepared in 10 mM NaOH. Volume of slurry was chosen considering the packing density of 2.2  $\text{g}\cdot\text{mL}^{-1}$  with 20% excess (11 mL and 22 mL for 50 and 100 mm long columns, respectively). Slurry was placed in the reservoir and the rest of the reservoir was filled with 10 mM NaOH solution. DIW was used as the pump fluid.

During the packing procedure, the pump was operated manually. A fast pressure increase is important to minimise sedimentation of the diamond particles. However, as mentioned in introduction, brittle diamond may be fractured if the pressure wave applied is too intense. Accordingly, the pressure program included a surge from 0 to 5500 psi within 2-3 seconds at the beginning of packing, followed by a further linear rise from 5500 psi to a target pressure (usually 10000 or 15000 psi) within 2-3 min. Pressure was held at a target level until 250 mL of water was pumped through the column. Then the slurry reservoir was

---

\* Author gratefully acknowledges Prof. Andrew Shalliker for the column provision and useful discussions of van Deemter experiments.

disconnected and the column was reconnected to an UHPLC instrument and conditioned by passing 6 mL of IPA at flow rate  $0.1 \text{ mL}\cdot\text{min}^{-1}$ . Finally, the column was conditioned with the mobile phase (*n*-hexane/IPA) at  $0.5 \text{ mL}\cdot\text{min}^{-1}$  until constant ( $\pm 1\%$ ) retention times were observed for the test substances.

Different packing temperatures were tried in order to obtain ideal packing conditions. If high temperature packing was used, packing was performed in two steps. First, pressure was increased to 5500 psi, and held until 30 mL of liquid had been eluted. After that, the pressure was released, slurry reservoir removed, and the column with extension was placed inside a column heater. After the required packing temperature was achieved, pressure was increased to its target value (usually 15000 psi) again, and the packing continued until 250 mL of liquid had passed through the column. After pressure was released, fittings were connected to the column while it was still hot.

## 2.4. Calculations

### 2.4.1. Sedimentation analysis of particle size distribution

Particle size distribution for HPHT diamond was established by sedimentation analysis. The main idea for the sedimentation analysis was taken from [8]. For a uniformly descending particle in liquid, gravitational force (including buoyancy) is equal to liquid friction. Archimedes law was used for calculating gravitational force, and Stokes law – for liquid friction (for spherical particles):

$$4/3\pi r^3 g(\rho_D - \rho_A) = 6\pi\eta r U \quad (\text{Equation 2.1})$$

Here,  $r$  is particle radius (m),  $g$  is gravitational constant ( $9.81 \text{ m}\cdot\text{s}^{-2}$ ),  $\rho_D$  is density of diamond ( $\text{kg}\cdot\text{m}^{-3}$ ),  $\rho_A$  is density of solvent A ( $\text{kg}\cdot\text{m}^{-3}$ ),  $\eta$  is viscosity of dispersant ( $\text{Pa}\cdot\text{s}$ ) and  $U$  is velocity of diamond particle ( $\text{m}\cdot\text{s}^{-1}$ ).  $U$  can be written as:

$$U(d_x) = H/t_x \quad (\text{Equation 2.2})$$

where  $U(d_x)$  is velocity of particle with diameter  $d_x$  ( $\text{m}\cdot\text{s}^{-1}$ ),  $H$  is the path length (height of cylinder for sedimentation, m), and  $t_x$  is the time for sedimentation for particle with size  $d_x$  (s). After substituting  $d = 2r$ , and combining Eqn. 2.1 and Eqn. 2.2, it can be written:

$$t_x = 18\eta H / (d_x^2 \cdot g(\rho_D - \rho_A)) \quad (\text{Equation 2.3})$$

This equation describes the time  $t_x$  when all particles with size  $d_x$ , will be completely sedimented in a cylinder of height  $H$  in solvent A. Clearly, sedimentation time correlates with the inverse second order of particle size.

The following setup was used for the sedimentation analysis (Fig. 2.1). A cylinder (21 cm height) was taken and filled with suspension of HPHT diamond. A glass plate, with a

diameter slightly smaller than that of the cylinder was submerged into the suspension, so it did not touch the bottom or the walls of the glass. By means of a scale beam and stainless steel wire, this plate was connected to a plummet on a balance. Therefore, during the experiment the weight of the plate with diamond sediment was increasing, and the weight of plummet on the balance was decreasing. The value from balance was recorded on a computer with a sampling rate of 1 Hz using an RSR232 Data Logger (software by Eltima, Frankfurt, Germany). A plot of plate weight v time was built afterwards and used for calculation of particle size distribution.

Fig. 2.2 presents the typical dependence obtained as described above. In the beginning, sedimentation of particles with all sizes happened, so the weight gain ( $W$ ) on the plate was highest and constant. This resulted in linear dependence of  $W$  on  $t$  at the beginning. After certain time  $t_{min}$ , all particles size bigger than  $d_{max}$  were sedimented, so the curvature was observed on the graph. As the time went on, more particle size fractions were completing their sedimentation, until finally all the smallest particles ( $d_{min}$ ) reached the plate by the time  $t_{max}$ . After this time weight of the plate was constant and the curve on the graph levelled off. Total weight of particles on the plate was  $W_0$  at the end of sedimentation.

As it is clear from Fig. 2.2, each time,  $t_x$ , can be matched to the weight of diamond sedimented during that time ( $W(t_x)$ ) and the fraction size,  $d_x$ , above which all particles have already completed sedimentation. Value of the intersection point between y-axis and tangent to the sedimentation curve at  $t_x$  yielded the weight,  $W_x$ , of all particles with size above  $d_x$ . The following formula was used to find  $W_x$  values, using the value of weight gradient at the moment,  $t_x$ :

$$W_x = W(t_x) - t_x \cdot (\partial W / \partial t)_x \quad (\text{Equation 2.4})$$

Accordingly, the weight fraction  $Q_x$  of particle with sizes above  $d_x$  was found as:

$$Q_x = W_x / W_0 = (W(t_x) - t_x \cdot (\partial W / \partial t)_x) / W_0 \quad (\text{Equation 2.5})$$

By taking the derivative of  $Q_x$  in respect to  $d_x$ , a classic particle size distribution was obtained, in terms of sedimentation time, rather than particle size:

$$q_x = \partial Q_x / \partial d_x = (1/W_0) \cdot \partial [W(t_x) - t_x \cdot (\partial W / \partial t)_x] / \partial d_x \quad (\text{Equation 2.6})$$

Here  $q_x$  is the fraction of particles with size  $d_x$ . In order to build this dependence in terms of particle size, it was necessary use Eqn. 2.3, which correlates these two parameters. Substituting Eqn. 2.3 into Eqn. 2.6 gives:

$$q_x = (1/W_0) \cdot \partial [W(t_x) - (18\eta H \cdot (\partial W / \partial t)_x) / (d_x^2 \cdot g(\rho_D - \rho_A))] / \partial d_x \quad (\text{Equation 2.7})$$

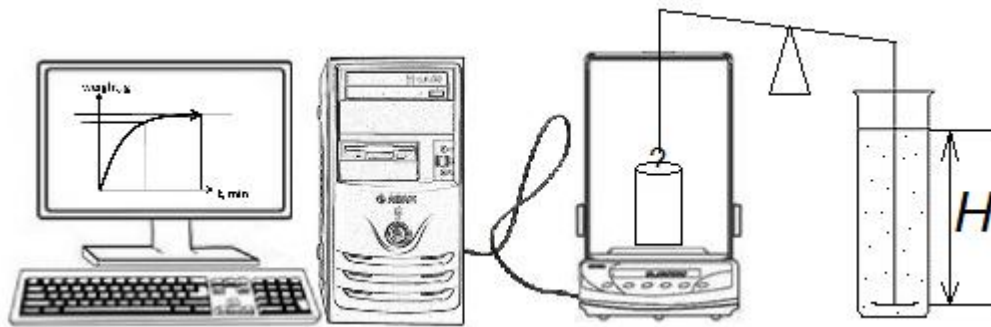


Fig. 2.1. Scheme of a setup for sedimentation analysis.

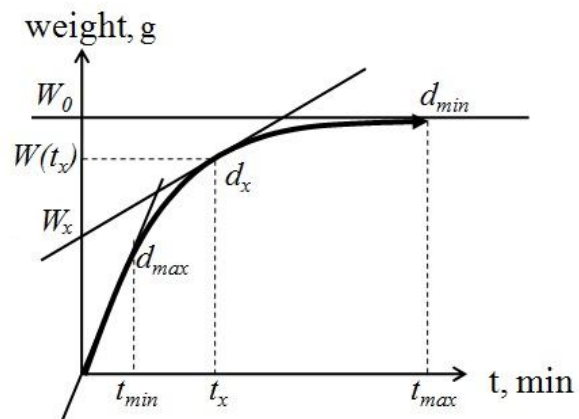


Fig. 2.2. Sedimentation curve (weight of diamond v time) obtained for calculation of particle size distributions. Each time,  $t_x$ , can be matched to the weight of diamond sedimented during that time ( $W(t_x)$ ) and the fraction size,  $d_x$ , above which all particles have already completed sedimentation.

This last equation was used to build particle size distributions. Values of  $W_0$  and  $W(t_x)$  were measured from sedimentation curve,  $d_x$  values were taken with increments of 0.1 or 0.2  $\mu\text{m}$ , and other values are constants.

#### 2.4.2. Determination of void volume and phase ratio of HPHT diamond column

On a daily basis the void volume was evaluated by the injection peak of hexane in NP-HPLC or ACN in HILIC/ANP chromatography modes. Additionally, the true void volume of the column was calculated by measuring the difference between weight of the column filled with either  $\text{CH}_2\text{Cl}_2$  ( $\rho = 1.326 \text{ g}\cdot\text{mL}^{-1}$ ) or hexane ( $\rho = 0.659 \text{ g}\cdot\text{mL}^{-1}$ ) at the room temperature (20 °C). The calculated volume of mobile phase in the column ( $V_M$ ) was  $352.8 \pm 3.5 \mu\text{L}$  for  $50 \times 4.6 \text{ mm}$  I.D. column at 20 °C, which matches the void volume ( $V_0$ ) calculated from the void time ( $t_0$ ) of 0.73 min measured from the peak of injected hexane at flow rate  $0.5 \text{ mL}\cdot\text{min}^{-1}$ . The volume of diamond particles in the column ( $V_S$ ) was also calculated by subtraction of  $V_M$  value from the volume of empty column as  $V_S = 830.5 - 352.8 = 477.7 \mu\text{L}$ .

It should be noted that the  $V_S$  value does not change with the variation of temperature or mobile phase composition, due to negligible thermal expansion of the diamond and absence of swelling in organic solvents.  $V_M(T)$ , however depends on the temperature due to the difference in thermal expansion of column body and stationary phase. Void volume of the instrument  $V_0(T)$  (which depends on the temperature) can be calculated at each temperature by carefully recording the solvent mismatch peak and multiplying this value by the flow rate:

$$V_0(T) = F \cdot t_0(T) \quad (\text{Equation 2.8})$$

Where  $F$  is flow rate ( $\text{mL}\cdot\text{min}^{-1}$ ) and  $t_0(T)$  is void time (min), which depends on temperature. This instrument void consists of the true volume of mobile phase in the column  $V_M(T)$  and volume of connectors and tubing ( $V_{C+T} = 11.7 \mu\text{L}$  which should not be considered in calculations of the phase ratio).  $V_M(T)$  can be found accordingly at each temperature:

$$V_M(T) = V_0(T) - V_{C+T} = F \cdot t_0(T) - V_{C+T} \quad (\text{Equation 2.9})$$

Finally, phase ratio can be calculated at each temperature:

$$\beta(T) = V_M(T)/V_S = (F \cdot t_0(T) - V_{C+T})/V_S \quad (\text{Equation 2.10})$$

Although usually for non-porous adsorbents phase ratio is calculated using the ratio of the surface area of stationary phase to the volume of mobile phase, in the present work this approach was not applied. This is because  $\beta$  values calculated in such manner would have the units of  $\text{m}^{-1}$  and depend on the units used, making the calculation of  $\log\beta$  meaningless. At the same time, no error is introduced in this work when  $\beta$  is defined as in the Eqn. 2.10, because only particles with the same size distribution are compared.

### 2.4.3. Van't Hoff plots

Van't Hoff's equation (Eqn. 2.11) was used for calculation of thermodynamic parameters of retention.

$$\ln k = -\Delta H^\circ/RT + \Delta S^\circ/R + \ln\beta(T) \quad (\text{Equation 2.11})$$

Here  $k$  is the retention factor,  $\Delta H^\circ$  is enthalpy,  $\Delta S^\circ$  is entropy and  $\beta(T)$  is column phase ratio. Retention factors were measured in the temperature interval 5 – 75 °C, and phase ratio was calculated at each temperature, as described in Section 2.4.2.

As mentioned above, due to the expansion of the column body, the column phase ratio exhibited a linear dependence on the temperature. A situation where the phase ratio is not constant was analysed by Chester and Coym [9], who proposed a way of calculating thermodynamic parameters using selectivity values instead of  $k$ , to account for the influence of the variable phase ratio on the thermodynamic parameters. However in [8] non-linear  $\ln\beta$  and  $k$  vs  $1/T$  plots were analysed, which is a more complicated setup, as compared to the linear plots observed for the HPHT diamond column. Therefore a more simple approach can be used for calculating enthalpy and entropy for diamond columns. In order to account for the linear change in phase ratio with temperature,  $\ln\beta$  can be presented in the form of:

$$\ln\beta = \text{const}_1/T + \text{const}_2 \quad (\text{Equation 2.12})$$

Accordingly, the van't Hoff equation can be written as:

$$\ln k = -\Delta H^\circ/RT + \Delta S^\circ/R + \text{const}_1/T + \text{const}_2 = (-\Delta H^\circ/R + \text{const}_1)/T + (\Delta S^\circ/R + \text{const}_2) \quad (\text{Equation 2.13})$$

Parameters  $\text{const}_1$  and  $\text{const}_2$  can be calculated from the  $\ln\beta$  vs  $1/T$  plot and substituted to Eqn. 2.13. Finally, by analysing the slope and y-intercept in the  $\ln k$  vs  $1/T$  plot and subtracting the values of  $\text{const}_1$  and  $\text{const}_2$ , the true enthalpy and entropy can be calculated for each compound.

### 2.5. Reference List

1. R.J. Hunter, Zeta potential in colloid science: principles and applications, Academic Press, London; New York, 1981.
2. L.S. Ettre, Nomenclature for Chromatography, Pure Appl.Chem., 65 (1993) 819-872.
3. J.R. Torres-Lapasio, J.J. Baeza-Baeza, M.C. Garcia-Alvarez-Coque, A model for the description, simulation, and deconvolution of skewed chromatographic peaks, Anal.Chem., 69 (1997) 3822-3831.

4. P.N. Nesterenko, O.N. Fedyanina, Properties of microdispersed sintered nanodiamonds as a stationary phase for normal-phase high performance liquid chromatography, *J.Chromatogr.A*, 1217 (2010) 498-505.
5. D.F. Mitev, A.T. Townsend, B. Paull, P.N. Nesterenko, Direct sector field ICP-MS determination of metal impurities in detonation nanodiamond, *Carbon*, 60 (2013) 326-334.
6. D.F. Mitev, A.T. Townsend, B. Paull, P.N. Nesterenko, Screening of elemental impurities in commercial detonation nanodiamond using sector field inductively coupled plasma-mass spectrometry, *J.Mater.Sci.*, 49 (2014) 3573-3591.
7. V.Ju. Dolmatov, Detonation nanodiamonds, NPO Professional (in Russian), Saint-Petersburg, 2011.
8. J.S. Smith, R. Gardenier, Determination of Particle Size Distributions by A Sedimentation Method, *Anal.Chem.*, 25 (1953) 577-581.
9. T.L. Chester, J.W. Coym, Effect of phase ratio on van't Hoff analysis in reversed-phase liquid chromatography, and phase-ratio-independent estimation of transfer enthalpy, *J.Chromatogr.A*, 1003 (2003) 101-111.



## Chapter 3. Preparation and characterisation of synthetic diamond stationary phase for liquid chromatography and optimisation of column packing procedure

### 3.1. Introduction

As discussed in Chapter 1, the majority of modern LC techniques are based on the use of silica based stationary phases, with polymer sorbents being the second most abundant. Since these silica and polymeric sorbents share some certain disadvantages in terms of their applicability under conditions of high temperature, pressure and aggressive mobile phases, carbon materials, especially diamond, are considered as a promising alternative.

Advantages of diamond based adsorbents for application in HPLC, such as chemical and mechanical stability, thermal conductivity and the possibility of surface modification have been discussed previously in Chapter 1. However, there are also several problems related to the use of HPHT diamond in HPLC, which need to be solved in order to prepare a suitable chromatographic column. First of all, HPHT diamond is a hard but brittle material, and no spherical particles are commercially available. Secondly, due to its non-porous structure, the surface area of HPHT diamond is quite small ( $5.1 \text{ m}^2 \cdot \text{g}^{-1}$  for  $1.55 \text{ }\mu\text{m}$  particles), so small particles have to be used in order to achieve sufficient column loading capacity. This also means that the application of ultra high pressure (UHPLC conditions) should be considered due to high backpressure associated with small particles. Furthermore, the properties of the diamond surface are hard to control, since they depend largely on manufacturing process and conditions of synthesis. Until now no standard approach has been accepted for the preparation of a uniform diamond surface [1]. Despite the fact that the development of a standardisation technique for diamond materials is outside of scope of this thesis, it is important to acquire all possible information about HPHT diamond properties. This information is especially important since chromatographic selectivity and adsorption properties, which are investigated here, cannot be explained without a complete understanding of the surface chemistry. Additionally, such information is required for the comparison of results obtained here with those obtained by other research groups using different sources of diamond. Overall, in the first part of this Chapter, the preparation and surface characterisation of HPHT diamond as a stationary phase will be presented. Special attention will be paid to the purification of diamond material and size fractionation of particles.

Another important aspect in the development of a new stationary phase is optimisation of the column packing procedure, which will be considered in the second part of this Chapter. The ultimate goal will be to elucidate a repeatable and reliable procedure for the preparation of columns with maximum possible efficiency. There is a plethora of information in the literature on column packing with conventional silica and polymeric stationary phases [2]. However, diamond is a very different material, and column packing conditions have still not been optimised. The development of a packing procedure for diamond particles is a non-trivial challenge which requires resolution of several complicating issues.

Firstly, diamond is a brittle material, and the pressure wave packing procedure, which is commonly used for packing silica, is not applicable. There are already some indications in the literature that a pressure wave may result in diamond particle fractures and formation of the ultrafine fragments which would negatively affect separation efficiency [3]. Another important issue is the high density of diamond ( $3.5 \text{ g}\cdot\text{cm}^{-3}$ ), which makes preparation of the stable diamond slurries complicated. Therefore, it is necessary to choose an appropriate slurry solvent with the required density and viscosity in order to avoid fast sedimentation during column packing. Otherwise, sedimentation can influence the quality of the bed and resultant column efficiency. Finally, other parameters, such as temperature, pressure and column conditioning need to be optimised, since they can also significantly influence both column efficiency and chromatographic peak shape.

Overall, there were a number of research problems that required addressing, and they are, therefore, investigated in this Chapter, including:

- Development of a purification procedure for HPHT diamond
- Characterisation of the purified diamond with various physical and chemical methods in order to establish its surface properties
- Selection of an appropriate slurry solvent for HPHT diamond, to reduce sedimentation rate and provide stable suspensions and dense firm sediments
- Preparation of HPHT diamond particles with improved shape and size distribution
- Elucidation of column packing procedure for the HPHT diamond stationary phase. Special attention will be paid to the investigation of the influence of packing pressure, temperature and after-packing column conditioning on the column performance.
- Comparison of the prepared HPHT diamond columns with other commercial and test column in terms of their performance and efficiency.

## **3.2. Experimental**

General information on materials, chemicals and instrumentation is summarised in Chapter 2. Information on the preparation of HPHT diamond material (including purification and fractionation), methods of investigation (titrations and sedimentation analysis), calculations (particle size distribution, void volume and phase ratio) and column packing procedure are also given in Chapter 2.

### **3.2.1. Calcination of HPHT diamond**

Calcination of HPHT diamond was done using Woodrow AF-3 furnace (Woodrow Kilns, Bankstown, NSW, Australia). Air and UHP N<sub>2</sub> were used. 1 g of diamond was used for each run. The heating rate was 5 °C per minute until a target temperature was reached (400 °C, 600 °C, 700 °C, 800 °C or 900 °C). After holding the target temperature for 1 hour, the sample was cooled down to room temperature at a rate of 10 °C per minute.

### **3.2.2. Determination of adsorption capacity of diamond**

Adsorption of aurointricarboxylic acid (ATA) was used in order to determine the adsorption capacity of HPHT diamond and how it is affected by calcination. ATA was purchased from Sigma-Aldrich (Castle Hill, NSW, Australia). 10 mL of 0.1 mM solution of ATA (0.422 mg of ATA) in water was added to 1 g of the HPHT diamond sample. After sonication for 30 s the mixture was set to equilibrate for ~10 min and finally centrifuged. The supernatant was separated and used for the determination of the remaining ATA concentration.

In a 25 mL volumetric flask, 5 mL of pH 5.0 sodium phosphate buffer (0.05 M) was placed, to which 15 mL of 0.25 mM Cu(NO<sub>3</sub>)<sub>2</sub> was added and mixed well. 2.5 mL of the supernatant with the unknown ATA concentration was added, and the volumetric flask was filled with DIW up to 25 mL. The flask was shaken vigorously and the formed Cu-ATA complex was detected at 520 nm using Metertech SP-8001 spectrophotometer (Nankang, Taipei, Taiwan).

## **3.3. Results and discussion**

### **3.3.1. Purification and characterisation of diamond packing material**

#### **3.3.1.1. Purification of HPHT diamond particles**

As previously reported, ICP-MS analysis of this HPHT diamond showed the presence of 2.96 wt. % of elemental impurities (H%, N% and O% are not counted) [4,5]. The major

impurities include  $25.3 \text{ mg}\cdot\text{g}^{-1}$  of Si,  $1.3 \text{ mg}\cdot\text{g}^{-1}$  of W,  $0.6 \text{ mg}\cdot\text{g}^{-1}$  of Ta,  $0.5 \text{ mg}\cdot\text{g}^{-1}$  of P,  $0.4 \text{ mg}\cdot\text{g}^{-1}$  of Al and  $0.3 \text{ mg}\cdot\text{g}^{-1}$  of each of Mn and S. The origin of silicon at such a high concentration level was due to the presence of 5.4 wt % of silica used as an anti-caking agent for the processing and storage of the diamond powder. The elevated concentrations of W and Ta are due to the reaction of diamond with construction materials containing these metals and formation of respective carbides during high temperature synthesis. These major impurities must be located at the surface of non-porous diamond particles and may significantly affect the adsorption and chromatographic properties of diamond. For this reason, before all experiments HPHT diamond particles were purified as described in Section 2.3.1, where the rationale for the selecting this particular purification procedure (firstly with boiling 40% NaOH, then with 5 M HNO<sub>3</sub>) is also provided.

In order to determine the successful removal of silica from the HPHT diamond, a test for the presence of silicates in wash solutions was performed. Wash solutions after the following treatment of HPHT diamond with 40 % NaOH were collected and acidified with concentrated HNO<sub>3</sub>. In the case of the formation of a white precipitate of SiO<sub>2</sub>·nH<sub>2</sub>O, indicating the presence of silicate in washoffs, treatment with boiling 40% NaOH had to be repeated. Accordingly, the purification procedure was repeated until no white precipitate was observed upon acidification.

EDS was additionally used to confirm the removal of the major impurities from HPHT diamond. This method allows the detection of elements heavier than Li at the level of 0.1 wt. % [6] and can be used to assess purification of diamond with regards to Si, W and Ta. EDS spectra of HPHT before and after the purification are shown in Fig. 3.1. Before the purification, a broad band at 1.7 – 1.8 keV composed of K $\alpha$  line 1.739 keV for Si and M lines 1.774 and 1.709 keV for W and Ta was observed. The purification procedure provided removal of these three elements (Si, W and Ta), as can be concluded from disappearance of the corresponding peak in Fig. 3.1. The presence of the other impurities, namely Mn, P and S was not detected in HPHT samples before and after purification due to a lack of EDS sensitivity towards these elements, presented in the original sample at concentration levels of 0.3 – 0.5 mg·g<sup>-1</sup> [4,5]. Both samples before and after purification showed peaks of Al from the aluminium plate used as a sample holder, and Pt from sputtering procedure before analysis. Overall, the purification of HPHT diamond provided sufficient removal of various impurities from the diamond surface, including silica, which can otherwise strongly contribute to the retention of organic substances.

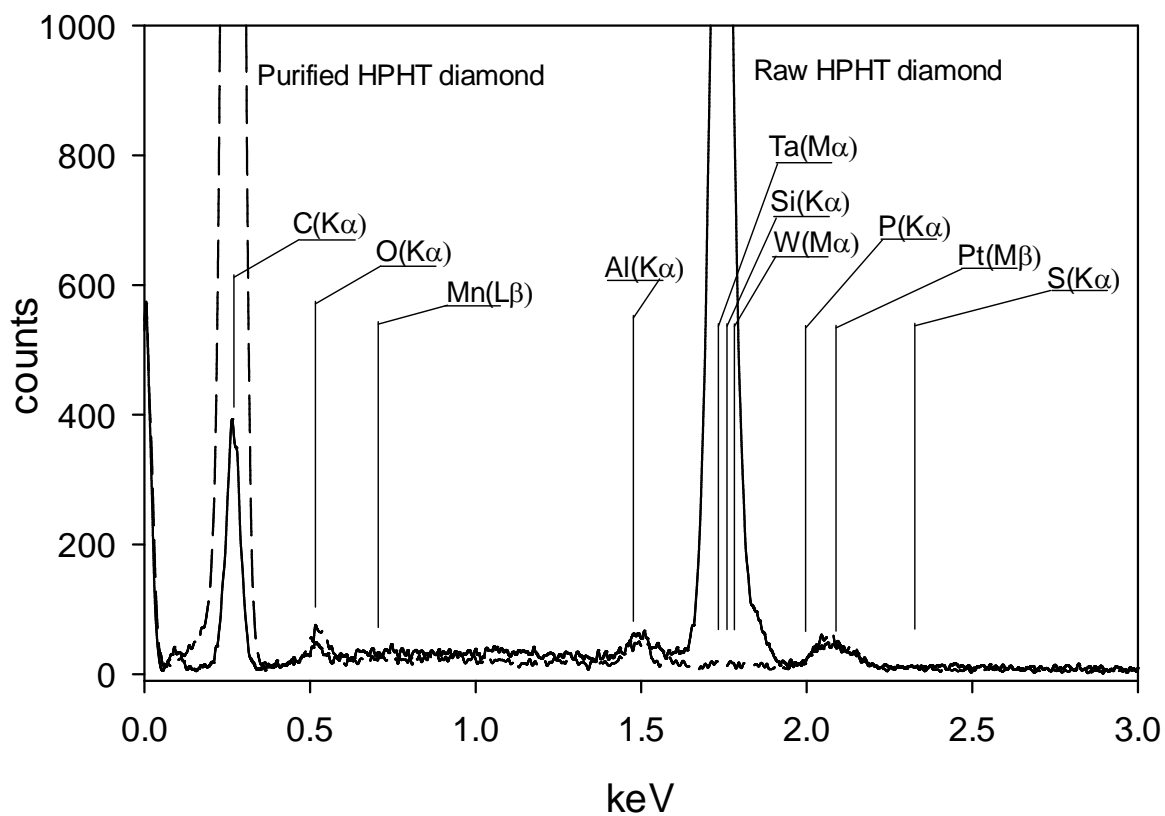


Fig. 3.1. EDS spectra of HPHT diamond before and after purification. Characteristic lines values taken from [7].

### 3.3.1.2. Surface characterisation of purified HPHT diamond

Since 5 M HNO<sub>3</sub> was applied to the purification of HPHT diamond (see Section 2.3.1), surface oxidation may occur, resulting in an increased concentration of oxygen containing groups [8]. Therefore, FTIR spectra were recorded to evaluate the presence of the functional groups and purity of the material (Fig. 3.2).

Both HPHT diamond samples before and after purification exhibited broad bands from 3000 to 3600 cm<sup>-1</sup> and a band at 1630 cm<sup>-1</sup>, which can be attributed to physically adsorbed water. This is in agreement with the previous reports on the hygroscopic properties of diamond [9], and indicates that the diamond surface is polar. Carbonyl related stretches  $\nu_{C=O}$  from carboxylic groups with characteristic band at 1730 cm<sup>-1</sup> are also clearly presented in both samples [10]. Interestingly the intensity of the  $\delta_{OH}$  band at 858 cm<sup>-1</sup> was higher for the purified sample, which can be due to a higher concentration of C-OH groups at the diamond surface. The intensity of a broad adsorption band at 1000-1100 cm<sup>-1</sup> was largely decreased after purification. Previously this band was attributed to silica by Loktev *et al.*, who had also observed its disappearance after purification procedure [11]. Interestingly, two sharp bands at 1385 cm<sup>-1</sup> and 2426 cm<sup>-1</sup> were only present in the diamond before purification. Presumably they belong to an unknown anticaking agent used by the manufacturer (Hunan Real Tech Superabrasive & Tool Co. Ltd., Changsha city, Hunan, China), and can also be removed during the purification procedure. It can be concluded from the IR spectra that the surface of purified HPHT diamond is a highly oxidised hydrophilic surface with a dominant presence of hydroxyl groups and smaller amount of carboxylic groups, and it is free of silica.

These conclusions about the surface state of HPHT diamond can also be confirmed using Raman spectroscopy (Fig. 3.3). According to Praver *et al.*, the Raman spectrum of diamond contains a characteristic first order line at 1325 cm<sup>-1</sup> [12], which can clearly be seen in Fig. 3.3 for both purified and non-purified samples. In contrast, bands at 1250 and 1650 cm<sup>-1</sup>, which are normally present in the spectra of diamond due to the amorphous carbon and sp<sup>2</sup> carbon impurities, respectively, are absent for both HPHT diamond samples. Therefore it is reasonable to conclude that even before the purification procedure, HPHT diamond did not contain “non-diamond” carbon.

Again, the band at 3000-3400 cm<sup>-1</sup> can be assigned to adsorbed water. Removal of silica can also be confirmed by Raman spectroscopy due to a decrease in a small band at 1050-1080 cm<sup>-1</sup>. This band is quite strong in the FTIR spectrum, but is a much weaker one in the Raman spectrum, which is in full agreement with literature data [13].

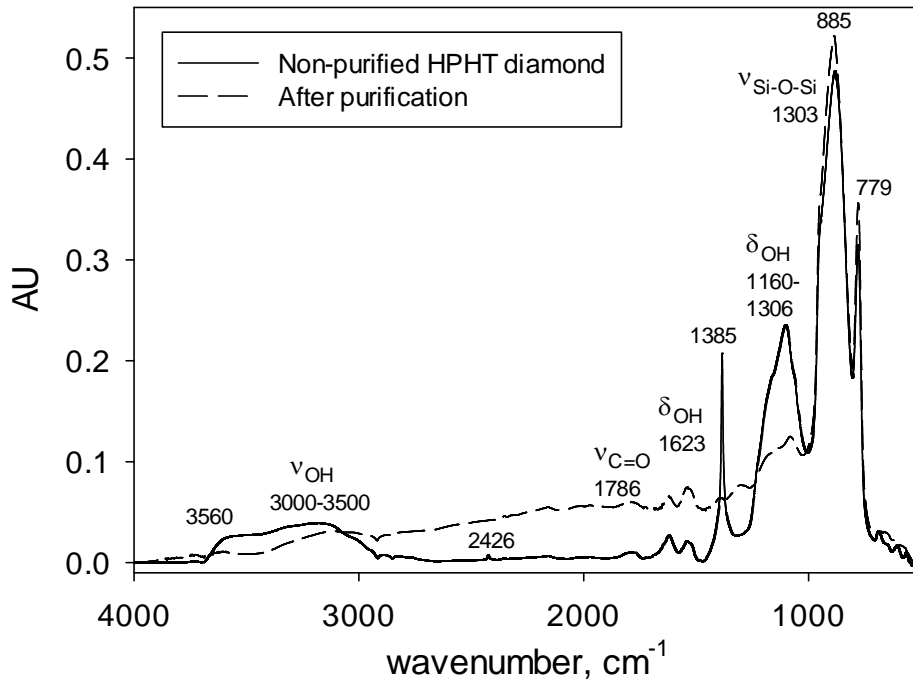


Fig. 3.2. FTIR spectra of HPHT diamond before and after purification (see Section 2.1 for details).

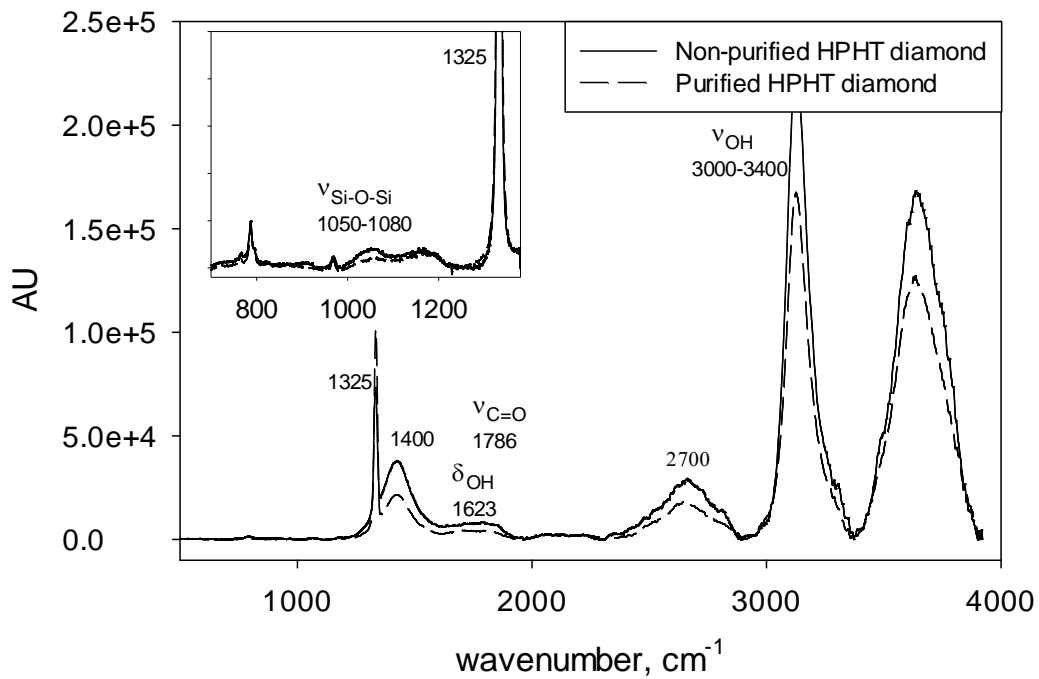


Fig. 3.3. Raman spectra of HPHT diamond before and after purification (see Section 2.1 for details).

Finally, some other bands were observed to decrease after purification, such as 1400 and 2700  $\text{cm}^{-1}$ , which, however, are unidentified.

The purification procedure has a strong impact on the  $\zeta$ -potential of HPHT diamond surface (see Fig. 3.4). Before purification, the  $\zeta$ -potential value was observed to decrease steadily towards a more alkaline pH, probably due to the presence of silica on the surface, while diamond after purification has two obvious regions. Under acidic conditions, the surface carries slightly negative charge ( $>-15$  mV), which starts to decrease rapidly between pH 5 and 7. This is related to the dissociation of COOH groups which are abundant on the surface of HPHT diamond according to the FTIR data (Fig. 3.2). The presence of hydroxyls and carboxyls at the surface of HPHT diamond provides a constant  $\zeta$ -potential of  $<-70$  mV for the purified HPHT diamond particles at pH values above 7, where dissociation of all functional groups with a labile proton takes place. Overall, the surface of HPHT diamond is negatively charged across the whole pH range, which is different from the  $\zeta$ -potential profile obtained for other form of diamond, such as MSDN [14].

### **3.3.1.3. Quantification of functional groups by means of acid base titration**

Once it had been found that carbonyl, hydroxyl and carboxyl groups were present on the surface of HPHT diamond, it was also necessary to understand what their concentration was. In order to do this, acid base titration experiments were performed as described in Sections 2.3.2 and 2.3.3. Three types of suspensions were used for the titration – 1 M NaCl aqueous, 80% ACN – 20% water and 80% MeOH – 20% water. 1 M NaCl was chosen rather than DIW in order to maintain a high ionic strength during titration and obtain better resolution of titrated groups [15]. Additionally, water – organic mixtures were tested in order to understand how the dissociation of surface groups is affected by the presence of organic solvents. According to the literature, an addition of 80% of organic solvent to solutions of carboxylic acids increases their pKa values by 1.5-3.0 units [16], so this study is important for the further understanding of chromatographic properties of HPHT diamond, when mobile phases containing polar organic solvent additives could be used.

Fig. 3.5 presents titration curve for HPHT diamond suspension in 1 M NaCl. As was described in Section 2.3.2, diamond with fully dissociated surface COOH groups was added to an excess of diluted HCl prior to the titration in order to protonate the surface. At the beginning of titration the pH of the suspension is acidic, so the first observed peak in the titration curve is related to the neutralisation of excessive HCl. The second peak appeared only a few millilitres after the first one, so it is hard to see it on the integral titration curve.



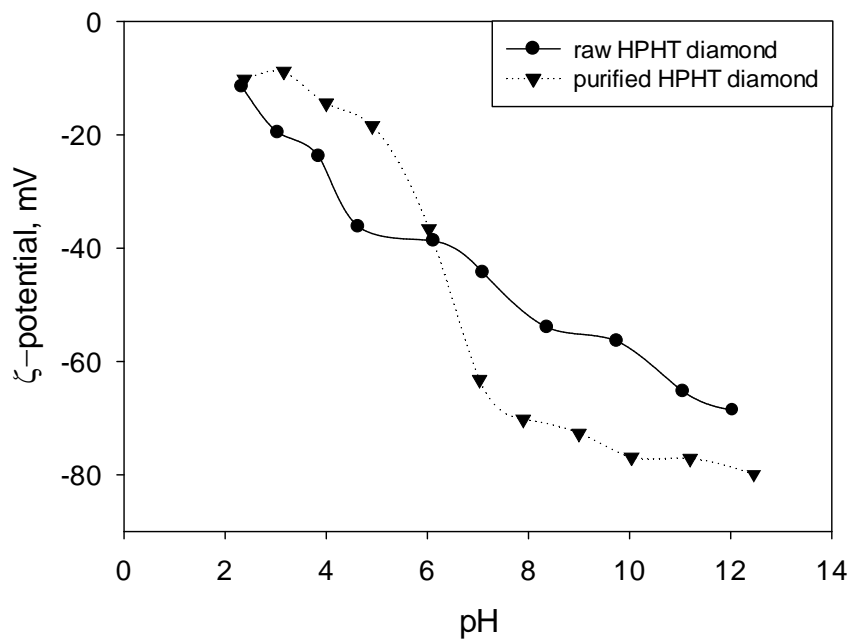


Fig. 3.4.  $\zeta$ -potential v pH curves for HPHT diamond before and after purification (see Section 2.1 for details).

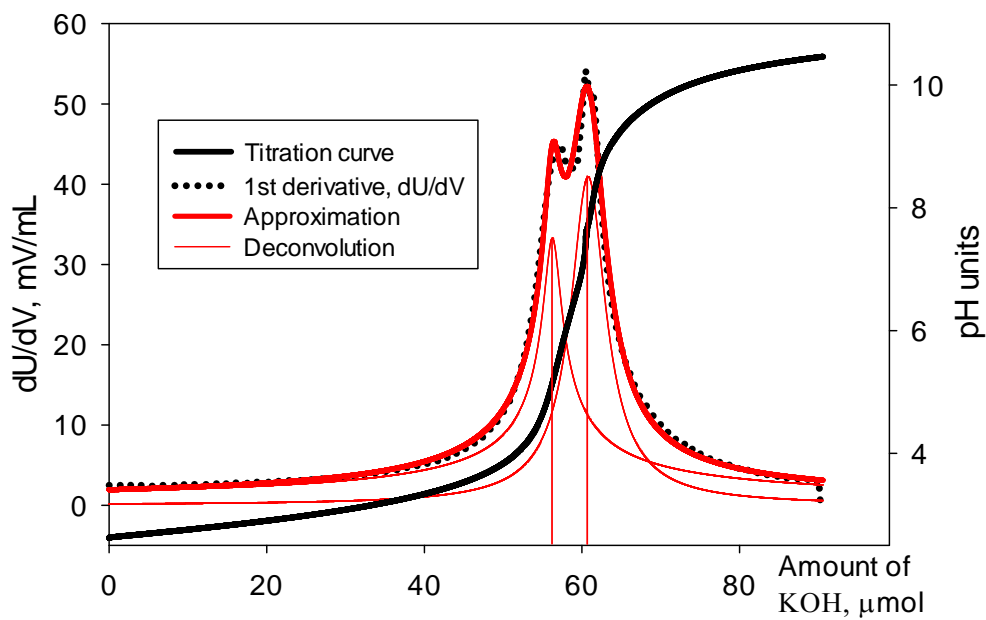


Fig. 3.5. Potentiometric titration of HPHT diamond in 1M NaCl and Gaussian peak-fitting.

However, the first derivative of the titration curve clearly shows two components in the mixture. A Gaussian peak-fitting procedure was applied, which provided the amount of titrant used for the neutralisation of excess of HCl, and for the titration of HPHT diamond. As shown in Table 3.1, the total amount of titrant used for the titration does not equal the amount of HCl added, which indicates that some residual NaOH was present in the HPHT diamond after the sedimentation procedure.

Potentiometric titration of the HPHT diamond suspensions was also performed in 80% ACN or MeOH suspensions of HPHT diamond (Fig. 3.6). In this situation a lesser amount of functional groups were expected to be detected, since it is known that the acidity (or basicity) of all groups decreases in the presence of organic solvents [16]. For both ACN and MeOH, resolution between peaks of neutralisation of excessive HCl and titration of COOH groups is poor, but the Gaussian peak-fitting of the first derivative of titration curve provided two peaks (Fig. 3.6). In contrast to the titration in 1 M NaCl, peaks for COOH groups were much broader for both ACN and MeOH. This is due to the large differentiating effect of organic modifiers, namely that the  $pK_a$  of some COOH groups may have similar values in 1 M NaCl, but differ significantly in the presence of organic solvent [16].

The data derived from all three titrations is summarised in Table 3.1, and provides useful information about the surface properties of HPHT diamond. As it could be expected, in 1 M NaCl, a much higher number of COOH groups is dissociated ( $4.5 \mu\text{mol}\cdot\text{g}^{-1}$ ) as compared to MeOH ( $2.5 \mu\text{mol}\cdot\text{g}^{-1}$ ) and ACN ( $2.3 \mu\text{mol}\cdot\text{g}^{-1}$ ). This is logical considering the increased  $pK_a$  values of carboxylic groups in organic-water mixtures, as compared with their true  $pK_a$  measured in water [17]. Accordingly, the dissociation of COOH groups in ACN is suppressed to a slightly higher extent than in MeOH. The value of  $4.52 \mu\text{mol}\cdot\text{g}^{-1}$  for the COOH groups detected on the surface of the HPHT diamond in 1 M NaCl corresponds to the value of 0.6 groups per  $\text{nm}^2$  (for comparison, this value for silica is  $\sim 4.6 \text{ nm}^{-2}$  [18]). The amount of the residual NaOH in HPHT diamond is consistent for all titration experiments and is at the level of  $\sim 7.5 \mu\text{mol}\cdot\text{g}^{-1}$ .

### **3.3.2. Fabrication of HPHT diamond particles with improved shape and particle size distribution**

The next step after purification and characterisation of HPHT diamond was to obtain fractions of HPHT diamond with a narrow particle size distribution and to improve particle shape. This is necessary in order to ensure a better packed bed, better peak shape, and column efficiency in HPLC.

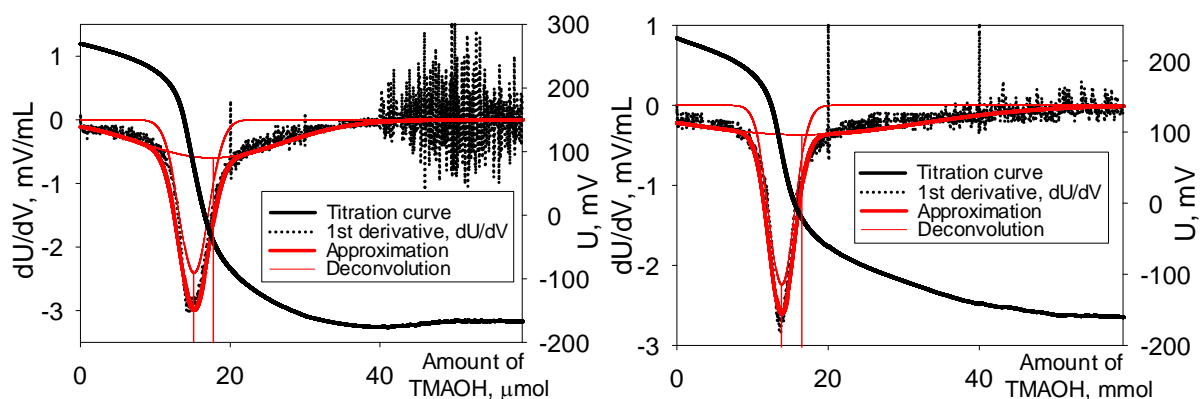


Fig. 3.6. Potentiometric titration of HPHT diamond in 80% ACN (left) and 80% MeOH solution and Gaussian peak-fitting.

Table 3.1. Calculation of the content of surface functional groups of HPHT diamond in different conditions\*.

	Dispersant		
	1 M NaCl	80% ACN	80% MeOH
Amount of HCl added initially, $\mu\text{mol}$	68.136	23.620	23.620
Amount of KOH or TMAOH used for neutralisation of excess of HCl, $\mu\text{mol}$	$56.126 \pm 0.004$	$13.813 \pm 0.004$	$13.816 \pm 0.004$
Amount of KOH or TMAOH used for titration of diamond, $\mu\text{mol}$	$4.523 \pm 0.004$	$2.340 \pm 0.004$	$2.480 \pm 0.004$
COOH on the diamond surface, $\mu\text{mol} \cdot \text{g}^{-1}$	$4.52 \pm 0.09$	$2.34 \pm 0.06$	$2.48 \pm 0.06$
Residual NaOH, $\mu\text{mol} \cdot \text{g}^{-1}$	$7.49 \pm 0.09$	$7.47 \pm 0.06$	$7.32 \pm 0.06$

\*Results are derived from deconvoluting titration curves in Fig. 3.5 and 3.6. Amount of COOH groups which can be titrated with  $\sim 5$  mM base was calculated by subtracting amount of titrant used for neutralisation of HCl from total amount of titrant used. Amount of residual NaOH in the HPHT diamond was calculated by subtracting total amount of titrant used from amount of HCl added initially. Further details are presented in Sections 2.3.2 and 2.3.3.

According to the literature, even a slight improvement in particle size distribution can drastically increase column efficiency for particles with the same mean size [19]. Usually, the  $D_{90/10}$  value is used to characterise particle size distribution, and means the diameter of particles at 90% distribution divided by the diameter at 10% distribution.

According to Henry, a decrease in  $D_{90/10}$  value from 1.4 to 1.1 results in 40% improvement in column efficiency [19]. In contrast, there is no clear evidence in the literature regarding the better efficiency of spherical particles over irregular ones [20]; however, generally this assumption is quite common. Therefore, a refinement of particle shape was attempted, with the aim of making more spherical particles, helping to decrease the backpressure of resultant packed columns.

According to the manufacturer, the original HPHT diamond particle size was between 1 and 2  $\mu\text{m}$ . A target fraction of 1.2-1.5  $\mu\text{m}$  was selected for isolation. Despite the fact that fractions with smaller sizes are harder to obtain, a 1.2-1.5  $\mu\text{m}$  fraction was preferred over a 1.5-2.0  $\mu\text{m}$  fraction for two reasons. Firstly, particles of smaller diameter should provide better column efficiency. Secondly, column loading capacity grows as a negative second order of particle size. Since HPHT diamond is a non-porous material, loading capacity could be a potential problem, so the application of 1.2 – 1.5  $\mu\text{m}$  particles as a stationary phase was investigated.

Fractionation by means of sedimentation is a proven method for narrowing particle size distribution. However, as it was mentioned above, HPHT diamond has an irregular shape with sharp edges and needled apexes, which need to be reduced. In order to achieve this, it was decided to first test calcination of HPHT diamond at high temperatures, which could help in the removal of sharp edges and surface defects. This is due to the fact that the carbon atoms near the edges have excessive energy and tend to be oxidised at lower temperatures [21].

### **3.3.2.1. Improvement of particle shape by means of thermal oxidation**

Prior to the investigation of the effect of calcination on the particle shape and size distribution, it was necessary to check the limits of thermal and chemical stability of HPHT diamond. Fig. 3.7 presents the results of TGA-DSC analysis of material carried out in UHP nitrogen atmosphere and in air. On the TGA curve under nitrogen it is clear that no weight loss is observed up to 1000  $^{\circ}\text{C}$ , which means that only negligible decomposition of some surface groups occurs. However, from the DSC curve under the nitrogen atmosphere it is clear that a phase transition from diamond to graphite happens at around 800  $^{\circ}\text{C}$ . This phase

transition is exothermic and results in a positive peak on the differential curve for the DSC signal. It is known that the rate of phase transition for diamond is extremely slow at temperatures below 1600 °C [22], however, the presence of certain metals can reduce these temperatures down to 650-970 °C [23]. Clearly, traces of W, Ta and Mn, which are present in the HPHT diamond may catalyse its phase transition at lower temperatures [5].

A different situation was observed during the heat treatment of diamond under air. Oxidation began at 600 °C and continued with the temperature gradient up to 800 °C. Usually, diamond is stable in air until 650 °C [24], but for diamond nanoparticles thermal oxidation can start at temperatures as low as 400 °C due to their excessive surface energy [25]. Therefore, the beginning of HPHT diamond oxidation under air at 600 °C in Fig. 3.7 is in good agreement with what could be expected for ~1 µm particles. Overall, HPHT diamond is stable to oxidation until 600 °C and stable towards graphitisation up to 800 °C. The temperature range of 25 to 700 °C was selected for further investigation, with a focus on the effect of calcination on particle shape and size distribution. Fig. 3.8 shows the SEM micrographs of HPHT diamond before and after calcination.

It is clear from Fig. 3.8 that heating of diamond at 400 °C and 600 °C does not have a visible influence on the particle shape. However, heating at 700 °C produced a small effect on the sharpness of the diamond particle edges. As noted in the beginning of this Section, surface and edge atoms possess excessive energy due to missing bonds, and are much more susceptible to oxidation. Therefore, oxidation of the HPHT diamond particles near the edges observed at 700 °C was expected. Although a reduction in visibly sharp edges was evident after calcination at 700 °C, this effect was obviously too small to have significant impact on the overall particle shape.

Despite the failed attempt to improve the particle shape by thermal oxidation, it was necessary to check the possibility of the removal of fine particles from the stock diamond material during heating.

Again, due to the excessive surface energy, smaller particles are expected to burn off at lower temperatures. As shown in Fig. 3.9, the low particle size cut-off value for HPHT diamond is 240 nm before calcination. After calcination, some reduction in the number of fine particles was observed, starting from 600 °C.

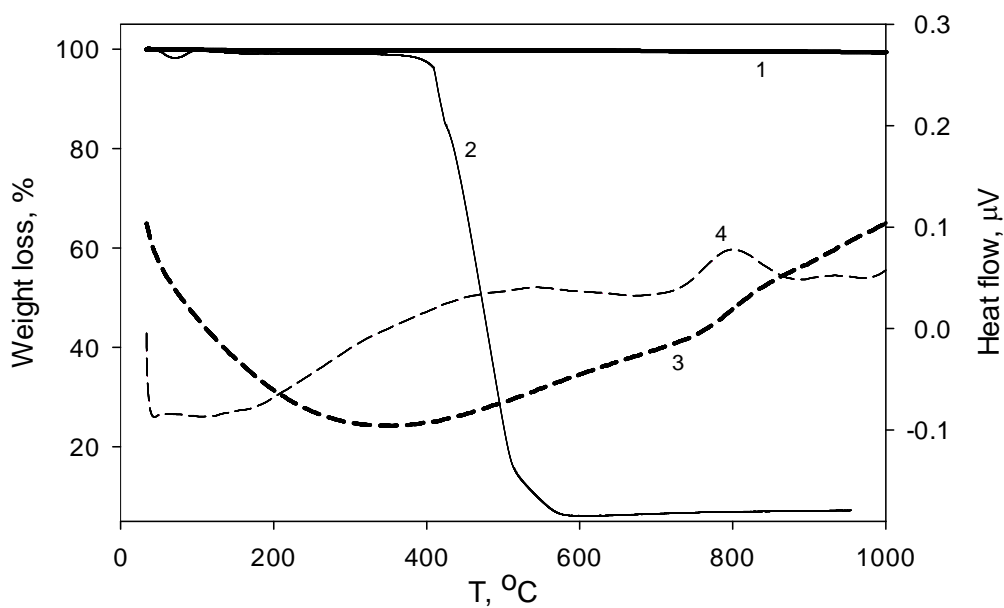


Fig. 3.7. TGA and DSC analysis of HPHT diamond. Bold solid line (1) is weight loss observed in UHP nitrogen, normal line (2) is weight loss observed in the air, bold dashed (3) is DSC signal in UHP nitrogen and simple dashed (4) is 1<sup>st</sup> derivative of DSC.

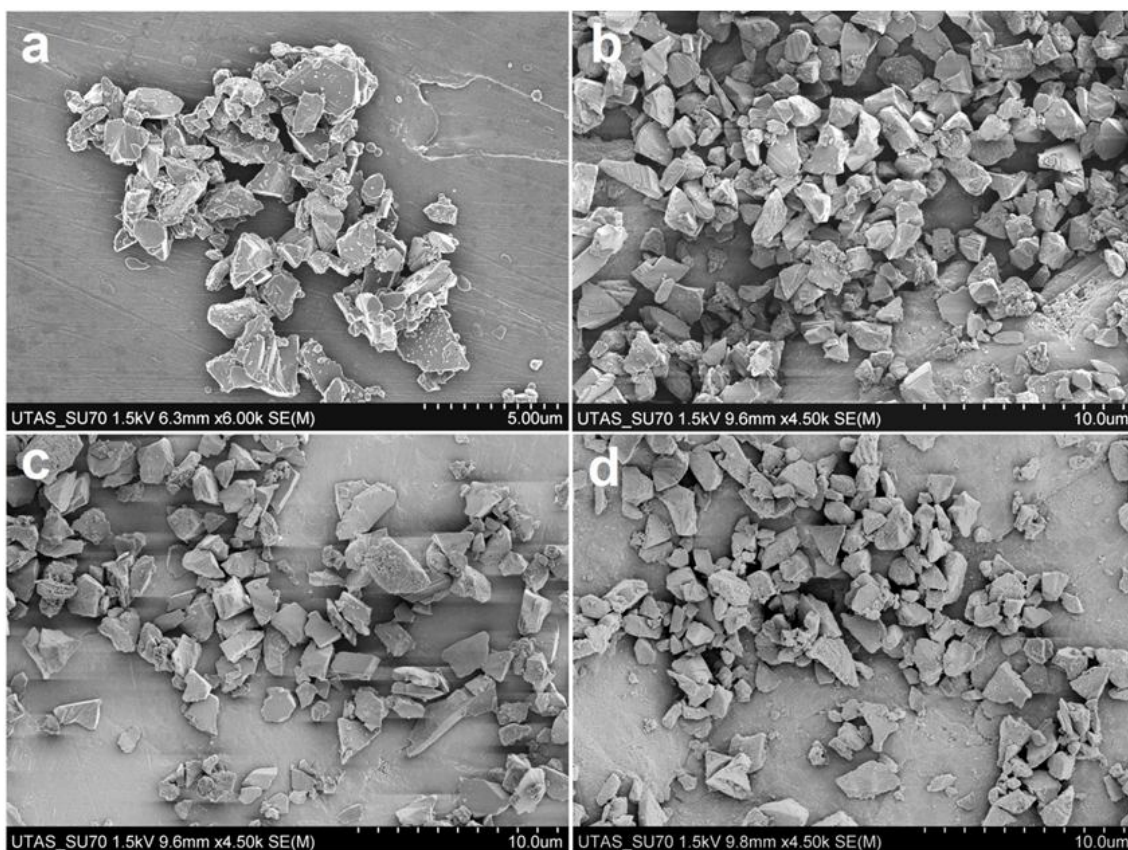


Fig. 3.8. SEM micrographs of HPHT diamond before (a) and after calcinations at 400 °C (b), 600 °C (c) and 700 °C (d).

A sample heated at 700 °C had the low particle size cut-off value of 280 nm. Further heating can improve this even more, but as previously mentioned, strong oxidation was observed at higher temperatures, along with graphitisation. Oxidation also results in more negative  $\zeta$ -potential for the samples heated above 700 °C, although samples heated below 700 °C did not change their surface charge significantly.

Fig. 3.10 shows the influence of calcination on the surface area of HPHT diamond and on its adsorption characteristics. As it could be expected, oxidation of smaller particles during heating causes a decrease in the surface area of the material. The original diamond had a surface area of  $5.6 \text{ m}^2 \cdot \text{g}^{-1}$ , while heating at 700 °C reduced this value to  $4.9 \text{ m}^2 \cdot \text{g}^{-1}$ . Oxidation at higher temperatures results in a further decrease to  $3.6 \text{ m}^2 \cdot \text{g}^{-1}$ . In order to assess the changes in adsorption capacity of HPHT diamond during calcination, the adsorption of aurintricarboxylic acid (ATA) on the diamond was investigated. ATA was chosen due to its flat structure and hydrophilic properties, which should provide a strong adsorption on HPHT diamond. As shown in Fig. 3.10, a reduction in surface area leads to a lower adsorption capacity of HPHT diamond towards ATA. Interestingly, the decrease in adsorption of ATA was much steeper than what was expected based on the surface area of the samples. Diamond heated at 900 °C had a 50% drop in surface area, but essentially did not adsorb ATA. Presumably, this is a result of a more negative  $\zeta$ -potential of -90 mV for oxidised HPHT diamond, which repels negatively charged ATA molecules.

Finally, the heating of diamond in air as a method for optimising particle structure is considered below in terms of its advantages and disadvantages. First of all, the sharp edges of the particles can be reduced during the oxidation at high temperatures, and this can potentially be beneficial for the preparation of a column with improved hydrodynamic characteristics. Similarly, the removal of fine particles and the decrease in HPHT diamond  $\zeta$ -potential is favourable and can improve the stability of suspensions and the quality of packed columns. On the other hand, all these effects are relatively small and do not compensate the 50% drop in the surface area of HPHT diamond, which is also a crucial parameter for the preparation of columns with sufficient loading capacity, as demonstrated with the adsorption capacity for ATA on oxidised HPHT diamond after heating, which was decreased substantially. Therefore, it was decided that the use of raw diamond was preferred over its calcinated derivatives, and was employed in further experiments. However, the desired improvement in particle size distribution was achieved *via* another technique – sedimentation (see Section 3.3.2.3).

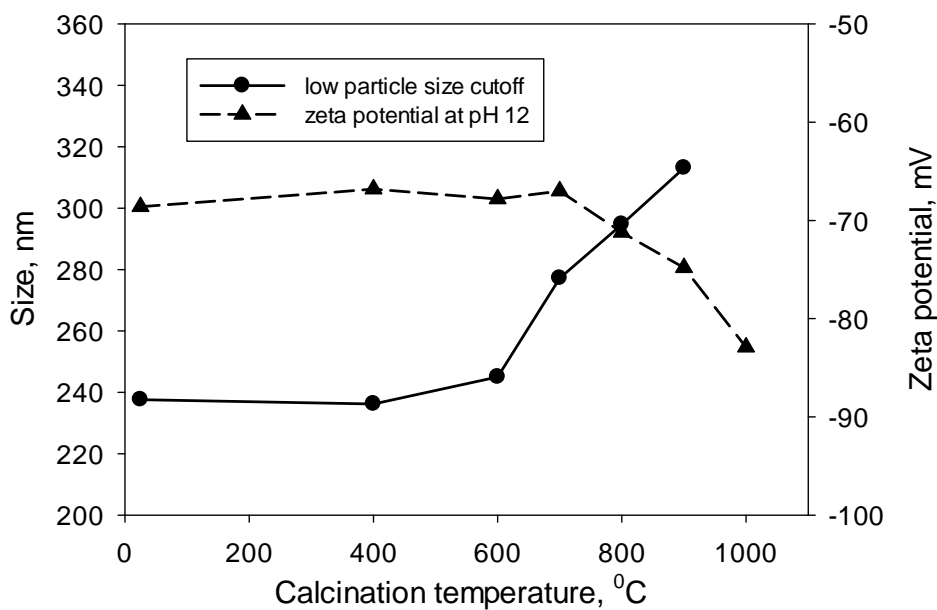


Fig. 3.9. Influence of heating temperature on the  $\zeta$ -potential of HPHT diamond (pH 10), and low particle size cut-off.

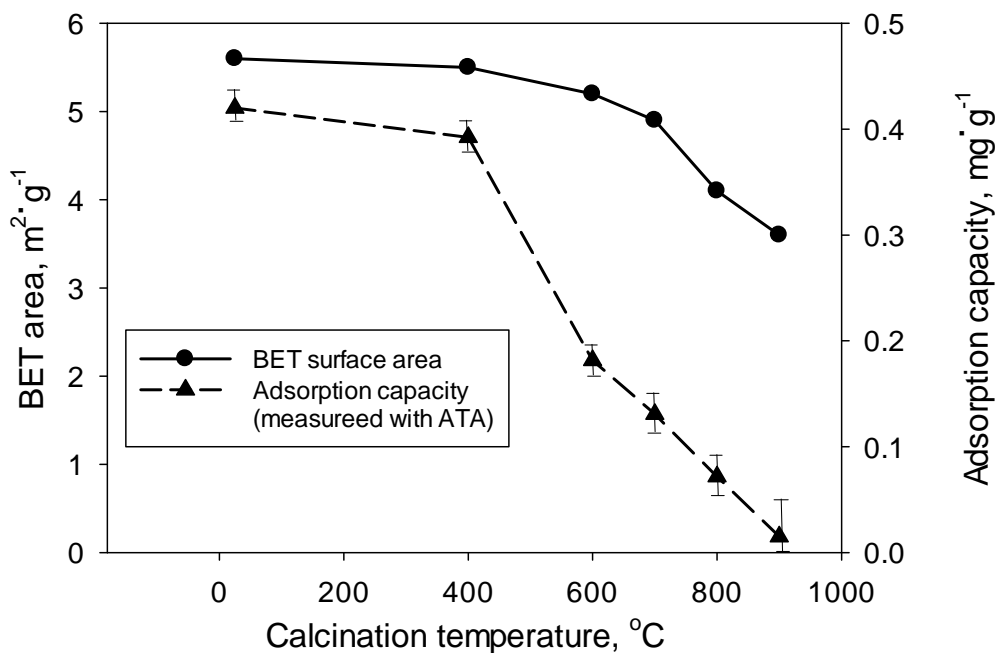


Fig. 3.10. Influence of heating temperature on the BET surface area of HPHT diamond, and on its adsorption capacity towards ATA.



### 3.3.2.2. Slurry solvent selection for particle sedimentation and column packing

According to the data provided by the manufacturer (Hunan Real Tech Superabrasive & Tool Co. Ltd., Changsha city, Hunan, China) the batch of HPHT diamond had particles with a size distribution between 1 and 2  $\mu\text{m}$ . Therefore, it was necessary to fractionate the material to obtain a more narrow distribution, which could provide improved performance in subsequent chromatographic experiments. One possible way of fractionating particles based on size is sedimentation [26]. This is not only an accepted method of fractionation of particles, but is also a way of preparing the particles with optimised geometry, providing similar flow resistance, which can be beneficial in chromatography. Other methods of improving particle size distribution, such as filtration or sieving, are based purely on the difference in linear dimensions. However, for irregular particles, flow resistance is not directly proportional to their size, since particle shape plays a significant role. Therefore, for our purposes, sedimentation was selected for the preparation of a diamond fraction with the desired narrow particle size distribution.

The first problem to be addressed is the determination of an optimal solvent for sedimentation. Properties of the solvent have a strong effect on the slurry behaviour during sedimentation and column packing [26]. A diamond slurry should be stable in terms of agglomeration, with slow particle sedimentation, which allows careful fractionation. The formation of a dense sediment which is hard to re-suspend is essential. Since diamond was shown to be a hydrophilic material with a range of oxygen containing groups at the surface (see Section 3.3.1.2), the use of polar solvents and their mixtures was the first investigated.

As discussed in Section 2.4.1, several factors influence the velocity of sedimentation. In an ideal case, when interactions between particles can be neglected, velocity is directly proportional to the difference between densities of the particle and the solvent. Accordingly, due to the high density of diamond ( $3.5 \text{ g}\cdot\text{cm}^{-3}$ ), high density solvents should be selected. This approach has never been reported before in the literature, since the density of non-porous silica is  $2.6 \text{ g}\cdot\text{cm}^{-3}$  and it can easily form compact sediments in water [26]. Secondly, sedimentation velocity is inversely proportional to solvent viscosity ( $\eta$ ), so viscous solvents need to be considered in order to provide lower sedimentation velocity (see Eqn. 2.1). Finally, in the case of strong interactions between particles, agglomeration stability of the suspension has to be achieved, and solvent properties should prevent agglomeration. Based on these factors a set of solvents was chosen, as presented in Table 3.2.

The solvents in Table 3.2 were compared based on their viscosity, density and polarity. NaOH was added to each solvent to give a concentration of 10 mM in order to provide a

maximum negative charge for the surface of HPHT diamond and to enhance particle repulsion. Since the velocity of each particle is a function of solvent viscosity, and the difference in density between diamond and solvent (see Eqn. 2.1), it is possible to introduce a parameter of relative velocity ( $U_A/U_W$ ). This relative velocity is the ratio of particle velocities in solvent A and water, respectively, in the ideal case of non-agglomerating particles (solvent polarity contribution is neglected).  $U_A/U_W$  values for different solvents can be derived from Eqn. 2.1:


$$U_A/U_W = (\eta_W/\eta_A) \cdot (\rho_D - \rho_A) / (\rho_D - \rho_W) \quad (\text{Equation 3.1})$$

where  $U_A$  is velocity of sedimentation in solvent A,  $U_W$  is velocity in water,  $\rho_D$  is density of diamond,  $\rho_A$  and  $\rho_W$  are densities of solvent A and water, respectively,  $\eta_W$  and  $\eta_A$  are corresponding viscosities. Values  $U_A/U_W$  are also presented in Table 3.2, and can provide some predictions on the velocity of diamond in different solvents.

Eight solvents were selected covering a large range of polarity and relative velocity. Special attention was paid to the use of very polar solvents to match the polarity of the diamond surface. Fig. 3.11 presents the correlation between the polarity and relative velocity of the solvents in Table 3.2, and demonstrates that the chosen range of solvents is sufficiently diverse.

Based on the values of relative velocities, an assumption was made that the solvents with low  $U_A/U_W$  values should provide better sedimentation conditions due to the slower moving particles. However, the experimental section of Table 3.2 indicates that this was not true for most of the solvents – recorded velocities in water and formamide were much lower than in other solvents. Obviously, this observation points to the fact that the polarity of solvent and its ability to form hydrogen bonds with HPHT diamond surface, thus preventing agglomeration, has a much stronger effect on the behaviour of the suspension. As shown in Table 3.2, six solvents out of eight are insufficiently polar to prevent agglomeration of HPHT diamond particles. Only water and formamide allowed the formation of true suspensions and satisfactory sediments. This is surprising, considering the fact that polarity of water/MeOH and water/IPA mixtures is only slightly less than that of water, but their viscosity is much higher. Presumably, the polarity of a solvent and its ability to form hydrogen bonds with the HPHT diamond surface has a very strong influence on the suspension stability, and cannot be fully compensated by lower relative velocities.

Table 3.2. Properties of solvents (taken from [27-29]) tested as a potential slurry dispersant for HPHT diamond, and sedimentational behaviour of such slurry. Each solvent contained 10mM NaOH to provide highly negative particle surface charge of particles.

		1. Water	2. MeOH	3. IPA	4. 50% water- 50% MeOH	5. 50% water- 50% IPA	6. 30% MeOH 70% IPA	7. Formamide	8. DMSO
Solvent properties	Polarity, normalised (E <sub>T</sub> <sup>N</sup> scale [27])	1.00	0.76	0.55	0.84	0.72	0.61	0.78	0.44
	Viscosity, cP	0.89	0.60	2.0	1.62	2.85	1.20	3.34	2.0
	Density, g·mL <sup>-1</sup>	1.000	0.792	0.786	0.912	0.926	0.786	1.129	1.101
	Calculated relative velocity, $U_A/U_W$ (see Eqn. 3.1)	1.00	1.61	0.48	0.57	0.32	0.81	0.25	0.43
Results of sedimentation experiments	Velocity observed, mm·min <sup>-1</sup>	<0.1	8	20	5	9	14	2	6
	Complete time for sedimentation, min	1000	12	5	15	10	7	80	13
	Visible agglomeration, Y/N	N	Y	Y	Y	Y	Y	N	Y
	Sediment height after 24 hours, mm	4	13	15	13	14	15	10	16
Image of sediment at the end of experiment									

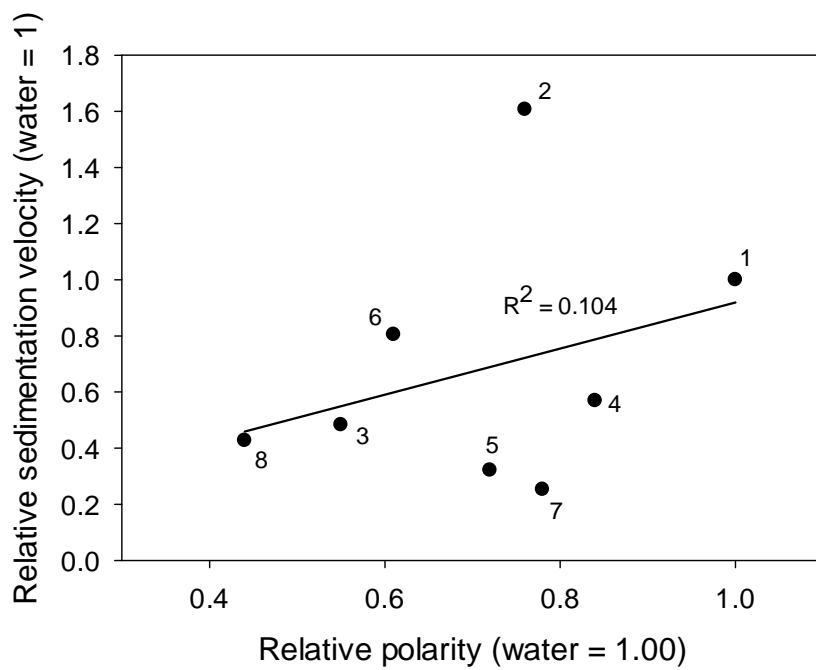


Fig. 3.11. Correlation between polarity and sedimentation velocity for eight solvents proposed for use as slurry dispersants. Solvents marked as in Table 3.2.

Therefore, the choice had to be made between water and formamide. Despite the fact that formamide is more dense and more viscous, and was supposed to provide four times slower sedimentation, it actually exhibited 12.5 times faster particle velocities. Again, the only explanation here is the 6% lower polarity of formamide and less stable suspensions. Nevertheless, the crucial factor favouring water over all other solvents is the formation of a much denser sediment, which is important for the following column packing procedure, where density of the packed particle bed is of highest priority. Thus, water (with 10 mM NaOH) was chosen for further investigations, including sedimentation analysis and column packing.

### 3.3.2.3. Sedimentation

HPHT diamond was subjected to sedimentations as described in Section 2.3.1, in order to improve particle size distribution. Two batches of diamond were prepared this way and compared with the original diamond. Fig. 3.12 presents the SEM images of these three diamond materials and their particle size distribution calculated by means of sedimentation analysis (see Section 2.4.1).

According to the manufacturer (Hunan Real Tech Superabrasive & Tool Co. Ltd., Changsha city, Hunan, China), the supplied fraction of HPHT diamond particles was between 1 and 2  $\mu\text{m}$ . This is obviously far from the accurate particle size distribution, as SEM images of the original diamond (Fig. 3.12, left) clearly show the presence of fine particles below 0.5  $\mu\text{m}$  as well as particles bigger than 2  $\mu\text{m}$ . The size distribution graph for the original HPHT diamond sample shows that although the majority of the particles are within 0.7-1.5  $\mu\text{m}$ , there is a considerable number of ultra-fine and large particles present. This material is unsuitable for the use in HPLC, and an additional particle fractionation based on size was required.

Two batches of fractionated HPHT diamond were prepared as described in Section 2.3.1. HPHT diamond in both batches exhibited a significantly improved size range, as can be seen from central and right images in Fig. 3.12. No particles below 0.5  $\mu\text{m}$  were present in either sample, which is a crucial criterion for obtaining a practical working backpressure for the resultant packed columns. Particle size distribution plots in Fig. 3.12 also confirm this hypothesis. For the first batch, most particles lie within the range 0.8-1.4  $\mu\text{m}$ , while for the second batch it is 1.3-2.0  $\mu\text{m}$ . Particle size distribution for all three diamond samples is compared in Table 3.3.

As it is shown in Table 3.3, the original HPHT diamond has a very broad particle size range 0.1-3.6  $\mu\text{m}$  with a mean of 1.1  $\mu\text{m}$ . This results in  $D_{90/10}$  value of 4.24.

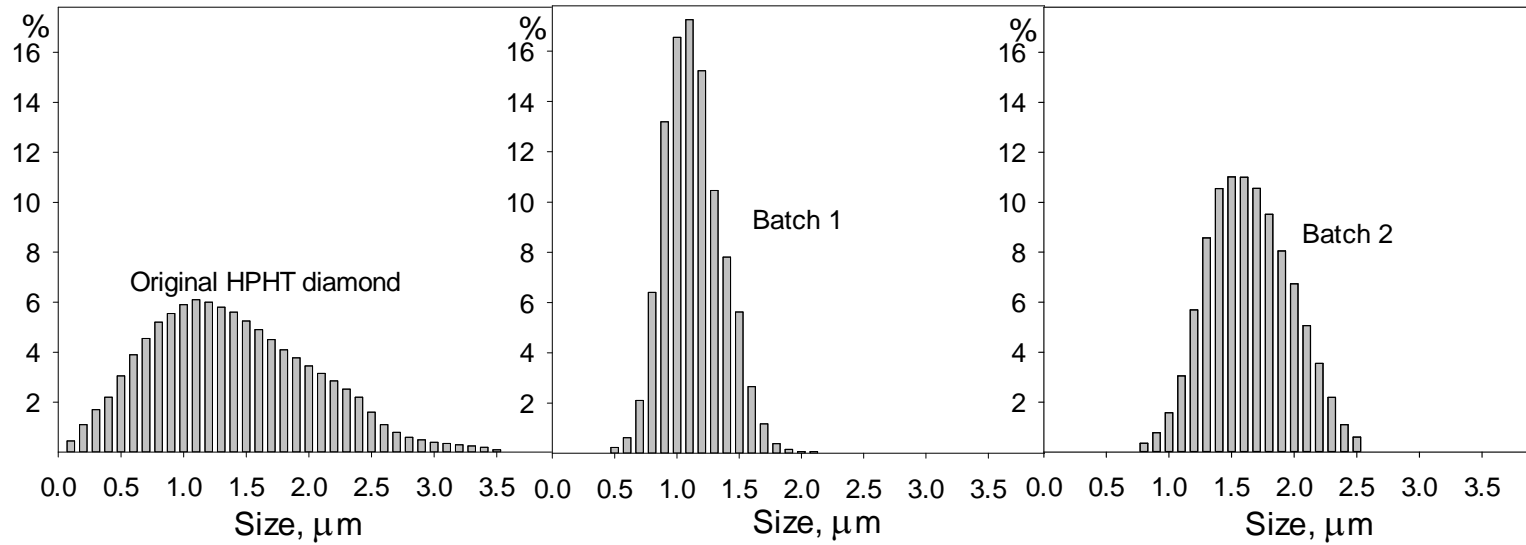
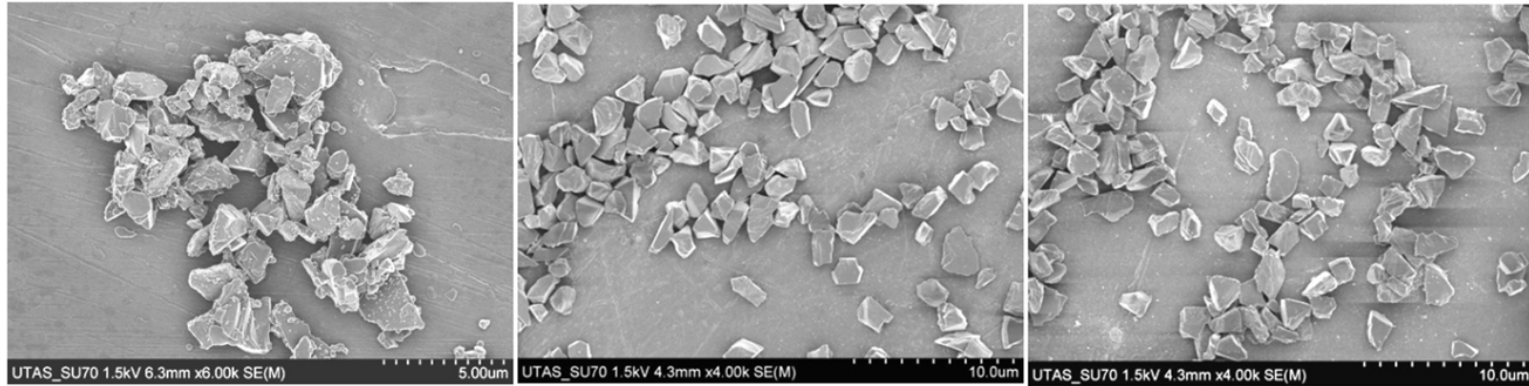


Fig. 3.12. SEM images of original (left), and two fractionated samples of HPHT diamond (batch 1 in the centre and batch 2 on the right). The particle size distribution is shown below the image of each sample, and calculated as described in Section 2.4.1.

Table 3.3. Properties of original and two isolated fractions of the HPHT diamond.

	Raw diamond	Batch 1	Batch 2
Smallest particle size, $\mu\text{m}$	0.1	0.5	0.8
Mean particle size, $\mu\text{m}$	1.1	1.1	1.55
Biggest particle size, $\mu\text{m}$	3.6	2.1	2.5
$D_{90/10}$ value	4.24	1.85	1.82

The first batch of diamond also had mean  $d_p$  value of 1.1  $\mu\text{m}$ , but the sedimentation allowed removal of the majority of fine and large particles, so the  $D_{90/10}$  value for the diamond particles in the first batch was 1.85. The first batch was obtained using sedimentation times of 24 and 12 hours ( $H = 21$  cm) for the removal of fine and large particles, respectively. For the second batch of diamond, these times were reduced to 18 and 6 hours. This allowed the production of fractions with bigger mean size (1.55  $\mu\text{m}$ ), while  $D_{90/10}$  values did not change significantly.

It should be noted that the particles used for packing of commercial HPLC columns have a much more narrow size range –  $D_{90/10}$  values of 1.15 or even 1.12 are quite common [30]. However, the values of 1.85 and 1.82 for HPHT diamond are certainly promising for a newly developing phase, where optimisation of particle shape and sedimentation procedure has not been fully optimised [31].

### **3.3.3. Development of column packing procedure for HPHT diamond**

#### **3.3.3.1. Influence of packing conditions on the performance of the column**

In the previous Section purification and fractionation procedures for HPHT diamond are described. It was found that HPHT diamond possesses a hydrophilic surface with an abundance of carbonyl, carboxyl and hydroxyl surface groups. The concentration of carboxyls is approximately 4.5  $\mu\text{mol}\cdot\text{g}^{-1}$ , and for OH groups this is  $\sim 5.5$   $\mu\text{mol}\cdot\text{g}^{-1}$ . Additionally, it was established that 10 mM aqueous NaOH is the best slurry dispersant for HPHT diamond. Despite its low density and viscosity, this solvent was the only medium where agglomeration of the HPHT diamond particles was substantially reduced.

As was discussed in Section 3.1, pressure-packing using a shock wave may result in fractures of brittle HPHT diamond particles [3]. Therefore, as a preliminary study it was decided to try an alternative approach involving “gravitational packing”\*. In order to carry out “gravitational packing”, an extra long (2 m long  $\times$  15 mm ID) column extension was connected to the column and filled with a diluted diamond slurry suspension (0.05  $\text{g}\cdot\text{mL}^{-1}$ ). The column with the extension was positioned upright and left for 1 week until HPHT diamond has completed sedimentation inside the column. Afterwards, the extension was removed and the column was connected to the pump at a pressure of 13,000 psi in order to compress the packed bed, thus avoiding the pressure shock wave. The described procedure proved satisfactory for a column with a large ID (7.8 mm), but presented two problems

---

\* The author gratefully acknowledges the suggestions from Dr John Ford regarding the column packing procedure for the HPHT diamond.



during packing of the standard 4.6 mm ID columns. Firstly, air bubbles were trapped between the column and the extension, which prevented sedimentation of HPHT diamond inside the column. Secondly, due to the use of such a long packing procedure (1 week), the particles were distributed inside the column based upon their size and sedimentation velocity (see Eqn. 2.1), which resulted in poor column efficiency and peak shape. Therefore, “gravitational packing” was not further utilised in the packing experiments. Instead, classic pressure packing was employed, involving a pressure gradient rather than a shock wave, in order to avoid HPHT diamond particle fractures (see Section 2.3.4).

According to Styskin *et al.*, the correct choice of slurry solvent for pressure packing is a key factor in the preparation of highly efficient columns [26]. Depending on the choice of solvent, three main techniques of packing can be utilised. First of all, the “balanced density” method requires the use of solvents with density comparable to that of the stationary phase in order to avoid fast sedimentation during packing. The second method utilises a highly viscous liquid for preparation of the slurry, also greatly reducing sedimentation velocity. Obviously for HPHT diamond these two methods cannot be applied, since only 10 mM NaOH is suitable (see Section 3.3.2.2). Therefore, a last method, referred to as “dynamic packing”, had to be explored.

“Dynamic packing” involves the use of solvent with a relatively low viscosity, such that packing is carried out quickly and sedimentation processes do not affect the quality of the packed bed. Usually, an extension before the column is used in this method in order to collect the excess of packing material including the smaller particle fractions. 10 mM NaOH should work well for “dynamic packing”, since its viscosity (0.89 cP) is low enough to allow rapid packing. In order to achieve further acceleration of the packing procedure, other parameters can be varied. For example, an increase in temperature and pressure of packing will lead to lower viscosity and a higher flow rate through the column, respectively, according to Eqn. 3.2.

$$\Phi = 100 \cdot \frac{\Delta P \cdot t_0 \cdot d_p^2}{\eta \cdot L^2} \quad (\text{Equation 3.2})$$

where,  $\Delta P$  is column backpressure (bar),  $t_0$  is void time (s),  $d_p$  is particle size ( $\mu\text{m}$ ),  $\eta$  is viscosity of mobile phase ( $\text{mPa}\cdot\text{s}$ ) and  $L$  is column length (mm). Table 3.4 summarises the parameters of four packing procedures, performed at different pressures and temperatures for packing 50 or 100 mm long 4.6 mm ID columns.

Clearly, a 50% increase in the packing pressure results in a big difference in column efficiency. Column 6, which was packed at 10000 psi, recorded an efficiency of 5211 plates

per meter, while a 50 mm column packed at 15000 psi (number 8) displayed efficiency of almost 37000 plates per meter. This result demonstrates a quicker packing procedure due to the higher pressure, and a reduced impact of sedimentation during packing on the quality of the packed bed. Surprisingly, an increase in temperature did not improve column efficiency, as can be concluded from comparison of columns 2 and 3. Presumably, the lower efficiency of column 3 can be attributed to the fact that a higher temperature leads to a lower viscosity of the slurry. A lower slurry viscosity enhances the rate of the sedimentation processes during the packing, which affects the uniformity of the packed bed.

The shape of chromatographic peaks for benzophenone obtained for each of the columns also confirms this hypothesis (Fig. 3.13). It is obvious from Fig. 3.13, that column 6 packed at 10000 psi displayed some packing problems, resulting in poor peak shape with several shoulders. Both columns 2 and 3 display severe peak fronting. However, column 2 shows more pronounced fronting at the beginning of benzophenone elution and a normal profile for the rest of the peak. In contrast, for column 3 the entire left portion of the peak is equally fronted. One of the possible reason is perhaps related to more intense sedimentation during packing caused by the higher temperature, disturbing a bigger section of the column, as compared to column 2.

The 50 mm long column 8 exhibited no peak fronting. Clearly, the use of a shorter column length and a faster packing process results in a reduced influence of sedimentation on the packed bed and improved column quality. The benzophenone peak for column 8 has some tailing, but considering the fact that the column packing conditions, as well as solvent composition, had not been optimised, this was deemed acceptable. Therefore, it was decided to use 50 mm columns and to conduct packing at 15000 psi and room temperature in further experiments. Packing pressure could be further increased and potentially improve column efficiency further, however, this work was limited by the maximum pressure of the pump used. Accordingly, the next step to improve column performance was to choose appropriate solvent systems for post-packing conditioning.

### **3.3.3.2. Influence of post-packing conditioning on the performance of the column**

There are no general rules about on choice of solvent systems for post-packing column conditioning [26]. Usually, the purpose of such conditioning is to compact the stationary phase and increase the column efficiency, as well as to provide a smooth transition between slurry solvent and the mobile phase in HPLC. Therefore, four conditioning systems were tested, as presented in Table 3.5.

Table 3.4. Performance of several HPHT diamond columns packed at different pressures and temperatures. All columns were packed from 10 mM NaOH diamond slurry without further conditioning/flushing.

	Column number			
	2	3	6	8
Dimensions, length × ID, mm	100 × 4.6	100 × 4.6	50 × 4.6	50 × 4.6
Packing temperature, °C	25	90	25	25
Packing pressure, psi	15000	15000	10000	15000
Void time, min	1.39	1.43	0.73	0.73
<i>k</i> , benzophenone	3.32	3.33	2.77	3.38
Efficiency, plates·m <sup>-1</sup> , benzophenone	55229	43547	5211	36942
Asymmetry@10%, benzophenone	1.52	1.64	1.80	1.78
Pressure at 0.1 mL·min <sup>-1</sup> of IPA and 25 °C, bar	303	296	139	148

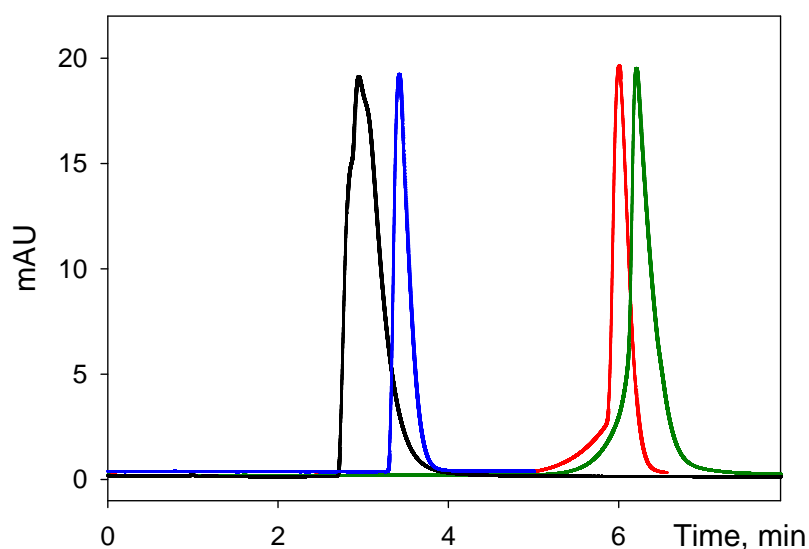


Fig. 3.13. Elution profile of benzophenone for four columns packed as described in Table 3.4: column 2 (red), 3 (green), 6 (black), 8 (blue). Mobile phase – 0.5 mL·min<sup>-1</sup> of 0.1% IPA in *n*-hexane, 1 μL injection of 50 mg·mL<sup>-1</sup> of propiophenone in mobile phase, 25 °C, UV detection at 254 nm.

Table 3.5. Performance of several HPHT diamond  $50 \times 4.6$  mm ID columns packed from 10 mM NaOH (aq.) and conditioned using different solvents. All columns were packed at 15000 psi and temperature 25 °C.

		Column number					
		04	05	11	12	13	14
1st flushing		Water	Water	IPA	10 mM HNO <sub>3</sub>	1 M aq. NH <sub>4</sub> Ac	Formamide
2nd flushing		-	-	-	water	water	IPA
Void time, min		0.94	0.94	1.11	0.95	0.96	0.94
k, propiophenone		1.03	1.05	0.85	0.88	0.84	0.88
Efficiency, plates·m <sup>-1</sup> , propiophenone		72580	70660	6340	57709	6259	20784
Asymmetry@10%, propiophenone		1.13	1.12	0.47	1.95	0.55	0.65
Van Deemter terms	$A \times 10^{-4}$ , cm	5.73±0.14	-	-	8.18±0.18	146±27	24.0±1.3
	$B \times 10^{-4}$ , cm <sup>2</sup> ·s <sup>-1</sup>	0.51±0.02	-	-	0.40±0.02	0.61±0.11	0.96±0.07
	$C \times 10^{-3}$ , s	2.80±0.08	-	-	6.56±0.13	16.2±2.2	11.9±0.8
R <sup>2</sup> for van Deemter model		0.997	-	-	0.993	0.858	0.981
Optimal linear velocity, mm·s <sup>-1</sup>		1.11	-	0.33	0.78	0.61	0.90
HETP at optimal velocity, μm		13.2	-	213	18.4	166	45.5
Pressure at 0.1 mL·min <sup>-1</sup> of IPA and 25 °C, bar		151	154	132	143	142	154

IPA (column 11) is compatible with both polar and non-polar solvents in HPLC, so it can provide a smooth transition between packing conditions and conditions of HPLC experiments. 10 mM HNO<sub>3</sub> (column 12) will protonate carboxylic groups on the diamond surface and decrease repulsion between particles, increasing packing density. A similar effect may be achieved using high ionic strength solutions (1 M NH<sub>4</sub>Ac, column 13), which can shield the surface charge of diamond particles and improve the packed bed. Column conditioning with formamide followed by flushing with IPA (column 14) can also provide a transition between aqueous and NP-HPLC solvents, but more smoothly than in the case of column 11, due to the use of polar formamide as an intermediate solvent. Finally, columns 4 and 5 were conditioned with DIW only and used for comparison. Table 3.5 summarises the parameters of column packing and their performance after conditioning with various solvents.

Useful information about the quality of packed columns can be obtained through van Deemter plots (Fig. 3.14 and Eqn. 3.3):

$$\text{HETP} = A + B/u + (C_s + C_m) \cdot u \quad (\text{Equation 3.3})$$

where  $A$  is eddy-diffusion term,  $B$  is longitudinal diffusion term, and  $C_s$  and  $C_m$  reflect resistance to mass transfer in stationary and mobile phases, respectively. According to the data provided in Fig. 3.14 and Table 3.5, conditioning did not improve column efficiency, as compared to column 4. The highest performance of 72580 plates·m<sup>-1</sup> was achieved using water for conditioning, while columns 11 and 13 exhibited low efficiencies. Column 11 also produced an unusually shaped van Deemter curve, where efficiency at very low flow rates and very high flow rates was higher than at intermediate flow rates. Therefore, the van Deemter plot for this column is not presented in Fig. 3.14. Due to the use of an intermediate conditioning reagent with high polarity (formamide), column 14 has shown improved efficiency, as compared to column 11, but performance of this column was still far below that of column 4.

The only conditioning approach which provided results comparable to using water was the conditioning with 10 mM HNO<sub>3</sub>. Column 12 has only 20% lower efficiency as compared to column 4, which is mostly due to a higher  $A$  and  $C$  terms in van Deemter equation (Eqn. 3.3). In contrast, the  $B$ -term is better for column 12 (0.40 versus 0.51), which indicates that protonation of carboxylic groups at the diamond surface can affect longitudinal diffusion. However, the packing density for column 12 is lower as compared to column 4, perhaps due to the aggregation of particles in the presence of nitric acid. This resulted in a higher  $A$ -term parameter and reduced HETP value for column 12. Though it was expected that use of 1 M NH<sub>4</sub>Ac will have similar effect on the packed bed, column 13 was very

poorly packed and only an had efficiency of  $6260 \text{ plates}\cdot\text{m}^{-1}$ . The differences observed between columns 12 and 13 could be attributed to adsorption of  $\text{NH}_4^+$  on the negatively charged diamond surface

Further comparison of column performance, depending on the conditioning, can be made based on the peak shape. As shown in Fig. 3.15, columns 11 and 13 have problems with packing, which resulted in the appearance of shoulders in the chromatographic peaks. Column 14 produced asymmetric peaks with extensive fronting. This is possibly caused by the strong adsorption of formamide on the surface of diamond, and difficulties in the complete removal of formamide *via* washing with IPA. This adsorbed formamide can result in the occurrence of multiple retention mechanisms in NP-HPLC and, consequently, in bad peak shapes. In the case of column 4, which has the best efficiency, the peak shape for propiophenone exhibited noticeable fronting. In contrast, the peak shape for column 12 was more symmetrical, but this column's overall efficiency was lower.

In conclusion, the best columns with HPHT diamond are produced by using 10 mM NaOH as slurry solvent, packing at room temperature and the highest possible pressure, whilst avoiding shock waves. Conditioning can be done either with water, or with 10 mM  $\text{HNO}_3$ , which helps to compact the bed and reduces peak fronting. This approach was used for the preparation of columns for further investigation in NP-HPLC and HILIC. While such packing procedures seem to provide columns of satisfactory quality, it would be interesting to compare the properties of HPHT diamond columns with the properties of columns packed with other carbon and silica sorbents.

### **3.3.3.3. Comparison of HPHT diamond column performance with other carbonaceous phases in HPLC**

The main concern regarding the application of HPHT diamond particles in HPLC is their non-porous structure and irregular shape. Though there are no proven advantages of using spherical particles over irregular particles in terms of separation efficiency in HPLC [20,32], the majority of work to-date has focused on the development of spherical porous or core-shell particles. Interestingly, the results of characterisation studies on 18 commercial columns indicated the tendency of reduced  $h$  values for irregularly shaped porous particles, when compared with spherical porous particles, with particle size less than  $5 \mu\text{m}$  [32]. Also, according to the literature, there appears to be only one work presenting van Deemter plots for a column packed with fine irregular nonporous particles [33].

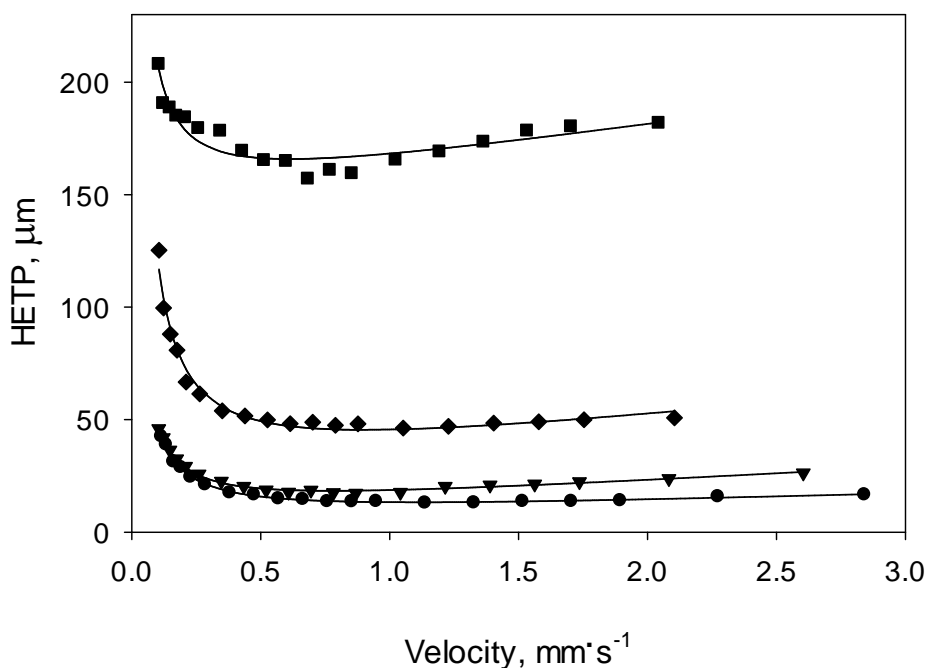


Fig. 3.14. Van Deemter curves for five columns (see Table 3.5): column 4 (circles), 12 (squares), 13 (diamonds) and 14 (downward triangles). Analyte – propiophenone, injection 1 μL, mobile phase – 0.1% of IPA in *n*-hexane, 25 °C.

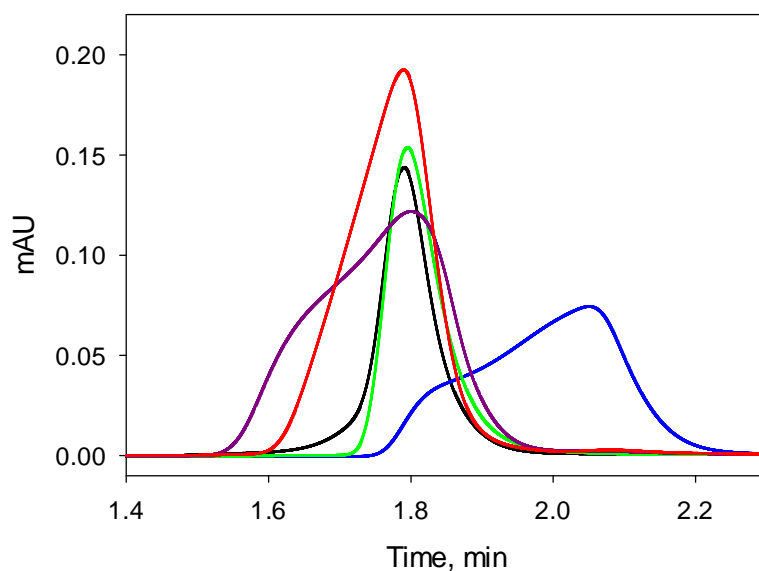


Fig. 3.15. Elution profile of propiophenone for five columns packed from 10 mM NaOH (aq.) and conditioned as described in Table 3.5: column 4 (black), 11 (blue), 12 (green), 13 (purple) and 14 (red). Mobile phase – 0.5 mL·min<sup>-1</sup> of 0.1% IPA in *n*-hexane, 1 μL injection of 50 mg·mL<sup>-1</sup> of propiophenone in mobile phase, 25 °C, UV detection at 254 nm.

The parameters  $A$ ,  $B$  and  $C = C_s + C_m$  in van Deemter equation (Eqn. 3.3) were calculated for columns packed with the nonporous angular HPHT diamond, spherical PGC, rounded porous MSDN, a spherical nanodiamond/polyamine composite and nonporous spherical silica particles. It is known that in order to achieve better accuracy in calculating the van Deemter parameters, largest possible range of linear velocities has to be examined [34]. In the case of HPHT diamond, linear velocities of 0.2 to 3.5 mm·s<sup>-1</sup> were examined, providing 20 data points. This allows an accurate and reliable calculation of  $A$ ,  $B$  and  $C$  coefficients and determination of the optimal flow rate. The corresponding data is presented in Table 3.6 and van Deemter plots for HPHT diamond and the PGC columns are presented in Fig. 3.16. The most significant contribution to the HETP value for the HPHT diamond column comes from the high values for the external obstruction  $\gamma$  parameter in the term  $B = 2\gamma D_m$ , responsible for longitudinal diffusion and eddy dispersion coefficient,  $\lambda$ , in the term  $A = 2\lambda d_p$ .

The calculated C-term of  $2.8 \cdot 10^{-3}$  s for HPHT diamond is lower than the values  $11.6 \cdot 10^{-3}$  s obtained for 5.0  $\mu\text{m}$  size porous PGC and  $9.07 \cdot 10^{-3}$  s for the 4.0  $\mu\text{m}$  size nanodiamond/crosslinked polyamine (ND/PAA) layer-by-layer structured composite phase. However, this value is still 5 times higher than the  $0.52 \cdot 10^{-3}$  s reported for nonporous spherical 1.5  $\mu\text{m}$  silica particles. This shows the potential application of HPHT diamond at higher flow rates (above optimal), without losing significant separation efficiency. Taking into consideration the excellent thermal and hydrolytic stability of HPHT diamond and its superior thermal conductivity, the use of elevated column temperatures might expand the possibilities of using such HPHT diamond columns for fast separations. The minimum HETP value of 13  $\mu\text{m}$  was obtained for a  $50 \times 4.6$  mm ID column packed with HPHT diamond at a linear velocity of 1.1 mm·s<sup>-1</sup>, and a flow rate of 0.52 mL·min<sup>-1</sup>. It should be noted that Liu [33] used a sophisticated procedure for slurry packing a capillary column (29.4 cm  $\times$  75  $\mu\text{m}$  ID) with 2  $\mu\text{m}$  synthetic diamond using ultrasonication of both slurry reservoir and capillary column and a pressure gradient up to 20,000 psi. The minimal HETP value of this column was 4.7  $\mu\text{m}$ , which is equivalent to 213,000 theoretical plates per meter. Interestingly, the HETP calculated for the column packed with similar synthetic diamond coated with a poly(butadiene) layer was significantly higher, with a value of 11.1  $\mu\text{m}$ .

Reduced plate height  $h$  is usually used for evaluation of quality of column packing:

$$h = \text{HETP}/d_p \quad (\text{Equation 3.4})$$

where HETP is height equivalent to theoretical plate at optimal flow rate.



Table 3.6. Comparison of van Deemter *A*-, *B*- and *C*- terms and related parameters for columns packed with HPHT diamond, PGC, nanodiamond/polyallylamine (ND/PAA) composite and nonporous silica.

Parameter	HPHT diamond column 4 <sup>a</sup>	HPHT diamond <sup>b</sup>	HPHT diamond <sup>c</sup>	polymer coated HPHT diamond <sup>b</sup>	ND/PAA <sup>d</sup>	PGC <sup>a</sup>	Micra C18 silica nonporous <sup>e</sup>
$d_p$ , $\mu\text{m}$	1.55	2.0	5.0	2.0	4.0	5.0	1.5
$D_{\text{pore}}$ , nm	nonporous	nonporous	nonporous	nonporous	28	25	nonporous
Column size: length (cm)	5.0	29.4	40.0	11.2	5.0	10.0	30.0
internal diameter	4.6 mm	75 $\mu\text{m}$	75 $\mu\text{m}$	75 $\mu\text{m}$	4.6 mm	4.6 mm	75 $\mu\text{m}$
Number of data points	20	17	22	7	12	22	52
$A \times 10^{-4}$ , cm	5.73±0.14	1.91 ± 0.15	N/A	5.51 ± 0.58	3.89	2.14±0.20	0.60 ± 0.29
$B \times 10^{-4}$ , cm <sup>2</sup> ·s <sup>-1</sup>	0.51±0.02	0.0845 ± 0.004	0.446 ± 0.037	0.163 ± 0.022	0.60	0.50±0.02	0.33 ± 0.02
$C \times 10^{-3}$ , s	2.80±0.08	2.17 ± 0.08	7.09 ± 0.21	5.45 ± 0.27	9.07	11.6±0.5	0.52 ± 0.07
$h = \text{HETP}/d_p$	8.04	2.35	1.82	5.55	4.65	3.48	2.07
HETP, $\mu\text{m}$	13.2	4.7	9.1	11.1	18.6	17.4	3.1

<sup>a</sup> - *n*-hexane – IPA (999:1, v/v), solute – propiophenone, 25 °C, this work (column 4).

<sup>b</sup> - 20 mM NH<sub>4</sub>Ac in water (pH 3.5) – acetonitrile (70:30, v/v), solute - 4-hydroxybenzoate, calculated from data [33]

<sup>c</sup> - 0.1% trifluoroacetic acid – acetonitrile (95:5, v/v), solute - phenol, calculated from data [33]

<sup>d</sup> - 0.1 % triethylamine in water – acetonitrile (40:60, v/v), solute - butylbenzene, 35 °C, calculated from data [35]

<sup>e</sup> - 100% acetonitrile, solute - nitromethane, from [33]

Usually, for a well packed chromatographic column, the  $h$  value is between 2 and 3, while for our HPHT diamond column 4,  $h$  was equal to only 8. Again, this indicates that the quality of column packing can be further improved. Obviously, a high  $h$  value is also connected to the relatively broad distribution of particle size (Fig. 3.7, right). Liu [33] achieved a remarkable quality of column packing using HPHT diamond 2  $\mu\text{m}$  particles with  $h = 2.35$ , which is similar to the value of 2.07 obtained for packing of 1.5  $\mu\text{m}$  nonporous silica.

Since column design for different HPLC column manufacturers can vary significantly, it was decided to determine how column design can influence the performance of the HPHT diamond stationary phase. Therefore, another 50  $\times$  4.6 mm ID column was packed using a column body from Thermo Fisher (see Section 2.3.4). Van Deemter plots for three compounds on this column are presented in Fig. 3.17. Clearly, the efficiency in the case of the Thermo Fisher column body was substantially lower than with the Phenomenex column bodies used for the other columns in this work (HETP was 28 and 13  $\mu\text{m}$  for Thermo Fisher and Phenomenex, respectively, at the optimal flow, rate see Fig. 3.16 and 3.17). The only difference between the columns from these two manufacturers is in the design and thickness of frits. Thermo Fisher employs thicker frits in the shape of a cap, while frits from Phenomenex are thinner and have a simple flat plate shape. Due to this difference, the void volume inside the frit, and the frit surface area is larger for Thermo Fisher columns. Apparently, this is a disadvantage in the case of using a stationary phase with low surface area, since extra band broadening may occur inside the frit and reduce the column efficiency. Therefore, Phenomenex columns were selected for further work herein.

#### **3.3.3.4. Comparison of HPHT diamond column hydrodynamic characteristics with other carbonaceous phases in HPLC**

The use of fine nonporous and irregularly shaped HPHT diamond particles in column packing raises a question about column permeability and kinetic chromatographic parameters. Generally, columns packed with fine irregular particles generate a high column backpressure, which could limit the flow rate of the mobile phase and the length of the column. Here, as a first step, the column resistance parameter  $\Phi$  was calculated according to Eqn. 3.2. In the case of a well packed column, Cramers *et al.* reported theoretical values for column resistance of 400 for spherical non-porous 10  $\mu\text{m}$  particles, up to 1550 for angular porous 10  $\mu\text{m}$  particles [36].  $\Phi$  for 50  $\times$  4.6 mm ID columns packed with the prepared HPHT diamond of average size of 1.6  $\mu\text{m}$  was found to be 1600.

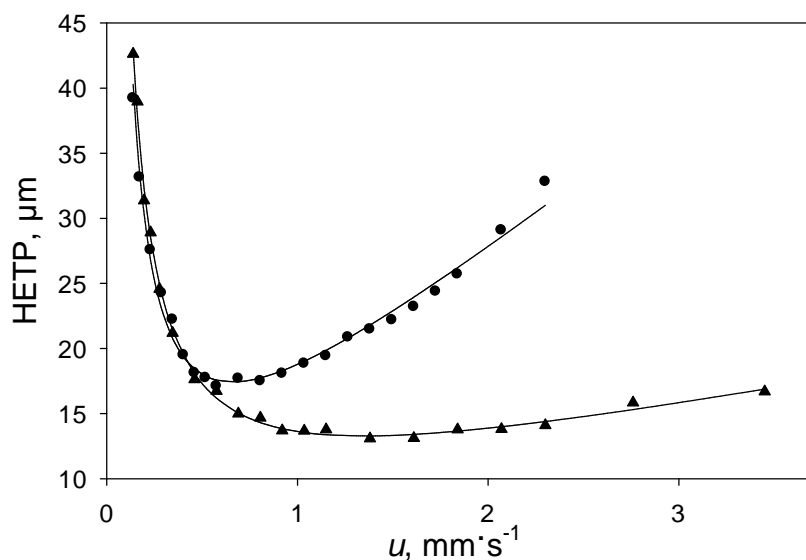


Fig. 3.16. Van Deemter plot obtained for  $50 \times 4.6$  mm ID (column 4) HPHT diamond (triangles) and Hypercarb  $5 \mu\text{m}$   $100 \times 4.6$  mm ID (circles) columns. Mobile phase: 0.1% of IPA in *n*-hexane, sample volume  $5 \mu\text{L}$  of  $0.05 \text{ mg}\cdot\text{mL}^{-1}$  of propiophenone in mobile phase, column temperature  $30 \text{ }^\circ\text{C}$ .

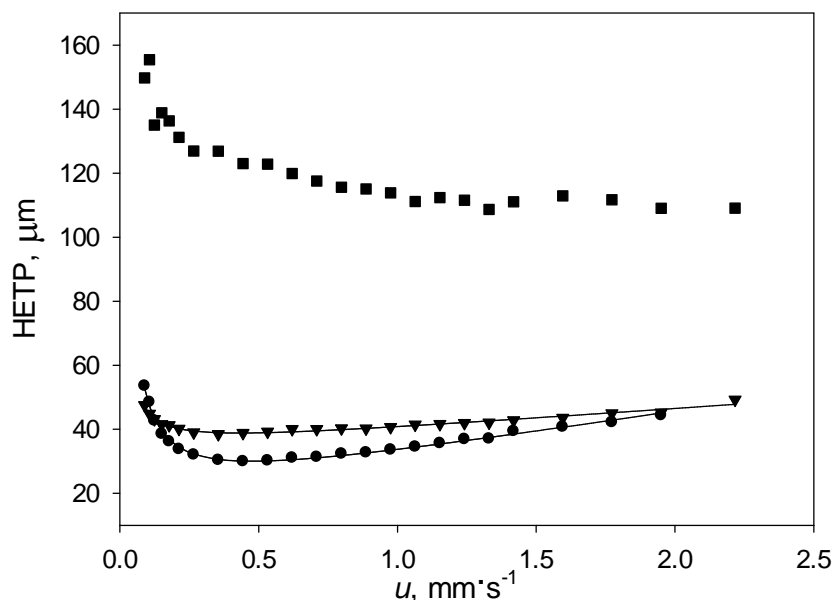


Fig. 3.17. Van Deemter plots obtained for  $50 \times 4.6$  mm ID HPHT diamond column packed into Thermo Fisher column body (see Section 2.3.4). Mobile phase: 0.1% of IPA in *n*-hexane, sample volume  $1 \mu\text{L}$ , column temperature  $30 \text{ }^\circ\text{C}$ . Solutes:  $0.05 \text{ mg}\cdot\text{mL}^{-1}$  of acetophenone (circles), benzophenone (triangles), dibenzylketone (squares) in mobile phase.

This is significantly higher than that reported by Giesche *et al.* [37] for non-porous spherical silica particles with  $d_p = 2.1 \mu\text{m}$ ,  $\Phi = 620$ . Apparently, such a high column resistance parameter is related to the irregular particle shape and a non-perfect particle size distribution.

### 3.3.3.5. Packing repeatability

As shown in Section 3.3.3.2, column 4 exhibited the best performance and peak shape out of all columns packed under different conditions, including variations in pressure, temperature, slurry solvent and conditioning solvents. Therefore, it was necessary to investigate the repeatability of the column packing procedure. Accordingly, another column (5) was packed using exactly the same packing conditions as column 4. This included packing at room temperature and pressure 15000 psi, using 10 mM NaOH for preparation of the slurry and using DIW as pump fluid and for conditioning. Finally, the two columns prepared by the same procedure were compared in terms of their performance and selectivity in HPLC (see Fig. 3.18 and Tables 3.5 and 3.7).

As shown in Fig. 3.18, the chromatograms for the same mixture of solutes obtained with column 4 and 5 generally looked very similar. According to Table 3.7,  $k$  values for all compounds were very close, and no more than 2-3% apart. The efficiency for these two columns is also very similar. However, column 5 exhibited strong peak fronting for all solutes. As shown later in Chapter 4, this peak fronting is not associated with column overloading. This fronting was observed for several other columns packed during this work, including columns 50 mm and 100 mm in length. There was no obvious trend as to when the column was showing fronted peaks, but it was observed to occur in about 50% of the columns packed. Following further investigation, the reason for this fronting was identified. It was related to the step involving disconnection of the column from the column extension. Since this procedure was performed manually, small volumes of sorbent were sometimes attached at the column extension, thus producing a tiny void volume at the column inlet, and in such cases peak fronting was observed. Despite the fact that this issue affected several columns in the current work, it is simply a technical error which is not foreseen to be relevant in the case of automated industrial column preparation, and is not connected with performance of the HPHT diamond stationary phase. Therefore, the peak fronting will be disregarded in subsequent Chapters.

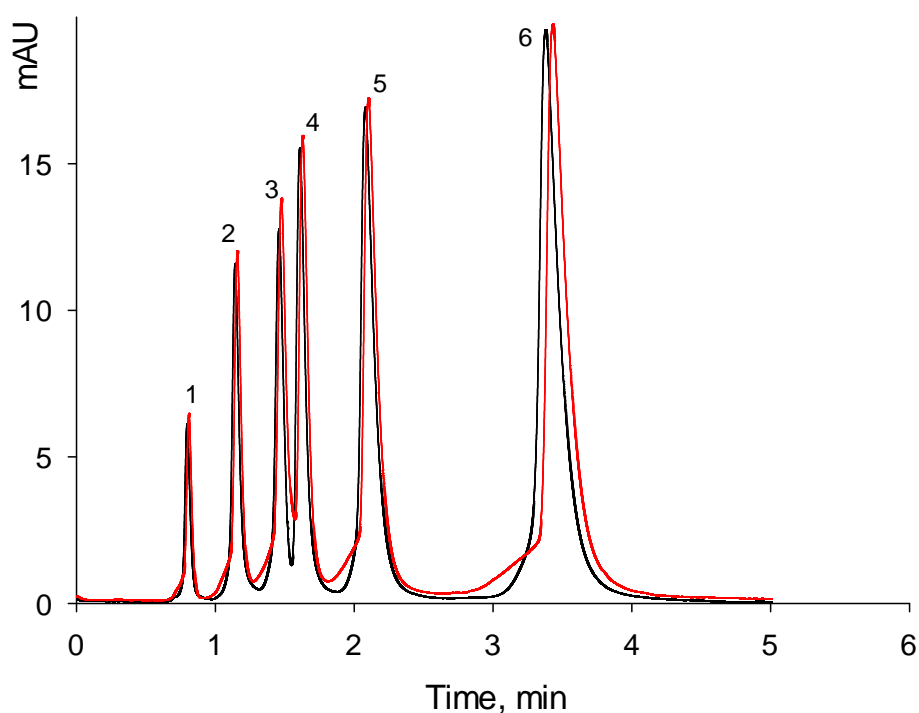


Fig. 3.18. Separation of a model mixture of analytes using two HPHT diamond columns packed at the same conditions – column 4 (black) and column 5 (red). Mobile phase: 0.1% of IPA in *n*-hexane, sample volume 1  $\mu\text{L}$  of  $0.05 \text{ mg}\cdot\text{mL}^{-1}$  in mobile phase, column temperature 25  $^{\circ}\text{C}$ . Analytes: anisole (1), nitrobenzene (2), benzaldehyde (3), propiophenone (4), acetophenone (5), benzophenone (6).

Table 3.7. Comparison of column 4 and 5 performance parameters. Conditions and analytes as in Fig. 3.18.

Peak	$k$			N, plates $\cdot\text{m}^{-1}$	
	Column 4	Column 5	$\Delta$ , %	Column 4	Column 5
1. Anisole	0.14	0.15	8.5	42300	44500
2. Nitrobenzene	0.63	0.65	3.5	51400	53000
3. Benzaldehyde	1.07	1.11	3.3	56000	54100
4. Propiophenone	1.29	1.33	2.8	61400	62100
5. Acetophenone	1.96	2.01	2.6	48300	50000
6. Benzophenone	3.76	3.78	0.5	56500	62000

### 3.4. Conclusions

Overall, despite several complications, a satisfactory method for preparation HPHT diamond columns has been developed. This method includes four steps. First of all, purification of HPHT diamond material with boiling 40% NaOH and 5 M HNO<sub>3</sub> provides complete removal of silica, metal admixtures, and other anticaking agents of unknown nature from the surfaces of diamond, as confirmed by FTIR, Raman and EDS methods. The resulting material has a negatively charged surface, populated with carboxyl, carbonyl and hydroxyl groups, of which the total content was ~10 μmol·g<sup>-1</sup>, as determined by means of potentiometric titration.

In the second step, it was shown, that calcination of HPHT diamond in air can smooth the sharp particle edges and reduce the number of fine particles due to their oxidation. However, such oxidative treatment had to be avoided in this work due to its negative impact on the surface area and adsorption capacity of HPHT diamond. Nevertheless, this calcination method could be re-considered in the future, in the case of preparation of porous stationary phases with other types of diamond, when a low surface area is not an issue.

Furthermore, a procedure for the isolation of HPHT diamond particles with a narrow size distribution through multiple sedimentations was developed. This allowed the preparation of HPHT diamond fractions with a mean particle size of 1.1 and 1.55 μm and D<sub>90/10</sub> value of ~1.8. The advantage of this fractionation method was that particles were selected based on their flow resistance rather than purely on their physical dimensions.

Finally, several column packing approaches were tested. It was shown that 10 mM NaOH is the best slurry solvent for hydrophilic HPHT diamond. Different packing conditions with variations in pressure, temperature and conditioning solvent were investigated. It was found that the best efficiency can be achieved by using DIW for the column conditioning. Room temperature is preferred over higher temperatures for column packing, and the packing pressure must be kept as high as possible.

Such procedures, as described above, provided columns with efficiencies of up to 72000 plates·m<sup>-1</sup> and asymmetry factors in the range 1.1-1.5 (conditions not optimised). Though such performance is not impressive when compared with modern commercial columns, it is comparable or even beyond that of other developing carbon and diamond stationary phases. It was decided that the column conditioned with DIW (column 4) would be used in NP-HPLC (Chapter 4), while the column conditioned with 10 mM HNO<sub>3</sub> (column 12) would be tested in HILIC mode (Chapter 5).

### 3.5. Reference List

1. A.P. Koshcheev, Thermodesorption mass spectrometry in the light of solution of the problem of certification and unification of the surface properties of detonation nanodiamonds, *Russ.J.Gen.Chem.*, 79 (2009) 2033-2044.
2. R.E. Majors, A review of HPLC column packing technology, *American Laboratory*, 35 (2003) 46-51.
3. A. Nuamthanom, P.M. Donaldson, J. Stokes, J.C. Ford, Reversed-Phase Liquid Chromatography on Columns Packed with Synthetic Diamonds, Duquesne University 2000 Summer Research Symposium, Pittsburgh, PA (2008)
4. D.F. Mitev, A.T. Townsend, B. Paull, P.N. Nesterenko, Direct sector field ICP-MS determination of metal impurities in detonation nanodiamond, *Carbon*, 60 (2013) 326-334.
5. D.F. Mitev, A.T. Townsend, B. Paull, P.N. Nesterenko, Screening of elemental impurities in commercial detonation nanodiamond using sector field inductively coupled plasma-mass spectrometry, *J.Mater.Sci.*, 49 (2014) 3573-3591.
6. J.J. Friel, X-ray and image analysis in electron microscopy, Princeton Gamma-Tech, Princeton, USA, 1995.
7. Tables of Physical & Chemical Constants (16th edition 1995), Kaye & Laby Online., 1995.
8. V.Ju. Dolmatov, Detonation nanodiamonds, NPO Professional (in Russian), Saint-Petersburg, 2011.
9. M.V. Korobov, N.V. Avramenko, A.G. Bogachev, N.N. Rozhkova, E. Osawa, Nanophase of water in nano-diamond gel, *J.Phys.Chem.C.*, 111 (2007) 7330-7334.
10. T. Jiang, K. Xu, FTIR study of ultradispersed diamond powder synthesized by explosive detonation, *Carbon*, 33 (1995) 1663-1671.
11. V.F. Loktev, V.I. Makalskii, I.V. Stoyanova, A.V. Kalinkin, V.A. Likholobov, V.N. Mitkin, Surface modification of ultradispersed diamonds, *Carbon*, 29 (1991) 817-819.
12. S. Praver, K.W. Nugent, D.N. Jamieson, J.O. Orwa, L.A. Bursill, J.L. Peng, The Raman spectrum of nanocrystalline diamond, *Chemical Physics Letters*, 332 (2000) 93-97.
13. A.G. Kalampounias, IR and Raman spectroscopic studies of sol-gel derived alkaline-earth silicate glasses, *B.Mater.Sci.*, 34 (2011) 299-303.
14. D.F. Mitev, A.T. Townsend, B. Paull, P.N. Nesterenko, Microwave-assisted purification of detonation nanodiamond, *Diam.Relat.Mater.*, 48 (2014) 37-46.

15. G.V. Lisichkin, Yu.A. Fadeev, A.A. Serdan, P.N. Nesterenko, P.G. Mingalev, D.B. Furman, Chemistry of grafted surface compounds (Khimiya privitykhpoverkhnostnykh soedinenii), Fizmatlit, Moscow, 2003.
16. X. Subirats, M. Roses, E. Bosch, On the effect of organic solvent composition on the pH of buffered HPLC mobile phases and the pK(a) of analytes - A review, Sep.Purif.Rev., 36 (2007) 231-255.
17. V. Verdolino, R. Cammi, B.H. Munk, H.B. Schlegel, Calculation of pK(a) Values of Nucleobases and the Guanine Oxidation Products Guanidinohydantoin and Spiroiminodihydantoin using Density Functional Theory and a Polarizable Continuum Model, J.Phys.Chem.B., 112 (2008) 16860-16873.
18. L.T. Zhuravlev, Concentration of Hydroxyl-Groups on the Surface of Amorphous Silicas, Langmuir, 3 (1987) 316-318.
19. R.A. Henry, Impact of Particle Size Distribution on HPLC Column Performance, LCGC N.Am., 32 (2014)
20. J.P.C. Vissers, E.C.J. Vandenhoef, H.A. Claessens, J. Laven, C.A. Cramers, Comparison of Spherically and Irregularly Shaped Stationary-Phase Packings in Microcolumn Liquid-Chromatography, J.Microcolumn Sep., 7 (1995) 239-245.
21. F. Rodrigue, P.A. Thrower, P.L. Walker, Kinetic Studies of Oxidation of Highly Oriented Pyrolytic Graphites, Carbon, 12 (1974) 63-70.
22. Y.L. Orlov, The mineralogy of the diamond, John Wiley & Sons Inc, New York, 1978.
23. Y.V. Butenko, V.L. Kuznetsov, A.L. Chuvilin, V.N. Kolomiichuk, S.V. Stankus, R.A. Khairulin, B. Segall, Kinetics of the graphitization of dispersed diamonds at "low" temperatures, J.Appl.Phys., 88 (2000) 4380-4388.
24. D.M. Crumpton, R.A. Laitinen, J. Smieja, D.A. Cleary, Thermal analysis of carbon allotropes - An experiment for advanced undergraduates, J.Chem.Educ., 73 (1996) 590-591.
25. V.Y. Dolmatov, Detonation synthesis ultradispersed diamonds: Properties and applications, Usp.Khim., 70 (2001) 687-708.
26. E.L. Styskin, L.B. Itsikson, E.V. Braude, Practical High-Performance Liquid Chromatography, Khimiya, Moscow, 1986.
27. C. Reichardt, Solvatochromic Dyes As Solvent Polarity Indicators, Chem.Rev., 94 (1994) 2319-2358.



28. I.M. Smallwood, Handbook of organic solvent properties, Elsevier Ltd., Sydney, Australia, 1996.
29. L.R. Snyder, Classification of Solvent Properties of Common Liquids, *J.Chromatogr.*, 92 (1974) 223-230.
30. Thermo Scientific, Thermo Scientific Accucore HPLC Columns Phase Overview (2012)
31. A.A. Peristy, O.N. Fedyanina, B. Paull, P.N. Nesterenko, Diamond based adsorbents and their application in chromatography, *J.Chromatogr.A*, 1357 (2014) 68-86.
32. R. Ohmacht, I. Halasz, Efficiency of Commercially Available Silicas in Hplc, *Chromatographia*, 14 (1981) 216-226.
33. Y. Liu, Investigation of novel microseparation techniques, PhD Thesis, Brigham Young University, 2007.
34. F. Gritti, G. Guiochon, The van Deemter equation: Assumptions, limits, and adjustment to modern high performance liquid chromatography, *J.Chromatogr.A*, 1302 (2013) 1-13.
35. L.A. Wiest, D.S. Jensen, C.H. Hung, R.E. Olsen, R.C. Davis, M.A. Vail, A.E. Dadson, P.N. Nesterenko, M.R. Linford, Pellicular Particles with Spherical Carbon Cores and Porous Nanodiamond/Polymer Shells for Reversed-Phase HPLC, *Anal.Chem.*, 83 (2011) 5488-5501.
36. C.A. Cramers, J.A. Rijks, C.P.M. Schutjes, Factors Determining Flow-Rate in Chromatographic Columns, *Chromatographia*, 14 (1981) 439-444.
37. H. Giesche, K.K. Unger, U. Esser, B. Eray, U. Trudinger, J.N. Kinkel, Packing Technology, Column Bed Structure and Chromatographic Performance of 1-2-Mu-M Non-Porous Silicas in High-Performance Liquid-Chromatography, *J.Chromatogr.*, 465 (1989) 39-57.

## Chapter 4. Chromatographic performance of synthetic polycrystalline diamond as a stationary phase in normal phase high performance liquid chromatography

### 4.1. Introduction

The growing interest to the application of the diamond based materials in high performance liquid chromatography (HPLC) has occurred over the last decade [1,2]. However, the majority of the work in this field is related to MSDN and composite sorbents, while the chromatographic performance of statically synthesised high pressure high temperature diamond (HPHT) has not been systematically studied. The only brief reports on this topic were presented by Ford *et al.* and Liu [3,4]. Until now, the most significant problem for the application of HPHT diamonds in chromatography was a lack of knowledge about their chemical and physical properties [5].

Chapter 3 of this work has been dedicated to the purification, fractionation and characterisation of the HPHT diamond stationary phase, as well as to the development of the column packing procedure. It was shown that suggested set of methods allows preparation of HPHT diamond material free of impurities and with the hydrophilic surface, saturated with hydroxyl, carbonyl and carboxyl groups. Additionally, the particle size distribution of HPHT diamond was improved by means of sedimentation, which allowed the isolation of fractions with mean particle sizes of 1.1 and 1.55  $\mu\text{m}$ , respectively. The repeatability of the suggested column packing procedure with the HPHT diamond stationary phase was shown, and good efficiency and peak shape were evidenced for the retention of model compounds on such columns.

Due to the hydrophilic properties of the surface of HPHT diamond (see Chapter 3.3.1.2), it was decided to start the investigation of its chromatographic properties using normal phase chromatography. (NP-HPLC). The main attention will be paid to the adsorption properties, retention mechanism and separation selectivity. The properties of HPHT diamond will be also compared with the properties of PGC and MSDN adsorbents.

### 4.2. Experimental

#### 4.2.1. Instrumentation

Two columns, Column 4 and Column 5 were used in this chapter. Their characterisation and packing procedures are given in Sections 2.3.4, 3.3.3.2 and 3.3.3.5. Column 5 was used for generation of all retention data and investigation of loading capacity

and influence of conditioning on retention factors. Column 4 was packed using exactly the same procedure and used in order to understand the repeatability of packing procedure (see Section 3.3.3.5). This column 4 was used for the separation of model mixtures (Fig. 4.7, 4.8 and 4.9).

#### **4.2.2. Column conditioning in NP-HPLC**

After column packing procedure was completed, column was flushed with IPA for 60 min at a flow rate of  $0.1 \text{ mL}\cdot\text{min}^{-1}$ . After that, *n*-hexane was pumped through at  $0.5 \text{ mL}\cdot\text{min}^{-1}$  for 50 min. Finally, the column was equilibrated with mobile phase until stable retention times were achieved within  $\pm 0.5\%$ .

In case of investigation of influence of column conditioning on retention factors, the following procedure was applied. Firstly, column conditioning included flushing with IPA for 20 min at a flow rate of  $0.1 \text{ mL}\cdot\text{min}^{-1}$ , then with DIW for 20 min at  $0.2 \text{ mL}\cdot\text{min}^{-1}$ . This was followed by flushing with target buffer for 1.5 h at  $0.2 \text{ mL}\cdot\text{min}^{-1}$ , before finally repeating flushing with DIW and IPA. After that, the column was equilibrated by pumping mobile phase until stable retention times were achieved within  $\pm 0.5\%$ .

### **4.3. Results and discussion**

#### **4.3.1. Characterisation of the prepared HPHT diamond fraction**

The prepared fraction of purified HPHT diamond displayed a narrow distribution of particles size between 0.5 and 2.0  $\mu\text{m}$  with a median at 1.6  $\mu\text{m}$ , as shown in Fig. 3.12, right. The resulting particles were mainly of angular shape, with a much reduced number of flakey and needle-shaped particles, as can be seen from the SEM image. The circularity of fractionated particles calculated as ratio  $2\cdot(S_p/P_p)^{1/2}$  where  $S_p$  is area of the particle and  $P_p$  is its perimeter, was notably improved, so the resistance to the flow of packed bed of these particles and operating pressure in chromatographic column should be less. Obviously this should also increase column efficiency.

The adsorption properties of HPHT diamond depend upon the surface chemistry and presence of reactive impurities, such as silica, which is a common anti-cake reagent in powders of industrial diamonds. According to the literature data, the surface of HPHT diamond has no or very low graphitic or  $sp^2$  carbon presence, with some amount of oxygen containing functional groups [6] and metal impurities [7]. The contact angle ( $\theta$ ) measured for the purified and seasoned single crystal (plane 1 1 1) of natural diamond, which is purer than synthetic HPHT diamond, is  $72 \pm 4$  degrees [8]. This indicates moderate hydrophobicity of

diamond surface. Obviously, fully oxidised at 400 °C natural diamond has more oxygen containing functional groups at the surface, which results in hydrophilic properties, with contact angle of  $32 \pm 2$  degrees (see Section 1.2.1). It should be noted that a fully oxidised diamond surface contains hydroxyl- or carboxyl- functional groups in concentrations up to 9.6 and  $10.5 \mu\text{mol}\cdot\text{m}^{-2}$ , respectively as reported by Gordeev *et al.*[9].

As 5 M  $\text{HNO}_3$  was used for purification, as described in Section 2.3.1, this may cause oxidation of HPHT diamond. According to FTIR data (Fig. 3.2) the surface of purified HPHT diamond is a highly oxidised hydrophilic surface with dominant presence of hydroxyl and carbonyl groups and smaller amount of carboxylic groups, and free of silica.

The presence of hydroxyls and carboxyls at the surface provides constant  $\zeta$ -potential of  $-60$  mV for the purified HPHT diamond particles at pH above 8, where dissociation for all functional groups with labile proton takes place. However, it was found that the surface of HPHT diamond is negatively charged across the whole pH range, which is different from the  $\zeta$ -potential profile obtained for MSDN. As shown in Fig. 4.1 the surface of the MSDN sample used in this work can be positively charged ( $+18$  mV) under acidic solutions with pH  $< 5.0$ , or negatively charged ( $-23$  mV) in alkaline solutions with pH  $> 10$ . These values of  $\zeta$ -potentials for MSDN are in a good agreement with data reported earlier for detonation nanodiamond obtained by using alternative purification schemes [27].

So, according to the obtained data the surface chemistry of HPHT diamond is populated with hydroxyls and carboxylic groups, together with chemisorbed water molecules, which results in polar hydrophilic properties. For this reason the HPHT diamond stationary phase should be used in normal-phase HPLC mode.

#### **4.3.2. Retention mechanism and separation selectivity**

Table 4.1 shows the retention factors ( $k$ ) for various aromatic substances obtained for columns packed with HPHT diamond, MSDN and PGC with *n*-hexane – IPA mobile phases. The  $k$  values for HPHT diamond column are in good agreement with properties of an adsorbent having a hydrophilic surface with negatively charged functional groups. As was mentioned previously, the surface of diamond contains hydroxy-, carbonyl- and a small amount of carboxy- functional groups. Accordingly, the retention of non-polar compounds such as alkanes and alkylbenzenes, with *n*-hexane mobile phase, is weak, except for polycyclic aromatic hydrocarbons (PAH), which exhibit stronger retention than other nonpolar solutes.

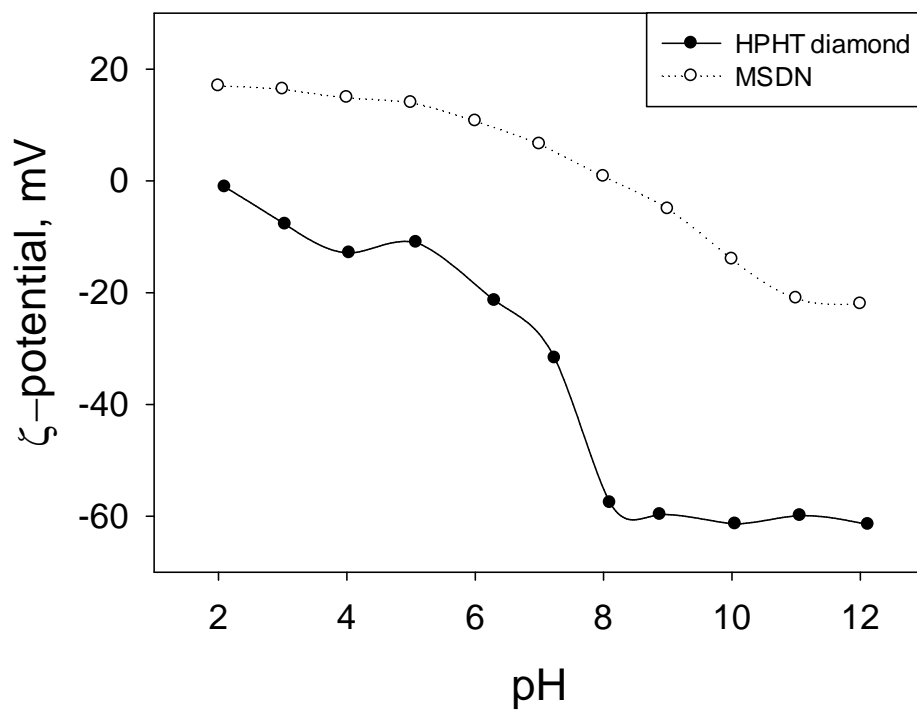


Fig. 4.1. Influence of pH on the  $\zeta$ -potential of HPHT diamond and MSDN measured for  $0.1 \text{ mg}\cdot\text{mL}^{-1}$  suspensions in  $1 \text{ M NaNO}_3$  at  $25^\circ\text{C}$ . pH of suspensions was adjusted with  $\text{HNO}_3/\text{NaOH}$ .

The elution of PAH from HPHT diamond column was achieved by using n-hexane containing 1% of IPA as mobile phase. A coplanar orientation of PAH molecules on the flat surface of crystal diamond and associated multiple interactions can be responsible for this. A linear dependence of  $\log k$  on number of  $\pi$ -electrons in PAH molecules was observed (Fig. 4.2), while the slope of the dependence (0.217) for HPHT diamond was lower than found for PGC (0.377) in this work, and is bigger than reported for bare silica with pure n-hexane (0.057) by Lanin *et al.* [10]. Also, PAHs are strongly retained on MSDN column and can be eluted with n-hexane containing 40% of IPA, while retention factors 0.21, 13.38 and  $> 200$  recorded for benzene, naphthalene and anthracene, respectively.

The retention of substituted benzenes on HPHT diamond column is stronger as compared to neutral alkyl benzenes. The following elution order was observed for mono-substituted derivatives of benzene: toluene  $<$  chlorobenzene  $<$  iodobenzene  $<$  benzyl chloride  $<$  anisole  $<$  nitrobenzene  $<$  methylbenzoate  $<$  benzaldehyde  $<$  alkyl phenyl ketones  $<$  benzonitrile  $<$  benzyl alcohol  $<$  phenol  $<$  benzoic acid, which is similar to the elution order reported for MSDN [11]. Very polar compounds such as phenols and benzoic acids, having labile protons in functional groups, are retained much stronger as compared with other solutes and the use of eluents containing 1-5% of IPA is required. The elution order of substituted benzenes obtained for PGC column is different, with much stronger retention observed for nitrobenzene, benzaldehyde and phenol.

As expected, the strongest retention is recorded for aromatic bases including pyridine and 4-chloroaniline, which is due to hydrogen bonding and electrostatic interactions of these molecules with OH and COOH groups at the surface of diamond. Thus, according to the classification of adsorbents introduced by Kiselev [12], the oxidised HPHT diamond can be identified as Type III adsorbent i.e. adsorbent having negatively charged groups (carbonyls, esters, carboxyls etc.). In adsorption liquid chromatography with binary mobile phases composed of solvents of very different polarity, the linear relationship between retention factor ( $k$ ) and molar fraction ( $X_B$ ) of polar solvent (solvent B) in the mobile phase can be described by the following equation (4.1) [13,14]:

$$\log k = a - n \cdot \log X \quad (\text{Equation 4.1})$$

where  $a$  and  $n$  are factors, and  $X$  is the mole fraction of polar solvent in the mobile phase. The  $\log k$ - $\log X$  plots obtained for 6 solutes are shown in Fig. 4.3.

Table 4.1. Retention factors ( $k$ ) of model compounds for HPHT diamond, MSDN and PGC columns. Mobile phase: IPA/*n*-hexane, 25 °C, sample: 1  $\mu$ L of 0.1 mg·mL<sup>-1</sup> solution of compound in mobile phase.

#	Compound	IPA, %	$k$ , HPHT	$k$ , PGC	IPA, %	$k$ , MSDN
1	Benzene		0.048	0.100		25.3
2	Toluene		0.049	0.108		18.6
3	Ethylbenzene		0.050	0.123		9.68
4	Propylbenzene		0.051	0.139		9.90
5	Butylbenzene	0	0.052	0.154		10.1
6	Pentylbenzene		0.055	0.169	0	10.3
7	<i>o</i> -Xylene		0.050	-		-
8	<i>m</i> -Xylene		0.053	-		-
9	<i>p</i> -Xylene		0.052	-		-
10	Chlorobenzene		0.072	-		-
11	Iodobenzene		0.088	-		-
12	Benzyl chloride		0.094	-		-
13	Anisole		0.15	0.45		3.75
14	Nitrobenzene		0.61	2.46		15.8
15	Methyl benzoate		0.68	1.31		10.6
16	Dimethoxybenzene		0.75	1.03		>50
17	Benzaldehyde		1.05	2.38		19.2
18	Acetophenone	0.1	1.91	1.73	2.5	22.0
19	Propiophenone		1.23	1.91		11.7
20	Butyrophenone		1.26	2.10		8.03
21	Valerophenone		1.28	2.32		6.09
22	Hexanophenone		1.32	2.67		4.91
23	Benzophenone		3.62	20.9		24.4
23a	Dibenzyl ketone		5.96	-		-
24	Biphenyl		0.38	3.65		>50
25	Benzonitrile		2.10	-		-
26	Benzyl alcohol		1.01	5.35		>50
27	Phenol		8.50	91.3		>50
28	Naphthalene		0.14	2.60		>50
29	Acenaphthene		0.14	7.69		>50
30	Fluorene	1	0.39	41.3		>50
31	Phenanthrene		1.64	-	50	-
32	Anthracene		1.96	-		-
33	Pyrene		4.86	-		-
34	Fluoranthene		5.50	-		-
35	Benzoic acid		0.51	1.33		>50
36	Propylbenzoic acid	5	0.42	1.70		>50
37	Heptylbenzoic acid		0.52	4.23		>50
38	4-chloroaniline		26.9	5.01		17.2
39	Pyridine	20	20.3	3.11		13.5

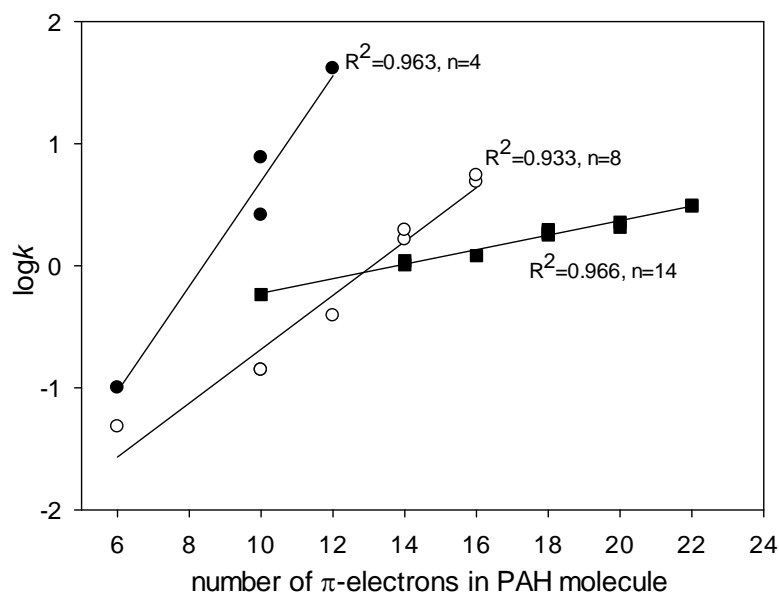


Fig. 4.2. The dependence of  $\log k$  of PAH on the number of  $\pi$ -electrons in the molecule. Data marked by (●) and (○) obtained in this work with Hypercarb and HPHT diamond columns, respectively. 1  $\mu\text{L}$  injections of  $100 \mu\text{g}\cdot\text{mL}^{-1}$  PAH solutions in mobile phase (*n*-hexane containing 1% of IPA), flow rate  $0.5 \text{ mL}\cdot\text{min}^{-1}$ , 210 bar, 25 °C. Data for silica column (■) and pure *n*-hexane as mobile phase is adapted from work [10].

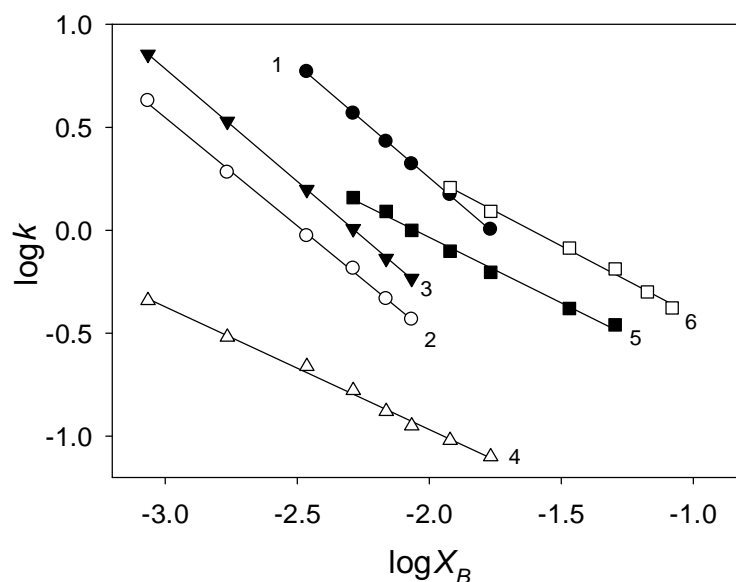


Fig. 4.3. The dependence of  $\log k$  of model substances on molar fraction ( $X$ ) of IPA in mobile phase.  $100 \times 4.6 \text{ mm}$  ID column, 1  $\mu\text{L}$  injections of  $100 \text{ mg}\cdot\text{l}^{-1}$  of solute in mobile phase, flow rate  $0.5 \text{ mL}\cdot\text{min}^{-1}$ , 210 bar, 25 °C. Solutes: benzyl alcohol (1), acetophenone (2), benzophenone (3), naphthalene (4), anthracene (5), pyrene (6).



The values of slopes obtained for acetophenone, benzophenone and benzyl alcohol ( $n = 1.1$ ) are significantly bigger than those obtained for naphthalene, anthracene and pyrene ( $n \sim 0.6$ ). This is a clear indication of difference in the retention mechanisms for these two classes of compounds. The retention of benzyl alcohol and alkyl phenyl ketones involves hydrogen bonding between carbonyl or hydroxyl group in the molecule of solute and hydroxy- and carboxy- groups on the surface of HPHT diamond. On the other hand, the retention of PAHs is rather associated with multiple non-specific interactions due to weak dispersive forces between planar PAHs molecules and flat surface of the diamond particles. There is a high probability of coplanar orientation of PAH molecules relative to diamond surface, which enhances the affinity of HPHT diamond toward number of  $n_C$  in aromatic structure of PAH as shown in Fig. 4.2. Obviously, the addition of IPA into the mobile phase produced a more significant effect on the hydrogen bonding of polar aromatic molecules than on the dispersive forces in the case of PAH molecules. Similar chromatographic properties have been reported for MSDN [11] (see also Table 4.1). Another carbonaceous adsorbent, Hypercarb, shows increased retention for solutes with a higher number of  $\pi$ -electrons in the molecule, as well as for phenols and benzoic acids having labile protons and retained through “polar retention effect on graphite” (PREG) mechanism [1].

This difference in retention mechanism between alkyl phenyl ketones and PAH molecules can be also supported by the values of adsorption enthalpies ( $\Delta H^\circ$ ) calculated from van Hoff plots (Eqn. 4.2) obtained for the HPHT diamond column over the temperature range 25–65 °C. Generally, parameter  $\beta$  representing phase ratio in the column is a characteristic constant for a given column. In this work  $\beta$  was calculated as described in Section 2.4.2. However, because of a huge difference in linear thermal expansion coefficients between diamond ( $\alpha_T = 0.05 \times 10^{-6} \text{ K}^{-1}$  [15]) and stainless steel ( $\alpha_T = 12.0 \times 10^{-6} \text{ K}^{-1}$  [15]), the variation of phase ratio  $\beta$  with temperature changes is expected. On this reason  $\beta$  value was calculated using void volume value measured at each temperature. It was found that  $V_0$  increases from 0.735 cm<sup>3</sup> at 25 °C to 0.743 cm<sup>3</sup> at 65 °C for 50 × 4.6 mm I.D. column (see Section 2.4.2). Thus, increase of temperature from 25 °C to 65 °C causes approximately 1.0% change in phase ratio for this column. The corresponding changes in  $\beta$  are counted in calculations of  $\Delta H^\circ$  values, as explained in Section 2.4.3. To underline this effect  $\ln\beta(T)$  term is used instead of  $\ln\beta$  as follows:

$$\ln k = -\Delta H^\circ/RT + \Delta S^\circ/R + \ln\beta(T) \quad (4.2)$$

Table 4.2. Adsorption enthalpy ( $\Delta H^\circ$ ) and entropy ( $\Delta S^\circ$ ) values calculated from ( $\ln k - 1/T$ ) plots for various substances on HPHT diamond column, using *n*-hexane/ IPA mobile phase, flow rate 0.5 mL·min<sup>-1</sup>. Values obtained for temperature range 25-65 °C.

Solute	$\Delta H^\circ$ , kJ·mol <sup>-1</sup>	$\Delta S^\circ$ , J·mol <sup>-1</sup> ·K <sup>-1</sup>
Nitrobenzene	1.90±0.13	10.7±0.7
Benzaldehyde	5.37±0.21	27.1±1.1
Propiophenone	4.75±0.18	26.8±1
Acetophenone	5.27±0.15	31.9±0.9
Benzophenone	5.85±0.09	39.7±0.6
Anisole	3.44±0.59	4.51±0.78
Dimethoxybenzene	1.26±0.06	15.9±0.7
Biphenyl	-14.2±1.5	-44.9±4.7
Naphthalene	-15.5±1.5	-48.3±4.6
Anthracene	-15.8±1.1	-46.2±3.4
Pyrene	-16.0±0.7	-39.3±1.6

As shown in Table 4.2,  $\Delta H^\circ$  values are negative for PAH molecules were indicative of an exothermic process, while endothermic effects were noted for polar alkoxybenzenes, alkyl phenyl ketones and benzaldehyde molecules. Indirectly, this confirms the difference in the retention mechanism for these classes of compounds. As expected, entropy  $\Delta S^\circ$  has a negative value for PAH flat molecules with limited number of degrees of freedom. At the same time, phenols and phenones which are retained due to hydrogen bonds have much higher entropy in the adsorbed state. This means that they have more degrees of freedom on the surface of stationary phase, than in the mobile phase. The probable explanation is that in adsorbed state molecules would gain extra entropy through more frequent formation of hydrogen bonds with hydroxyls on diamond surface, since at low IPA content H-bonds with surface hydroxyls can be prevalent. However, energy of this H-bonds could be smaller than in solution (for example due to lower acidity of surface OH groups), which results in positive enthalpy values.

As was said previously, void volume increase with temperature was observed due to the expansion of stainless steel column body (while diamond expansion is negligible). This resulted in up to 50% peak broadening at higher temperatures. Therefore, separations at high temperatures are not presented in this work, as initially planned. However it should be mentioned, that this problem does not diminish the potential of using thermally stable diamond based stationary phases in high-temperature liquid chromatography. Further research in this area will be focused on possibility of using chromatographic tubing made of Ti or Zr alloys having very low thermal expansion coefficients.

#### **4.3.3. Influence of column conditioning on the retention in NP-HPLC**

Since the ionisable oxygen containing functionalities are present on the surface of HPHT diamond, it is important to know how the state of the surface can influence the retention of various solutes in NP-HPLC. Especially, carboxylic groups may have a strong impact on the retention, since they can be in protonated or deprotonated forms with various counter-ions. The retention factors for three model compounds on the HPHT diamond column after conditioning with different pH buffer solutions are shown in Table 4.3.

Clearly, flushing the column with alkaline solutions, such as 10 mM NaOH or KOH, turns the surface carboxyls into the anionic form, which results in a strong negative surface charge ( $\sim -80$  mV, see Fig. 3.4). This weakens hydrogen bonding and leads to smaller  $k$  values, as compared to the unconditioned column, or column conditioned at neutral pH (6.5).

Table 4.3. Influence of column conditioning with various pH buffers on the retention of solutes in NP-HPLC. Mobile phase – 0.1% of IPA in *n*-hexane.

Column conditioning	<i>k</i>		
	Benzaldehyde	Acetophenone	Benzophenone
Before conditioning	1.05	1.91	3.62
Sodium hydroxide, pH 12.0	0.93	1.26	1.87
Potassium hydroxide, pH 12.0	0.93	1.26	1.87
10 mM Sodium phosphate buffer, pH 12.0	0.99	1.45	2.29
10 mM Sodium carbonate buffer, pH 12.0	0.98	1.44	2.27
10 mM Sodium phosphate buffer, pH 6.5	1.06	1.91	3.59
Phosphoric acid, pH 2.0	0.37	0.59	0.83
Nitric acid, pH 2.0	1.01	1.61	3.19
Sulfuric acid, pH 2.0	1.00	1.60	3.14
Methanesulphonic acid, pH 2.0	0.99	1.60	3.13

In the case of using carbonate and phosphate buffers with pH 12, similar decrease in the retention times was observed, but to a lower extent due to the weak basic character of these buffers. No significant influence of counter-ion of carboxyl groups ( $\text{Na}^+$  or  $\text{K}^+$ ) on the retention was registered. Flushing column with the acids (pH 2.0) turns the surface carboxyls to protonated form and reduces surface charge close to the zero value (see Section 3.3.1.2). This results in stronger retention of model solutes, than in the case of column conditioning with the alkaline solvents. However,  $k$  values after the conditioning with acids are still smaller than before conditioning. Apparently, this is due to the adsorption of anions on the diamond surface. Especially, this is clear in the case of using phosphate buffer with pH 2.0. Strong interaction between diamond surface and phosphate is known in literature [16]. Regarding other anions, there is a lack of data on their adsorption on diamond (see Chapter 6), which complicates the explanation of the observed phenomena.

#### **4.3.4. Comparison with other carbonaceous adsorbents**

As discussed above, the surface chemistry and matrix properties of HPHT diamond are different from other carbonaceous adsorbents, including MSDN, where significant amounts of graphitic carbon is presented at the surface, and also fully graphitic adsorbents, as PGC.

##### **4.3.4.1. Comparison with MSDN**

It was shown that the retention of polar solutes such as phenols or benzoic acids on MSDN in methanol–water and acetonitrile–water based mobile phases is defined by acidity of phenol and carboxylic group, respectively [17,18], which was explained by the presence of conducting  $sp^2$ -carbon layer on the surface of detonation diamond. In this work the same set of phenols was used to check the retention properties of HPHT. Table 4.4 contains data on retention of various phenols for HPHT diamond under NP-HPLC conditions and data reported for MSDN under RP-HPLC/HILIC mode [17]. In general, a good correlation ( $R^2 = 0.901$ ,  $n = 13$ ) between the retention of phenols on HTHP diamond and on MSDN was observed, which indicates a similarity in the retention mechanism. However, a few exceptions were noted in a group of phenols with strong electron-acceptor substituents, such as nitro- or multiple chloro-groups. For these compounds, the retention was unexpectedly high on HPHT diamond, which could be due to ion-dipole interactions between charged groups on the diamond surface and the polarised aromatic ring of the solute molecule. Obviously, such interactions are stronger in the case of HPHT diamond, which surface is more saturated with the charged groups as compared with MSDN (see Fig. 4.1).

Table 4.4. Retention data for substituted phenols on HPHT diamond column (mobile phase – 10% of IPA in *n*-hexane, 25 °C, 1  $\mu$ L injections of 100  $\text{mg}\cdot\text{l}^{-1}$  of solute in mobile phase), and on MSDN diamond in 90% of acetonitrile in water [17].  $\text{pK}_a$  in water and  $\log P$  values are taken from [17].  $\text{pK}_a$  in IPA are taken from [19].

№	Compound	$\text{pK}_a$ in IPA	$\text{pK}_a$ in water	$\log P$	$k$ , HPHT diamond	$k$ , MSDN
5	2-tertbutyl-4-methyl phenol	-	11.7	3.97	0.09	0.09
7	2,6-diisopropylphenol	-	11.1	4.43	0.13	-
6	2,4-dimethylphenol	-	10.6	2.30	0.40	1.05
4	4-methylphenol	-	10.3	1.94	0.77	0.86
2	4-methoxyphenol	-	10.1	1.58	2.08	1.42
1	Phenol	13.7	9.99	1.46	1.25	1.04
3	2-methoxyphenol	-	9.98	1.32	5.90	2.09
9	4-chlorophenol	15.31	9.41	2.39	2.31	1.93
10	4-bromophenol	14.3	9.17	2.59	2.31	3.70
8	2-chlorophenol	15.83	8.56	2.15	3.94	3.25
14	3-nitrophenol	13.92	8.36	2.00	>90	7.07
11	2,4-dichlorophenol	14.48	7.89	3.06	24.4	9.67
12	2,5-dichlorophenol	-	7.51	3.06	21.5	19.9
15	2-nitrophenol	13.3	7.23	1.79	>90	12.5
13	2,6-dichlorophenol	13.58	6.79	2.75	30.0	38.4
16	2,4,6-trichlorophenol	12.55	6.23	3.69	>90	45.3
17	Pentachlorophenol	-	4.74	5.12	>90	87.9

The  $\log k$  values for substituted phenols on HPHT column are well-correlated ( $R^2 = 0.873$ ,  $n = 13$ ) with the pKa of the phenol groups in water (Table 4.4). It should be noted that a stronger correlation ( $R^2 = 0.977$ ) for the same set of solutes is reported before for MSDN column in acetonitrile-water mobile phase [17]. At the same time, no correlation ( $R^2 = 0.104$ ,  $n = 13$ ) was recorded between  $\log k$  and hydrophobicity of phenols expressed as  $\log P$ . This confirms the conclusion regarding hydrophilic properties of the HPHT diamond surface (Section 3.3.1.2).

An important question has been raised whether it is appropriate to correlate  $k$  obtained in *n*-hexane based mobile phases with pKa of phenols in water solutions. Generally, it is rather hard to find information about pKa values for different compounds in non-aqueous solutions. Therefore, majority of researchers prefer to use aqueous pKa in order to explain retention behaviour. In Table 4.4 several pKa values presented for IPA, which, however were not measured but calculated [19]. Clearly, there is no correlation between pKa in water and IPA for this set of phenols. Accordingly, correlation between  $k$  and acidity in water in such case would not make sense. On the other hand, calculated pKa values often are far away from the measured values, and some researchers believe that correlation between aqueous and non-aqueous acidity has to be strong [20]. Overall, there is no agreement in this matter, but it is obviously a very important issue, since explanation of a large segment of chromatographic experiments is affected.

The separation selectivity ( $\alpha = k_2/k_1$ ) towards positional isomers was checked for MSDN and HPHT diamond columns. Similar values of  $\alpha$  for a pair of *o*- and *p*-chlorophenols of 1.71 and 1.68 were obtained for HPHT diamond and MSDN, respectively. However, more significant differences in separation selectivity were observed for *o*- and *p*-methoxyphenols, with  $\alpha = 2.83$  for HPHT diamond, and  $\alpha = 1.47$  for the MSDN column. Possibly, this is due to higher volume of methoxy- group as substituent in ortho position, which could be responsible for shielding of phenol group and some sterical hindrance effects within microporous structure of MSDN.

The difference in separation selectivity between two diamond based columns can be also connected with presence of conducting graphene type  $sp^2$ -carbon layer at the surface of MSDN at the top of non-conducting diamond cores (see Section 1.2.3). Accordingly, phenols with labile protons (low pKa value) can easily induce dipoles upon the surface of the MSDN, which cause stronger retention of corresponding molecules. Another reason is the possibility of hydrogen-bonding and ion-induced dipole interactions between benzene derivatives and protons from OH- and COOH- groups at the surface of HPHT diamond column.

#### 4.3.4.2. The effect of alkyl chain length on retention of alkylbenzenes and alkyl phenyl ketones

In Section 4.3.4.1 the properties of HPHT diamond and MSDN columns are compared using different solvents systems as the mobile phase, which could be a reason for some disagreement between obtained data. Therefore, the additional experiments on the comparison of separation selectivity of HTHP diamond, MSDN and PGC columns in NP-HPLC mode was carried out. The values of retention factors obtained for 40 solutes are presented in Table 4.1. Generally, much higher  $k$  values are recorded for MSDN column, which is due to the highly polar surface and well developed surface area of  $191 \text{ m}^2 \cdot \text{g}^{-1}$ . Therefore, a higher concentration of more polar solvent is required for the elution of some solutes, while PAH cannot be eluted from MSDN column even with 50% of IPA in *n*-hexane as eluent.

To compare PGC and HPHT diamond selectivity the corresponding orthogonality plot is built for 28 compounds representing various classes of aromatic compounds (see Fig. 4.4). Despite the difference in content of IPA in mobile phases used for elution of model compounds, a strong correlation ( $R^2 = 0.952$ ) between logarithms of retention factors ( $\log k$ ) for the set of 17 model compounds marked with open shapes in Fig. 4.4 is recorded. At the same time, there is a visible difference between of these adsorbents towards three groups of compounds including PAH, alkyl phenyl ketones and aromatic bases. Clearly, the known effect of co-planar coordination of flat PAH molecules upon the planar structure of PGC surface is responsible for  $\pi$ - $\pi$  stacking and for the stronger retention of PAH on Hypercarb column. The increased affinity of HPHT diamond as compared with PGC column is also recorded for alkyl phenyl ketones, which can be attributed to hydrogen bonding between keto- groups of solutes and hydroxyl groups at the surface of HPHT diamond. Obviously, the presence of negatively charged carboxyls and hydroxyls at the surface of HPHT diamond is responsible for the stronger retention of aromatic bases, as compared with neutral PGC. Surprisingly, no visible contribution of PREG mechanism (polar retention effect on graphite) in retention of very polar organic substances (phenol, carboxylic acids etc.) on PGC column is reflected by the orthogonality plot.

Finally, three carbonaceous phases are compared by retention of monoalkylbenzenes and alkyl phenyl ketones with varied length of alkyl substituent. This model was used before for the description of the properties of silica, alumina, MSDN and PGC [21], and chemically modified silica [22,23]. Here, the corresponding plots were obtained for HPHT diamond, MSDN and PGC columns with *n*-hexane and *n*-hexane– IPA mixture as the eluent (Fig. 4.5).



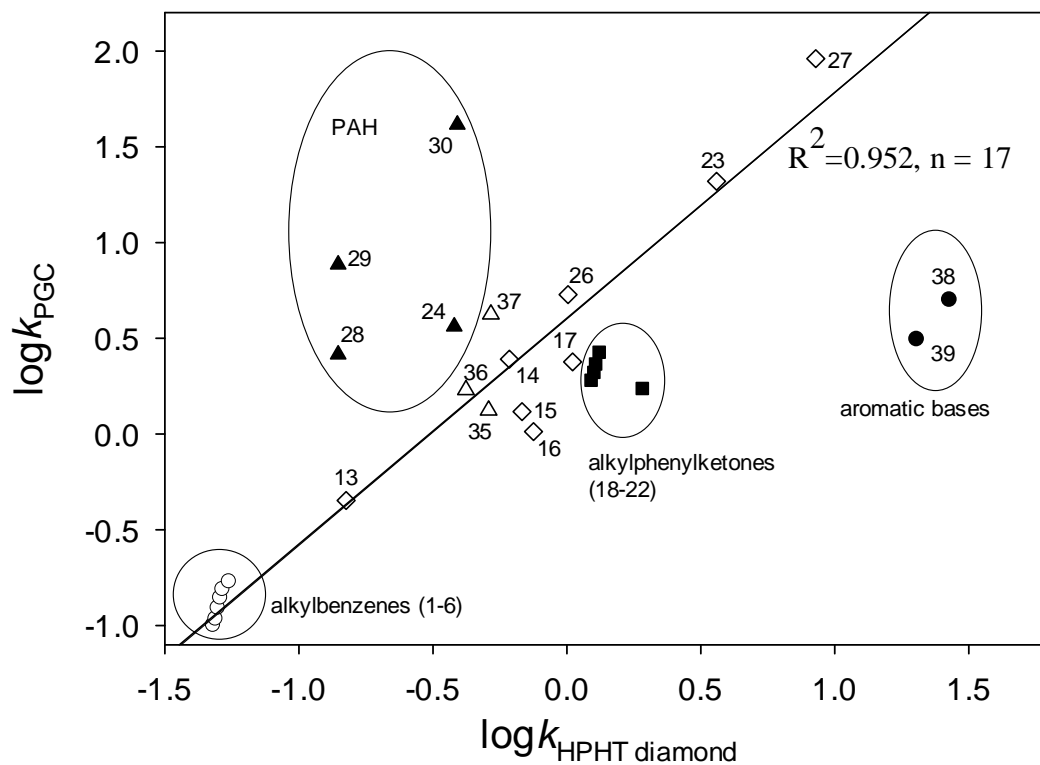


Fig. 4.4. Orthogonality of retention factors ( $\log k$ ) obtained for 28 aromatic compounds on HPHT diamond and PGC columns in NP-HPLC. Solutes: ( $\blacktriangle$ ) – PAH, ( $\blacksquare$ ) – alkyl phenyl ketones, ( $\bullet$ ) – aromatic bases, ( $\circ$ ) – alkylbenzenes, ( $\Delta$ ) – alkanolic acids, ( $\diamond$ ) – miscellaneous aromatic compounds. All compounds are numbered according to Table 4.1. Eluent: varied concentration of IPA in *n*-hexane: 0.1% for compounds from 13 to 24, 1% for compounds from 26 to 30, 5% for compounds from 35 to 37, and 20% for compounds 38 and 39, respectively. Linear regression is presented for 17 data points marked by open circles, triangles and diamonds.

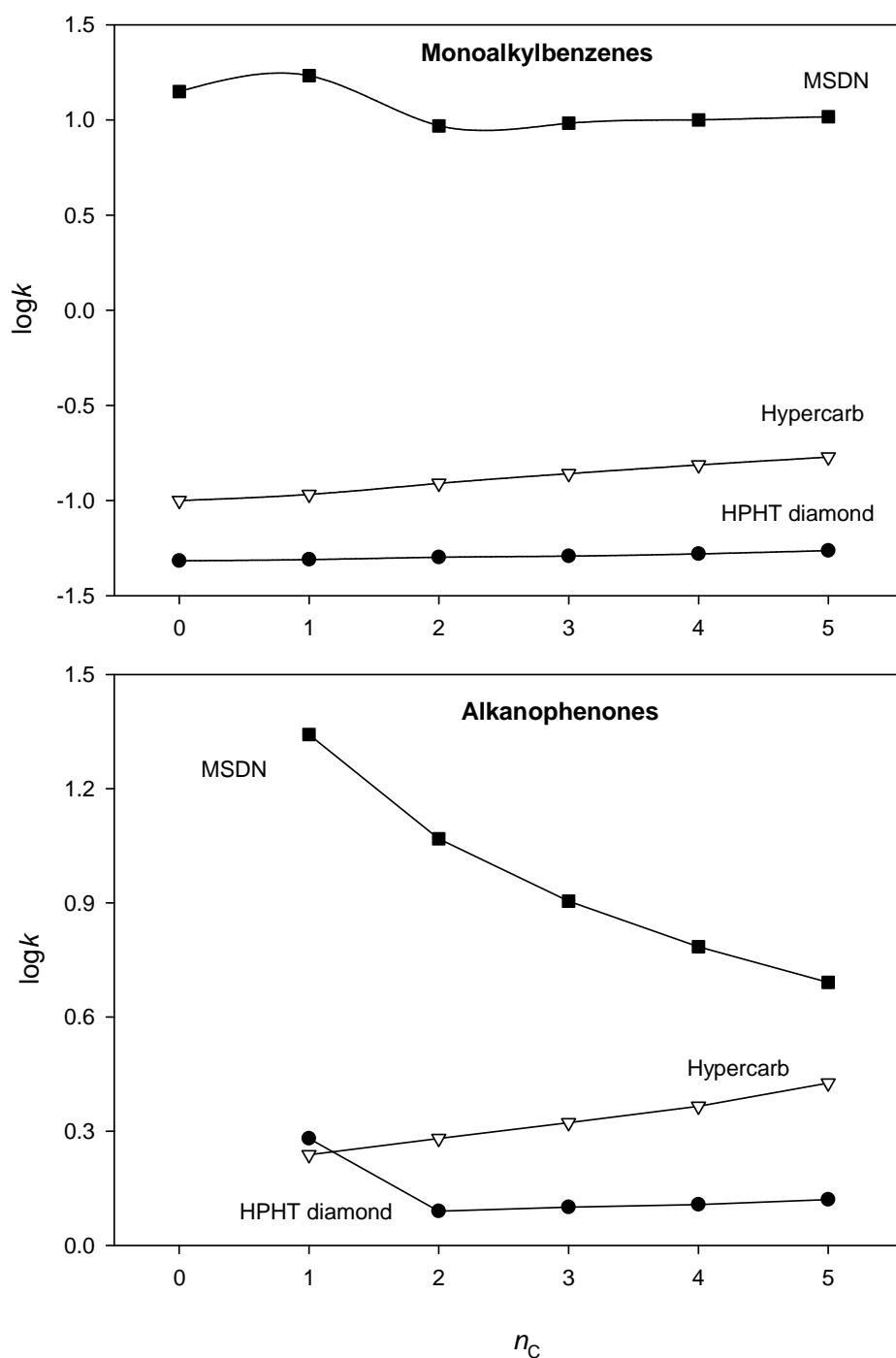


Fig. 4.5. Dependence of  $\log k$  on the carbon atom number in alkyl chain for mono-substituted benzenes (upper figure, benzene to pentylbenzene, mobile phase – *n*-hexane) and phenones (lower figure, acetophenone to hexanophenone, mobile phase – 0.1% of IPA in *n*-hexane). Comparison between HPHT diamond, PGC and MSDN columns.

The increase of the length of alkyl chain increases the retention of both alkylbenzenes and alkylphenones on PGC column, but more slightly on HPHT and not in MSDN column. This is in agreement with the results of Nesterenko *et al.* who observed this effect for the retention of dialkylphthalates on MSDN in NP-HPLC [11]. Possibly, this effect is connected with size-exclusion phenomenon for long chain molecules the fine porous structure of MSDN, having trimodal distribution of pores size with maxima at 0.7, 1.4 and 3.1 nm [24].

### **4.3.5. Chromatographic performance**

#### **4.3.5.1. HPHT diamond column loading capacity**

Maximum column loading capacity of the column was determined by the injection of 1–12  $\mu\text{L}$  of sample with constant concentration of  $2 \mu\text{g}\cdot\text{mL}^{-1}$  solution of acetophenone in mobile phase and by injection of 1  $\mu\text{L}$  of acetophenone solution with varied concentration from  $1 \mu\text{g}\cdot\text{mL}^{-1}$  to  $1000 \mu\text{g}\cdot\text{mL}^{-1}$ . The corresponding plots of  $\log k$ , number of theoretical plates and peak asymmetry against amount of injected acetophenone are presented in Fig. 4.6.

The visible drop in all three parameters occurred for the injections of 1  $\mu\text{L}$  of acetophenone solution in mobile phase with concentration higher than  $100 \mu\text{g}\cdot\text{mL}^{-1}$ , which is mass equivalent of 0.1  $\mu\text{g}$  or 0.83 nanomols. Assuming area of acetophenone molecule is  $0.4 \text{ nm}^2$  means that the surface area occupied by solute molecules during such injection is  $0.0002 \text{ m}^2$ . At the same time, during 1  $\mu\text{L}$  injection, sample band will occupy 0.283% of column volume (void volume is  $352.8 \mu\text{L}$ ). Such volume will contain  $0.00283 \cdot 8.9 = 0.0252 \text{ m}^2$  of diamond surface ( $8.9 \text{ m}^2$  per 50 mm column). Therefore, surface coverage with acetophenone within this sample band will equal  $0.0002/0.0252 = 0.00794 \approx 0.8\%$ , which corresponds to Henry region of adsorption (low surface coverage). Therefore, it can be claimed that no column overloading was evidenced under conditions used in this paper (injection volume 1  $\mu\text{L}$  and sample concentrations below  $100 \mu\text{g}\cdot\text{mL}^{-1}$ ).

#### **4.3.5.2. Separations with HPHT diamond column**

The separation of model mixture of 8 compounds within 6 min on the  $50 \times 4.6 \text{ mm ID}$  HPHT diamond column is shown in Fig. 4.7. All chromatographic peaks exhibit modest fronting and almost no tailing except for the peak of dibenzyl ketone. The possible reason for peak fronting for early eluting peaks can be associated with low surface area of  $5.1 \text{ m}^2\cdot\text{g}^{-1}$  for nonporous HPHT diamond particles.

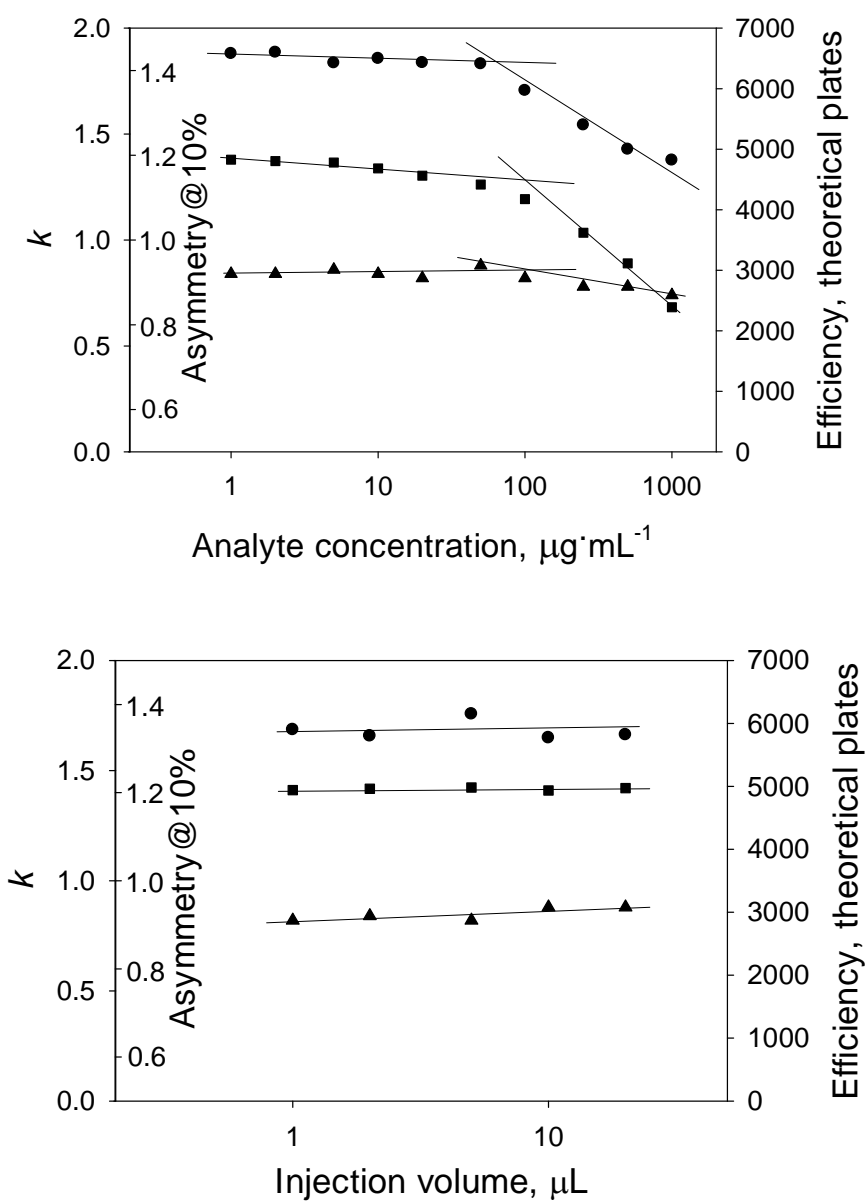


Fig. 4.6. Influence of solute concentration and injection volume on the performance of  $50 \times 4.6$  mm ID HPHT diamond column. Mobile phase – 0.15% of IPA in *n*-hexane,  $0.5 \text{ mL}\cdot\text{min}^{-1}$ ,  $30^\circ\text{C}$ . Injections of acetophenone in mobile phase ( $V = 1 \mu\text{L}$  in upper figure, and  $C = 2 \mu\text{g}\cdot\text{mL}^{-1}$  in bottom figure). Plotted: retention factor (squares), efficiency (circles) and peak asymmetry at 10% height (triangles).

This value is relatively small as compared to surface area of  $100 - 500 \text{ m}^2 \cdot \text{g}^{-1}$  for majority of mesoporous adsorbents (mean pore diameter  $D_{\text{pore}} = 2-50 \text{ nm}$ ) used in HPLC, but they are close to the values of surface area for macroporous silica adsorbents such as LiChrospher 4000 ( $d_p = 7 \text{ }\mu\text{m}$ ,  $S_{\text{BET}} = 6 \text{ m}^2 \cdot \text{g}^{-1}$ ,  $D_{\text{pore}} = 400 \text{ nm}$ ) and Spherosil XOC-005 ( $d_p = 7 \text{ }\mu\text{m}$ ,  $S_{\text{BET}} = 10 \text{ m}^2 \cdot \text{g}^{-1}$ ,  $D_{\text{pore}} = 300 \text{ nm}$ ) [25]. Also, due to the higher density of diamond ( $3.5 \text{ g} \cdot \text{cm}^{-3}$ ) as compared with nonporous silica ( $2.2 \text{ g} \cdot \text{cm}^{-3}$ ), the mass of diamond in chromatographic column is bigger (1.75 g per  $50 \times 4.6 \text{ mm}$  ID column), corresponding to a surface area of  $8.9 \text{ m}^2$  per column. This is sufficient to carry out the chromatographic experiments at appropriate conditions without column overload. The peak tailing for dibenzyl ketone could be due to delocalisation of electron density in a molecule, where the central carbonyl carbon atom has electrophilic character and the two adjacent carbon atoms are slightly nucleophilic. Such polarisation may lead to the multi-point interaction with polar groups at the surface of diamond and resulted in as lower kinetics of desorption, which is responsible for peak tailing.

As it was shown above, the estimated loading capacity value is 0.83 nanomols per column. Though this value is  $\sim 10$  times smaller than in case of conventional silica columns, it should not contribute to peak fronting, if low volumes of diluted samples are used. Therefore, the most probable factor causing peak fronting in Figs. 4.7 and 4.8 is non-ideal column packing.

Asymmetry factors  $As_{10}$  for obtained peaks were between 1.15–1.60, which is acceptable for the majority of applications. The maximum efficiency of 128,000 theoretical plates per meter was recorded for the peak of benzophenone (Table 4.5). The retention of PAHs increases strongly with increase in number of aromatic rings (Table 4.1), so the separation of the mixture of benzene, naphthalene, anthracene and pyrene was obtained only with gradient elution (Fig. 4.8).

Fig. 4.9 presents a separation of a commercial pesticide “VC175 Tropical Strength Mould Killer” (The Flood Company Australia, Padstow, NSW, Australia) using HPHT diamond column. According to the manufacturer, the sample consists of  $<10\%$  of 2-n-octylisothiazoline-3-one (octhiline, main component), and  $>75\%$  of isobutyric acid monoester with 2,2,4-trimethylpentane-1,3-diol (solvent). Remaining  $\sim 15\%$  were not specified. From the separation (Fig. 4.9), it is clear that at least 4 components are present. The first peak on the chromatogram is clearly a solvent peak ( $k = 0.24$ ), since it absorbs weakly at 220 nm, as expected for an ester without aromaticity (UV data is not available for this compound). Apparently, second peak ( $k = 0.62$ ) is octhiline. In order to confirm this, separation was repeated using different detection wavelength, and the intensity of this peak followed the UV

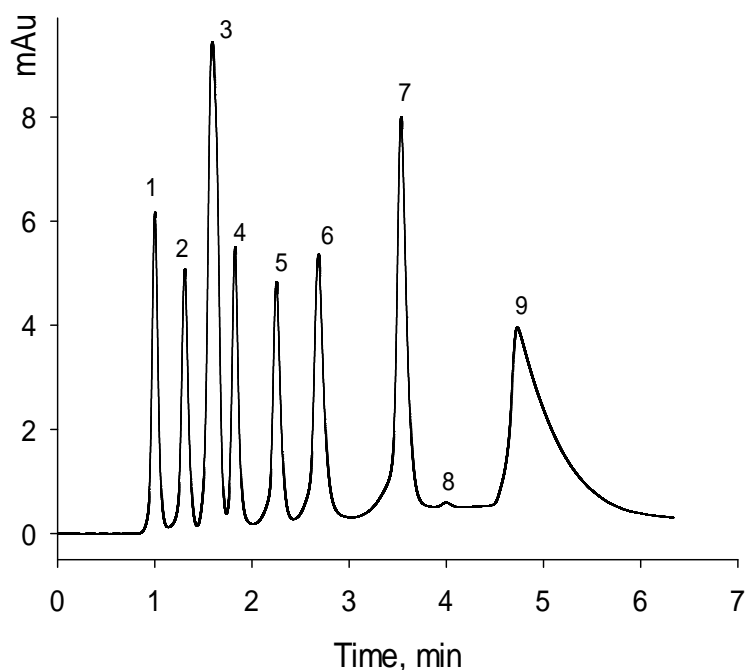


Fig. 4.7. Separation of test mixture on  $50 \times 4.6$  mm ID HPHT diamond column. Mobile phase – 0.1% of IPA in *n*-hexane, flow rate  $0.5 \text{ mL} \cdot \text{min}^{-1}$ , 210 bar,  $25 \text{ }^\circ\text{C}$ , sample volume  $3 \text{ } \mu\text{L}$ , detection at 254 nm. Solutes: anisole (1), nitrobenzene (2), benzaldehyde (3), propiophenone (4), acetophenone (5), benzoquinone (6), benzophenone (7), unknown compound (8), dibenzyl ketone (9).

Table 4.5. Retention parameters, separation efficiency and peak symmetry calculated for the peaks shown in Fig. 4.7.

Peak	$t_R$ , min	$k$	N, plates $\cdot\text{m}^{-1}$	Peak asymmetry @10%
1. Anisole	1.00	0.14	25600	1.05
2. Nitrobenzene	1.31	0.49	36300	1.04
3. Benzaldehyde	1.59	0.81	19700	1.14
4. Propiophenone	1.82	1.07	79600	1.08
5. Acetophenone	2.25	1.56	85400	1.06
6. Benzoquinone	2.68	2.05	77500	1.08
7. Benzophenone	3.53	3.01	128200	1.09
8. Unknown	3.99	3.53	-	1.14
9. Dibenzyl ketone	4.72	4.36	17700	2.87

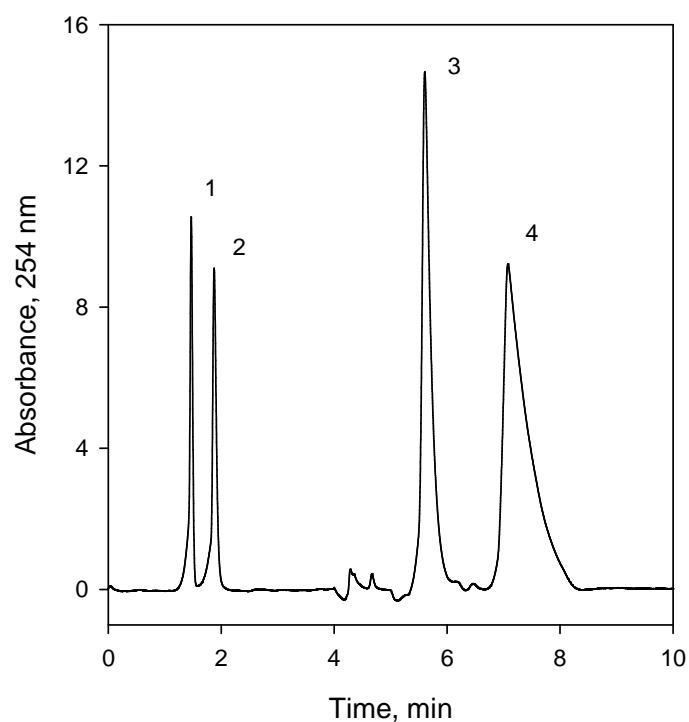


Fig. 4.8. Separation of PAHs on  $100 \times 4.6$  mm ID HPHT diamond column. Gradient elution: 0 – 1.5 min: 0.15%; 1.5 – 5 min: from 0.15% to 5%; 5 – 10 min: 5% of IPA in *n*-hexane, flow rate  $0.5 \text{ mL} \cdot \text{min}^{-1}$ , 440 bar,  $25 \text{ }^\circ\text{C}$ , sample volume  $1 \text{ } \mu\text{L}$ , detection at 254 nm. Solutes: benzene (1), naphthalene (2), anthracene (3) and pyrene (4).

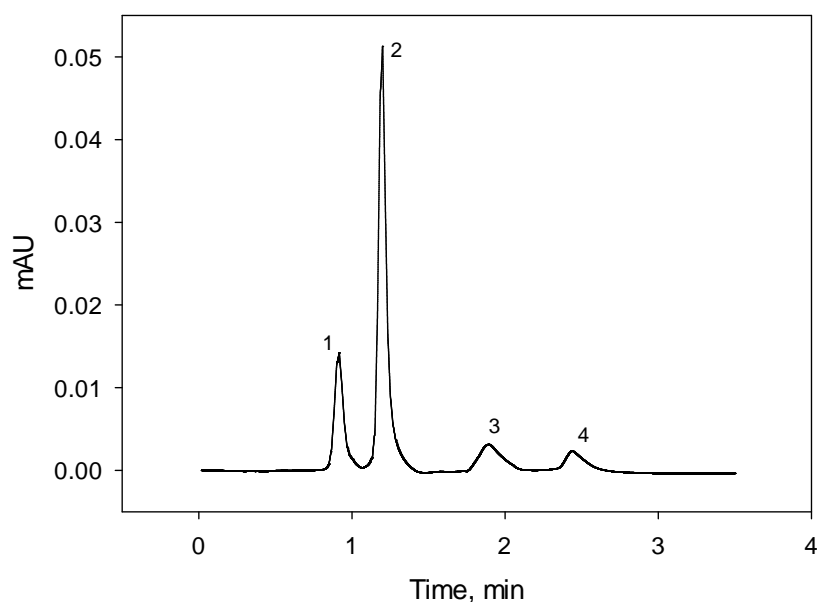


Fig. 4.9. Separation of VC175 Tropical Strength Mould Killer on  $50 \times 4.6$  mm ID HPHT diamond column. Flow rate –  $0.5 \text{ mL} \cdot \text{min}^{-1}$  of *n*-hexane, 210 bar,  $25 \text{ }^\circ\text{C}$ , injection  $1 \text{ } \mu\text{L}$  of  $100 \text{ } \mu\text{g} \cdot \text{mL}^{-1}$  of sample in *n*-hexane, detection at 220 nm. See text for peak description.

spectra obtained in [26] (maximum at 280 nm). Chromatograms obtained at other wavelength are not shown here since intensity of peaks 1 and 4 was insufficient. Peak 3 ( $k = 1.56$ ) is presumably an overlap of two compounds which cannot be resolved (conclusion based upon the peak shape). It was not possible to establish the nature of these compounds since their adsorption at different wavelength did not match the spectra of any compounds commonly present in octhilonone samples [26]. Finally, fourth peak ( $k = 2.29$ ) is probably 6-Methoxy-2-methylbenzothiazol, based on its UV adsorption data from [26]. Overall, such separation demonstrates the potential of application of HPHT diamond for analysis of pesticide samples.

#### **4.4. Conclusions**

The obtained results show the potential of using angular nonporous particles of HPHT diamond as a stationary phase in HPLC. The high separation efficiency in combination with superior thermal and chemical stability makes diamond an interesting alternative to porous graphitic carbon for liquid chromatography at high temperatures and pressures. It was found that the loose synthetic diamond has hydrophilic surface and can be used in classic type of NP HPLC. Depending on properties of the solute the retention mechanism may include electrostatic interactions with carboxylic groups, hydrogen bonding with hydroxyl groups and donor–acceptor type interactions involving aromatic rings of solutes acting as hydrogen acceptors.

Remarkably, HPHT diamond showed different retention selectivity as compared with other type of diamond based adsorbent MSDN and porous graphitic carbon. Future work in this area should aim for improving of packing HPHT diamond columns and development of ways for hydrophobization of HPHT diamond to be used in RP HPLC. Special attention should be paid to column design and search for alternative column body materials with low thermal expansion, which is essential for diamond applications in high-temperature LC.

#### **4.5. Reference List**

1. L. Pereira, Porous graphitic carbon as a stationary phase in HPLC: Theory and applications, *J.Liq.Chromatogr.R.T.*, 31 (2008) 1687-1731.
2. C. West, C. Elfakir, M. Lafosse, Porous graphitic carbon: A versatile stationary phase for liquid chromatography, *J.Chromatogr.A*, 1217 (2010) 3201-3216.
3. Y. Liu, Investigation of novel microseparation techniques, PhD Thesis, Brigham Young University, 2007.



4. A. Nuamthanom, P.M. Donaldson, J. Stokes, J.C. Ford, Reversed-Phase Liquid Chromatography on Columns Packed with Synthetic Diamonds, Duquesne University 2000 Summer Research Symposium, Pittsburgh, PA (2008)
5. B.I. Kharisov, O.V. Kharissova, L. Chavez-Guerrero, Synthesis Techniques, Properties, and Applications of Nanodiamonds, *Synth.React.Inorg., Metal-Organic, Nano-Metal Chem.*, 40 (2010) 84-101.
6. A. Krueger, Beyond the shine: recent progress in applications of nanodiamond, *J.Mater.Chem.*, 21 (2011) 12571-12578.
7. D.F. Mitev, A.T. Townsend, B. Paull, P.N. Nesterenko, Screening of elemental impurities in commercial detonation nanodiamond using sector field inductively coupled plasma-mass spectrometry, *J.Mater.Sci.*, 49 (2014) 3573-3591.
8. J.O. Hansen, R.G. Copperthwaite, T.E. Derry, J.M. Pratt, A Tensiometric Study of Diamond (111) and (110) Faces, *J.Colloid Interf.Sci.*, 130 (1989) 347-358.
9. S.K. Gordeev, E.P. Smirnov, Influence of Chemical Nature of Diamond Surface on Its Adsorption Properties, *Colloid J.USSR*, 44 (1982) 492-494.
10. S.N. Lanin, Y.S. Nikitin, A.A. Pyatygin, S.M. Staroverov, The Effect of the Structure of Bonded Cyanoalkyl Stationary Phases on Their Selectivity in the Liquid-Chromatographic Separation of Polynuclear Aromatic-Hydrocarbons, *Chromatographia*, 27 (1989) 147-155.
11. P.N. Nesterenko, O.N. Fedyanina, Y.V. Volgin, Microdispersed sintered nanodiamonds as a new stationary phase for high-performance liquid chromatography, *Analyst*, 132 (2007) 403-405.
12. A.V. Kiselev, Ya.I. Yashin, *Gas-adsorption chromatography*, New York : Plenum Press, 1969.
13. S.N. Lanin, M.Y. Ledenkova, Y.S. Nikitin, Influence of the concentration of adsorbate and modifier in the mobile phase on retention in high-performance liquid chromatography, *J.Chromatogr.A*, 797 (1998) 3-9.
14. L.R. Snyder, H. Poppe, Mechanism of Solute Retention in Liquid-Solid Chromatography and the Role of the Mobile Phase in Affecting Separation - Competition Versus Sorption, *J.Chromatogr.*, 184 (1980) 363-413.
15. P.N. Nesterenko, P.R. Haddad, Diamond-related materials as potential new media in separation science, *Anal.Bioanal.Chem.*, 396 (2010) 205-211.
16. Y.W. Zhu, X.Q. Shen, Z.J. Feng, X.G. Xu, B.C. Wang, On the zeta-potential of nanodiamond in aqueous systems, *J.Mater.Sci.Technol.*, 20 (2004) 469-471.

17. O.N. Fedyanina, P.N. Nesterenko, Regularities of Chromatographic Retention of Phenols on Microdispersed Sintered Detonation Nanodiamond in Aqueous-Organic Solvents, *Russ.J.Phys.Chem.A*, 84 (2010) 476-480.
18. O.N. Fedyanina, P.N. Nesterenko, Regularities of retention of benzoic acids on microdispersed detonation nanodiamonds in water-methanol mobile phases, *Russ.J.Phys.Chem.A*, 85 (2011) 1773-1777.
19. J. Jover, R. Bosque, J. Sales, Neural network based QSPR study for predicting pK(a) of phenols in different solvents, *QSAR Comb.Sci.*, 26 (2007) 385-397.
20. D.D. Perrin, *Dissociation Constants of Organic Bases in Aqueous Solution*, Butterworths, London, 1972.
21. P.N. Nesterenko, O.N. Fedyanina, Properties of microdispersed sintered nanodiamonds as a stationary phase for normal-phase high performance liquid chromatography, *J.Chromatogr.A*, 1217 (2010) 498-505.
22. P.N. Nesterenko, V.V. Krotov, S.M. Staroverov, Chromatographic properties of silica-gel with bonded quinine, *Russ.J.Phys.Chem.*, 65 (1991) 1415-1418.
23. P.A. Sutton, P.N. Nesterenko, Retention characteristics of aromatic hydrocarbons on silica and aminopropyl-modified monolithic columns in normal-phase HPLC, *J.Sep.Sci.*, 30 (2007) 2900-2909.
24. G.N. Yushin, S. Osswald, V.I. Padalko, G.P. Bogatyreva, Y. Gogotsi, Effect of sintering on structure of nanodiamond, *Diam.Relat.Mater.*, 14 (2005) 1721-1729.
25. A.A. Lur'e, *Khromatograficheskie materialy (Chromatographic materials)*, Khimiya, Moscow, 1976.
26. R. Matissek, R. Lehnguth, Analysis of Microbiocidal Isothiazolones .5. Ultraviolet Spectrophotometric Investigation in Consideration of Selected Compounds for Quantitative High-Performance Liquid-Chromatographic Analysis According to the Internal Standard Method, *Fresen.Z.Anal.Chem.*, 328 (1987) 108-111.

## Chapter 5. Chromatographic behaviour of synthetic high pressure high temperature diamond in hydrophilic interaction liquid chromatography

### 5.1. Introduction

As it was shown in Chapters 3 and 4, HPHT diamond possesses a hydrophilic surface with a high content of hydroxyl, carbonyl and carboxyl groups. Accordingly, it was applied in NP-HPLC and exhibited retention for various classes of solutes with polar functional groups. NP-HPLC involves the use of a polar stationary phase and less polar mobile phase. Therefore, it was decided to investigate the behaviour of the HPHT diamond column in other variants of NP-HPLC, which is aqueous normal phase (ANP) and hydrophilic interaction liquid chromatography (HILIC).

ANP and HILIC modes of HPLC usually employ water-ACN or water-MeOH mobile phases with a high ( $\geq 70\%$ ) content of organic solvent [1]. Polar sorbents, such as unbonded silica, amino, and zwitterionic phases are the most commonly used [2]. Solute-sorbent interactions usually occur within the partially immobilised water-rich layer, which is formed near the hydrophilic surface of stationary phase [3]. While in both HILIC and ANP it is generally suggested that hydrophilic interactions are responsible for retention, the main difference between these two modes being the retention mechanism. In HILIC, retention occurs due to the partitioning of solutes between the water-enriched layer and the bulk mobile phase [3], resembling that in RP-HPLC, where the partitioning between ACN-enriched layer and the mobile phase is evident [4]. In contrast, ANP is a variation of adsorption chromatography, where the following adsorption mechanisms of retention are known: hydrogen bonding, ion-exchange, ion-pairing and dipole-dipole interactions [5,6].

Due to this difference in the retention mechanism, mobile phase composition affects retention in HILIC and ANP modes in various ways. According to Hemstrom and Irgum [1], in the case of the partitioning mechanism, a direct correlation between  $\log k$  and concentration of stronger eluting component has to be observed (Eqn. 5.1), while surface adsorption mechanism is described by Snyder-Soczewinski model (Eqn. 5.2):

$$\text{Partitioning model:} \quad \log k = \log k_{org} - S \cdot \varphi_w \quad (\text{Equation 5.1})$$

$$\text{Adsorption model:} \quad \log k = \log k_w - A_s/n_w \cdot \log X_w \quad (\text{Equation 5.2})$$

Here,  $k_{org}$  is the retention factor in 100% of the weaker mobile phase component (organic solvent),  $\varphi_w$  is volume fraction of the eluting species (water),  $S$  is slope,  $k_w$  is retention factor in the stronger component (water),  $X_w$  is molar fraction of stronger

component (water), and  $A_S$  and  $n_w$  are cross-sectional areas of molecules of solute and water, respectively.

As discussed in Chapter 4, the HPHT diamond stationary phase exhibits retention in NP-HPLC due to dipole-dipole interactions and hydrogen bonding. Accordingly, such interactions should be expected to take place in ANP mode as well. In contrast, the existence of a partitioning mechanism is questionable, due to low surface area of diamond and its non-porous nature, thus complicating the formation of a stable water-enriched layer. Nevertheless, such possibilities should be eliminated experimentally. Overall, the main goal of this Chapter was to investigate the chromatographic properties of non-modified HPHT diamond in HILIC and ANP chromatography. Special attention was paid to selectivity issues, retention mechanisms, column efficiency, as well as similarities and contrasts with other carbon sorbents. In order to achieve a better understanding of the retention mechanism, different mobile phases covering a wide pH range and several types of pH buffers were explored. The following classes of solutes were used as model compounds: amines and heterocyclic nitrogen containing compounds, nucleobases, phenols, and carboxylic acids. This choice of compounds allowed the investigation of molecules varying in chemical nature, and, thus, the evaluation of different retention mechanisms, including anion and cation exchange, hydrogen bonding (donor and acceptor) and partitioning. A list of solutes is given in Table 5.1.

## **5.2. Experimental**

General information on materials, chemicals and instrumentation is given in Chapter 2. Information on the preparation of HPHT diamond material (including purification and fractionation), methods of investigation (titrations and sedimentation analysis), calculations (particle size distribution, void volume and phase ratio), and column packing procedure is also given in Chapter 2. Column 12 ( $50 \times 4.6$  mm ID, see Section 3.3.3.2 and Table 3.5) was used for all experiments. Prior to using in HILIC and ANP mode, the HPHT diamond column was conditioned by passing 6 mL of IPA at a flow rate of  $0.1 \text{ mL} \cdot \text{min}^{-1}$ , followed by flushing with DIW for 60 minutes at  $0.3 \text{ mL} \cdot \text{min}^{-1}$ . DIW was also flushed through the column for 15 min at  $0.3 \text{ mL} \cdot \text{min}^{-1}$  before changing the type of mobile phase or pH buffer type.

## **5.3. Results and discussion**

### **5.3.1. Characterisation of the prepared HPHT diamond column**

Properties of HPHT diamond and the column characteristics are described in detail in Chapter 3. Here it is just important to outline that the surface area of the HPHT diamond is

5.1 m<sup>2</sup>·g<sup>-1</sup>, or 8.9 m<sup>2</sup> per 50 × 4.6 mm ID column. The ζ-potential curve for the HPHT diamond is also given in Section 3.3.1.2, which shows that the surface of diamond is almost neutral at pH<3, whilst highly negative at pH>7.5 (see Fig. 3.4). However, in order to better understand the population of functional groups on the surface of diamond, acid-base titration experiments were carried out using suspensions of HPHT diamond in both aqueous and organic solvents (see Section 3.3.1.3).

According to acid-base titration experiments, three classes of surface groups can be identified on the HPHT diamond, based on their acidity and reactivity (see Section 3.3.1.3). The first type are the carboxylic groups, which are acidic with pK<sub>a</sub> = 4.5-5. The second type are hydroxyls with an electron-withdrawing group nearby, which provides their acidic character (pK<sub>a</sub> value for these groups is between 8 and 12). These two types of groups can potentially be protonated or dissociated depending on the pH, and are responsible for the decrease in ζ-potential at higher pH values. Finally, there are weak hydroxyl and carbonyl groups, which will not dissociate under any buffer pH and, therefore, cannot contribute to electrostatic/ion-exchange based retention. However, they are responsible for the hydrophilic character of diamond surface, and can participate in H-bonding or other hydrophilic interactions.

It was also shown in Section 3.3.1.3, that the cation exchange capacity of HPHT diamond was 4.5 μmol·g<sup>-1</sup> which corresponds to the value of 0.6 nm<sup>-2</sup>. This represents a high degree of functionalisation (for comparison, the value for silica is 4.6 nm<sup>-2</sup> [7]). However, it was also shown in Section 3.3.1.3 that the degree of dissociation and acidity of surface groups is strongly affected by the nature of the mobile phase. In 1 M NaCl, a much higher percentage of COOH groups could be dissociated (4.5 μmol·g<sup>-1</sup>), as compared to MeOH (2.5 μmol·g<sup>-1</sup>) and ACN (2.3 μmol·g<sup>-1</sup>). This is logical considering the much higher pK<sub>a</sub> values for carboxylic groups in organic-water mixtures, compared to their true pK<sub>a</sub> [8]. Accordingly, dissociation in ACN is suppressed to a slightly higher extent than in MeOH due to its aprotic character.

Overall, the results from Chapter 3 provide a clear image about surface functional groups and their concentration. Such information is impossible to obtain from the literature data, but is important and useful in the explanation of the diamond column performance in the HILIC/ANP separation mode.

### 5.3.2. Behaviour of HPHT diamond in acetonitrile based mobile phases

Prior to discussing the main findings about the performance of the HPHT diamond column, information about the dissociation constants ( $pK_a$ ) for solutes used in this work are summarised in Table 5.1. This information is of crucial importance, as chromatographic experiments were conducted at different mobile phase composition and pH values.

Fig. 5.1 presents the results of a preliminary investigation of the HPHT diamond column operated in HILIC/ANP mode, namely influence of the ACN content on the retention of the test library of compounds. This experiment was carried out using DIW-ACN mixture for the mobile phase, without the addition of a buffer. For the majority of compounds, classic HILIC behaviour was observed at ACN mobile phase content above 70-80% [9]. Nucleobases (except uracil) exhibit strong retention under HILIC conditions, while other compounds were only moderately retained. Interestingly, a complete selectivity inversion was observed for compound pairs 4-hydroxybenzenesulphonic acid/4-chloroaniline, 4-hydroxybenzenesulphonic acid/2,4-dinitrophenol, and adenine/adenosine.

From the analysis of the data, presented in Fig. 5.1, it is possible to make some assumptions about the retention mechanism on HPHT diamond. As mentioned in Section 5.1, HILIC is based on the partitioning of the solute between mobile phase and a water-enriched layer at the surface of sorbent, as opposed to classic normal phase, which implies molecular adsorption due to various types of interactions. Therefore, in the case of a partitioning mechanism, a direct correlation between  $\log k$  and the concentration of the stronger eluting mobile phase component has to be observed (Partitioning model, Eqn. 5.1). In the case of surface adsorption, a logarithmic correlation will be observed (Adsorption model, Eqn. 5.2). Therefore, plotting  $\log k$  v content of the stronger solvent in the mobile phase, as both logarithmic and linear plots, can provide an indication as to whether partitioning or adsorption mechanism is dominant.

Table 5.2 summarises the squared correlation coefficients for approximation of retention v water content dependence, using the Partitioning model and Adsorption model. As can be concluded from the Table 5.2, the Adsorption model (Eqn. 5.2) describes the observed influence of mobile phase on retention better than the Partitioning model (Eqn. 5.1). This implies that retention is likely to be more dependent upon adsorption than partitioning. For the mobile phase comprising 10-20% of aqueous buffer, it is usually assumed that a combination of partitioning and adsorption mechanisms are present [10]. However, in case of non-porous HPHT diamond, having a flat surface, the formation of a semi-bonded water-rich layer is complicated, and the thickness of this layer would likely be negligible.

Table 5.1. pKa values for the substances used in this Chapter. All data presented for diluted water solutions at 25°C, and taken from [11], unless stated otherwise.

Basic compounds, $\mu = 0.0$ M	pKa <sub>1</sub>	pKa <sub>2</sub>	pKa <sub>3</sub>
Adenine	4.17 <sup>(NH<sup>+</sup>)</sup>	9.86 <sup>(NH)</sup>	-
Cytosine	4.58 <sup>(NH<sup>+</sup>)</sup>	12.20 <sup>(NH)</sup>	-
Uracil	-	9.46 <sup>(NH)</sup>	13.49 <sup>(NH)</sup>
Adenosine	3.5 <sup>(NH<sup>+</sup>)</sup>	12.42 <sup>(2-OH)</sup>	-
Thymidine	-	9.80 <sup>(NH)</sup>	12.86 <sup>(NH)</sup>
4-chloroaniline	3.98 <sup>(NH<sub>3</sub><sup>+</sup>)</sup>	-	-
Pyridine	5.20 <sup>(NH<sup>+</sup>)</sup>	-	-
Acidic compounds, $\mu = 0.1$ M			
Benzenesulphonic acid	<sup>a</sup> 0.70 <sup>(SO<sub>3</sub>H)</sup>	-	-
4-hydroxybenzenesulphonic acid (4-HBSA)	<sup>a</sup> 0.70 <sup>(SO<sub>3</sub>H)</sup>	9.05 <sup>(OH)</sup>	-
2,4-dinitrophenol	3.92 <sup>(OH)</sup>	-	-
Salicylic acid	2.80 <sup>(COOH)</sup>	13.4 <sup>(OH)</sup>	-
4-hydroxybenzoic acid	4.37 <sup>(COOH)</sup>	8.98 <sup>(OH)</sup>	-
2,3-dihydroxybenzoic acid (2,3-DHBA)	2.68 <sup>(COOH)</sup>	9.84 <sup>(3-OH)</sup>	-
2,4-dihydroxybenzoic acid (2,4-DHBA)	3.13 <sup>(COOH)</sup>	8.64 <sup>(4-OH)</sup>	<sup>a</sup> 14.00 <sup>(2-OH)</sup>
2,5-dihydroxybenzoic acid (2,5-DHBA)	2.75 <sup>(COOH)</sup>	10.05 <sup>(5-OH)</sup>	-
2,6-dihydroxybenzoic acid (2,6-DHBA)	1.00 <sup>(COOH)</sup>	13.10 <sup>(OH)</sup>	-
3,4-dihydroxybenzoic acid (3,4-DHBA)	4.3 <sup>(COOH)</sup>	8.75 <sup>(4-OH)</sup>	13.00 <sup>(3-OH)</sup>
3,5-dihydroxybenzoic acid (3,5-DHBA)	3.86 <sup>(COOH)</sup>	9.02 <sup>(OH)</sup>	10.54 <sup>(OH)</sup>
5-sulphosalicylic acid	strong <sup>(SO<sub>3</sub>H)</sup>	2.48 <sup>(COOH)</sup>	11.85 <sup>(OH)</sup>
1,5-naphthalenedisulphonic acid	strong <sup>(SO<sub>3</sub>H)</sup>	<sup>b</sup> 0.57 <sup>(SO<sub>3</sub>H)</sup>	-
3,5-dinitrosalicylic acid	0.3 <sup>(COOH)</sup>	7.07 <sup>(OH)</sup>	-

<sup>a</sup> Data taken from [12]

<sup>b</sup> Data taken from [13]

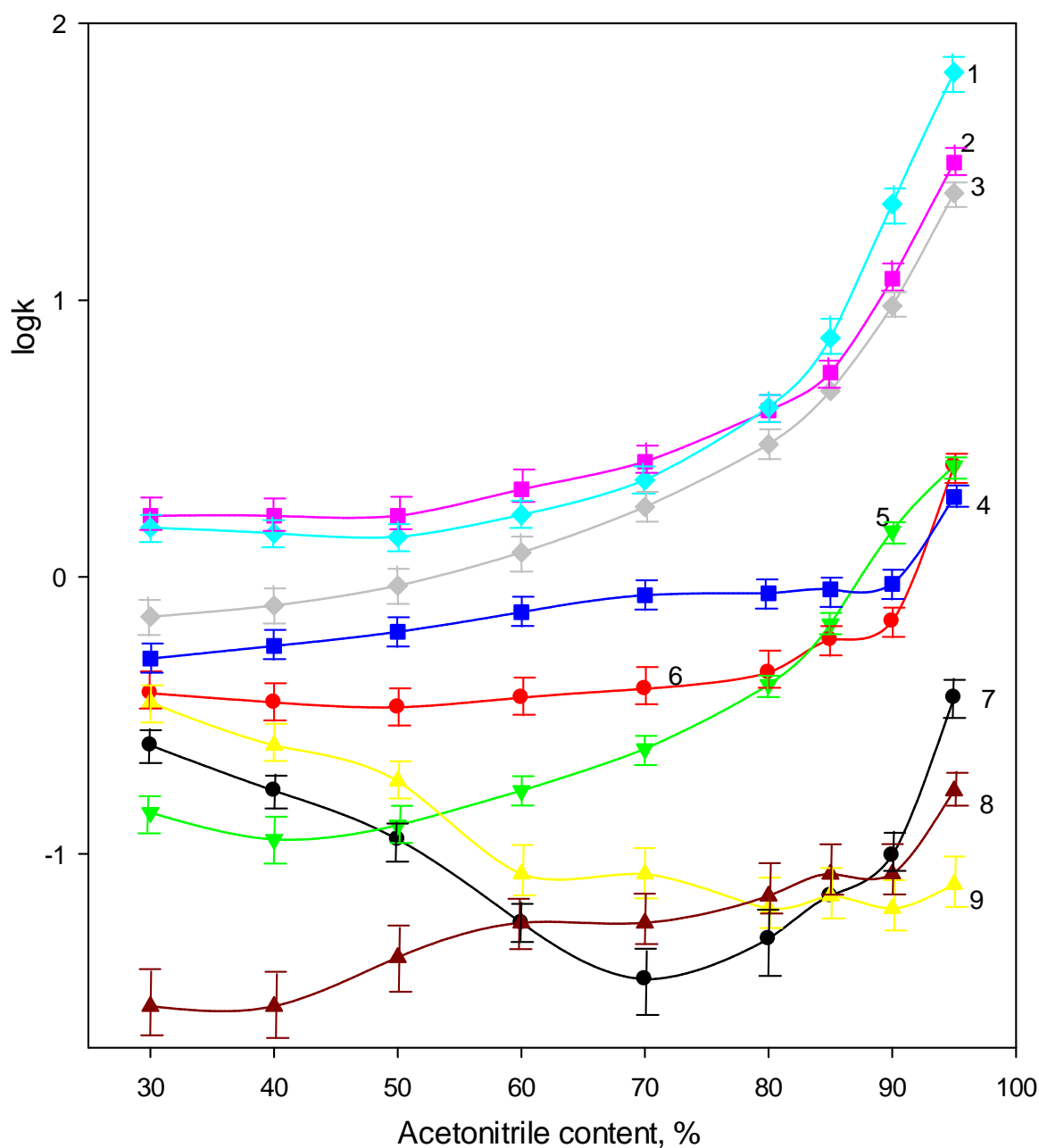


Fig. 5.1. Influence of the ACN content in mobile phase on  $k$  of several compounds over the HPHT diamond column. Mobile phase – DIW/ACN,  $0.5 \text{ mL} \cdot \text{min}^{-1}$ ,  $2 \text{ } \mu\text{L}$  injections, sample concentration  $0.05 \text{ mg} \cdot \text{mL}^{-1}$ , UV detection at  $254 \text{ nm}$ . Solutes: adenosine (1), adenine (2), cytosine (3), 4-HBSA (4), pyridine (5), BTMA (6), 2,4-dinitrophenol (7), uracil (8), 4-chloroaniline (9),  $n=3$ .



Table 5.2.  $R^2$  values (n=3) for the approximation of retention factors obtained in water-ACN and water-MeOH (see Fig. 5.1 and Fig. 5.5) mobile phases (5-30% aqueous in increments of 5%) with Eqn. 5.1 (Partitioning model) and Eqn. 5.2 (Adsorption model). Fig. 8.1 in Supplementary section presents the corresponding plots from the Fig. 5.1 and 5.5 in terms of linear and logarithmic functions of the mobile phase composition.

	ACN		MeOH	
	Partitioning model	Adsorption model	Partitioning model	Adsorption model
2,4-dinitrophenol*	0.810	0.976	-	-
BTMA	0.689	0.913	0.821	0.979
4-HBSA	0.955	0.963	-	-
Pyridine*	0.503	0.779	-	-
Adenine	0.881	0.994	0.847	0.981
Adenosine	0.912	0.988	0.902	0.955
Cytosine	0.921	0.996	0.939	0.991
Uracil*	0.787	0.935	0.979	0.976

\* Solutes marked with asterisk exhibited low retention in one or both mobile phases ( $k < 0.2$ ), which may affect the accuracy of the approximation procedure.

For instance, it was claimed that non-porous silica sorbents cannot form a semi-bonded water layer as efficiently as low-crosslinked ion exchangers, and the partitioning mechanism does not play a major role for such sorbents [1]. Therefore, it is quite likely that this conclusion is valid for the HPHT diamond as well, due to its even lower surface area. In contrast, the adsorption properties of diamond surface are well-known, and indeed can provide sufficient retention, as it was shown in Chapter 4 for NP-HPLC mode. Therefore, it can be stated that the ANP chromatography term should be used when describing retention in mobile phases with high organic.

Since it is thus assumed that adsorption of solutes on the surface of HPHT diamond is responsible for retention, it becomes necessary to evaluate which exact adsorption mechanisms are involved in the interaction between diamond and various solutes, and how these mechanisms are affected by pH and the buffer selection. As it was described in Section 5.1, ion-exchange, hydrogen bonding, and dispersive forces are usually associated with ANP chromatography, so these types of interaction should be considered.

#### **5.3.2.1. Influence of pH and type of buffer**

Two buffering systems have been investigated in regards to their influence on the retention times, namely ammonium formate buffer (adjusted with either ammonia or formic acid), and trifluoroacetate (TFA) buffer. As it can be seen from Fig. 5.2, the addition of a buffer slightly reduces the retention factors for the majority of compounds, as compared to a non-buffered mobile phase of the same ACN/water ratio (Fig. 5.1). This indicates that electrostatic interactions do play an important role in the retention mechanism, when no buffer is included and ionic strength is low. Higher ionic strength, arising from the addition of a buffer, results in suppression of such interactions and slightly decreased retention.

Other evidence that ion-exchange interactions are significant for several classes of compounds, can be found by comparing the retention data in Fig. 5.2 with the  $\zeta$ -potential v pH curve for HPHT diamond (Fig. 3.4). For example, adenosine, cytosine, adenine, pyridine and 4-chloroaniline have pKa values in the range of 3.5-5.2 (see Table 5.1), and are positively charged under acidic conditions. Accordingly, in Fig. 5.2 the graphs for these compounds exhibit curvature near their pKa values, and much stronger retention at low pH is observed (Plots 1, 3, 4, 8 and 10). This means that ion-exchange interactions with the negatively charged surface of diamond is their primary mechanism of retention, and deprotonation of these compounds at higher pH leads to significant decrease in  $k$  values.

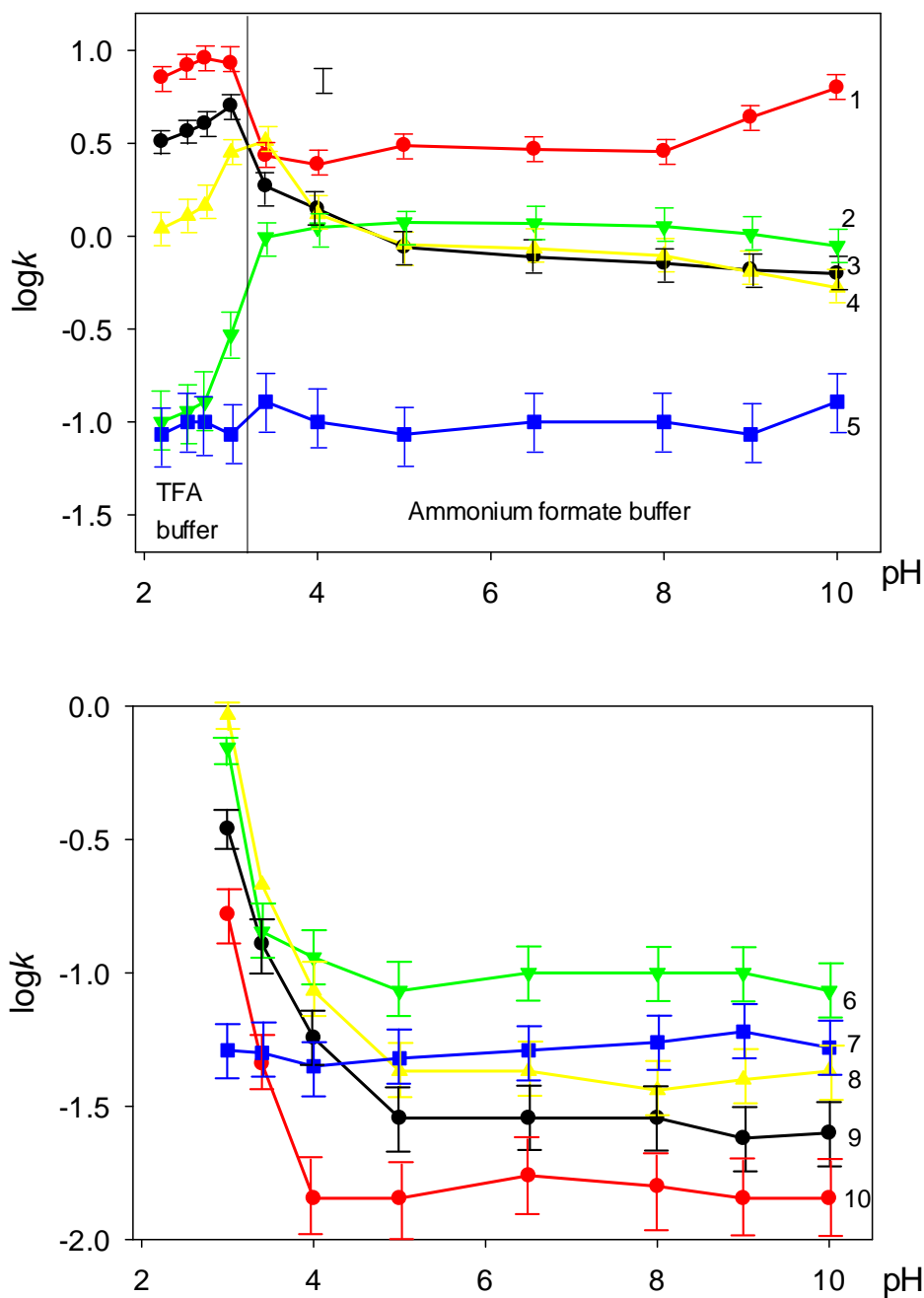


Fig. 5.2. Influence of type of buffer and its pH on the retention of several compounds on the HPHT diamond column. Mobile phase – 85%ACN – 15% 10 mM buffer (TFA and ammonium formate in upper figure, ammonium formate in bottom figure), 0.5 mL·min<sup>-1</sup>, injection volume 2 μL, sample concentration 0.05 mg·mL<sup>-1</sup>, UV detection at 254 nm. Solutes: adenosine (1), BTMA (2), adenine (3), cytosine (4), uracil (5), 4-HBSA (6), BSA (7), pyridine (8), 2,4-dinitrophenol (9), 4-chloroaniline (10).

Interestingly, after a sharp increase in  $k$  values for the solutes between pH 3-5 (due to the protonation of nitrogen), some solutes (compounds 1, 3 and 4) exhibit a slight decrease of retention with pH. This likely correlates with the drop in the  $\zeta$ -potential of the diamond surface (see Fig. 3.4), which reduces the electrostatic forces between these solutes and the stationary phase. Similarly, BTMA (plot 2 in Fig. 5.2, top), which carries a fixed positive charge, is retained over the majority of neutral pH (i.e. pH 3.5-10), when diamond has a strong negative charge. However, in the region of lower pH (i.e. pH<3.5), the  $\zeta$ -potential of diamond rapidly increases, which results in weaker retention for BTMA.

Overall, ion-exchange interactions explain the retention of positively charged species on the HPHT diamond column well. However, such hypothesis is clearly not sufficient for the explanation of the strong retention of adenosine at neutral pH, when its molecule is not charged, as well as rise in retention of negatively charged 4-HBSA and 2,4-dinitrophenol at  $\sim$ pH 5. Presumably, hydrogen bonding may be responsible for these phenomena. This assumption can be confirmed by comparing the data for 4-HBSA and benzenesulphonic acid (BSA) (plots 6 and 7 in Fig. 5.2). Clearly, the BSA molecule (lacking OH group) cannot be involved in hydrogen bonding interactions, and as such, this compound is not retained under any conditions. In contrast, the 4-HBSA molecule exhibits a significant rise in retention at pH values below 4, and the only reason for this is an interaction with the phenolic OH group.

Similarly, the retention of 2,4-dinitrophenol is attributed to hydrogen bonding between the OH group and the surface of HPHT diamond. This also correlates well with the weak retention of 4-HBSA and 2,4-dinitrophenol over the pH range 4-10, when these molecules are deprotonated (see Table 5.1), and when diamond has a strong negative charge (see Fig. 3.4). Clearly, under these conditions electrostatic repulsion between solutes and the stationary phase decreases retention. However, as the pH is reduced, the surface of diamond becomes almost neutral, so these molecules are no longer repelled and begin to retain *via* hydrogen bonding.

As was mentioned in Section 5.1, another class of interaction which can be present in ANP chromatography are dispersive interactions. From the results presented in Fig. 5.1 and 5.2, it is unlikely that dispersive forces contribute significantly to retention on the diamond column. As it will be shown later in Fig. 5.6, longer alkyl chains actually result in decreased  $k$  values for BTBA, as compared to BTMA. Since BTMA and BTBA are similar compounds, the only difference in their retention is due to the different length of alkyl chains. Therefore, earlier elution of BTBA infers that its butyl fragments interact with mobile phase more than when compared to the methyl groups of BTMA. This is not surprising, considering the low

hydrophobicity of HPHT diamond (see Section 3.3.1), especially in comparison with 85% of ACN in mobile phase. Overall, dispersive interactions can be neglected when evaluating the behaviour of HPHT diamond in ANP mode.

### 5.3.2.2. Operation under alkaline conditions

Since HPHT diamond possesses excellent stability over the whole pH range, it was interesting to investigate how it operates under alkaline conditions ( $\text{pH} > 11.5$ ). This pH range is almost never used with conventional silica sorbents due to their hydrolytic instability, but represents significant interest. According to the discussion in Section 3.3.1.2 and from Fig. 3.4, the surface of diamond is negatively charged at high pH ( $\zeta = -80$  mV at  $\text{pH} \geq 10$ ). Therefore, HPHT diamond can potentially exhibit properties of a weak cation-exchanger. Additionally, other hydrophilic retention mechanisms (including hydrogen bonding, partitioning and dispersive forces) need to be considered again, since under different mobile phase and pH conditions, they may be more significant. Fig. 5.3 presents the results on retention of several compounds in 85% ACN – 15% aqueous mobile phase, with hydroxide concentration 5-50 mM in water phase. Four hydroxide solutions were tested: NaOH, KOH, TMAOH and  $\text{NH}_4\text{OH}$ .

First of all, the plot for BTMA (Fig. 5.3) gives a clear indication that a cation exchange mechanism is dominant. An almost linear dependence of  $\log k$  on  $\log C$  was observed, according to the cation exchange principles. Moreover, the slopes for elution of BTMA with NaOH, KOH and TMAOH were very close to the value of 1.0, which is in full agreement with ion exchange theory for two competing monovalent cations [14]. A lower slope in case of  $\text{NH}_4\text{OH}$  is due to the fact that ammonia is a weak electrolyte, and its eluting power is lower, as compared to other hydroxides.

Another confirmation of the presence of an ion exchange mechanism was that  $k$  values increased in series,  $\text{NaOH} < \text{KOH} < \text{TMAOH}$  for the majority of compounds. Such behaviour can be linked to the radii of hydrated ionic spheres for these ions, which decrease in series  $\text{NaOH} > \text{KOH} > \text{TMAOH}$  [15]. Accordingly, TMAOH exhibits the strongest retention on the surface of HPHT diamond (which is cation-exchanger due to presence of carboxyls, see Section 3.3.1.2), while NaOH retained much less. Therefore, in the presence of TMAOH, most compounds exhibited stronger retention.

In order to evaluate the contribution of hydrogen bonding to retention on HPHT diamond at high pH, plots for 4-HBSA and BSA are compared in Fig. 5.3.

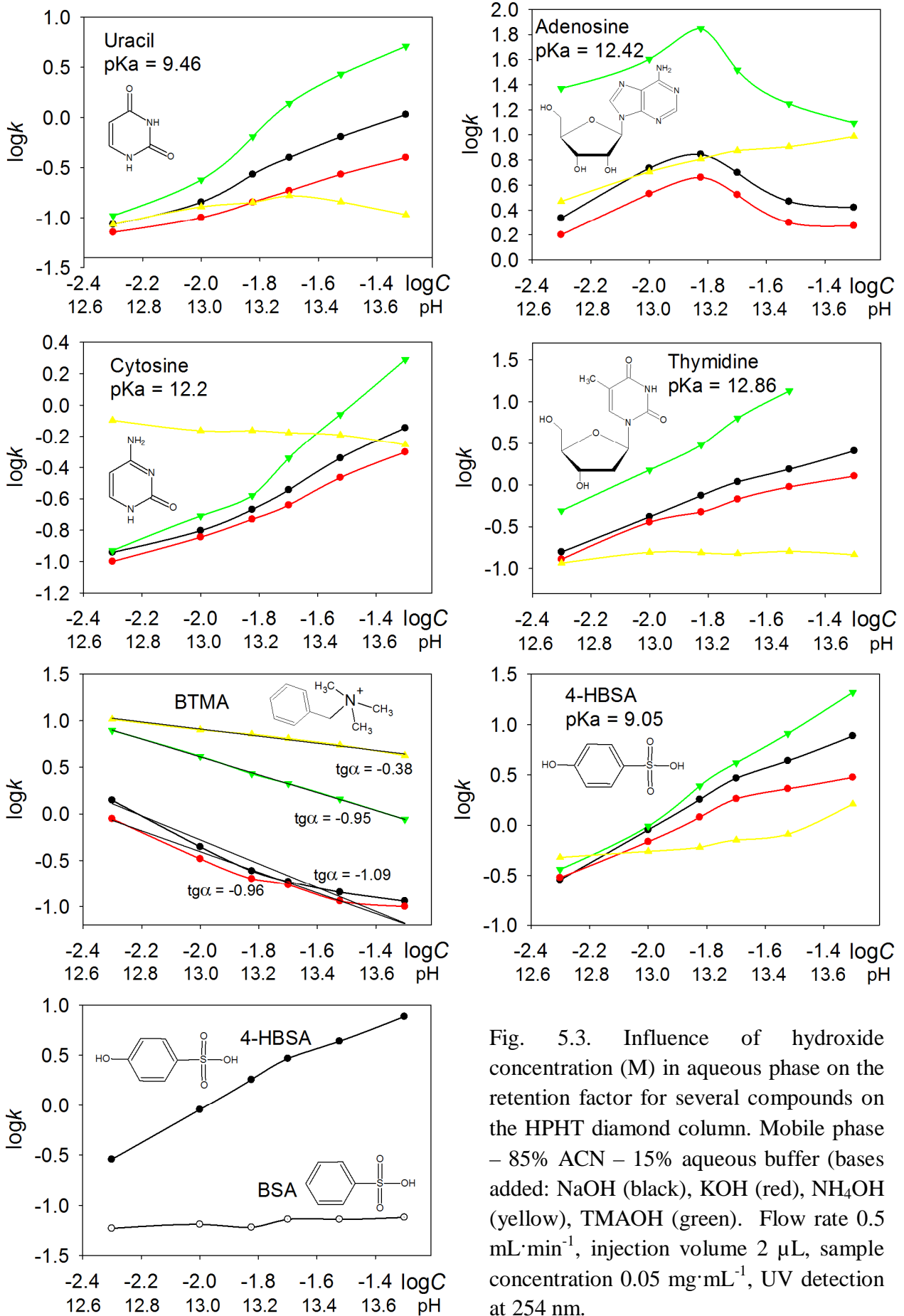


Fig. 5.3. Influence of hydroxide concentration (M) in aqueous phase on the retention factor for several compounds on the HPHT diamond column. Mobile phase – 85% ACN – 15% aqueous buffer (bases added: NaOH (black), KOH (red),  $\text{NH}_4\text{OH}$  (yellow), TMAOH (green)). Flow rate  $0.5 \text{ mL}\cdot\text{min}^{-1}$ , injection volume  $2 \mu\text{L}$ , sample concentration  $0.05 \text{ mg}\cdot\text{mL}^{-1}$ , UV detection at 254 nm.

As mentioned in the previous section, BSA cannot participate in hydrogen bonding since it does not have an OH group. As a result, this compound is unretained over the whole range of concentrations of NaOH in the mobile phase (Fig. 5.3). In contrast, 4-HBSA is retained much stronger, and its retention increases at higher pH. This fact confirms that a hydrogen bonding mechanism is present, and indicates that the energy of hydrogen bonds is higher with increased hydroxide concentration.

Nucleobases (uracil, cytosine, adenosine and thymidine (Fig. 5.3) are also retained under alkaline conditions, similarly as described above for 4-HBSA. Again, hydrogen bonding for these molecules is quite likely, but an explanation is needed as to why these molecules exhibit stronger retention at higher pH. Clearly, ion exclusion cannot be proposed to explain such behaviour. The reason is that cytosine, uracil and thymidine are not charged within this pH range (see Table 5.1), hence cannot be involved in ion exclusion interactions. Another reason is that surface of HPHT diamond is non-porous, and its exclusion volume is negligible. Therefore, hydrogen bonding strength is very likely to increase at higher hydroxide pH, which would explain the observed increase in retention.

There are two main factors which will influence strength of hydrogen bonds under alkaline conditions. Firstly, the higher ionic strength in more concentrated solutions will obviously decrease the H-bonding energy, due to the screening effect and lower dielectric constant of the mobile phase [16]. Secondly, higher OH<sup>-</sup> concentrations will result in less H-bonding between water and solute molecules, thus increasing strength of hydrogen bonds between HPHT diamond and solutes. Clearly, this second factor is more prevalent in this situation, since the difference in dielectric constants between 5 mM and 50 mM solutions is less than 1% [17]. Stronger H-bonding leads to increased retention for these four solutes at higher pH.

Interesting behaviour was observed for the most retained molecule, adenosine, which displayed a retention maximum (Fig. 5.3). Adenosine is not charged in the presence of 5-10 mM of hydroxide (pK<sub>a</sub> = 12.4, see Table 5.1) and behaves similarly to other nucleobases initially – *k* increases with increasing concentration of hydroxide in the mobile phase. However, one of the hydroxyls of the ribose moiety deprotonates at pH 12.4, and so retention of adenosine begins to decrease in accordance to ion-exchange principle.

### **5.3.2.3. Selectivity of retention in water – ACN mixtures**

At this point it is already quite clear, that the mechanism of retention on HPHT diamond is complicated, and many aspects need to be considered, such as pH, ionic strength,

nature of the buffer, the surface state of diamond, and specificity of the solute under experimental conditions. However, it is easy to see from the data presented above, that retention factors for some compounds have very different trends under varying mobile phase conditions. For example, uracil which was not retained in unbuffered conditions, as well as in TFA and ammonium formate buffers, began to display retention under alkaline conditions. In contrast, adenine which was the most strongly retained compound when using DIW, exhibited much lower retention in acidic and neutral buffers, and was not retained at all at high pH. Fig. 5.4 shows a chromatogram of four and five compounds obtained with different mobile phases – using TFA or NaOH.

In TFA buffer (pH 2.7), cytosine, adenine, and adenosine are protonated, while uracil is in neutral form (see Table 5.1). Alternatively, in the presence of 50 mM NaOH, imide nitrogen of uracil, adenine or thymidine will lose a proton and become negatively charged. As it was discussed previously, one of ribosyl OH groups in adenosine has a  $pK_a$  value of 12.4, which makes this molecule also negatively charged in presence of 50 mM NaOH. In contrast, the deoxyribose fragment in the thymidine molecule, lacking this very OH group, remains neutral. Overall, in acidic conditions uracil is neutral, and other compounds are positively charged. In alkaline conditions, cytosine is neutral, while other compounds carry negative charge, and charge of adenosine is on the carbohydrate moiety. Combined with the fact that the surface of diamond also becomes negative at  $pH > 7$ , from being neutral in TFA, and the fact that TFA enhances ion pairing for positively charged solutes [18,19], while NaOH strengthens H-bonding (see Section 5.3.2.2), this results in the selectivity reversal observed in Fig. 5.4. Clearly, with so many variables, more experiments are required in order to precisely establish what happens on the surface of HPHT diamond.

### **5.3.3. Performance of HPHT diamond in methanol based mobile phases**

As discussed in Chapter 3, in 80% MeOH 6% more surface groups of the HPHT diamond are dissociated, as compared to 80% ACN. At the same time, MeOH is more active in disrupting H-bonds ( $pK_a$  of MeOH is ~15,  $pK_a$  of ACN is 25 [20]). Therefore, more ion-exchange contribution and less hydrogen bonding could be expected by substituting these two organic modifiers. Influence of MeOH on the retention factors of different compounds is presented in Fig. 5.5.

Again, the classic curvature of the retention plot in the area of higher methanol contents was observed, similar to aqueous ACN buffers. However, generally, much lower retention times were recorded in the case of MeOH based mobile phases.



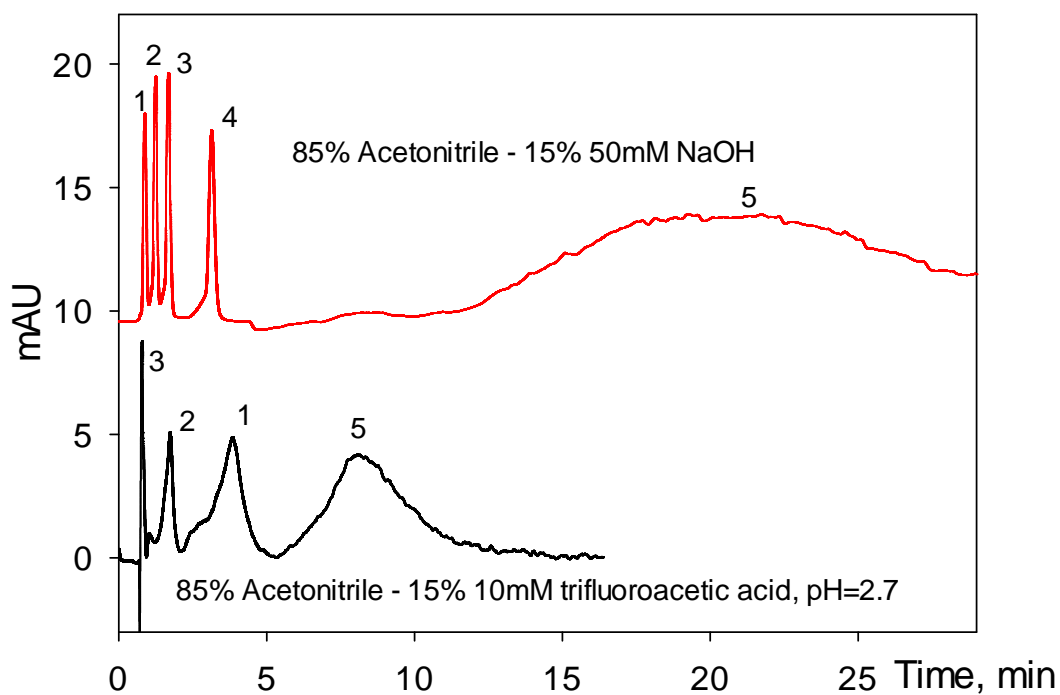


Fig. 5.4. Separation of five and four model compounds with the HPHT diamond column using two different mobile phases. Flow rate  $0.5 \text{ mL}\cdot\text{min}^{-1}$ , column temperature  $25^\circ\text{C}$ , injection volume  $2 \mu\text{L}$ , total sample concentration  $0.05 \text{ mg}\cdot\text{mL}^{-1}$ , UV detection at  $254 \text{ nm}$ . Solutes: 1 – adenine, 2 – cytosine, 3 – uracil, 4 – thymidine, 5 – adenosine.

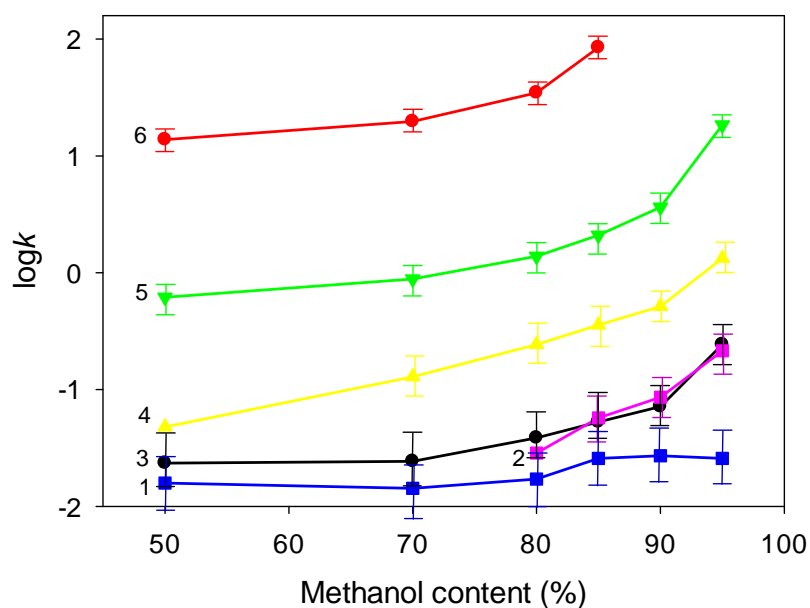


Fig. 5.5. Influence of MeOH content in the mobile phase on the retention of different compounds on the HPHT diamond column. Flow rate  $0.5 \text{ mL}\cdot\text{min}^{-1}$ , column temperature  $25^\circ\text{C}$ , injection volume  $2 \mu\text{L}$ , sample concentration  $0.05 \text{ mg}\cdot\text{mL}^{-1}$ , UV detection at  $254 \text{ nm}$ . Solutes: 1 – 4-HBSA, 2 – uracil, 3 – adenine, 4 – cytosine, 5 – BTMA, 6 – adenosine.

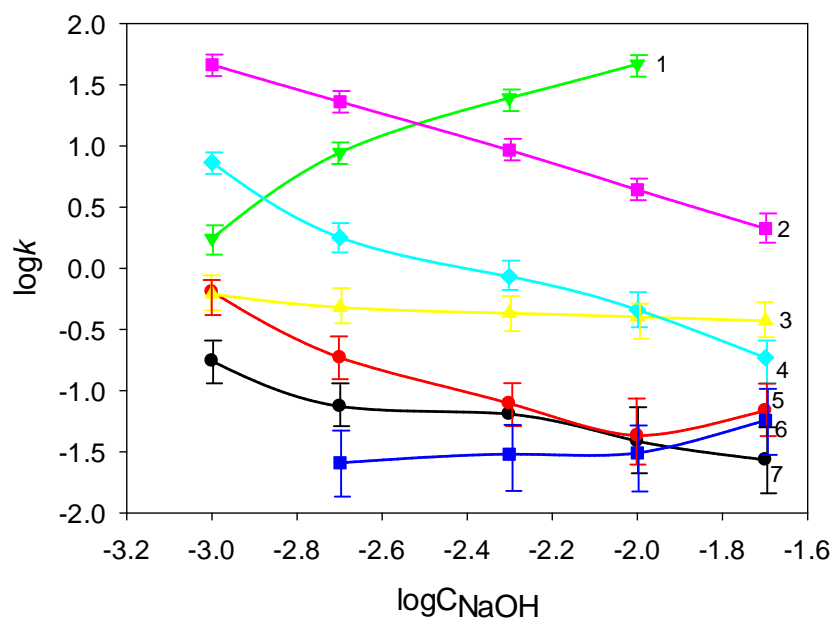


Fig. 5.6. Influence of concentration of NaOH in aqueous phase on the retention of different compounds on the HPHT diamond column. Mobile phase: 85% MeOH – 15% aqueous, flow rate  $0.5 \text{ mL}\cdot\text{min}^{-1}$ , column temperature  $25^\circ\text{C}$ , injection volume  $2 \text{ ul}$ , sample concentration  $0.05 \text{ mg}\cdot\text{mL}^{-1}$ , UV detection at  $254 \text{ nm}$ . Solutes: 1 – adenosine, 2 – BTMA, 3 – cytosine, 4 – BTBA, 5 – adenine, 6 – 4-HBSA, 7 – uracil.

This makes sense considering the stronger eluting power of methanol [9]. As it was already said, the retention dependence on methanol content is best described in terms of the Snyder-Soczewinski model (see Table 5.1 and Section 5.3.2.), similarly to what was found for ACN in Section 5.3.2.

However, if we consider retention of the solutes in 85% MeOH – 15% aqueous NaOH (Fig. 5.6), the situation appears to be quite different from that observed for similar ACN based mobile phases (Fig. 5.3). First of all, greater retention of positively charged species (BTMA and BTBA) should be mentioned. This correlated with the assumption that stronger cation-exchange character of the HPHT diamond exists in presence of MeOH, when more COOH groups are dissociated (see Section 3.3.1.3). Accordingly, the retention of 4-HBSA decreased as compared to that seen for ACN based mobile phase, since hydrogen bonding is suppressed. As it was mentioned in Section 5.3.2.2, in ACN the retention of several compounds increased with the concentration of NaOH in the mobile phase (see Fig. 5.3) due to stronger hydrogen bonding. In contrast, the retention of these compounds in MeOH based mobile phase is either constant (for neutral at this conditions cytosine) or decreasing (for the positive molecules of uracil and adenine).

#### **5.3.4. Selectivity of HPHT in ACN and MeOH based mobile phases**

Since different retention factors for compounds were observed in the presence of MeOH and ACN based mobile phases, the selectivity of the HPHT diamond in these two mobile phases was compared. Fig. 5.7 compares the retention of four compounds which exhibited the greatest differences. Cytosine, which is neutral at the conditions of the experiment, had very close retention times in MeOH and ACN based mobile phases for the whole range of NaOH concentrations investigated. However, for the other compounds, a large difference between two organic modifiers was recorded. 4-HBSA is not retained at any tested concentration of NaOH in MeOH based mobile phases, but in the presence of acetonitrile its retention factor increases with the pH of mobile phase. Therefore, at 20 mM NaOH the difference in the retention of 4-HBSA in MeOH and ACN based mobile phases is quite significant. The opposite is true for positively charged BTMA and BTBA: in both mobile phases their retention decreases with NaOH concentration. Nevertheless,  $k$  for BTMA is about one order of magnitude higher in the presence of MeOH, than in ACN, and for BTBA  $k$  is about 4 times higher. Such big differences in the retention makes it potentially possible to vary column selectivity by switching between MeOH and ACN within the mobile phase. A set of separations is presented in Fig. 5.8 to confirm this hypothesis.

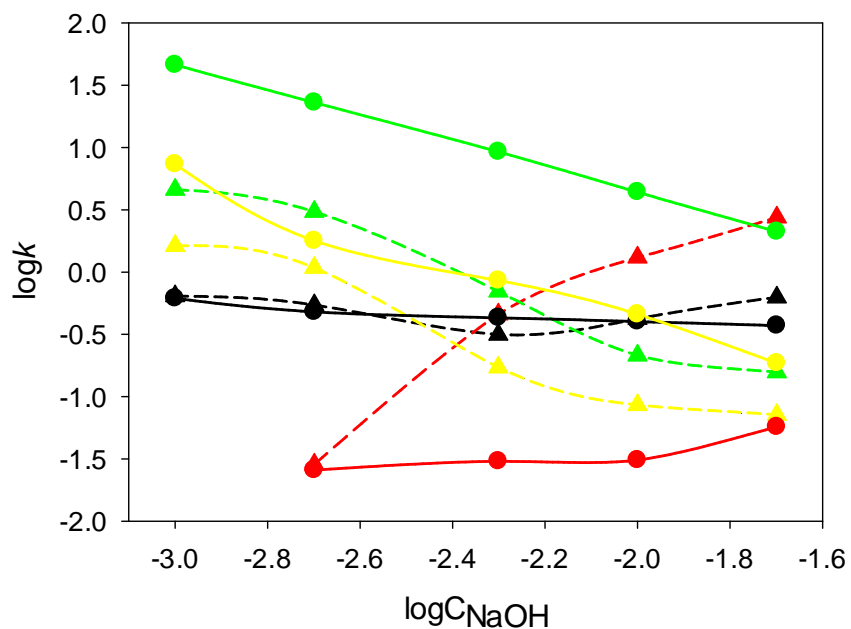


Fig. 5.7. Comparison of retention variation with NaOH concentration in aqueous phase between ACN and MeOH based mobile phases. Mobile phase: 15% aqueous – 85% organic (triangles for ACN, circles for MeOH). Flow rate  $0.5 \text{ mL}\cdot\text{min}^{-1}$ , column temperature  $25^\circ\text{C}$ , injection volume  $2 \mu\text{L}$ , sample concentration  $0.05 \text{ mg}\cdot\text{mL}^{-1}$ , UV detection at  $254 \text{ nm}$ . Solutes: BTMA (green), BTBA (yellow), cytosine (black), 4-HBSA (red).

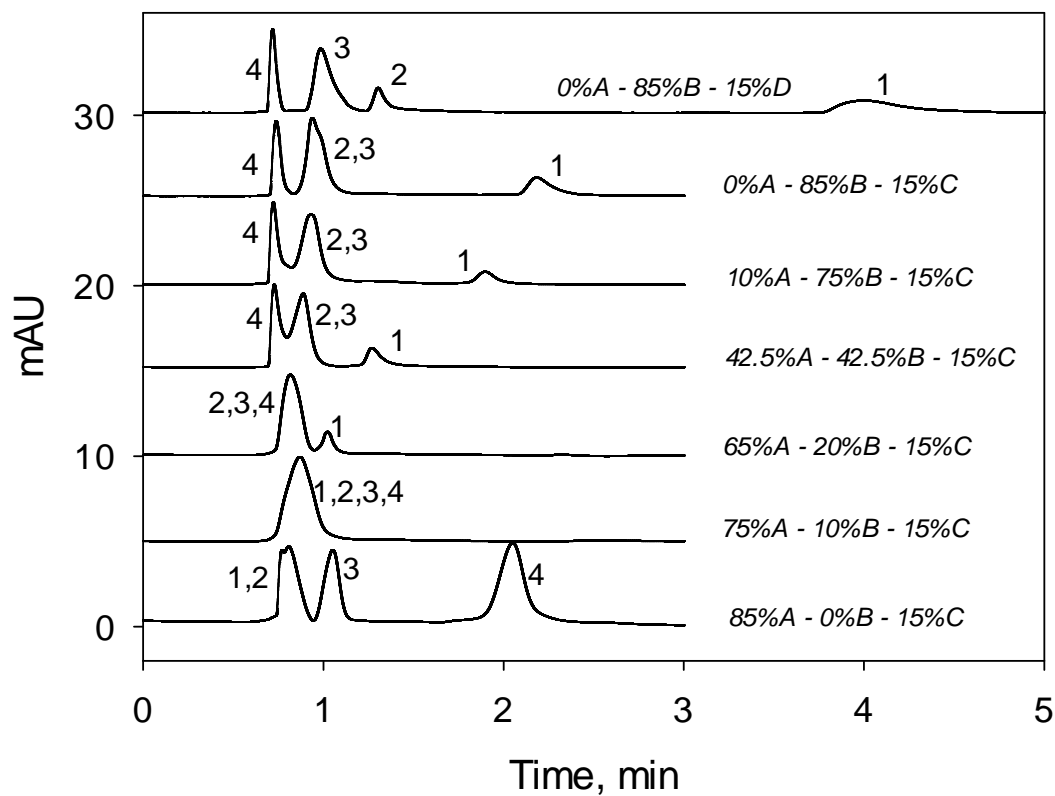


Fig. 5.8. Changing the selectivity of HPHT diamond column by replacing ACN in the mobile phase with MeOH. Mobile phase as designated in the picture (A = ACN, B = MeOH, C = 20 mM NaOH, D = 10 mM NaOH). Flow rate  $0.5 \text{ mL}\cdot\text{min}^{-1}$ , column temperature  $25^\circ\text{C}$ , injection volume  $2 \mu\text{L}$ , sample concentration  $0.05 \text{ mg}\cdot\text{mL}^{-1}$ , UV detection at 254 nm. Solutes: 1– BTMA, 2 – BTBA, 3 – cytosine, 4 – 4-HBSA.

When using a mobile phase with 85% of ACN, BTMA and BTBA elute in the void, while cytosine is retained slightly, and 4-HBSA is retained strongly. Substituting 10% of ACN with MeOH, however, greatly reduces the retention of 4-HBSA, so all compounds elute as a single peak. Further increase in the percentage of MeOH in the mobile phase leads to 4-HBSA starting to be unretained, and the peak of BTMA showing increasing retention. When 85% MeOH – 0% ACN mobile phase is applied, the 4-HBSA peak is fully resolved from cytosine, while the cytosine and BTBA peaks still overlap, and BTMA has a greater retention. Finally, a decrease in the concentration of NaOH in the aqueous fraction down to 10 mM allows complete separation of cytosine and BTBA.

Overall, it is clear that a complete reversal of selectivity for the HPHT diamond column is observed when 85% ACN is replaced with 85% MeOH. This substitution does not influence the retention of cytosine on the HPHT diamond. However, the addition of small amounts of MeOH drastically reduced the retention of 4-HBSA, which is an indication of a hydrogen bonding retention mechanism for this molecule. The  $k$  for BTMA and BTBA are almost linearly correlated with the percentage of MeOH in the mobile phase, according to the ion-exchange mechanism of their retention. To our knowledge, there is no evidence in the literature on such selectivity reversal for silica columns in water-ACN-MeOH mixtures. Usually, use of MeOH or other alcohols instead of ACN leads to poorer efficiency and only has negligible influence on selectivity [21,22], at least for bare silica and amino columns. A slight influence on selectivity can be achieved by substituting ACN with THF, as was shown for high-purity silica stationary phase for separation of epirubicin analogues [23]. However, this selectivity change could be also achieved by adjusting the pH value of the mobile phase, and is connected with different apparent pKa values of solutes in ACN and THF, rather than with different retention mechanisms.

Since such an unusual change in selectivity (based on the organic modifier) was revealed for the HPHT diamond column, it was interesting to investigate more on the retention of different compounds in ACN and MeOH based mobile phases. Fig. 5.9 presents the selectivity chart obtained for 26 model compounds in 80% organic – 20% aqueous 20 mM NaOH for both ACN and MeOH. Higher aqueous content (20%) was used in order to obtain more retention factors for compounds which could not be eluted under 15% aqueous mobile phase. Clearly, there is a difference between selectivities of HPHT diamond column under these two mobile phases.

First of all, the retention of positively charged quaternary ammonium compounds is stronger in 80% MeOH mobile phase due to enhanced ion-exchange interactions.

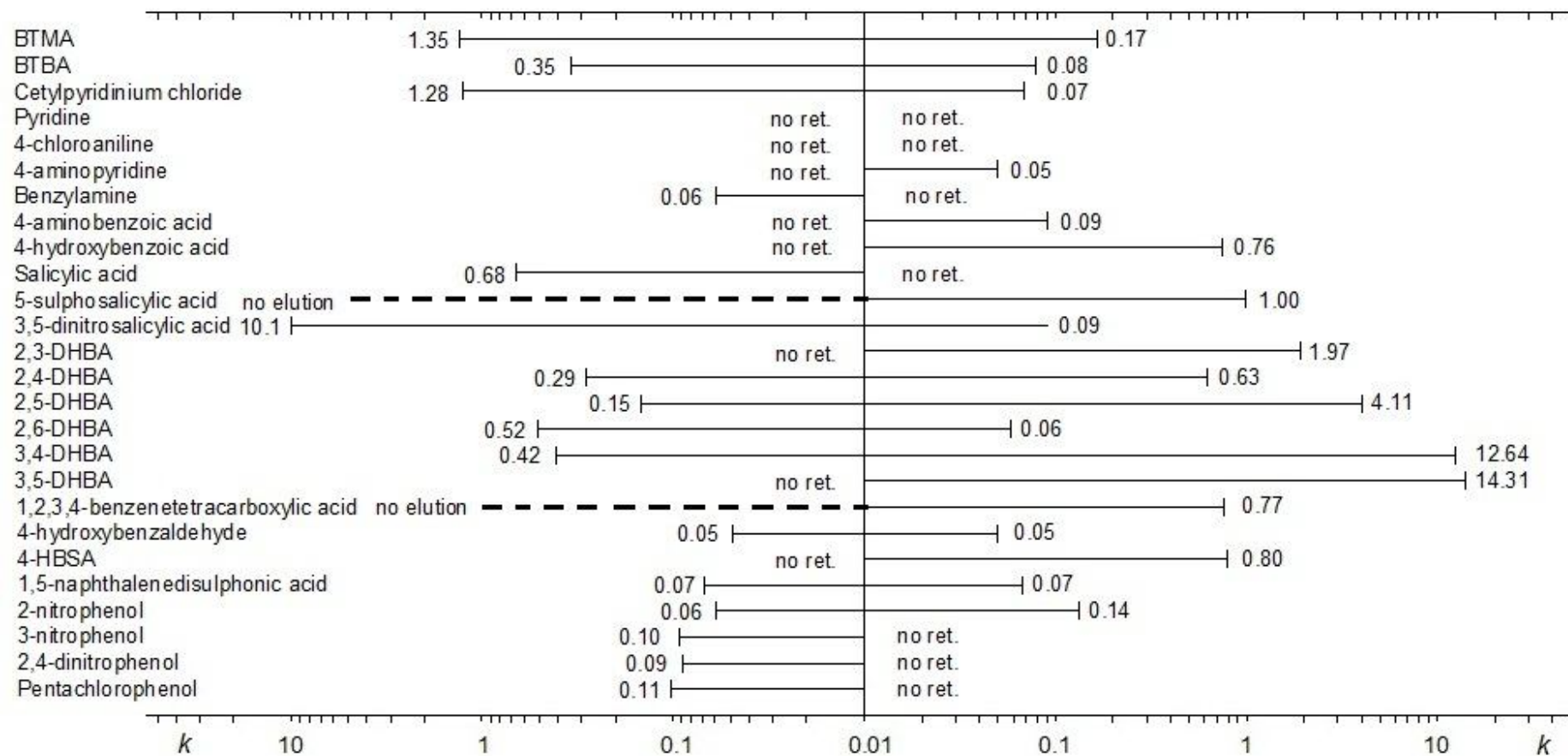


Fig. 5.9. Selectivity of HPHT diamond in ACN and MeOH based mobile phases. Flow rate  $0.5 \text{ mL}\cdot\text{min}^{-1}$ , detection UV 254 nm, column temperature  $25^\circ\text{C}$ , injection volume  $2 \mu\text{L}$ , sample concentration  $0.05 \text{ mg}\cdot\text{mL}^{-1}$ , UV detection at 254 nm.

Secondly, the derivatives of salicylic acid are also better retained in 80% MeOH. On the other hand, the majority of the other phenolic compounds have greater retention in 80% ACN. Obviously, this is a result of the stronger hydrogen bonding interactions for such compounds, which are suppressed in 80% MeOH but not in 80% ACN.

Special attention should be paid to the selectivity of retention for the positional isomers of dihydroxybenzoic acid (DHBA). As it is clear from the chart, in ACN based mobile phases DHBA isomers with at least one OH group in the meta position have stronger retention, while 2,4-DHBA and 2,6-DHBA are retained weakly. The opposite is true for the selectivity in MeOH: ortho- and para- isomers of DHBA are retained longer. Previously, Wan *et al.* have found that *o*-, *p*- and *m*- isomers can be well resolved on graphitic carbon rather than octadecyl silica, and associated this with the solute interactions with the flat surface of PGC [24]. Presumably, a similar effect can take place on the flat surface of the HPHT diamond, providing different retention factors for the isomers of DHBA.

### 5.3.5. Thermodynamics of retention on HPHT diamond in ANP chromatography

Useful information about interactions between solutes and the surface of stationary phase can be obtained by investigating the thermodynamics of retention and calculating retention entropy and enthalpy. Van't Hoff's equation (Eqn. 5.3) was used for calculations of these parameters.

$$\ln k = -\Delta H^\circ/RT + \Delta S^\circ/R + \ln\beta(T) \quad (\text{Equation 5.3})$$

Here  $k$  is retention factor,  $\Delta H^\circ$  is enthalpy,  $\Delta S^\circ$  is entropy and  $\beta(T)$  is column phase ratio. The retention factors were measured in the temperature interval 5 – 75 °C, and phase ratio was calculated at each temperature, as described in Section 2.4.3. Here it should be mentioned that possibly due to the expansion of the column body, column phase ratio exhibited a linear dependence on the temperature. This dependence as well as  $\ln k$  vs  $1/T$  plots for several compounds is given in Fig. 5.10.

In Chapter 4, about a 1% change in phase ratio was evident due to the column expansion in the temperature range between 25 and 65 °C. In the current Chapter, a much larger temperature interval was considered (5-75 °C), so an even greater influence of phase ratio variation on the  $\Delta H^\circ$  and  $\Delta S^\circ$  values was expected. The approach to consider this effect in the evaluation of the thermodynamic parameters is given in Section 2.4.3.

It is clear from the Table 5.3 that the linearity factors for all compounds are high, and no graph curvature was evidenced for any of the solutes.



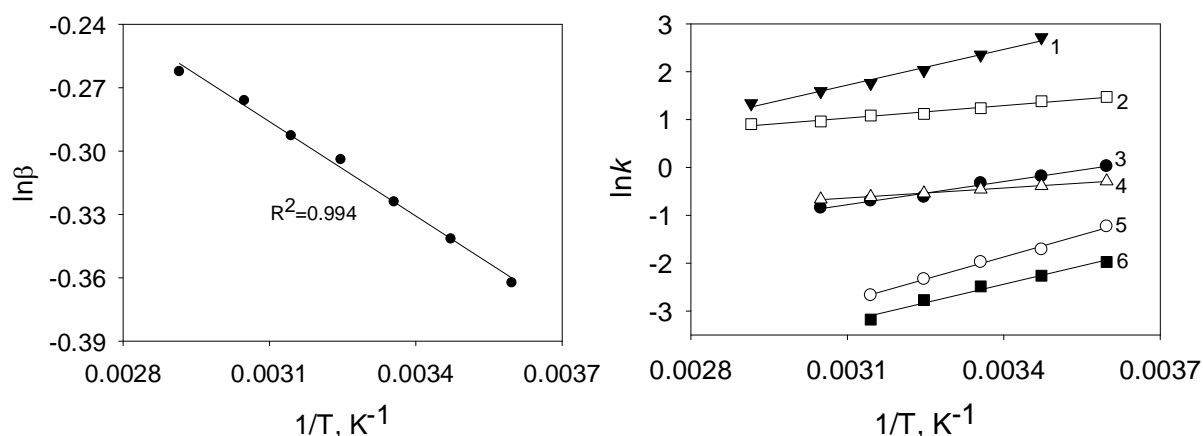


Fig. 5.10. Temperature influence on the phase ratio of HPHT diamond column (left) and on retention of several compounds (right). Method of calculating phase ratio is given in Section 2.4.3. Retention factors were obtained in 85% ACN – 15% 20 mM NaOH, flow rate  $0.5 \text{ mL}\cdot\text{min}^{-1}$ , sample concentration  $0.05 \text{ mg}\cdot\text{mL}^{-1}$ , UV detection at 254 nm. 1 – adenosine, 2 – 4-HBSA, 3 – uracil, 4 – cytosine, 5 – adenine, 6 – BTMA;  $R^2$  for van't Hoff's plots are also given in Table 5.3.

Table 5.3. Enthalpy and entropy of the retention of several compounds on the HPHT diamond column, obtained over the temperature range 5-75 °C. Mobile phase 85% ACN – 15% 20 mM NaOH, flow rate  $0.5 \text{ mL}\cdot\text{min}^{-1}$ , UV detection at 254 nm, sample concentration  $0.05 \text{ mg}\cdot\text{mL}^{-1}$ .

Compound	$\Delta H^\circ, \text{kJ}\cdot\text{mol}^{-1}$	$\Delta S^\circ, \text{kJ}\cdot\text{mol}^{-1}\cdot\text{K}^{-1}$	Linearity, $R^2$
Uracil	$-14.6\pm 1.0$	$-49.4\pm 3.3$	0.986
Adenine	$-26.9\pm 2.6$	$-104\pm 10$	0.994
Adenosine	$-21.9\pm 0.9$	$-51.1\pm 2.0$	0.985
Cytosine	$-7.00\pm 0.39$	$-24.6\pm 1.4$	0.998
BTMA	$-22.6\pm 2.8$	$-94.3\pm 11.6$	0.980
4-HBSA	$-8.47\pm 0.42$	$-15.3\pm 0.8$	0.981

This indicates that a single retention mechanism is dominant for each solutes in a given mobile phase (85% ACN – 15% 20 mM NaOH). All enthalpy values are negative, which means that retention is exothermic in nature. This makes sense assuming that the main mechanisms are ion exchange and hydrogen bonding, which are both known to be enthalpy driven [25]. Accordingly, the entropy values are negative, which corresponds to a decrease in number of degrees of freedom for the solute molecules in the adsorbed state. It should be also added that  $\Delta H^\circ$  and  $\Delta S^\circ$  values may potentially be not constant over the studied temperature range, which can cause slight curvature in the graphs for example for adenosine and cytosine.

#### **5.4. Conclusions**

In this work the main fundamental regularities of retention on the HPHT diamond surface are discussed. Classic HILIC type dependencies were observed in both ACN/water and MeOH/water mobile phases. However, a molecular adsorption mechanism rather than partitioning was established to be responsible for the retention, which means that ANP nomenclature needs to be used. Influence of different mobile phases on the retention of different compounds was studied, and three main retention mechanisms were confirmed for the HPHT diamond. At neutral pH, the retention is primarily determined by hydrogen bonding mechanism, while in acidic conditions ion-exchange mechanism is favourable. At high pH, the main mechanism was dependent on the type of organic modifier: mostly hydrogen bonding was present for ACN based mobile phase, and both ion-exchange and hydrogen bonding were observed in presence of MeOH.

Presented results show the high potential of application of the HPHT diamond in ANP mode of chromatography. The diamond columns were tested within a broad pH range (2.2-12.7) and temperature (5-75 °C) and were shown to be physically and chemically stable. Selectivity of this stationary phase is unique and can be greatly varied by choosing pH, buffer and MeOH/ACN ratio in the mobile phase. Increasing MeOH content enhances the retention of cations on the HPHT diamond, while use of ACN provides stronger retention for neutral and negatively charged solutes.

#### **5.5. Reference List**

1. P. Hemstrom, K. Irgum, Hydrophilic interaction chromatography, *J.Sep.Sci.*, 29 (2006) 1784-1821.
2. Y. Guo, S. Gaiki, Retention behavior of small polar compounds on polar stationary phases in hydrophilic interaction chromatography, *J.Chromatogr.A*, 1074 (2005) 71-80.

3. A.J. Alpert, Hydrophilic-Interaction Chromatography for the Separation of Peptides, Nucleic-Acids and Other Polar Compounds, *J.Chromatogr.*, 499 (1990) 177-196.
4. J.G. Dorsey, K.A. Dill, The Molecular Mechanism of Retention in Reversed-Phase Liquid-Chromatography, *Chem.Rev.*, 89 (1989) 331-346.
5. P. Jandera, Stationary and mobile phases in hydrophilic interaction chromatography: a review, *Anal.Chim.Acta*, 692 (2011) 1-25.
6. P. Jandera, Stationary phases for hydrophilic interaction chromatography, their characterization and implementation into multidimensional chromatography concepts, *J.Sep.Sci.*, 31 (2008) 1421-1437.
7. L.T. Zhuravlev, Concentration of Hydroxyl-Groups on the Surface of Amorphous Silicas, *Langmuir*, 3 (1987) 316-318.
8. V. Verdolino, R. Cammi, B.H. Munk, H.B. Schlegel, Calculation of pK(a) Values of Nucleobases and the Guanine Oxidation Products Guanidinohydantoin and Spiroiminodihydantoin using Density Functional Theory and a Polarizable Continuum Model, *J.Phys.Chem.B.*, 112 (2008) 16860-16873.
9. B. Buszewski, S. Noga, Hydrophilic interaction liquid chromatography (HILIC)-a powerful separation technique, *Anal.Bioanal.Chem.*, 402 (2012) 231-247.
10. A. Berthod, S.S.C. Chang, J.P.S. Kullman, D.W. Armstrong, Practice and mechanism of HPLC oligosaccharide separation with a cyclodextrin bonded phase, *Talanta*, 47 (1998) 1001-1012.
11. A.E. Martell, R.M. Smith, R.J. Motekaitis, NIST Database 46, National Institute of Standards and Technology, U.S. Dept. of Commerce, c2004, Gaithersburg, MD (2004).
12. D.D. Perrin, Dissociation Constants of Organic Bases in Aqueous Solution, Butterworths, London, 1972.
13. J.A. Dean, Lange's handbook of chemistry, McGraw-Hill, New-York, USA, 1998.
14. J.S. Fritz, D.T. Gjerde, Ion Chromatography, Wiley, New-York, USA, 2009.
15. R.A. Cox, Acids and Bases. Solvent Effects on Acid-Base Strength, *Angew.Chem.Int.Edit.*, 52 (2013) 7638-7638.
16. A. Levy, D. Andelman, H. Orland, Dielectric Constant of Ionic Solutions: A Field-Theory Approach, *Phys.Rev.Lett.*, 108 (2012) 227801-227806.
17. R. Buchner, G.T. Hefter, P.M. May, Dielectric relaxation of aqueous NaCl solutions, *J.Phys.Chem.A.*, 103 (1999) 1-9.

18. S. Mysling, G. Palmisano, P. Hojrup, M. Thaysen-Andersen, Utilizing Ion-Pairing Hydrophilic Interaction Chromatography Solid Phase Extraction for Efficient Glycopeptide Enrichment in Glycoproteomics, *Anal.Chem.*, 82 (2010) 5598-5609.
19. J. Dai, P.W. Carr, Role of ion pairing in anionic additive effects on the separation of cationic drugs in reversed-phase liquid chromatography, *J.Chromatogr.A*, 1072 (2005) 169-184.
20. I.M. Smallwood, *Handbook of organic solvent properties*, Elsevier Ltd., Sydney, Australia, 1996.
21. B.A. Olsen, Hydrophilic interaction chromatography using amino and silica columns for the determination of polar pharmaceuticals and impurities, *J.Chromatogr.A*, 913 (2001) 113-122.
22. J.C. Valette, C. Demesmay, J.L. Rocca, E. Verdon, Separation of tetracycline antibiotics by hydrophilic interaction chromatography using an amino-propyl stationary phase, *Chromatographia*, 59 (2004) 55-60.
23. R.P. Li, J.X. Huang, Chromatographic behavior of epirubicin and its analogues on high-purity silica in hydrophilic interaction chromatography, *J.Chromatogr.A*, 1041 (2004) 163-169.
24. Q.H. Wan, M.C. Davies, P.N. Shaw, D.A. Barrett, Retention behavior of ionizable isomers in reversed phase liquid chromatography: A comparative study of porous graphitic carbon and octadecyl bonded silica, *Anal.Chem.*, 68 (1996) 437-446.
25. A.V. Kisilev, *Intermolecular interaction in adsorption and chromatography*, Visshaja Shkola, Moscow, 1986.

## Chapter 6. Ion-exchange properties of microdispersed sintered detonation nanodiamond

### 6.1. Introduction and literature review

According to the information presented in Chapters 3-5, diamond possesses a hydrophilic surface, saturated with carboxyl, carbonyl and hydroxyl groups. The presence of  $\sim 10 \mu\text{mol}\cdot\text{g}^{-1}$  of carboxyls and hydroxyls provides a negative  $\zeta$ -potential for the particles at  $\text{pH} > 7$  of  $-80 \text{ mV}$ , while under acidic conditions, the  $\zeta$ -potential is almost neutral (see Section 3.3.1.2). Diamond particles with such surface properties can provide several types of adsorption interactions. For example, in NP-HPLC (Chapter 4), it was shown that the retention of compounds with polar groups (ketones, phenol, carboxylic acids and amines) is predominantly based upon hydrogen bonding, whereas polycyclic aromatic hydrocarbons (PAH) were retained due to  $\pi$ - $\pi$  stacking. In contrast, contribution of hydrophobic (dispersive) interactions was not evident due to the low surface area of HPHT diamond. In ANP chromatography (Chapter 5), the main retention mechanisms were shown to be hydrogen bonding and ion-exchange. The partitioning mechanism was not obvious, and this was credited to the low surface area and non-porous structure of diamond particles. Therefore, the last type of interaction, which can potentially be significant on such diamond sorbents and needs to be investigated more carefully, is ion-exchange.

There are some obvious indications that diamond should possess the properties of an ion-exchange adsorbent. First, the negatively charged surface, described above, should enable the adsorption of cations. This was demonstrated in Sections 5.3.2 and 5.3.3 for the BTMA cation. Also, using NaOH, KOH, TMAOH and  $\text{NH}_4\text{OH}$  mobile phase solutions resulted in different retention factors for the same model compounds (see Section 5.3.2.2). This indicates that the adsorption of cations from the mobile phase takes place and influences the chromatographic properties of the HPHT diamond column. However, it is likely that the diamond surface possesses diphilic character and adsorption of both cations and anions can occur. Evidence for such an assumption is the variation in retention times in NP-HPLC for the diamond column when flushed with several different acids at  $\text{pH} 2.0$  (Section 4.3.3). The most reasonable explanation for this effect is the adsorption of anions on the surface of diamond. In addition, it was shown that the negatively charged molecules (phenols and carboxylic acids) are retained on the diamond column with water-ACN mobile phases (see Chapter 5.3.4). Therefore, in this Chapter a more systematic investigation of the ion-

exchange properties of diamond will be undertaken. The kinetics of ion-exchange interactions are much slower than for the other types of interactions [1], including hydrogen bonding and dispersive interactions. Therefore it was decided to first check the adsorption of anions and cations on diamond adsorbents, before moving on to chromatographic investigations.

The number of publications based upon the ion-exchange properties of diamond is very low. Most research in this area has been dedicated to the study of the cation-exchange properties of diamond, while information on the adsorption of anions is limited. This is due to the fact that negatively charged oxygen-containing groups are normally present on the surface of nanodiamond [2], which makes adsorption of cations favourable. For example, one of the first papers in this field reports that the surface of detonation nanodiamond (DND) exhibits acidic character. In this work potentiometric titration was employed to confirm the ability of DND to adsorb alkali and alkali earth cations [3]. The majority of studies have investigated DND, while no data is available for HPHT diamond. This can be attributed to the small surface area of HPHT diamond, which complicates conducting such adsorption experiments.

Regarding the adsorption of alkali and alkali earth metals, the following selectivity was observed for DND:  $\text{Ca}^{2+} > \text{Ba}^{2+} > \text{Li}^+ > \text{Na}^+ > \text{K}^+$  [4]. This series matches the selectivity reported earlier for oxidised synthetic diamond [5], and is typical for carboxylic cation exchangers in alkaline media [6]. In the case of non-oxidised DND, however, an alternative selectivity was reported ( $\text{Na}^+ > \text{K}^+ > \text{Li}^+$ ). Zhukov *et al.* suggest that the pKa values of the different types of carboxylic groups on the non-oxidised DND can account for this difference [7]. It was shown that oxidative purification with mineral acids is essential for preparation of DND with cation exchange properties, and, depending on the purification, capacities of up to 0.6-0.9 mmol·g<sup>-1</sup> can be achieved [4].

While the adsorption mechanism of alkali and alkaline earth metals involves electrostatic interactions with surface carboxyl groups [5], the adsorption mechanism for transition metals is more complicated. Several research groups have studied the adsorption of different metals onto DND, such as Fe<sup>2+</sup> [8], Ni<sup>2+</sup> [9], Al<sup>3+</sup> [10], Fe<sup>3+</sup> [9,11] and Rh<sup>3+</sup> [12]. Though little attention was paid to the actual adsorption mechanism and selectivity, it is generally concluded that complexation is the one of the most probable mechanisms for the adsorption of transition metals [8,9]. In these studies two other factors that can influence adsorption of transition metals were also mentioned. First, the presence of sp<sup>2</sup>-carbon has a strong impact on the adsorption of transition metals [11,13,14]. The optimal ratio between diamond and sp<sup>2</sup>-carbon was shown to be 80:20 – this provided highest adsorption of Fe<sup>3+</sup>, Ni<sup>2+</sup>, Cr<sup>3+</sup>, Pb<sup>2+</sup>, Cd<sup>2+</sup>. Second, the hydrophobicity of the particles plays an important role

[13]. Surprisingly, the capacity of DND with a hydrophobic surface was about twice that of DND with a hydrophilic surface. A hydrophobic surface of DND was achieved through calcination at 250 °C in Ar atmosphere or by electrochemical treatment.

The following selectivity of adsorption of transition metals on DND was reported by Bogatyreva *et al.*:  $\text{Fe}^{3+} > \text{Ni}^{2+} > \text{Cr}^{3+} > \text{Pb}^{2+} > \text{Cd}^{2+}$  [11,13,14]. This differs from the selectivity series known for transition metals on common carboxylic cation exchangers [15]. Unfortunately, the authors of these studies [11,13,14] did not present their opinions on the reasons for such unusual selectivity.

The adsorption capacity for transition metals on DND sorbents ( $S = 150 \text{ m}^2 \cdot \text{g}^{-1}$ ) is between 0.2 and 0.5  $\text{mmol} \cdot \text{g}^{-1}$  as reported by Bogatyreva *et al.* [11,13,14]. This exceeds the literature values for activated carbon ( $S = 422 \text{ m}^2 \cdot \text{g}^{-1}$ ) and oxidised carbon ( $S = 425 \text{ m}^2 \cdot \text{g}^{-1}$ ), but is in agreement with the concentration of acidic carboxyl groups on the DND surface ( $1.3 \text{ group} \cdot \text{nm}^{-1}$ ) [16]. Furthermore, the modification and purification procedures applied can affect the adsorption capacity of DND significantly, as was shown by Chukhaeva and Cheburina [17]. The highest capacity (0.4-0.5  $\text{mmol} \cdot \text{g}^{-1}$ ) was obtained using ozone purification, and was reported to be due to an increased number of peroxy- groups on the surface of DND. Generally, C=O and -COOH groups are responsible for the adsorption of cations, but peroxy-groups can potentially contribute to the adsorption of cations as well.

Overall, DND exhibits a significant cation exchange capacity and selectivity due to its negatively charged surface. In contrast, the examples of adsorption of anions on DND are rare. Only a small number of the DND samples reported have positive  $\zeta$ , which facilitates their interaction with anions [18]. Adsorption of anions, such as  $\text{AuCl}_4^-$ ,  $\text{AsO}_3^{3-}$ ,  $\text{AsO}_4^{3-}$ ,  $\text{Cr}_2\text{O}_7^{2-}$ ,  $\text{MoO}_4^{2-}$ , and  $\text{WO}_4^{2-}$ , has been investigated [9,12,19,20], but only  $\text{Cr}_2\text{O}_7^{2-}$ ,  $\text{MoO}_4^{2-}$  and  $\text{WO}_4^{2-}$  can be adsorbed on the DND surface at pH 5.0 [19]. Adsorption values of 30%, 65% and 100% were reported, respectively, however the actual adsorption capacity was not mentioned. The authors have proposed that the positive surface charge of DND and its anion adsorption are due to the presence of protonated amino groups on the DND surface. However, adsorption of  $\text{Cu}^{2+}$  (which can be used as proof of the presence of amino groups) was not observed during these experiments. Therefore, the reasons for the high selectivity towards  $\text{MoO}_4^{2-}$  and  $\text{WO}_4^{2-}$  remain unclear. Though it is indeed possible that without oxidative purification DND can exhibit a positively charged surface [21], this effect is usually linked to fixed charges or the protonation of pyrones, rather than amino groups [22].

Finally, it has to be added that some computational efforts have been made recently in order to investigate the interactions between diamond surface and ions [23]. Despite the fact

that results obtained so far with this approach lack the experimental confirmation, in future such method may become beneficial.

Overall, the ion exchange properties of DND appear to be complex. Several mechanisms for retention of cations and anions on the surface of DND are suggested, but most data is inconclusive and the need for a more systematic investigation is evident. Therefore, the current Chapter aims to investigate the ion-exchange properties of DND. The HPHT diamond employed in previous Chapters cannot be used for adsorption experiments due to its lower surface area. Adsorption of both cations and anions on DND will be studied, with the focus on transition metals and simple inorganic anions. Since there is evidence that the adsorption of cations and anions can potentially influence each other [24], experiments will be planned in a way which allows the assessment of such influence.

## **6.2. Experimental**

General information on materials, chemicals and instrumentation is provided in Chapter 2. All adsorption experiments were carried out using microdispersed sintered detonation nanodiamond (MSDN), purchased from ALIT (Kiev, Ukraine) and characterised by Novikov *et al.* [8]. Before each experiment, MSDN was purified using the following procedure. First, it was washed with 5 M HNO<sub>3</sub> in order to remove metal impurities, then with 1 M NaOH to remove anionic impurities, and again with 5 M HNO<sub>3</sub> to ensure all surface groups were protonated. Following this, the excess of HNO<sub>3</sub> was removed by flushing MSDN several times with deionised water, until the pH of the MSDN suspension was in the range 4.5-5.

The adsorption properties of MSDN were determined based upon the experiments investigating different types of buffers, pH, solute concentration and volume, and adsorption time. For the adsorption experiments, 0.2 g of MSDN was placed within a plastic vial with 10 mL of the ion solution at the required concentration and pH. After approximately 30 min (which was sufficient time to achieve equilibrium, see Section 6.3.2.2), the vials were centrifuged, and the supernatant collected for the subsequent filtering and the determination of the remaining ion concentration using IC or UV spectrometry.

### **6.2.1. Experiments with transition metals**

A Thermo Fisher Dionex (Sunnyvale, CA, USA) ion chromatography system was used for the analysis of the transition metal concentrations during the sorption experiments. This consisted of an AS50 thermal compartment and an autosampler with an IP25 isocratic pump and AD25 absorbance detector. An IonPac CS16 250 × 3.0 mm ID column was installed. A



UV spectrophotometer Metertech SP-8001 (Nankang, Taipei, Taiwan) was used for the spectrophotometric determination of metal concentrations following reaction with complexometric indicators. A  $1.00 \times 10^{-4}$  M solution of 4-(2-pyridylazo)resorcinol (PAR) in 0.1 M sodium tetraborate buffer (pH 9.18) was used for the determination of  $Zn^{2+}$ ,  $Mn^{2+}$ ,  $Co^{2+}$ ,  $Ni^{2+}$ ,  $Cd^{2+}$ ,  $Cu^{2+}$ ,  $Fe^{3+}$ . A  $1.00 \times 10^{-4}$  M solution of Chromazurol-S in 0.1 M hexamine buffer (pH=6.0) was used for the determination of  $Al^{3+}$ . The following wavelengths were chosen for complex concentration determinations: 490 nm for the complexes of  $Zn^{2+}$ ,  $Co^{2+}$ ,  $Fe^{3+}$ ,  $Ni^{2+}$ , 493 nm for the complex of  $Mn^{2+}$ , 486 nm for the complex of  $Cu^{2+}$ , 487 nm for the complex of  $Cd^{2+}$ , and 545 nm for the complex of  $Al^{3+}$ .

Two types of buffer solutions were used for the assessment of buffer influence on the adsorption of cations on MSDN, namely a sodium acetate buffer across pH 4-6, and sodium phosphate buffer over pH 3-9. For more acidic or basic solutions, either  $HNO_3$  or  $NaOH$  was employed, respectively. 0.1 M  $HNO_3$  was used as eluent for the desorption of metal cations from MSDN.

### 6.2.2. Experiments with anions

A Thermo Fisher (Sunnyvale, CA, USA) ICS-2000 ion chromatograph equipped with an AS autosampler was employed for the analysis of anion solutions following sorption experiments on MSDN. An AS19 250  $\times$  4.0 mm ID column with a 40 mM KOH mobile phase was used for the determination of  $NO_3^-$ ,  $SO_4^{2-}$ ,  $ClO_4^-$ ,  $Cl^-$ ,  $I^-$ , and  $PO_4^{3-}$  concentrations. A column temperature of 30 °C and a 1 mL $\cdot$ min $^{-1}$  flow rate were chosen. Conductivity detection (ICS-2000) was applied, and background conductivity was suppressed using an ASRS 300 4 mm suppressor.  $B_4O_7^{2-}$  and  $C_2O_4^{2-}$  concentrations were obtained using ion-exclusion chromatography, using a Dionex ICE-AS6 250  $\times$  9.0 mm ID column and 1 mL $\cdot$ min $^{-1}$  of 10 mM  $H_2SO_4$  mobile phase. Conductivity was suppressed using an AMMS ICE-II ion-exclusion suppressor with 3 mL $\cdot$ min $^{-1}$  of 40 mM  $NaOH$  as the regenerant.

### 6.2.3. Adsorption isotherms

Isotherms of adsorption of cations and anions on MSDN were determined via a series of experiments. Solutions of increasing ion concentrations (0 to 100  $\mu$ mol $\cdot$ mL $^{-1}$ ) were employed to investigate the adsorption on MSDN (0.2 g), the solution volume was held constant (5ml). Adsorption values ( $A$ ,  $\mu$ mol $\cdot$ g $^{-1}$ ) were calculated for each sample according to the formula:

$$A = (C_0 - C) \cdot V/m \quad (\text{Equation 6.1})$$

where  $C$  is ion concentration after sorption ( $\mu\text{mol}\cdot\text{mL}^{-1}$ ),  $C_0$  – ion concentration before sorption ( $\mu\text{mol}\cdot\text{mL}^{-1}$ ),  $V$  is volume of solute (mL) and  $m$  is amount of MSDN (g). Adsorption values were plotted versus ion concentration remaining in the solution ( $C$ ).

Langmuir and Freundlich equations (Eqn. 6.2 and Eqn. 6.3, respectively) were applied to describe the adsorption isotherms:

$$A = A_{max} \cdot K_L \cdot C / (1 + K \cdot C) \quad (\text{Equation 6.2})$$

where  $A_{max}$  represents the limit of adsorption with the increasing concentration and can be compared to the adsorption capacity.  $K_L$  here describes the isotherm gradient at low concentrations and is connected with the distribution coefficient ( $K_D$ ).

$$A = K_F \cdot C^{1/n} \quad (\text{Equation 6.3})$$

where  $K_F$  can be compared with the distribution coefficient. Correlation factors ( $R^2$ ) between the experimental and simulated isotherms were calculated in order to understand how well Langmuir or Freundlich laws were obeyed.

### 6.3. Results and discussion

#### 6.3.1. Characterisation of MSDN

As discussed in Chapter 1, the properties of DND and MSDN can vary significantly depending on synthesis conditions and purification procedures. Therefore, prior to adsorption experiments, MSDN was characterised using the physical and chemical methods detailed below. All characterisation data refers to MSDN purified as described in Section 6.2.

##### 6.3.1.1. Scanning electron microscopy

Fig. 6.1 shows the SEM micrographs of MSDN particles used in this work. Sintered agglomerates have particle sizes between 0.5 and 2  $\mu\text{m}$ . Each of these agglomerates is composed of much smaller nanoparticles of 10-30 nm in size, as can be seen on the SEM image under higher magnification. Nanoparticles form a porous 3D structure which increases the surface area for MSDN. According to the manufacturer, the surface area of MSDN is 150  $\text{m}^2\cdot\text{g}^{-1}$  and the pore size is equal to 3 nm [8].

##### 6.3.1.2. Surface characterisation

The FTIR spectrum of MSDN is presented in Fig. 6.2. The broad absorption band at 3000-3600  $\text{cm}^{-1}$  corresponds to O-H stretching mode, and can be attributed to adsorbed water, hydroxyl groups and the OH of the carboxyl groups. The characteristic band at 1735  $\text{cm}^{-1}$  is due to the C=O stretching of the carbonyl.

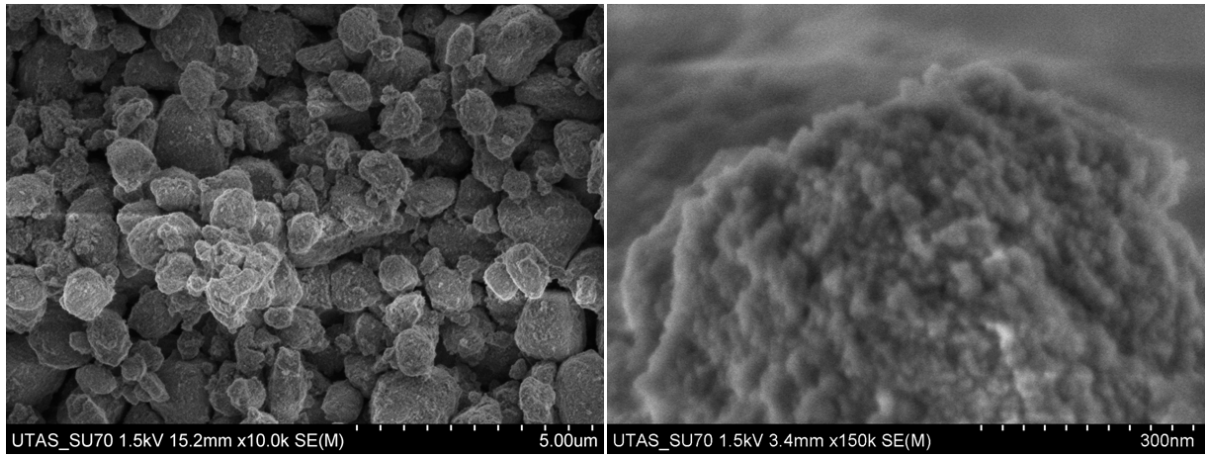


Fig. 6.1. SEM images of MSDN (see Section 2.1 for details).

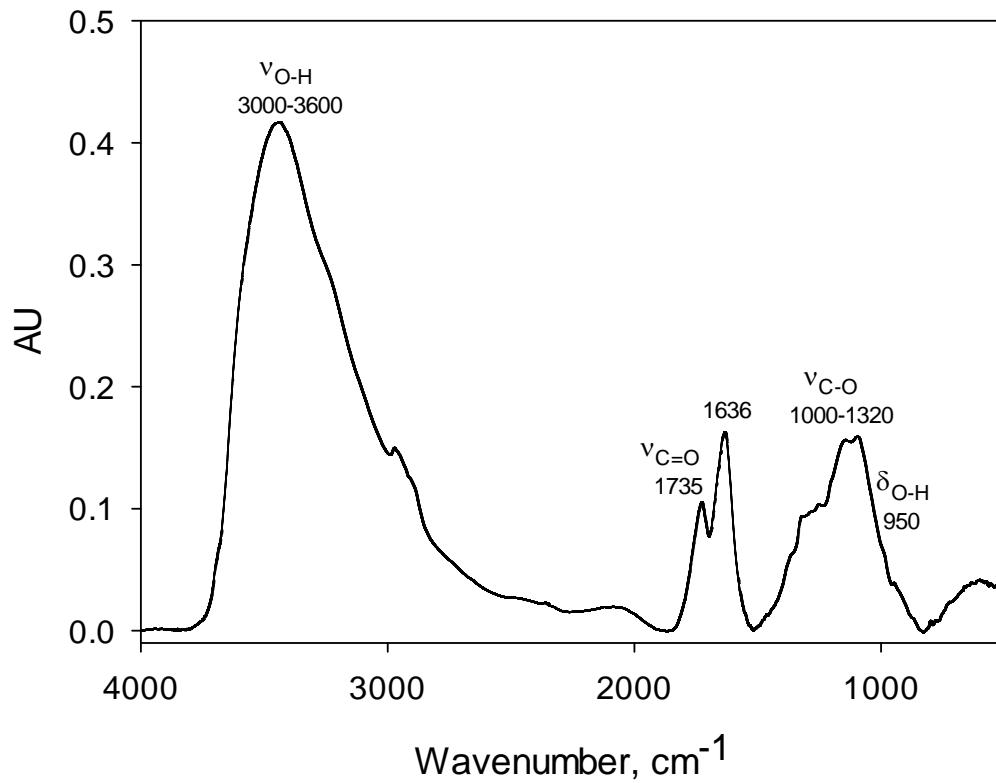


Fig. 6.2. FTIR spectrum of HPHT diamond before and after purification (see Section 6.2 for the purification procedure).

The band at 1000-1320  $\text{cm}^{-1}$  is related to C-O stretches in the hydroxyl groups. The spectra highlights the hydrophilic character of the MSDN is due to the presence of oxygen-containing functional groups. Overall, the observed FTIR spectrum is typical for DND [25].

Fig. 6.3 presents the  $\zeta$ -potential v pH dependence for MSDN. Under the acidic conditions MSDN exhibits a positive  $\zeta$ -potential of +17 mV. This value reduces with the increase in pH, with an isoelectric point observed at pH 8.0. Under alkaline conditions the  $\zeta$ -potential of MSDN drops down to -23 mV. It is common that the  $\zeta$ -potential of nanodiamond can be very different depending on the origin, purification and modification of the material [26]. Nanodiamond with  $\zeta$ -potentials between -60 and +60 mV have been described by different research groups [22,27]. Whereas negative  $\zeta$ -potentials in alkaline conditions can be explained by dissociation of the hydroxyl and carboxyl groups, reasons for the positive  $\zeta$ -potential can be more complicated. The simple explanation could involve nitrogen-containing functionalities. However, here according to the FTIR spectrum (Fig. 6.2) this is unlikely since no N-H or C-N bands were evident. However, it is known that the surface of MSDN particles contain graphitic layers of  $sp^2$ -carbon [28]. According to Paci, the main reason for the positive  $\zeta$ -potential is protonation of pyrone, chromene and phenol functional groups which are quite common on the graphitic surface of MSDN [22]. The structure of these groups is presented in Fig. 6.4.

### 6.3.2. Investigation of adsorption of metals

#### 6.3.2.1. pH dependence

Fig. 6.5 shows adsorption curves for 8 metal cations –  $\text{Zn}^{2+}$ ,  $\text{Mn}^{2+}$ ,  $\text{Co}^{2+}$ ,  $\text{Ni}^{2+}$ ,  $\text{Cd}^{2+}$ ,  $\text{Cu}^{2+}$ ,  $\text{Fe}^{3+}$ , and  $\text{Al}^{3+}$  in 0.05 M phosphate buffer. The graph shows how all metals except  $\text{Co}^{2+}$  and  $\text{Ni}^{2+}$  may be adsorbed on MSDN at a certain pH. Triple charged cations ( $\text{Fe}^{3+}$  and  $\text{Al}^{3+}$ ) have significantly higher adsorption in the low pH range (1-3). Doubly charged transition metals can be divided in 2 groups. The first group is cations  $\text{Zn}^{2+}$ ,  $\text{Cd}^{2+}$ ,  $\text{Mn}^{2+}$  and  $\text{Cu}^{2+}$ . Adsorption of these cations increased over the pH range 3-6. The second group is  $\text{Co}^{2+}$  and  $\text{Ni}^{2+}$ , which apparently interact only weakly with the surface of MSDN. It is clear from Fig. 6.5 that the selectivity for the adsorption of transition metals on MSDN is  $\text{Al}^{3+} > \text{Fe}^{3+} > \text{Cu}^{2+} > \text{Mn}^{2+} > \text{Zn}^{2+} > \text{Ni}^{2+} > \text{Co}^{2+} > \text{Cd}^{2+}$ . This series is different from that which is commonly observed on other carboxylic exchangers [15] or carbon sorbents [29]. For example, the retention order  $\text{Cu}^{2+} > \text{Ni}^{2+} > \text{Co}^{2+} > \text{Zn}^{2+} > \text{Mn}^{2+}$  was observed for oxidised active carbon by Strelko *et al.* [29].

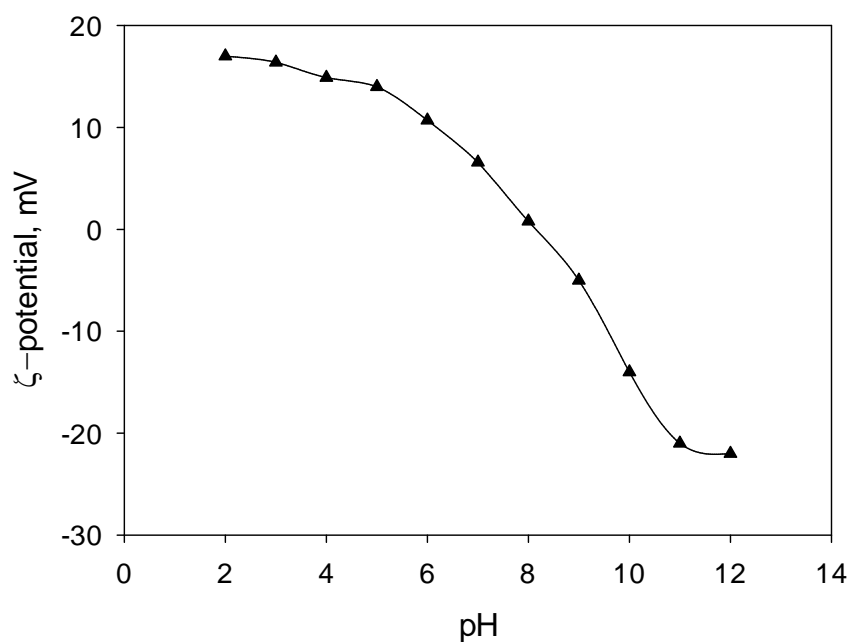


Fig. 6.3.  $\zeta$ -potential dependence on pH for MSDN. Measured for  $100 \mu\text{g}\cdot\text{mL}^{-1}$  water suspension of MSDN ( $\mu = 0.01 \text{ M}$ ), pH adjusted with NaOH or  $\text{HNO}_3$

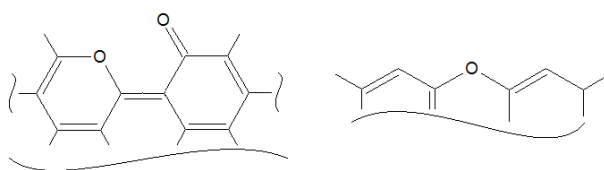


Fig. 6.4. Structure of pyrone (left) and chromene (right) functional groups, protonation of which can provide positive  $\zeta$ -potential for MSDN under acidic conditions. Adopted from [22].

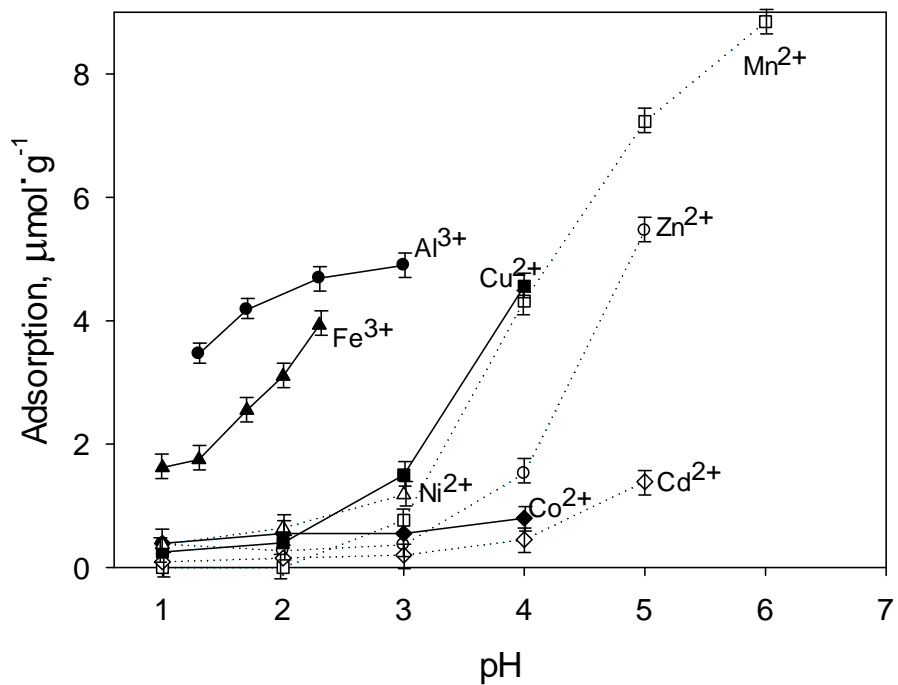


Fig. 6.5. Dependence of adsorption of various metals on MSDN (0.2 g) on pH, from 10 mL of  $10\ \mu\text{g}\cdot\text{mL}^{-1}$  solution in 0.05 M sodium phosphate buffer.

The high selectivity displayed by both oxidised active carbon and MSDN sorbents towards  $\text{Cu}^{2+}$  is a consequence of the fact that  $\text{Cu}^{2+}$  often forms distorted and more stable octahedral complexes [29]. However, for the other cations of transition metals ( $\text{Ni}^{2+}$ ,  $\text{Co}^{2+}$ ,  $\text{Zn}^{2+}$ , and  $\text{Mn}^{2+}$ ) an almost opposite retention order was observed. This reversal points towards a unique retention mechanism for MSDN.

It is known that only a cation exchange retention mechanism is observed with oxidised active carbon for transition metals ions [29]. In contrast, at least 3 retention mechanisms were reported previously for MSDN [30], including interaction with the two types of carboxylic groups with different pKa, interaction with hydroxyls and complexation. Moreover, for diamond sorbents complexation may play a major role in adsorption, as compared to electrostatic interaction.

The above mentioned information correlates well with the data in Fig. 6.5. Metals such as  $\text{Cu}^{2+}$ ,  $\text{Zn}^{2+}$  and  $\text{Mn}^{2+}$ , which are known for their ability to form complexes with carboxylic groups, are adsorbed at lower pHs. At the same time,  $\text{Co}^{2+}$  and  $\text{Ni}^{2+}$  should be mostly adsorbed via a simple cation exchange mechanism, which explains why they are not adsorbed under acidic conditions. An investigation of their adsorption at pH above 5-6 was impossible due to hydrolysis and formation of insoluble phosphates. In the case of triple charged cations, interaction mechanisms are more difficult to elucidate, as  $\text{Fe}^{3+}$  and  $\text{Al}^{3+}$  exhibit different adsorption trends. The stronger interaction for  $\text{Fe}^{3+}$  and  $\text{Al}^{3+}$  can be due to their triple charge and consequently greater electrostatic attraction to the diamond surface, as was previously observed for the triple charged lanthanides and actinides under acidic conditions [31,32].

Regarding adsorption capacity, the highest value of  $9 \mu\text{mol}\cdot\text{g}^{-1}$  was observed for  $\text{Mn}^{2+}$ . However, this value is not high compared to activated carbon ( $200\text{-}300 \mu\text{mol}\cdot\text{g}^{-1}$ , [29]) or the commercial carboxylic cation exchangers ( $\sim 1 \text{ mmol}\cdot\text{g}^{-1}$ , [15]). However, it should be taken into account, that the surface area of MSDN is only  $150 \text{ m}^2\cdot\text{g}^{-1}$ , which is  $\sim 6$  times lower than the value for activated carbon ( $850 \text{ m}^2\cdot\text{g}^{-1}$ ) and other commercial sorbents (up to  $1000 \text{ m}^2\cdot\text{g}^{-1}$ ) [8].

### 6.3.2.2. Kinetics of adsorption

Fig. 6.6 shows data on adsorption kinetics of  $\text{Cu}^{2+}$  and  $\text{SO}_4^{2-}$  on MSDN. Adsorption capacity is reached after approximately 10 minutes and the curves obey classic 1<sup>st</sup> order kinetics (Fig. 6.6, left). This demonstrates slow kinetics of ion-exchange interactions as compared with the other types of adsorption interactions, and is in accordance with the literature [1].

Fig. 6.6 (right) was obtained by carrying out sorption of a constant amount of  $\text{Cu}^{2+}$  (100  $\mu\text{g}$ ) on 0.2 g of MSDN from increasing volumes of buffer solution at pH 5. The coefficient of  $\text{Cu}^{2+}$  distribution between the diamond surface and the buffer media was calculated from this curve. The distribution ratio ( $K_d$ ) was found to be 280  $\text{mL}\cdot\text{g}^{-1}$  at pH 4. This value is in the same range as the  $K_d$  values for transition metal adsorption on industrially used carboxylic cation exchangers [15].

### 6.3.2.3. Buffer dependence

As discussed earlier, hydroxyl groups on the MSDN surface can possess both cation and anion exchange properties. As such, the adsorption of anions and cations at different pH can interfere with each other. Previously, some indication of co-adsorption of  $\text{NO}_3^-$  and  $\text{Cu}^{2+}$  on diamond was obtained by Dolenko *et al.* [33]. To confirm this hypothesis, we investigated the influence of the buffer composition on  $\text{Cu}^{2+}$  adsorption. The dependences obtained are shown in Fig. 6.7.

For both sodium acetate and sodium phosphate buffers, adsorption of  $\text{Cu}^{2+}$  on MSDN starts at pH 3.0. However, in the case of sodium phosphate buffer, complete (100%)  $\text{Cu}^{2+}$  adsorption was achieved at pH 5, while in the case of the sodium acetate buffer, complete adsorption of  $\text{Cu}^{2+}$  was not achieved even up to pH 6 (highest possible value for sodium acetate buffer). Such a significant difference in adsorption from various buffers in the same pH range indicates that there is a strong buffer influence on the adsorption mechanism. Strong interaction between phosphate and diamond surface was established previously [34]. It will be shown hereafter, that  $\text{PO}_4^{3-}$  ions can be adsorbed more strongly than  $\text{CH}_3\text{COO}^-$  on the diamond surface due to the higher charge and greater interaction with various functionalities. So, the adsorbed phosphate can act as an additional adsorption site for  $\text{Cu}^{2+}$  cations. Additionally, very low solubility constant for  $\text{Cu}_3(\text{PO}_4)_2$  ( $k_{\text{sp}} = 1.4 \cdot 10^{-37}$ ) can influence the adsorption. Another reason for such a significant difference between sodium acetate and sodium phosphate buffers is that acetate can form complexes with copper. Weaker adsorption of these complexes upon the MSDN surface may be related to different adsorption mechanisms.

### 6.3.2.4. Isotherms of adsorption

In the case of using a buffer for maintaining a certain pH, the concentration of buffer is much higher than the concentration of the solute, so the buffer influence on adsorption is not surprising.



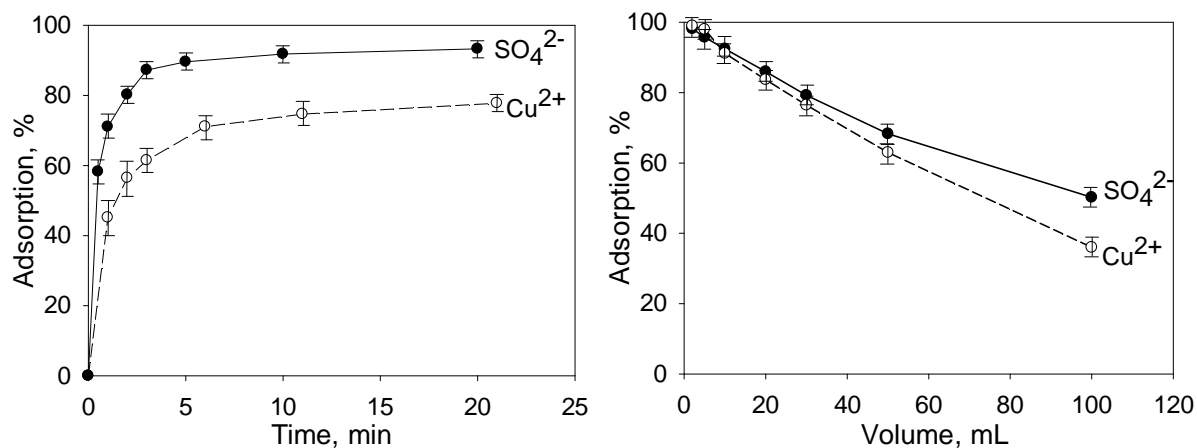


Fig. 6.6. Dependence of Cu<sup>2+</sup> and SO<sub>4</sub><sup>2-</sup> adsorption on MSDN (0.2 g) on time (left), and on solution volume (right). Left figure: 10 mL of 0.0625 mM CuSO<sub>4</sub> solution in 0.05 M sodium phosphate buffer (pH 5.0). Right figure: 0.625 μmol of Cu<sup>2+</sup> in various volumes (1 to 100 mL) of 0.05 M sodium phosphate buffer (pH 5.0).

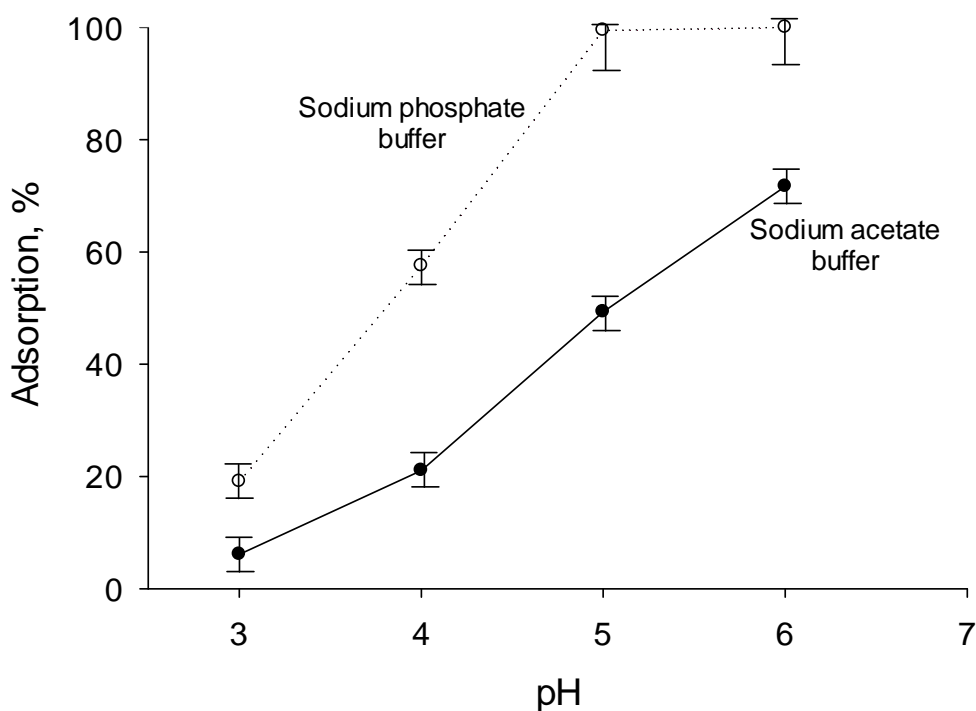


Fig. 6.7. Adsorption of Cu<sup>2+</sup> on MSDN (0.2 g) depending on the buffer pH for sodium phosphate and sodium acetate buffers. Experiments were done from 10 mL of 10 μg·mL<sup>-1</sup> Cu<sup>2+</sup> solution in 0.05 M buffer (100% adsorption = 100 μg of Cu<sup>2+</sup>).

However, it is interesting to understand whether the counter ions in the  $\text{Cu}^{2+}$  salts used also have an influence on  $\text{Cu}^{2+}$  adsorption, despite their concentration being much smaller than the concentration of anions within the buffers. Fig. 6.8 presents the  $\text{Cu}^{2+}$  adsorption isotherm on MSDN for different  $\text{Cu}^{2+}$  salts with different counter-ions. No buffer was added; this experiment was carried out with only deionised water as the solvent.

As it can be seen from Fig. 6.8, the counter ion has a great influence on the shape of the  $\text{Cu}^{2+}$  adsorption isotherm and overall adsorption capacity. In the case of a  $\text{SO}_4^{2-}$  counter ion, there are at least 3 distinct regions on the isotherm, while isotherms of  $\text{Cl}^-$  and  $\text{NO}_3^-$  counter ions behave similarly and have only two regions. The fact that adsorption isotherms have several steps is quite uncommon and indicates that the mechanism of interaction between MSDN and  $\text{Cu}^{2+}$  is complicated and is influenced by the counter ion adsorption. Other researchers, who have investigated adsorption isotherms for heavy metals on the other graphite-type carbon materials, have shown that the surface of these materials contains only one type of active site [35]. That means that a fundamental difference exists between the adsorption properties of diamond and graphite based adsorbents, though some authors have described the structure and composition of diamond surface as being very similar to a graphite layer [36].

The case with the numerous steps on an adsorption isotherm was analysed by Tolner, who established that “multi-step isotherms can be calculated additively from the adsorption isotherms of the individual “steps” [37] and derived an extended Langmuirian type equation for their description (Eqn. 6.4):

$$A = \sum_{i=1}^S \frac{a_i * k_i * [(C-b_i) + abs(C-b_i)]^{n_i}}{2^{n_i + k_i} * [(C-b_i) + abs(C-b_i)]^{n_i}} \quad (\text{Equation 6.4})$$

Here,  $A$  is adsorption ( $\mu\text{mol}\cdot\text{g}^{-1}$ ),  $a_i$  is adsorption limit of the step  $i$  on the adsorption isotherm ( $\mu\text{mol}\cdot\text{g}^{-1}$ ),  $k_i$  is isotherm gradient for the step  $i$  ( $\text{mL}\cdot\mu\text{mol}^{-1}$ ),  $C$  is concentration ( $\mu\text{mol}\cdot\text{mL}^{-1}$ ),  $b_i$  is the concentration limit at which the adsorption mechanism of the step  $i$  comes into action ( $\mu\text{mol}\cdot\text{mL}^{-1}$ ), and  $n_i$  is the degree of association at the step  $i$ . In the case of two and three step adsorption (Fig. 6.8) where association degree is 1 at each step (positively charged  $\text{Cu}^{2+}$  cations do not form associates), Eqn. 6.4 can be simplified as:

$$A = \frac{a_1 * k_1 * C}{1 + k_1 * C} + \frac{a_2 * k_2 * [(C-b_2) + abs(C-b_2)]}{2 + k_2 * [(C-b_2) + abs(C-b_2)]} + \frac{a_3 * k_3 * [(C-b_3) + abs(C-b_3)]}{2 + k_3 * [(C-b_3) + abs(C-b_3)]} \quad (\text{Equation 6.5})$$

Eqn. 6.5 was used in order to approximate adsorption isotherms in Fig. 6.8. Obtained parameters for all three isotherms as well as  $R^2$  values are presented in the Table 6.1

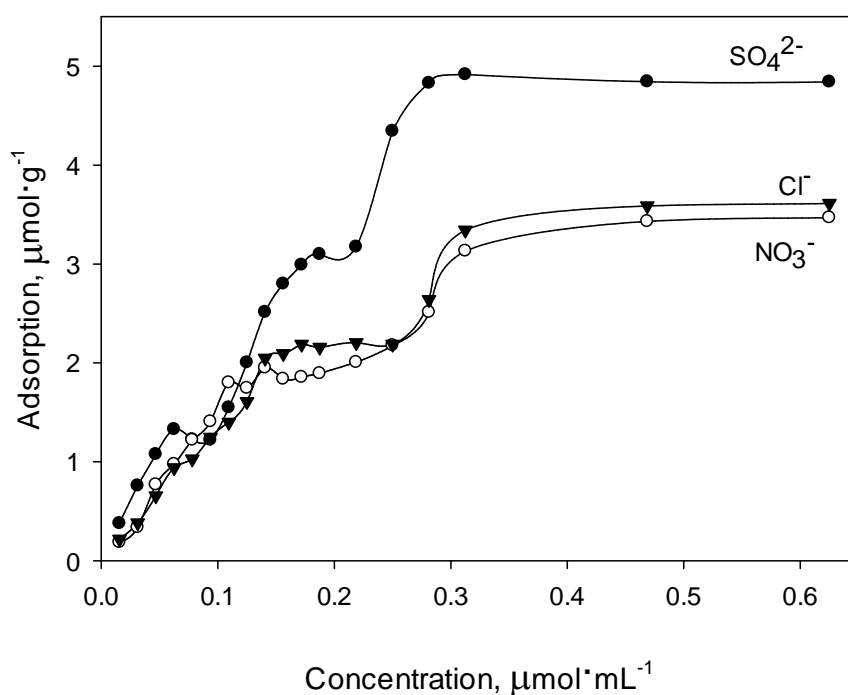


Fig. 6.8. Adsorption isotherm for  $\text{Cu}^{2+}$  on MSDN (0.2 g) from 10 mL of  $\text{CuSO}_4$  solutions with various  $\text{Cu}^{2+}$  concentrations.

Table 6.1. Calculated parameters for optimisation of the adsorption isotherms in Fig. 6.8 with the Eqn. 6.5.

	$\text{CuSO}_4$	$\text{Cu}(\text{NO}_3)_2$	$\text{CuCl}_2$
$a_1, \mu\text{mol}\cdot\text{g}^{-1}$	$2.07\pm 0.14$	$3.51\pm 0.27$	$4.38\pm 0.38$
$a_2, \mu\text{mol}\cdot\text{g}^{-1}$	$2.31\pm 0.23$	$0.70\pm 0.09$	$0.53\pm 0.06$
$a_3, \mu\text{mol}\cdot\text{g}^{-1}$	$1.16\pm 0.10$	-	-
$k_1, \text{mL}\cdot\mu\text{mol}^{-1}$	$20.0\pm 2.3$	$6.93\pm 0.71$	$4.81\pm 0.39$
$k_2, \text{mL}\cdot\mu\text{mol}^{-1}$	$20.1\pm 2.4$	$7770\pm 690$	$7970\pm 730$
$k_3, \text{mL}\cdot\mu\text{mol}^{-1}$	$109\pm 9$	-	-
$b_2, \mu\text{mol}\cdot\text{mL}^{-1}$	$0.11\pm 0.01$	$0.28\pm 0.02$	$0.28\pm 0.03$
$b_3, \mu\text{mol}\cdot\text{mL}^{-1}$	$0.22\pm 0.02$	-	-
$R^2$	0.992	0.981	0.980

As seen from the Table 6.1, in the case of  $\text{Cu}^{2+}$  adsorption from chloride and nitrate solutions, the third term in Eqn. 6.5 can be neglected, since there are only two steps on the adsorption isotherms for  $\text{Cu}(\text{NO}_3)_2$  and  $\text{CuCl}_2$ . In contrast, adsorption of  $\text{CuSO}_4$  has to be described with the full Eqn. 6.5, and all eight parameters can be calculated. Clearly, since adsorption isotherms for  $\text{Cu}(\text{NO}_3)_2$  and  $\text{CuCl}_2$  are almost identical, the values of their calculated descriptors in the Table 6.5 are also similar. Generally, the Eqn. 6.5 describes multistep adsorption of  $\text{Cu}^{2+}$  well, as indicated by  $R^2$  values close to 1. This means that adsorption of Langmuir type was observed for  $\text{Cu}^{2+}$  on MSDN, where different adsorption mechanisms dominate within various concentration ranges.

A probable explanation for the numerous steps on the adsorption isotherms can involve the  $\zeta$ -potential – pH dependence for MSDN (see Fig. 6.3). Without a buffer, the pH of MSDN suspension is around 4.5-5. Average surface charge is positive at this pH (+14 mV), and  $\text{Cu}^{2+}$  adsorption is decreased due to the electrostatic repulsion. At the same time, counter anions can be adsorbed at this pH (see Section 6.3.3), modifying the MSDN surface and decreasing the surface charge. In the case of the doubly charged  $\text{SO}_4^{2-}$  counter ion, this effect would be greater than for the singly charged  $\text{Cl}^-$  or  $\text{NO}_3^-$ . Thus, the interaction with adsorbed anions can provide an additional step on the  $\text{CuSO}_4$  adsorption isotherm and lead to a higher  $\text{Cu}^{2+}$  adsorption capacity in the case of  $\text{CuSO}_4$ , as compared to those of  $\text{CuCl}_2$  and  $\text{Cu}(\text{NO}_3)_2$ . Total  $\text{Cu}^{2+}$  adsorption capacity was found to be  $5 \mu\text{mol}\cdot\text{g}^{-1}$  for  $\text{CuSO}_4$  and  $3.5 \mu\text{mol}\cdot\text{g}^{-1}$  for  $\text{CuCl}_2$  and  $\text{Cu}(\text{NO}_3)_2$ .

Fig. 6.9 confirms that the evidence that the presence of  $\text{SO}_4^{2-}$  in the solution is the reason for the increased  $\text{Cu}^{2+}$  adsorption on MSDN. It is clear that an increase in the presence of  $\text{SO}_4^{2-}$  anions leads to a higher adsorption of  $\text{Cu}^{2+}$ , while, the addition of an appropriate amount of  $\text{NO}_3^-$  (to adjust same ionic strength) did not cause a significant rise in  $\text{Cu}^{2+}$  adsorption (Fig. 6.9, left). It will be shown later in Section 6.3.3, that MSDN under acidic conditions displays anion exchange properties. So, adsorbed  $\text{SO}_4^{2-}$  can act as an additional adsorption site for  $\text{Cu}^{2+}$ . However, the ionic strength can also influence the adsorption of  $\text{Cu}^{2+}$ , (Fig. 6.9, right).

As shown in Fig. 6.9 (right), with increasing ionic strength the adsorption of  $\text{Cu}^{2+}$  increases significantly until  $\mu = 0.05 \text{ M}$  after which it levels off. This may indicate that the adsorption mechanism for  $\text{Cu}^{2+}$  on the MSDN surface is chelation based. In the case of ion-exchange, increasing ionic strength would lead to a decline in adsorption levels due to the lower  $\zeta$ -potential at the MSDN surface at higher ionic strength values.

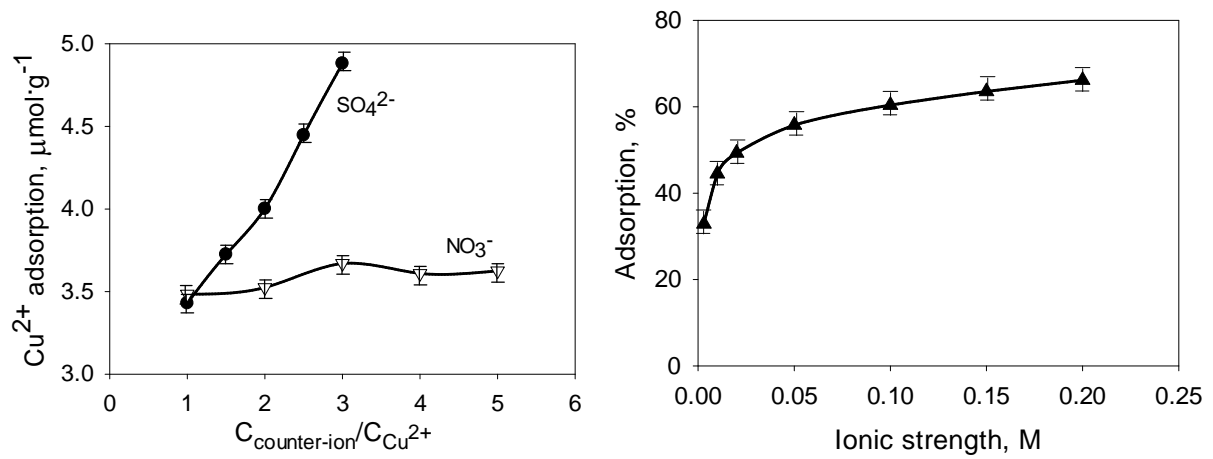


Fig. 6.9. Influence of nature of anion (left) and ionic strength (right) on Cu<sup>2+</sup> adsorption on MSDN (0.2 g). 10 mL of 10 μg·mL<sup>-1</sup> Cu<sup>2+</sup> solution was used. Left figure: Na<sub>2</sub>SO<sub>4</sub> or NaNO<sub>3</sub> were added to increase counter ion/Cu<sup>2+</sup> ratio. Right figure: ionic strength was maintained with NaNO<sub>3</sub>.

As shown in Fig. 6.3, the  $\zeta$ -potential of MSDN is about +14 mV at pH 5.0, therefore the surface of the MSDN should repulse positively charge  $\text{Cu}^{2+}$  cations. However, due to complexation  $\text{Cu}^{2+}$  can still be adsorbed. Increasing ionic strength can reduce the value of the positive  $\zeta$ -potential and subsequently promote  $\text{Cu}^{2+}$  adsorption.

### 6.3.3. Investigation of anion adsorption

Once it was found that counter ions have influence on the metal cation adsorption on MSDN, the nature of MSDN interaction with the simple inorganic anions required investigation.

Fig. 6.10 shows adsorption isotherms for 8 inorganic anions on MSDN and Table 6.2 presents the distribution coefficients ( $K_D$ ) for anion adsorption as well as an approximation of adsorption isotherms with Langmuir and Freundlich models (Eqn. 6.2 and 6.3).

From the Table 6.2 it is clear that the adsorption of anions obeys the Langmuir equation better than the Freundlich model (except for  $\text{PO}_4^{3-}$ , which behaviour will be explained hereafter). This makes sense if a chemical monolayer adsorption is assumed, when anions interact with functionalities on the MSDN surface and are not able to drift along the surface. Adsorption capacities for anions are at the level of  $50\text{-}150 \mu\text{mol}\cdot\text{g}^{-1}$ , which significantly exceeds the values for cations. This is the first time that such significant anion adsorption capacity was revealed for nanodiamond.

Distribution coefficients for anion adsorption over MSDN increase in series:  $\text{CH}_3\text{COO}^- < \text{Cl}^- < \text{B}_4\text{O}_7^{2-} < \text{ClO}_4^- < \text{I}^- < \text{SO}_4^{2-} < \text{C}_2\text{O}_4^{2-}$ . This sequence is different from common anion-exchange selectivity known for most amino and quaternary ammonium anion exchangers, which is reported as:  $\text{B}_4\text{O}_7^{2-} < \text{CH}_3\text{COO}^- < \text{Cl}^- < \text{I}^- < \text{C}_2\text{O}_4^{2-} < \text{SO}_4^{2-} < \text{ClO}_4^-$  [38]. Though some anions exhibit similar selectivity as these anion exchange series, the high  $K_D$  values for  $\text{B}_4\text{O}_7^{2-}$  and  $\text{C}_2\text{O}_4^{2-}$  and low  $K_D$  for  $\text{ClO}_4^-$  indicate that some other mechanism is taking place together with the anion-exchange interactions.

The FTIR spectrum (Fig. 6.2) suggests that there is a high abundance of hydroxyl groups present on the MSDN surface. Hydroxyls were not dissociated at the pH of the experiment; however they can contribute to adsorption by providing hydrogen bonds with anions. Also, it is known that diol and polyol surface groups are able to form complexes with  $\text{B}_4\text{O}_7^{2-}$  anions [39]. This can explain the unusually high  $K_D$  for  $\text{B}_4\text{O}_7^{2-}$  in our experiments (as compared to common anion exchangers which interact with borate weakly).

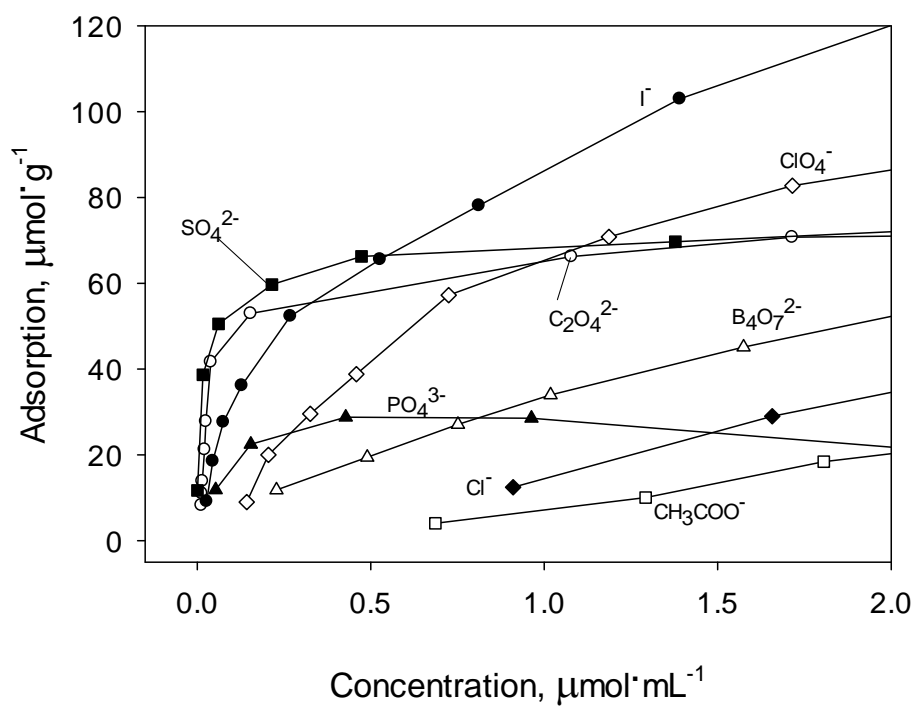
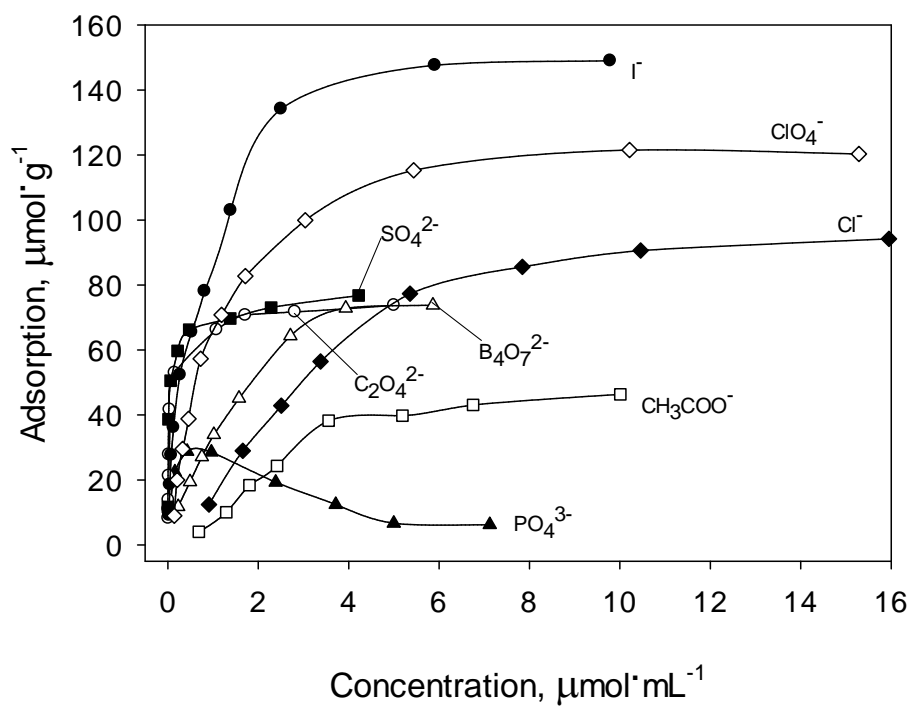


Fig. 6.10. Isotherms of adsorption on MSDN for 8 inorganic anions from 5 mL solutions of sodium salts of increasing concentration. (Bottom figure gives a magnified view in the area of low initial concentration of anions)

Table 6.2. Adsorption capacity and distribution coefficients for anion adsorption on MSDN and adsorption modelling with Langmuir and Freundlich equations.

Anion	Experiment		Langmuir model (Eqn. 6.2)			Freundlich model (Eqn. 6.3)		
	$K_D, \text{mL}\cdot\text{g}^{-1}$	$A_{max}, \mu\text{mol}\cdot\text{g}^{-1}$	$R^2$	$K_L, \text{mL}\cdot\mu\text{mol}^{-1}$	$A_{max}, \mu\text{mol}\cdot\text{g}^{-1}$	$R^2$	$n$	$K_F$
$\text{C}_2\text{O}_4^{2-}$	870±70	74±2	0.988	21±2.0	73±4	0.930	4.5±0.7	58±9
$\text{B}_4\text{O}_7^{2-}$	45±3	74±2	0.994	0.50±0.05	104±5	0.974	2.0±0.3	34±5
$\text{CH}_3\text{COO}^-$	10±1	47±1	0.971	0.20±0.02	75±4	0.937	1.73±0.30	14±2
$\text{Cl}^-$	17±2	95±2	0.985	0.21±0.02	131±6	0.943	2.12±0.30	29±4
$\text{I}^-$	325±21	150±4	0.992	1.55±0.16	160±8	0.970	3.11±0.50	81±12
$\text{SO}_4^{2-}$	552±44	77±2	0.979	59±6	71±4	0.963	7.3±1.1	67±10
$\text{ClO}_4^-$	90±8	121±3	0.998	0.94±0.10	134±6	0.941	3.10±0.50	58±9



Since FTIR has also shown MSDN to have a lot of hydroxyl functionalities, the presence of diols on the MSDN surface is likely and can provide strong retention of borate through the complexation.

Furthermore, it was revealed by means of ICP-MS that even purification with acids cannot completely remove metal impurities from the surface of MSDN [40]. Metal cations, such as  $\text{Ca}^{2+}$ ,  $\text{Sr}^{2+}$  and  $\text{Ba}^{2+}$  are still present in MSDN and can interact with anions such as  $\text{C}_2\text{O}_4^{2-}$  or  $\text{PO}_4^{3-}$ . Thus, metal impurities present on MSDN surface can potentially contribute to the adsorption mechanism for certain anions (i.e.  $\text{C}_2\text{O}_4^{2-}$ ), changing the selectivity of anion adsorption on MSDN. Overall, the combination of anion exchange, interaction with hydroxyl/diol groups and interaction with metals impurities can collectively result in the observed unusual distribution coefficients for inorganic anions on MSDN.

As shown in Fig. 6.10, the shape of an adsorption isotherm for  $\text{PO}_4^{3-}$  is different from that observed for the other anions. The initial part of isotherm matches those for the other anions, but with increasing phosphate concentration, adsorption suddenly drops down and remains low even for the high  $\text{Na}_3\text{PO}_4$  concentrations. A likely explanation for this behaviour is that both the MSDN suspension and the  $\text{Na}_3\text{PO}_4$  solution used in this experiment have properties of a pH buffer with  $\text{pK}_a$  of  $\sim 5$  and  $\sim 12$ , respectively. Therefore, at low  $\text{Na}_3\text{PO}_4$  concentrations the pH of the system is determined by the MSDN particles and equals  $\sim 5$ . At this pH, MSDN particles are positively charged (see Fig. 6.3) which enables  $\text{H}_2\text{PO}_4^-$  adsorption on MSDN. This is in full agreement with literature data, since strong  $\text{H}_2\text{PO}_4^-$  interaction with hydroxyls on diamond surface under acidic pH has been reported [34]. However, addition of a higher concentration of  $\text{Na}_3\text{PO}_4$  leads to a substantial rise in pH due to the basicity of  $\text{PO}_4^{3-}$  and this changes the  $\zeta$ -potential to negative values. Accordingly, the adsorption of  $\text{HPO}_4^{2-}$  starts to decrease due to the electrostatic repulsion from the MSDN surface. A strong influence of  $\text{PO}_4^{3-}$  concentration on the  $\zeta$ -potential of nanodiamond was also confirmed by Zhu *et al.* [41]. This effect is not evident for the other anions (such as  $\text{SO}_4^{2-}$ ,  $\text{Cl}^-$ , or  $\text{ClO}_4^-$ ), as they are anions of strong acids and do not possess the buffering capacity of  $\text{PO}_4^{3-}$ .  $\text{B}_4\text{O}_7^{2-}$  has buffering capacity, but as it was mentioned above, the adsorption mechanism for  $\text{B}_4\text{O}_7^{2-}$  is different and related to complexation with diol groups. In the case of  $\text{B}_4\text{O}_7^{2-}$ , increasing pH should actually provide greater adsorption, since it was shown that the stability of  $\text{B}_4\text{O}_7^{2-}$  – diol complexes actually increases at higher pH values [42].

Results in Fig. 6.11 serve to prove all these hypotheses. Here the amount of solute was constant and the only variable was the pH of the solution, maintained with  $\text{HNO}_3/\text{NaOH}$ . It is

clear that for both  $\text{H}_2\text{PO}_4^-$  and  $\text{SO}_4^{2-}$  a drop in adsorption is observed at pH 7, which is close to the isoelectric point for MSDN (pH 8). Therefore, it is likely that an anion-exchange mechanism is responsible for the adsorption of  $\text{H}_2\text{PO}_4^-$  and  $\text{SO}_4^{2-}$ , since the adsorption values are higher in the pH range when MSDN is positively charged and can be involved in electrostatic attraction with the anions. In the case of  $\text{B}_4\text{O}_7^{2-}$ , the adsorption value is minimal at acidic pH, and gradually goes up with the pH increases. As was shown by Tan, the complexation between  $\text{B}_4\text{O}_7^{2-}$  and surface hydroxyls would release protons, and result in a pH decrease [42]. Therefore, high pH helps to remove the excess of protons and facilitates the complex formation between  $\text{B}_4\text{O}_7^{2-}$  and hydroxyls of the MSDN surface, thus increasing adsorption.

Fig. 6.6 presents the kinetics of adsorption (left) and the dependence of amount of  $\text{SO}_4^{2-}$  (and  $\text{Cu}^{2+}$ ) adsorbed on solution volume (right). Here the kinetics of adsorption for  $\text{Cu}^{2+}$  and for  $\text{SO}_4^{2-}$  is similar: the curve levels off at ~20 minutes for both cation and anion (Fig. 6.6, left). Fig. 6.6 (right) can be used to calculate the distribution coefficient for  $\text{SO}_4^{2-}$  more accurately. According to this experiment, the distribution coefficient for  $\text{SO}_4^{2-}$  is  $563 \pm 16 \text{ mL} \cdot \text{g}^{-1}$ , which is consistent with the value obtained from the  $\text{SO}_4^{2-}$  adsorption isotherm ( $552 \pm 44 \text{ mL} \cdot \text{g}^{-1}$ , see Table 6.2).

#### 6.4. Conclusions

Adsorption properties of detonation nanodiamond material prepared by the sintering method have been investigated. It was shown that the adsorption properties of MSDN are conditioned by surface charge and functionalities. Depending on the pH, the  $\zeta$ -potential of the diamond surface can be positive or negative, which enables the adsorption of both anions and cations. This is the first time that such significant anion adsorption capacity ( $50 - 150 \mu\text{mol} \cdot \text{g}^{-1}$ ) has been observed with MSDN. The anion exchange capacity far exceeds the cation exchange capacity of this material ( $< 5 \mu\text{mol} \cdot \text{g}^{-1}$ ). However, it should be considered that due to hydroxide precipitation, adsorption experiments for cations cannot be conducted at high pH, where the adsorption capacity can be expected to increase significantly, as the  $\zeta$ -potential is negative at these conditions. Adsorption on the MSDN surface is chemical in nature and obeys Langmuir law. It was confirmed that at least 3 mechanisms can be responsible for adsorption behaviour of MSDN, including ion-exchange, complex formation and influence of metal impurities. Anions of strong acids interact generally through ion exchange, while  $\text{B}_4\text{O}_7^{2-}$  is adsorbed through complex formation with hydroxyl. Interaction with metal impurities can increase distribution coefficient for such anions as  $\text{SO}_4^{2-}$  and  $\text{C}_2\text{O}_4^{2-}$ .

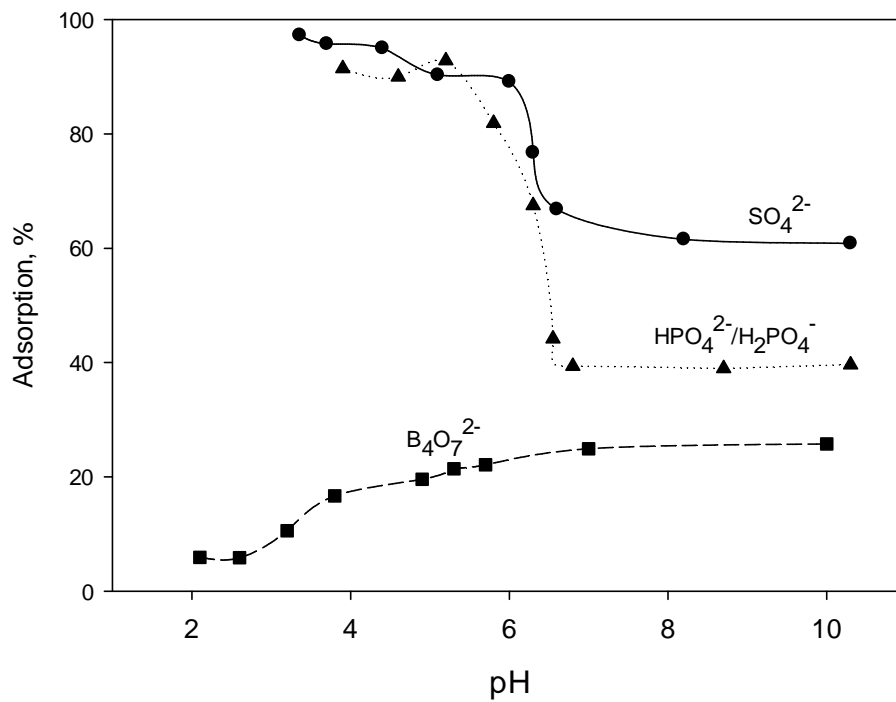


Fig. 6.11. pH influence on phosphate, sulphate and borate adsorption on MSDN (0.2 g). From 10 mL of 100  $\mu\text{mol}\cdot\text{mL}^{-1}$  solution. NaOH/HNO<sub>3</sub> was used to adjust pH and ionic strength ( $\mu = 0.01$  M)

It is the first time when the combination of these three mechanisms was established for MSDN adsorption properties. Distribution coefficients for anions over MSDN were calculated, ranging between 10 and 870 mL·g<sup>-1</sup> for various anions. Selectivity for anions differs from that on common anion-exchangers, but can be explained considering the identity of MSDN surface.

### 6.5. Reference List

1. A.V. Kisilev, Intermolecular interaction in adsorption and chromatography, Visshaja Shkola, Moscow, 1986.
2. G. Bogatyreva, V. Maevsky, M. Marinich, Y. Nikitin, I. V. Poltoratsky, A. Kozlovsky, V, EPR and physicochemical properties of composite materials based on nanodispersed diamonds, *J.Superhard.Mater.*, 27 (2005) 1-66.
3. V.I. Kuchuk, E.V. Golikova, Y.M. Chernoberezhskii, Potentiometric Titration of A Natural Diamond Micropowder, *Colloid J.USSR*, 46 (1984) 982-987.
4. G.A. Chiganova, Investigation of surface properties of ultradispersed diamond, *Colloid J.*, 56 (1994) 266-268.
5. S.K. Gordeev, O.G. Taushkanova, E.P. Smirnov, L.M. Martynova, Reaction of Solutions of Alkali Hydroxides and Alkali Earth Metals with Diamond Preparations, *Zh.Obshch.Khim.*, 53 (1983) 2426-2428.
6. Y.A. Kokotov, Ionites and ion exchange, Leningrad: Chemistry, 1980.
7. A.N. Zhukov, F.R. Gareeva, A.E. Aleksenskii, A.Y. Vul, Surface charge of detonation nanodiamond particles in aqueous solutions of simple 1: 1 Electrolytes, *Colloid J.*, 72 (2010) 640-646.
8. N.V. Novikov, G.P. Bogatyreva, M. Voloshin, M.A. Marinich, V.I. Padalko, Yu.S. Slavinsky, Nanostructured porous diamond powders and properties of their surface, *J.Superhard.Mater.*, 6 (2002) 4-10.
9. G. Bogatyreva, M. Voloshin, M. Marinich, V. Malogolovets, V. Gvyazdovskaya, V. Gavrilova, Surface and electrochemical properties of dynamically synthesized nanodiamond, *J.Superhard.Mater.*, 21 (1999) 40-43.
10. G.A. Chiganova, V.A. Bondar, A.S. Chiganov, Electrophoretic Behavior of Hydrosols of Ultradisperse Diamond and Modification of Its Surface, *Colloid J.Russ.Acad.Sci.*, 55 (1993) 774-775.
11. G.P. Bogatyreva, M. Marinich, G.A. Bazalii, Application of nanocarbon materials for purification of biological media, *Ele.Com.Eng.*, 55 (2010) 34-38.

12. N.A. Skorik, A.L. Krivozubov, A.P. Karzhenevskii, B.V. Spitsyn, Physicochemical study of the nanodiamond surface, *Prot.Met.Phys.Chem.Surf.*, 47 (2011) 54-58.
13. G.P. Bogatyreva, M. Marinich, G.A. Bazalii, G.D. Ilnitskaya, Adsorption processes in biological media on the surface of new diamond nanopowders, *Nanosystems, nanomaterials, nanotechnologies*, 8 (2010) 851-859.
14. G. Bogatyreva, M. Marinich, G.A. Bazalii, V. Gvyazdovskaya, Adsorbents for Biological Environments Based on Nano-diamond Polycrystalline Powders, *Nanosystems, nanomaterials, nanotechnologies*, 6 (2008) 1227-1236.
15. Z. Hubicki, D. Kolodynska, Ion Exchange Technologies, InTech, Rijeka, Croatia, 2015
16. G.A. Chiganova, D.A. Chul'myakova, L.E. Mordvinova, T.I. Petrova, A Nickel-Substituted Form of Nanodiamonds and Its Catalytic Activity in Decomposition of Hydrogen Peroxide, *Russ.J.Appl.Chem.*, 85 (2012) 177-181.
17. S.I. Chukhaeva, L.A. Cheburina, Sorption activity of nanodiamonds on cesium, *J.Superhard.Mater.*, 2 (2000) 43-48.
18. W. Hongthani, D.J. Fermin, Layer-by-Layer assembly and redox properties of undoped HPHT diamond particles, *Diam.Relat.Mater.*, 19 (2010) 680-684.
19. H. Sakurai, N. Ebihara, E. Osawa, M. Takahashi, M. Fujinami, K. Oguma, Adsorption characteristics of a nanodiamond for oxoacid anions and their application to the selective preconcentration of tungstate in water samples, *Anal.Sci.*, 22 (2006) 357-362.
20. G.P. Bogatyreva, M.A. Marinich, V.L. Gvyazdovskaya, Diamond - an adsorbent of a new type, *Diam.Relat.Mater.*, 9 (2000) 2002-2005.
21. E.P. Smirnov, O.G. Taushkanova, V.B. Aleskovskii, The Cation and Anion-Exchange Properties of Diamonds, *Dokl.Akad.Nauk SSSR+*, 290 (1986) 901-904.
22. J.T. Paci, H.B. Man, B. Saha, D. Ho, G.C. Schatz, Understanding the Surfaces of Nanodiamonds, *J.Phys.Chem.C.*, 117 (2013) 17256-17267.
23. M.Z. Hossain, T. Kubo, T. Aruga, N. Takagi, T. Tsuno, N. Fujimori, M. Nishijima, Adsorbed states of K on the diamond (100)(2 x 1) surface, *Diam.Relat.Mater.*, 9 (2000) 162-169.
24. A.A. Peristy, P.N. Nesterenko, B. Paull, Adsorption of inorganic ions by sintered detonation nanodiamond, HPLC-2013, Hobart, Australia (2013)
25. T. Jiang, K. Xu, FTIR study of ultradispersed diamond powder synthesized by explosive detonation, *Carbon*, 33 (1995) 1663-1671.

26. V.Y. Dolmatov, Detonation synthesis ultradispersed diamonds: Properties and applications, *Usp.Khim.*, 70 (2001) 687-708.
27. N. Gibson, O. Shenderova, T.J.M. Luo, S. Moseenkov, V. Bondar, A. Puzyr, K. Purto, Z. Fitzgerald, D.W. Brenner, Colloidal stability of modified nanodiamond particles, *Diam.Relat.Mater.*, 18 (2009) 620-626.
28. G.N. Yushin, S. Osswald, V.I. Padalko, G.P. Bogatyreva, Y. Gogotsi, Effect of sintering on structure of nanodiamond, *Diam.Relat.Mater.*, 14 (2005) 1721-1729.
29. V. Strelko, D.J. Malik, Characterization and metal sorptive properties of oxidized active carbon, *J.Colloid Interf.Sci.*, 250 (2002) 213-220.
30. P.N. Nesterenko, O.N. Fedyanina, Y.V. Volgin, P. Jones, Ion chromatographic investigation of the ion-exchange properties of microdisperse sintered nanodiamonds, *J.Chromatogr.A*, 1155 (2007) 2-7.
31. M. Arisaka, M. Watanabe, T. Kimura, Selective adsorption of trivalent actinides from lanthanides onto activated carbons in acidic aqueous solution, *J.Nucl.Mater.*, 407 (2010) 116-118.
32. M. Watanabe, T. Kimura, Adsorption of actinides on diamond surface, International Conference on Diamond and Carbon Materials 2012, Granada, Spain (2012)
33. T.A. Dolenko, S.A. Burikov, K.A. Laptinskiy, T.V. Laptinskaya, J.M. Rosenholm, A.A. Shiryayev, A.R. Sabirov, I.I. Vlasov, Study of adsorption properties of functionalized nanodiamonds in aqueous solutions of metal salts using optical spectroscopy, *J.Alloys Compd.*, 586 (2014) S436-S439.
34. R. Caterino, R. Csiki, M. Wiesinger, M. Sachsenhauser, M. Stutzmann, J.A. Garrido, A. Cattani-Scholz, G. Speranza, S.D. Janssens, K. Haenen, Organophosphonate biofunctionalization of diamond electrodes, *ACS Appl.Mater.Inter.*, 6 (2014) 13909-13916.
35. A. Seco, C. Gabaldon, P. Marzal, A. Aucejo, Effect of pH, cation concentration and sorbent concentration on cadmium and copper removal by a granular activated carbon, *J.Chem.Technol.Biot.*, 74 (1999) 911-918.
36. A.E. Aleksenskii, M.V. Baidakova, A.Y. Vul', V.I. Siklitskii, The structure of diamond nanoclusters, *Phys.Solid State*, 41 (1999) 668-671.
37. L. Tolner, The Determination of Parameters of Multi-Step Adsorption Isotherm by Sequential Simplex Optimization, *Applied Ecology and Environmental Research*, 6 (2008) 111-119.

38. C.A. Finch, *Ion Exchangers; properties and applications*, Walter de Gruyter, Berlin, New York, 1993.
39. B.B. Pappin, M.J. Kiefel, T.A. Houston, *Carbohydrates - Comprehensive Studies on Glycobiology and Glycotechnology*, InTech, Croatia, 2012
40. D.F. Mitev, A.T. Townsend, B. Paull, P.N. Nesterenko, Direct sector field ICP-MS determination of metal impurities in detonation nanodiamond, *Carbon*, 60 (2013) 326-334.
41. Y.W. Zhu, X.Q. Shen, Z.J. Feng, X.G. Xu, B.C. Wang, On the zeta-potential of nanodiamond in aqueous systems, *J.Mater.Sci.Technol.*, 20 (2004) 469-471.
42. X.M. Tan, N.Y. Huang, H.Q. Xie, Complexation between borate ion and hydroxyl groups of phenol-formaldehyde resol resin, *J.Wuhan Univ.Technol.*, 17 (2002) 14-18.

## Chapter 7. General conclusions and future work

### 7.1. Conclusions

The overall aim of this work was to develop a stationary phase based on HPHT diamond for the application within HPLC. The main investigation focused on the preparation and characterisation of HPHT diamond particles, the development of the column packing procedure and testing of the synthetic polycrystalline high pressure high temperature (HPHT) diamond columns under different modes of HPLC, including NP and ANP modes. Additionally, the cation and anion exchange properties of diamond were evaluated. Special attention was paid to the selectivity of diamond sorbents, retention and adsorption mechanisms, column performance, efficiency and stability under a range of temperatures, pressures and mobile phases.

Initially, a careful analysis of the literature available in the field was completed. It was found that several types of diamond based materials, including DND, MSDN and diamond/polymer composites, have been tested previously in varied modes of chromatography, such as GC, RP-HPLC, HILIC and IC. To-date the efficiency of diamond stationary phases has been generally low, due to the broad particle size distribution and irregular shape. Moreover, no fundamental investigations of retention mechanisms and selectivity have been reported in the literature. Partially this deficiency is related to the complex surface chemistry of diamond and to the fact that a standard approach for purification and unification of diamond materials is not available. Several research groups have tried to achieve high efficiency and good selectivity of diamond based stationary phases by using composite materials of diamond with other sorbents, including polymers, silica, and various forms of carbon. However, such composite materials did not exhibit the advantages of pure diamond, especially in terms of thermal and mechanical stability and resistivity to solvents.

Based on the information obtained during the literature review, it was decided to investigate HPHT diamond. This material is commercially available, inexpensive and is suitable for the investigation of chromatographic performance of pure diamond particles. Nevertheless, the properties of HPHT diamond in normal phase, HILIC, reversed-phase and ion chromatography have not been studied.

Here our work has shown that the purification with boiling 40% NaOH and 5 M HNO<sub>3</sub> is required in order to remove the impurities from the surface of HPHT diamond. Such



purification allows preparation of material with a silica and metal impurities content below the limits of detection using EDS (see Section 3.3.1.2), and leads to a highly hydrophilic diamond surface. According to the FTIR, Raman, EDS and titration experiments, the diamond surface contains hydroxyls, carbonyls and carboxyls, with a total content of acidic groups of  $10 \mu\text{mol}\cdot\text{g}^{-1}$ . This results in a negative charge of the HPHT diamond surface ( $\zeta$ -potential at  $\text{pH} > 7$  was  $-70\text{mV}$ ).

Particle size distribution of HPHT diamond phase can be improved by means of sedimentation. According to our results, 10 mM NaOH is the best slurry dispersant for HPHT diamond, and allows the formation of stable suspensions which form a dense sediment. By doing multiple sedimentations in the presence of 10 mM NaOH it was possible to isolate two fractions of the HPHT diamond material with an average particle size of 1.1 and 1.55  $\mu\text{m}$ .  $D_{90/10}$  values were reduced from 4.24 for original diamond down to  $\sim 1.8$  for its fractionated derivative. Since 10 mM NaOH provides the most stable suspensions for HPHT diamond, it was also used as a slurry solvent for column packing.

Column packing procedure has never been optimised before for diamond based stationary phases. However, as was shown in this work, it is an important matter which has a crucial effect on the performance of columns packed with the HPHT diamond. It was found that the best results can be achieved by column packing from 10 mM NaOH (aq.) at room temperature and using highest pressure possible. Column conditioning also has a strong influence on the column's performance. Flushing with DIW results in higher column efficiency, while conditioning with 10 mM  $\text{HNO}_3$  provides a better peak shape. A new developed packing procedure was used to repeatably prepare columns with HETP values of  $\sim 13 \mu\text{m}$ .

Due to the high polarity of HPHT diamond surface, it was decided to investigate it in classic normal phase liquid chromatography first, since until now no reference is available in the literature about the use of non-porous microcrystalline diamond in NP-HPLC. IPA/*n*-hexane mobile phase was used with IPA content below 1%. Despite the low surface area ( $5.1 \text{ m}^2\cdot\text{g}^{-1}$ ) and non-porous character of particles, a column loading capacity of  $0.1 \mu\text{g}$  (acetophenone) per column ( $50 \times 4.6 \text{ mm ID}$ ) was established. This allowed the use of the diamond columns under appropriate conditions without column overloading. Depending on the properties of the solute, the retention mechanism in NP-HPLC may include electrostatic interactions with carboxylic groups, hydrogen bonding with hydroxyl groups and donor–acceptor type interactions involving aromatic rings of solutes acting as hydrogen acceptors. Interestingly, the HPHT diamond showed a different retention selectivity than other types of

carbon based adsorbents, such as MSDN and porous graphitic carbon. Especially, strong retention on the HPHT diamond column was observed for alkylphenyl ketones, phenolic compounds and nitrogen containing molecules. The HPHT diamond column exhibited efficiencies of up to 128,000 plates·m<sup>-1</sup>. This is the highest value to-date achieved for diamond based adsorbents in liquid chromatography, and can be further improved by using a diamond fraction with a narrower size distribution. Model separations of 4, 6 and 9 compounds within 5-8 min were shown. Additionally, an application of the HPHT diamond column towards the analysis of pesticide othilinone was presented.

Since HPHT diamond exhibited potential in classic NP-HPLC, it was decided to test its performance in the other types of NP, namely ANP and HILIC modes. Typical ANP/HILIC behaviour was observed for HPHT diamond column in both ACN/water and MeOH/water mobile phases. It was established that molecular adsorption rather than partitioning mechanism was responsible for the retention of solutes in both mobile phases. The column was tested over the broad range of pH and using different pH buffering systems. Three main types of interactions were observed depending on the mobile phase composition and pH. In TFA buffer and pH<3.5 strong retention of positively charged species was observed due to the ion-exchange interactions, while hydrogen bonding was responsible for the retention of neutral and negatively charged molecules. At the same time, only hydrogen bonding was confirmed during operation under ammonium acetate buffer in pH range 4-10. Due to this combination of retention mechanisms, the HPHT diamond column exhibited distinctive retention selectivity in HILIC/ANP mode of chromatography, different from that reported for common silica and polymeric stationary phases [1].

For the first time, the excellent hydrolytic stability of diamond was exploited in HPLC by using the HPHT diamond columns in HILIC/ANP chromatography under alkaline conditions. It was shown that a combination of hydrogen bonding and ion exchange was responsible for the retention of solutes under alkaline conditions, with the exact retention mechanism depending upon the mobile phase composition. In presence of ACN based mobile phase, ion-exchange interactions are suppressed due to an aprotic nature of the solvent, and the retention is mainly conditioned by hydrogen bonding. Alternatively, using a MeOH based mobile phase leads to disruption of hydrogen bonds, but enhances the ion-exchange retention mechanism because of the higher degree of dissociation of surface groups. Therefore, different selectivities were observed for several classes of solutes under these two mobile phases. In ACN/water retention of phenols and carboxylic acids is stronger, while quaternary ammonium salts, amines and nitro compounds are retained more in MeOH/water. Due to this

effect, it was possible to achieve a complete selectivity reversal for a model mixture of 4 compounds by gradually replacing ACN in the mobile phase with MeOH. Previously, no influence of ACN/MeOH ratio in the mobile phase on the selectivity of diamond based stationary phases was reported.

In both NP and ANP modes of chromatography evidence has been obtained showing the strong influence of surface state and especially adsorbed anions and cations on the retention factors for the HPHT diamond column. In NP, column conditioning with different solvents (NaOH, KOH, acids with pH 2.0) lead to significant variation of retention factors for model compounds. Similarly, in ANP using NaOH, KOH and TMAOH of equal concentration in the mobile phase resulted in different retention factors for nucleobases and other compounds. Therefore, an assumption was made that adsorbed cations and anions on the diamond surface were responsible for the observed effects. Though some preliminary studies on adsorption of cations on diamond sorbents have been carried out, most of the data is not conclusive, while information about adsorption of anions on diamond is limited to the only publication by Sakurai *et al.* [2]. Therefore, a comprehensive investigation of ion-exchange properties of diamond was performed.

In order to evaluate the adsorption of cation and anions on the diamond surface, MSDN was used rather than HPHT diamond due to the higher surface area and larger particle size. The affinity series  $\text{Fe}^{3+} > \text{Al}^{3+} > \text{Cu}^{2+} > \text{Mn}^{2+} > \text{Zn}^{2+} > \text{Cd}^{2+} > \text{Co}^{2+} > \text{Ni}^{2+}$  was found for MSDN, and adsorption capacity for these metals did not exceed  $5 \mu\text{mol}\cdot\text{g}^{-1}$ . Counter ions can contribute to the adsorption mechanism for transition metals, and buffer influence on the adsorption of transition metals was revealed. For this reason, the adsorption of inorganic anions ( $\text{CH}_3\text{COO}^-$ ,  $\text{Cl}^-$ ,  $\text{B}_4\text{O}_7^{2-}$ ,  $\text{ClO}_4^-$ ,  $\text{I}^-$ ,  $\text{SO}_4^{2-}$ ,  $\text{C}_2\text{O}_4^{2-}$ ,  $\text{PO}_4^{3-}$ ) on MSDN was investigated. Adsorption capacity for inorganic anions was at levels of  $50\text{-}150 \mu\text{mol}\cdot\text{g}^{-1}$ , depending on the anion. For the first time such anion exchange capacity for inorganic anions is demonstrated for detonation nanodiamond, exceeding its cation-exchange capacity. Electrostatic interactions, formation of complexes with hydroxyls and interactions with metal impurities contribute to the anion adsorption mechanism, so anion adsorption selectivity over MSDN is different from common anion exchangers. Adsorption of anions on MSDN is chemisorption and obeys Langmuir law. pH affects adsorption of  $\text{SO}_4^{2-}$ ,  $\text{PO}_4^{3-}$  and  $\text{B}_4\text{O}_7^{2-}$  differently due to their different adsorption mechanism.

## 7.2. Future work

According to the results obtained in this work, several directions look promising and should be investigated more carefully in the future.

First, in the current work only hydrophilic diamond was employed, which restricted its applications area to the normal phase modes of chromatography. Therefore, methods for the hydrophobisation of diamond need to be developed. Such hydrophobic material can be then used in RP-HPLC or ion-pair chromatography.

Another interesting opportunity lies in the preparation of diamond based composites. This approach is currently under investigation by several groups, but the majority of researchers prefer to use silica or polymers for composite preparation. However, such additives will reduce the mechanical and chemical stability of the diamond stationary phase, which is the main advantage of using diamond materials in HPLC. Therefore, a more promising option is preparation of diamond-carbon and diamond-nanodiamond composites. This is challenging due to the complexity of diamond surface chemistry and complications related to the grafting of functional groups to the diamond surface. Nevertheless, a successful method would allow the preparation of spherical particles with well-developed surface, potentially core-shell and with narrow particle size distribution, which are also stable at high temperatures and over the entire pH range. Preliminary results in this field have been obtained by Kondo *et al.*, who prepared ND/CVD diamond composites and employed them in RP-HPLC [3]. Despite the relatively low efficiency of the prepared stationary phase, the authors have demonstrated great potential of such composites for HPLC applications.

Additionally, more attention should be dedicated to use of diamond stationary phases at elevated temperatures (>100 °C). Such increases in temperature should lead to better column performance, higher efficiency and faster analysis time. Potentially, diamond columns can be used under supercritical conditions as well. In the current work, application of diamond at high temperatures was limited by the expansion of stainless steel column bodies, resulting in a drop of efficiency. Therefore, focus should be made on the development of columns made of materials with negligible thermal expansion, such as Ni alloys, as well as Zr and Ti.

### **7.3. Reference List**

1. M.E.A. Ibrahim, Y. Liu, C.A. Lucy, A simple graphical representation of selectivity in hydrophilic interaction liquid chromatography, *J.Chromatogr.A*, 1260 (2012) 126-131.
2. H. Sakurai, N. Ebihara, E. Osawa, M. Takahashi, M. Fujinami, K. Oguma, Adsorption characteristics of a nanodiamond for oxoacid anions and their application to the selective preconcentration of tungstate in water samples, *Anal.Sci.*, 22 (2006) 357-362.
3. T. Kondo, M. Kobayashi, T. Saito, Y. Kadota, T. Kameshima, T. Aikawa, T. Kawai, M. Yuasa, Micrometer-sized mesoporous diamond spherical particles, *Diam.Relat.Mater.*, 43 (2014) 72-79.

## Chapter 8. Supplementary information

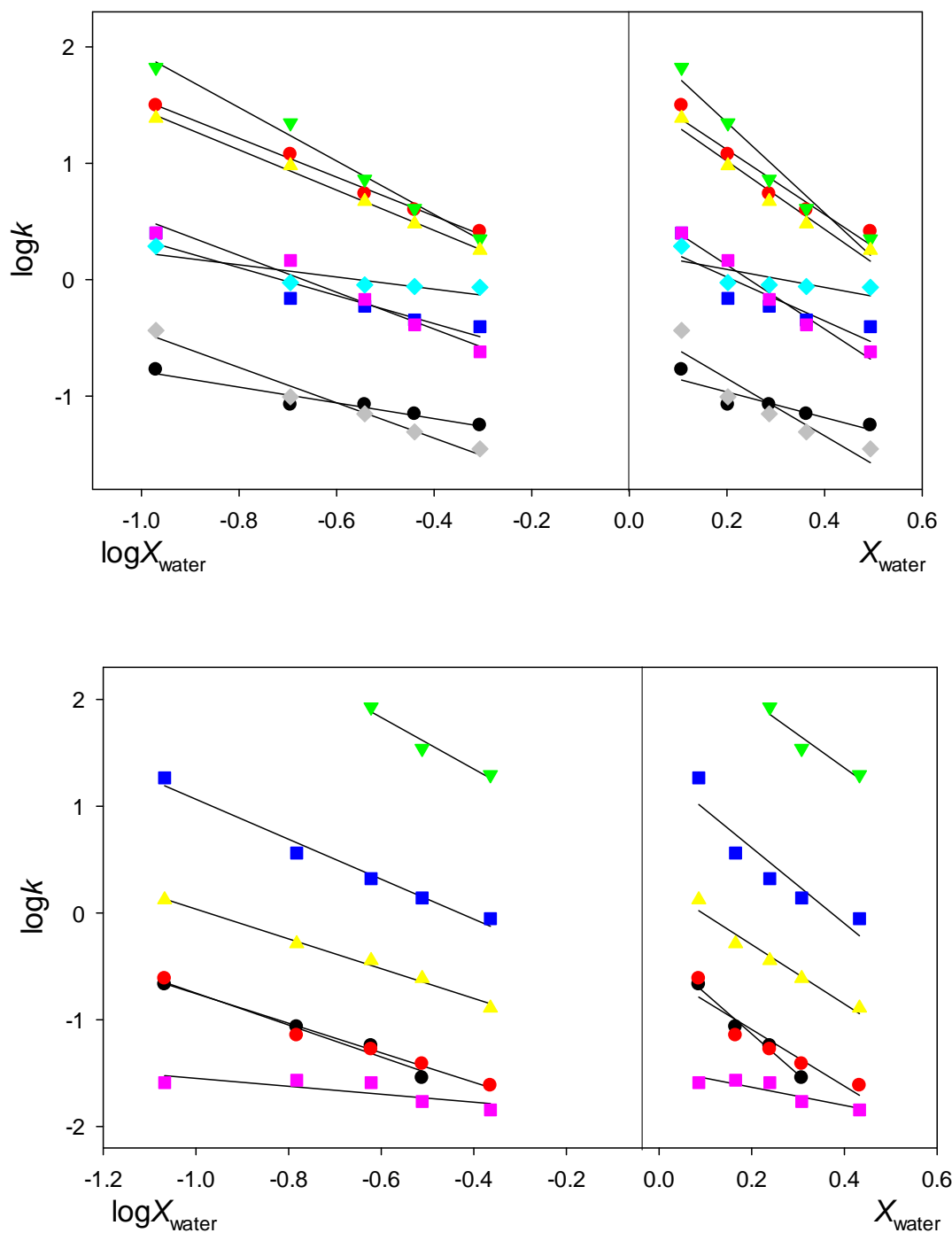


Fig. 8.1. Re-built retention data from Fig. 5.1 (upper figure) and Fig. 5.5 (bottom figure) in terms of molar water content in the mobile phase ( $X_{\text{water}}$ ) and logarithm of molar water content in the mobile phase ( $\log X_{\text{water}}$ ).  $R^2$  values for this approximation are given in the Table 5.2. Analytes: adenosine (green), adenine (red), cytosine (yellow), 4-HBSA (pink), pyridine (light blue), BTMA (dark blue), 2,4-dichlorophenol (grey), uracil (black). For the experimental details see Sections 5.3.2 and 5.3.3 and Fig. 5.1 and 5.5.